

The primary applications of wire EDM are found in tool and die manufacturing, as well as in engine and medical technology. It is predominantly used for producing high-value components and often serves as the final critical manufacturing step. Consequently, process reliability and repeatability are of utmost importance and can be ensured through intelligent control and automation solutions. In this context, the growing digitalization of manufacturing processes, driven by Industry 4.0, highlights the need for data-driven approaches in wire EDM.

The aim of this work was to develop a data-driven model for evaluating the wire EDM process, primarily based on continuously recorded electrical process data to ensure the model's transferability and general validity. Machine learning models were trained on this process data to enable real-time evaluation of the process based solely on electrical signals. The objective was to achieve this by developing a regression model to assess quality and a classification model to evaluate productivity. The scientific framework of this study is shaped by the data analysis methods and techniques employed, and the structure of the work is accordingly aligned with the development of data-driven models.

A system was first developed to enable the real-time recording of temporally and spatially resolved individual discharges within the continuous wire EDM process. Following systematic data processing, including data reduction and feature extraction, characteristic values were subsequently correlated with process productivity and product quality. Building on these initial process data insights, a regression model was created to predict product quality. For this purpose, a neural network was trained to estimate the component's curvature based on continuously recorded data, achieving high prediction accuracy and explaining a significant portion of the data variability. Process productivity was assessed through a classification model using a deep learning approach, where various neural network architectures were explored. The results demonstrated high accuracy, particularly noteworthy given that all evaluations were conducted using entirely unseen data. The findings were applied to develop a Digital Twin in an industrial context, capable of visualizing the real-time curvature of the workpiece on a dashboard using continuously processed data.

ISBN 978-3-98555-260-3



9 783985 552603

Data-driven Model for Process Evaluation in Wire EDM

Ugur Küpper



Ugur Küpper

# Data-driven Model for Process Evaluation in Wire EDM



Data-driven Model for Process Evaluation in Wire EDM

## Datengetriebenes Modell zur Prozessbewertung in der Drahtfunkenerosion

Von der Fakultät für Maschinenwesen  
der Rheinisch-Westfälischen Technischen Hochschule Aachen  
zur Erlangung des akademischen Grades eines  
Doktors der Ingenieurwissenschaften  
genehmigte Dissertation

vorgelegt von

Ugur Küpper, geb. Tombul

### **Berichter/in:**

Univ.-Prof. Dr.-Ing. Thomas Bergs

Univ.-Prof. Dr.-Ing. Dr.-Ing. E. h. Dr. h. c. Dr. h. c. Fritz Klocke

Tag der mündlichen Prüfung: 20. Dezember 2024

Diese Dissertation ist auf den Internetseiten der Universitätsbibliothek online verfügbar.



# ERGEBNISSE AUS DER PRODUKTIONSTECHNIK

**Ugur Küpper**

## Data-driven Model for Process Evaluation in Wire EDM

**Herausgeber:**

Prof. Dr.-Ing. Dipl.-Wirt. Ing. G. Schuh

Prof. Dr.-Ing. C. Brecher

Prof. Dr.-Ing. R. H. Schmitt

Band 6/2025





**Bibliografische Information der Deutschen Nationalbibliothek**

Die Deutsche Nationalbibliothek verzeichnet diese Publikation in der Deutschen Nationalbibliografie; detaillierte bibliografische Daten sind im Internet über <https://portal.dnb.de> abrufbar.

Ugur Küpper:

Data-driven Model for Process Evaluation in Wire EDM

1. Auflage, 2025

Gedruckt auf holz- und säurefreiem Papier, 100% chlorfrei gebleicht.

Copyright Apprimus Verlag, Aachen, 2025

Wissenschaftsverlag des Instituts für Industriekommunikation und Fachmedien  
an der RWTH Aachen

Steinbachstr. 25, 52074 Aachen, Deutschland

Internet: [www.apprimus-verlag.de](http://www.apprimus-verlag.de), E-Mail: [info@apprimus-verlag.de](mailto:info@apprimus-verlag.de)

Alle Rechte, auch das des auszugsweisen Nachdruckes, der auszugsweisen oder vollständigen Wiedergabe, der Speicherung in Datenverarbeitungsanlagen und der Übersetzung, vorbehalten.

Printed in Germany

ISBN 978-3-98555-260-3

# Vorwort und Danksagung

## *Preamble and Acknowledgement*

Die vorliegende Arbeit entstand während meiner Tätigkeit als wissenschaftlicher Mitarbeiter am Werkzeugmaschinenlabor WZL der Rheinisch-Westfälischen Technischen Hochschule (RWTH) Aachen und am Fraunhofer-Institut für Produktionstechnologie (IPT) in Aachen.

Herrn Prof. Dr.-Ing. Thomas Bergs, Inhaber des Lehrstuhls für Technologie der Fertigungsverfahren (heute Manufacturing Technology Institute MTI), danke ich für die stetige Unterstützung meiner Tätigkeit und die fachliche und persönliche Förderung. Herrn Prof. Dr.-Ing. Dr.-Ing. E. h. Dr. h. c. Dr. h. c. Fritz Klocke, ehemaliger Inhaber des Lehrstuhls für Technologie der Fertigungsverfahren, danke ich herzlichst für die Übernahme des Koreferats, für die eingehende Durchsicht des Manuskripts sowie für die bereichernden Gespräche und Anmerkungen zu meiner Dissertation. Die fachliche und persönliche Unterstützung beider hat ein motivierendes Arbeitsumfeld geschaffen, in dem ich stets sehr gerne gearbeitet habe.

Ebenfalls möchte ich mich bei Herrn Prof. Dr.-Ing. Christian Hopmann, Inhaber des Lehrstuhls für Kunststoffverarbeitung, für die Übernahme des Prüfungsvorsitzes herzlichst bedanken. Außerdem danke ich Frau Prof. Dr.-Ing. Kirsten Bobzin, Inhaberin des Lehrstuhls für Oberflächentechnik im Maschinenbau, für die Übernahme des Prüfungsbeisitzes.

Für die konstruktive Zusammenarbeit innerhalb des von dem Bundesministerium für Bildung und Forschung (BMBF) geförderten Projektes „KI-Erosion“ gilt mein herzlicher Dank allen beteiligten Personen. Besonderen Dank möchte ich hier Herrn Dr.-Ing. Markus Ohlenforst, Herrn Dr.-Ing. Martin Peterek, Herrn Akshay Paranjape von IconPro und Herrn Mike Brinkmann von der WBA Aachen aussprechen. Darüber hinaus danke ich allen Partnern aus dem Industriearbeitskreis „Elektroerosive Bearbeitung“ für die vielen Anregungen, die zur Erstellung dieser Dissertation beigetragen haben. Insbesondere möchte ich mich bei Herrn Dr.-Ing. David Welling für die exzellente Unterstützung und Zusammenarbeit bedanken. Durch seine wohlwollende Förderung hat er mir während seiner Tätigkeit beim Maschinenhersteller Makino viele Möglichkeiten gegeben, meine fachlichen Fähigkeiten weiterzuentwickeln und wertvolle berufliche Erfahrungen zu sammeln, wofür ich ihm sehr dankbar bin.

Ein großer Dank geht an Dr.-Ing. Tim Herrig sowie Dr.-Ing. Andreas Klink, die mich als Oberingenieure stets gefördert und einen großen Beitrag zu meiner persönlichen Entwicklung geleistet haben. Ein besonderer Dank gilt meinen aktiven und ehemaligen Kollegen aus der Abteilung Abtragende Fertigungsverfahren, die fachlich, insbesondere aber auch menschlich für eine unvergessliche Zeit am Institut gesorgt haben. Vielen Dank an Dr.-Ing. Simon Harst, Lukas Heidemanns, Dr.-Ing. Lars Hensgen, Raphael Hess, Dr.-Ing. Maximilian Holsten, Dr.-Ing. Mehnoush

Mohammadnejad, Dr.-Ing. Marcel Olivier, Timm Petersen, Dr.-Ing. Sebastian Schneider, Daniel Schulze Brock, Gregor Smeets, Florian Sous, Elio Tchoupe Sambou, Lukas Welschof, Jan Wittenburg und Dr.-Ing. Dr. rer. nat. Markus Zeis.

Weiterhin bedanke ich mich herzlich für die intensive Durchsicht meines Manuskripts und das hilfreiche Feedback bei Herrn Daniel Schulze Brock, Herrn Dr.-Ing. Sebastian Schneider, Herrn Dr.-Ing. Maximilian Holsten, Herrn Dr.-Ing. Simon Harst, Herrn Dr.-Ing. Andreas Klink und Herrn Prof. Dr. Phil Koshy.

Für die Unterstützung bei allen experimentellen und praktischen Arbeiten möchte ich mich bei Herrn Marcel Bauer und Herrn Aron Salm bedanken. Daneben bedanke ich mich bei Herrn Robert Seidner und Herrn Sascha Kamps für die Unterstützung mit ihrer Expertise in der Signaldatenerfassung.

Die Anfertigung des Manuskripts wäre in dieser Art und Weise ohne die Arbeit meiner studentischen Hilfskräfte sowie den Einsatz der Bachelor- und Masterarbeiter nicht möglich gewesen. Daher möchte ich mich bei den Herren Daniel Schulze Brock, Kai Woltering, Andreas Pertzborn, Elio Tchoupe Sambou, Benedikt Despineux, Adrian Spahn und Haolin Jiang.

Darüber hinaus danke ich allen aktiven und ehemaligen Kegelbrüdern des Kegelclubs „Funke, Span, Gefüge“, welche für ein monatliches Entkommen aus dem Institutsalltag gesorgt haben. Hervorheben möchte ich hierbei insbesondere Dr.-Ing. Tobias Seelbach und Dr.-Ing. Thomas Pullen. Ich habe die Zeit am Institut als großartig empfunden und denke gerne an die vielen schönen Momente zurück.

Daneben waren auch meine Freunde aus meiner Schul- und Studienzeit eine große Stütze in den letzten Jahren und haben stets für den nötigen Ausgleich gesorgt. Ein besonderer Dank geht dabei an meine ältesten und engsten Freunde Lukas Welschof, Christoph Marquis und Marco Caputo.

Ein tiefer Dank gilt meinen Schwiegereltern Theo und Andrea. Ich danke euch, dass ihr mir von Anfang an das Gefühl gegeben habt zur Familie zu gehören. Meiner Mutter Hanife danke ich für ihre unermüdliche Fürsorge und dafür, dass sie uns eine Kindheit ermöglicht hat, die sie selbst nie hatte.

Für die aufgebrachte Geduld und bedingungslose Unterstützung möchte ich meiner Frau Eva und meinem Sohn Elias danken. Beide haben für diese Arbeit auf einen Teil gemeinsamer Zeit verzichten müssen und gaben mir trotzdem immer den notwendigen Rückhalt. Danke Eva, dass du seit über 16 Jahren an meiner Seite bist und mir klar gemacht hast, was wirklich wichtig im Leben ist und was Familie bedeutet.

**für Elias**

*Du hast Macht über deinen Geist –  
nicht über äußere Ereignisse. Erkenne  
das, und du wirst Stärke finden.*

Marcus Aurelius



## **Abstract**

The main areas of application for wire EDM are in tool and die making, as well as in engine and medical technology. It is mainly used in the production of high-priced products and is often the last decisive manufacturing technology. The process reliability and repeatability of this technology are therefore particularly important and can be guaranteed by correspondingly intelligent control and automation solutions. This, along with the digitalization of manufacturing processes in the context of Industry 4.0, requires the use of data-driven approaches in wire EDM.

The objective of the present work was therefore to develop a data-driven model for the evaluation of the wire EDM process. This was to be based primarily on continuously recorded physical respectively electrical process data in order to ensure the transferability and general validity of the model. Machine learning models were trained with process data to evaluate the process solely based on the electrical process signals evaluated in real-time. This goal was to be achieved by developing a regression model to evaluate quality and a classification model to evaluate productivity. The scientific design framework in this work is determined in particular by the methods and techniques used in data analysis and the structure of the work is designed accordingly for the development of data-driven models.

To this end, a system was first developed for the real-time recording of time and spatially resolved characterized individual discharges in the continuous process. After data processing, including systematic data reduction and feature extraction, characteristic values were correlated with process productivity and product quality in the following step.

Based on the initial findings from the process data, a regression model was developed to evaluate product quality. For this purpose, a neural network was trained that predicts the curvature of the component based on continuously recorded data. The model shows good prediction accuracy and explains a significant part of the data variability. The productivity of the process was evaluated using a classification model. A deep learning approach was used, in which various forms of neural networks were used for the model architecture. The results showed high accuracy, especially considering that all tests were performed with completely unknown data.

Finally, it was shown how the findings can be transferred to the development of a Digital Twin in an industrial setting. In cooperation with an AI software manufacturer and a wire EDM user, a Digital Twin was developed that can map the generated curvature of the workpiece in a dashboard using data processed in real-time.



## Kurzfassung

Die Hauptanwendungsgebiete der Drahtfunkenerosion liegen im Werkzeug- und Formenbau sowie in der Triebwerks- und Medizintechnik. Dort kommt sie vor allem bei der Fertigung von hochpreisigen Produkten zum Einsatz und wird oft als letzte maßgebende Fertigungstechnologie eingesetzt. Daher sind die Prozesssicherheit und Wiederholbarkeit dieser Technologie besonders wichtig und können durch entsprechend intelligente Regelungen und Automatisierungslösungen gewährleistet werden. Dies und die Digitalisierung von Fertigungsprozessen im Kontext von Industrie 4.0 erfordern daher den Einsatz von datengetriebenen Lösungen in der Drahtfunkenerosion.

Die Zielsetzung der vorliegenden Arbeit bestand demnach darin, ein datengetriebenes Model zur Bewertung des Drahtfunkenerosionsprozesses zu entwickeln. Dieses sollte vor allem auf kontinuierlich aufgezeichneten physikalischen bzw. elektrischen Prozessdaten beruhen, um eine Übertragbarkeit und Allgemeingültigkeit des Modells zu gewährleisten. Mit den Prozessdaten wurden KI-Modelle trainiert, um den Prozess nur auf Basis der in Echtzeit ausgewerteten elektrischen Prozesssignale zu bewerten. Dieses Ziel sollte durch die Entwicklung eines Regressionsmodells zur Bewertung der Qualität und eines Klassifikationsmodells zur Bewertung der Produktivität realisiert werden. Der wissenschaftliche Gestaltungsrahmen wird in dieser Arbeit besonders durch die Methoden und Techniken in der Datenanalyse bestimmt, und der Aufbau der Arbeit ist entsprechend für die Entwicklung datengetriebener Modelle ausgelegt.

Zu diesem Zweck wurde zunächst ein System zur echtzeitfähigen Erfassung von zeit- und orts aufgelösten charakterisierenden Einzelentladungen im kontinuierlichen Prozess entwickelt. Nach der Datenaufbereitung mit systematischer Datenreduktion und Merkmalsextraktion wurden im nächsten Schritt charakteristische Prozesskennwerte mit der Prozessproduktivität und der Produktqualität korreliert.

Basierend auf den ersten Erkenntnissen der Prozessdaten wurde ein Regressionsmodell zur Bewertung der Produktqualität entwickelt. Dazu wurde ein neuronales Netz trainiert, das die Wölbung des Bauteils anhand kontinuierlich aufgezeichneter Daten vorhersagt. Das Modell zeigt eine gute Vorhersagegenauigkeit und erklärt einen erheblichen Teil der Datenvariabilität. Die Produktivität des Prozesses wurde mithilfe eines Klassifikationsmodells bewertet. Es wurde ein Deep-Learning-Ansatz angewandt, bei dem verschiedene Formen neuronaler Netze für die Modellarchitektur verwendet wurden. Die Ergebnisse zeigten eine hohe Genauigkeit für die Teilmodelle, insbesondere unter Berücksichtigung, dass alle Validierungen mit völlig unbekannten Daten durchgeführt wurden.

Abschließend wurde im letzten Kapitel gezeigt, wie die Erkenntnisse in die Entwicklung eines Digitalen Zwillings in einem industriellen Umfeld überführt werden können. In kooperativer Arbeit mit einem KI-Software Hersteller und einem Drahtfunkenerosionsanwender konnte ein Digitaler Zwilling entwickelt werden, der durch in Echtzeit verarbeitete Daten die erzeugte Kontur des Werkstücks in einem Dashboard abbilden kann.





# Table of Contents

## Inhaltsverzeichnis

<b>1</b>	<b>Introduction.....</b>	<b>1</b>
<b>2</b>	<b>State of the Art.....</b>	<b>5</b>
2.1	Fundamentals of Wire EDM .....	5
2.2	Use of Data in Wire EDM .....	13
2.3	Machine Learning Methods.....	21
2.4	Machine Learning in Wire EDM.....	26
2.5	Summary and Conclusions .....	35
<b>3</b>	<b>Objective and Tasks.....</b>	<b>37</b>
<b>4</b>	<b>Data Acquisition and Processing in Wire EDM.....</b>	<b>41</b>
4.1	Offline Measurement of Single Discharge Energies.....	41
4.2	Online Measurement of Process Parameters.....	46
4.3	Online Measurement of Spatially Resolved Single Discharges.....	49
4.4	Data Agglomeration .....	59
4.5	Summary and Conclusions .....	68
<b>5</b>	<b>Analysis of Evaluation Criteria in Wire EDM.....</b>	<b>71</b>
5.1	Exploratory Data Analysis for the Productivity.....	71
5.2	Exploratory Data Analysis for the Workpiece Quality .....	77
5.3	Summary and Conclusions .....	91
<b>6</b>	<b>Regression Model for Quality Evaluation.....</b>	<b>93</b>
6.1	Data Processing.....	93
6.2	Feature Engineering.....	101
6.3	Regression Model Architecture .....	105
6.4	Training the Regression Model .....	109
6.5	Testing the Regression Model.....	111
6.6	Summary and Conclusions .....	115
<b>7</b>	<b>Classification Model for Productivity Evaluation.....</b>	<b>117</b>
7.1	Data Generation.....	118
7.2	Data Processing and Defining Classes .....	121
7.3	Classification Model Architecture .....	126
7.4	Testing the Classification Models.....	132
7.5	Summary and Conclusions .....	140
<b>8</b>	<b>Development of a Digital Twin.....</b>	<b>141</b>
<b>9</b>	<b>Summary and Outlook .....</b>	<b>147</b>
<b>10</b>	<b>References .....</b>	<b>155</b>
<b>11</b>	<b>Appendix .....</b>	<b>179</b>



# Formula Symbols and Abbreviations

## Formelzeichen und Abkürzungsverzeichnis

### Capital Letters

$C$	$\mu\text{m}$	Curvature
$E$		Model error
$F1\text{-Score}$		Harmonic mean of precision and recall
$K$		Kurtosis
$K_S$		Correction factor for FPGA calibration
$K_T$		Correction factor for FPGA limit detection
$K_U$		FPGA current limit defined by user
$P$	$\text{W}$	Power
$R$	$\Omega$	Resistance
$R^2$		Coefficient of determination
$R_a$	$\mu\text{m}$	Average surface roughness
$R_{ab}$		Ratio of abnormal discharges
$R_z$	$\mu\text{m}$	Surface roughness value
$S$		Scaling factor
$V_w$	$\text{mm}^2/\text{min}$	Material removal rate
$W_e$	$\text{mJ}$	Discharge energy

### Small Letters

$\bar{x}_M$		Mode
$\hat{I}_e$	$\text{A}$	Maximum discharge current
$\bar{I}_e$	$\text{A}$	Average discharge current
$\bar{U}_e$	$\text{V}$	Average discharge voltage
$\hat{U}_i$	$\text{V}$	Open circuit voltage
$a$	$\text{mm}$	Nozzle distance
$a_{\text{lower}}$	$\text{mm}$	Lower nozzle distance
$a_{\text{upper}}$	$\text{mm}$	Upper nozzle distance
$d$	$\text{mm}$	Wire diameter
$\Theta_{\text{max}}$		Error factor

$f$	Hz	Frequency
$f_{current}$		Sample rate of the current measurement device
$f_e$	Hz	Effective pulse frequency
$f_{oscilloscope}$	Hz	Sample rate of the oscilloscope
$f_p$	Hz	Pulse frequency
$f_{voltage}$	Hz	Sample rate of the voltage measurement device
$g_k$		Gradient at iteration k
$h$	mm	Workpiece height
$i$	A	Current
$i_e$	A	Discharge current
$i_{lower}$	A	Current of the lower wire head
$i_{total}$	A	Total current
$i_{upper}$	A	Current of the upper wire head
$k_i$		Statistical factor for discharge distribution
$l$	mm	Cutting length
$m$		Slope
$n_{bins}$		Number of bins
$n_d$		Total number of discharges
$p$	bar	Flushing pressure
$p$		Precision
$q$		Quantile
$r$		Bravais-Pearson correlation coefficient
$r$	mm	Radius
$r$		Recall
$res$		Resolution
$r_n$		Ratio of normal discharges
$r_{SP}$		Spearman correlation coefficient
$s$	Hz	Sampling rate
$s_F$	mm	Frontal working gap
$s_L$	mm	Lateral working gap
$s_l$	mm	Lower cutting kerf
$s_u$	mm	Upper cutting kerf

$t$	s	Time
$t$	mm	Thickness
$t_0$	$\mu\text{s}$	Pulse interval time
$t_d$	$\mu\text{s}$	Ignition delay time
$t_e$	$\mu\text{s}$	Discharge duration
$t_{e,n}$	$\mu\text{s}$	Discharge duration of normal discharges
$t_{e,s}$	$\mu\text{s}$	Discharge duration of short circuits
$t_i$	$\mu\text{s}$	Pulse duration
$t_{\text{measure}}$	s	Measurement duration
$t_p$	$\mu\text{s}$	Pulse cycle time
$U$	V	Voltage
$v_D$	m/s	Wire run-off speed
$v_f$	mm/min	Feed rate
$W_{e,n}$	J	Normal discharge energy
$W_{e,s}$	J	Short circuit energy
$W_{\text{local}}$	J	Local discharge energy
$x$		x-Position
$z$		z-Position
$\Delta i$	A	Current difference
$\Delta t$	s	Averaging time
$\Delta y$	mm	Lateral infeed

**Greek Letters**

$\eta_k$		Learning rate
$\tau_a$		Kendall's tau coefficient
$\mu_k$		Momentum coefficient
$\alpha$	°	Conicity angle
$\alpha$	%	Proportion of training data
$\gamma$		Skewness
$K$	S/m	Electrical conductivity
$\lambda$		Frequency ratio
$\rho$	kg/m <sup>3</sup>	Density
$\sigma$		Standard deviation

**Abbreviations**

ADAM	Adaptive Moment Estimation
AI	Artificial Intelligence
ANFIS	Adaptive Neuro-Fuzzy Inference System
ANN	Artificial Neural Network
API	Application Programming Interface
BM	Base Material
BO	Bayesian Optimization
CCD	Central Composite Design
CFD	Computational Fluid Dynamics
CMM	Coordinate Measuring Machine
CNN	Convolutional Neural Network
CV	Coefficient of Variation
DIN	German Institute for Standardization
DOE	Design of Experiments
DT	Digital Twin
EDA	Exploratory Data Analysis
EDM	Electrical Discharge Machining
EPP	Electrical Process Parameter
et al.	lat.: et alii engl.: and others
FEM	Finite Element Method
FFT	Fast Fourier Transformation
FIFO	First In First Out
FPGA	Field Programmable Gate Array
GA	Generic Algorithm

GP	Gaussian Processes
GRU	Gated Recurrent Unit
HAZ	Heat-Affected Zone
HTLBO	Hybrid Teaching and Learning-Based Optimization
KW	Kerf Width
LRNN	Layer Recurrent Neural Network
LSTM	Long Short-Term Memory
MAE	Mean Absolute Error
MAPE	Mean Absolute Percentage Error
MC	Main Cut
ML	Machine Learning
MOPSO	Multi-Objective Particle Swarm Optimization
MRR	Material Removal Rate
MSE	Mean Squared Error
MSP	Machine Setting Parameter
NN	Neural Network
PC	Power Consumption
PINN	Physics-Informed Neural Network
PSO	Particle Swarm Optimization
ref	Reference
RL	Recast Layer
RMSE	Root Mean Squared Error
RNN	Recurrent Neural Network
RSM	Response Surface Methodology
SEM	Scanning Electron Microscope
SHAP	SHapley Additive exPlanations



Sinking EDM	Sinking Electrical Discharge Machining
SR	Shift Register
std.	Standard
SVM	Support Vector Machine
T	Tool
TC	Trim Cut
TLBO	Teaching–Learning-Based Optimization
TOPSIS	Technique for Order of Preference by Similarity to Ideal Solution
VI	Virtual Instrument
W	Workpiece
wb	Wire break
wire EDM	Wire Electrical Discharge Machining
WL	White Layer
WLT	White Layer Thickness
WW	Wire Wear

# 1 Introduction

The demand for companies to achieve climate neutrality in the future among the regular competition is driving them to continuously improve the efficiency of the products they manufacture on the one hand and to make production as efficient as possible on the other [BUND21]. In addition, there are economic challenges, especially in high-wage countries such as Germany, which require not only an increase in productivity and product quality but also a reduction in costs in order to remain competitive as a production location compared to low-wage countries [BREC11]. In addition, many sectors need to find solutions to the growing shortage of skilled workers in the manufacturing industry [BURS24]. In order to achieve this in production, individual production technologies or entire process chains are being optimized and automated. Automation requires stable and adaptive processes that no longer require manual intervention. However, the flexibility of individual processes, which is required in many areas, poses major challenges due to continuously changing conditions [BREC11].

In the context of Industry 4.0, data-driven automation systems are required and seen as an enabler for high competitiveness of manufacturing companies in high-wage countries. In order to develop such systems and implement them in a holistic ecosystem, so-called Digital Twins (DTs) are being developed due to the increasing possibilities of digitalization. In this work, the definition by Bergs et al. [BERG20c, BERG21] is applied, which describes a DT in the context of manufacturing technology as follows: *“The digital twin of an asset is the virtual representation of its physical state - state changes are described by models and supported by data.”* These could, for example, include process-related changes in the state of a workpiece. According to Shao et al. [SHAO20], a Digital Twin differs from a traditional simulation model through its regular connection to the real physical object in the sense of monitoring. According to the CIRP Encyclopedia of Production Engineering, the DT is a virtual image of a real device, object, machine, service or intangible asset that describes its properties and behavior using models, data and information within its life cycle [STAR19]. An up-to-date and comprehensive overview of the DT methodology in all areas of production technology can be found in [JONE20].

The implementation of Digital Twins for individual manufacturing technologies is necessary in order to digitalize production holistically. Electrical discharge machining (EDM) is usually used as an alternative manufacturing process for high-priced products [KLOC14a]. Advantages over other manufacturing technologies include the high flexibility and accuracy. Due to the increasing demand for materials with high thermomechanical strength, wire EDM is increasingly being used for a variety of applications, e.g. in tool and die making as well as in the aerospace industry [BOOS18, HEID21]. In particular, monitoring and automation of the EDM process results in the need for integration into networked adaptive production in the context of Industry 4.0. However, the use of process data in wire EDM represents a major challenge for the development of a DT. Due to a high amount of data generated by millions of individual discharges in the single-digit microsecond range and a stochastic process behavior, a valid data

acquisition and processing system must first be developed and implemented. A subsequent analysis should link existing expert knowledge and existing physical models with the data in order to generate new insights into the process and to relate a data-driven system for process monitoring and optimization to improve productivity and quality. The use of artificial intelligence (AI) methods is a promising approach for this.

The performance of AI and the potential to solve complex problems have increased rapidly in recent years. At the latest since the introduction of the chatbot ChatGPT from the company OpenAI, the whole topic of AI has taken on a much more practical character in society [RAY23]. AI methods have played a role in people's everyday lives for much longer and the use of AI in manufacturing companies is also increasing [JAVA23, PART24, ROCK24]. The most important prerequisite for a well-functioning AI model is a sufficiently large amount of data with high data quality, which can be evaluated on the basis of various factors as named in [ASKH13].

Even though the application of AI methods in wire EDM has already been dealt with in many works, it has not yet been possible to develop valid models that have been trained on the basis of sufficiently large amounts of data and retain their validity even under changed process conditions. For this reason, in this thesis a system is initially developed and implemented in this work, with which physical process data can be continuously recorded. By processing the data in real time, a memory for the high data volumes is realized. However, it is systematically validated that no irrelevant information is lost by reducing the amount of data; on the contrary, the density of information is increased.

In practice, wire EDM typically involves a main cut followed by one or more trim cuts, which sequentially enhance accuracy and surface quality. Since the main cut has a significant impact on productivity and contour accuracy, the main cut machining is examined in this thesis.

Based on the data, AI-based models are developed in this thesis, which enable both quantitative predictions regarding component quality and qualitative predictions regarding process performance. These predictions are realized in regression and classification models using various AI methods. To this end, the relevant input and output parameters are first systematically identified and evaluated. Subsequently, a sufficiently high number of experiments are carried out with defined process conditions and data is generated in order to train, validate and test the models. Finally, the findings are transferred to a concept that enables machine users to digitize, monitor and optimize their processes using external software simply by equipping a data acquisition system without data science expertise. For this purpose, the findings are transferred to the development of a DT in an industrial environment.

## Einleitung

Die Forderung nach Klimaneutralität im regulären Wettbewerb treibt die Unternehmen dazu an, zum einen den Wirkungsgrad der hergestellten Produkte kontinuierlich zu verbessern und zum anderen auch die Fertigung möglichst effizient zu gestalten [BUND21]. Hinzu kommen insbesondere in Hochlohnländern wie Deutschland wirtschaftliche Herausforderungen, die neben einer Steigerung der Produktivität und Produktqualität auch die Reduzierung der Kosten erfordern, um als Produktionsstandort weiterhin konkurrenzfähig gegenüber Niedriglohnländern zu bleiben [BREC11]. Zusätzlich müssen viele Branchen Lösungen für den wachsenden Fachkräftemangel in der produzierenden Industrie finden [BURS24]. Um dies in der Fertigung zu realisieren, werden einzelne Fertigungstechnologien oder ganze Prozessketten optimiert und automatisiert. Die Automatisierung setzt stabile und adaptive Prozesse voraus, die keine manuellen Eingriffe mehr benötigen. Die Flexibilität einzelner Prozesse, die in vielen Bereichen gefordert wird, stellt jedoch aufgrund sich kontinuierlich verändernder Bedingungen große Herausforderungen dar [BREC11].

Im Kontext von Industrie 4.0 werden datengetriebene Automatisierungssysteme gefordert und als Enabler für eine hohe Konkurrenzfähigkeit der produzierenden Unternehmen in Hochlohnländern gesehen. Um solche Systeme zu entwickeln und in ein ganzheitliches Ökosystem zu implementieren, werden durch die zunehmenden Möglichkeiten der Digitalisierung sogenannte Digital Twins (DT) entwickelt. In dieser Arbeit findet die Definition von Bergs et al. [BERG20c, BERG21] Anwendung, die einen DT im Kontext der Fertigungstechnologie wie folgt beschreibt: *„Der digitale Zwilling eines Assets ist das virtuelle Abbild seines physikalischen Zustands - Zustandsänderungen sind beschrieben durch Modelle und gestützt durch Daten.“* Diese könnten zum Beispiel prozessbedingte Zustandsänderungen eines Werkstücks sein. Nach Shao et al. [SHAO20] unterscheidet sich ein DT von einem traditionellen Simulationsmodell durch seine regelmäßige Verbindung zum realen physikalischen Objekt im Sinne eines Monitorings. Nach der CIRP Enzyklopädie der Produktionstechnik ist der DT ein virtuelles Abbild eines realen Geräts, Objekts, einer Maschine, einer Dienstleistung oder eines immateriellen Assets, das dessen Eigenschaften und Verhalten anhand von Modellen, Daten und Informationen innerhalb seines Lebenszyklus beschreibt [STAR19]. Einen aktuellen und umfassenden Überblick über die Methodik des DT in allen Bereichen der Produktionstechnik gibt [JONE20].

Die Implementierung von DTs für einzelne Fertigungstechnologien ist notwendig, um die Produktion ganzheitlich zu digitalisieren. Die Funkenerosion (EDM) wird meist als alternatives Fertigungsverfahren für hochpreisige Produkte eingesetzt [KLOC14a]. Die Vorteile gegenüber anderen Fertigungstechnologien sind die hohe Flexibilität und Genauigkeit. Aufgrund der steigenden Nachfrage nach Werkstoffen mit hoher thermomechanischer Festigkeit wird die Drahtfunkenerosion zunehmend für eine Vielzahl von Anwendungen eingesetzt, z. B. im Werkzeug- und Formenbau sowie in der Luftfahrtindustrie [BOOS18, HEID21]. Dabei ergibt sich insbesondere aus der Überwachung und Automatisierung des Erodierprozesses die Notwendigkeit der

Einbindung in eine vernetzte adaptive Produktion im Kontext von Industrie 4.0. Die Nutzung von Prozessdaten in der Drahtfunkenerosion stellt dabei jedoch eine große Herausforderung für die Entwicklung eines DT dar. Aufgrund der prozessbedingt hohen Datenmenge durch Millionen von einzelnen Entladungen im einstelligen Mikrosekundenbereich und des stochastischen Prozessverhaltens muss zunächst eine valide Datenerfassung und -verarbeitung entwickelt und implementiert werden. Eine anschließende Analyse soll vorhandenes Expertenwissen und bestehende physikalische Modelle mit den Daten verknüpfen, um zum einen neue Erkenntnisse über den Prozess zu generieren und zum anderen ein datengetriebenes System zur Prozessüberwachung und -optimierung zur Verbesserung von Produktivität und Qualität zu realisieren. Dazu ist die Anwendung von Methoden der Künstlichen Intelligenz (KI) ein vielversprechender Ansatz.

Die Leistungsfähigkeit von KI und das Potential komplexe Probleme zu lösen sind in den vergangenen Jahren rasant gestiegen. Spätestens seit der Einführung vom Chatbot ChatGPT der Firma OpenAI hat das ganze Thema KI einen wesentlich praxisnäheren Charakter in der Gesellschaft erhalten [RAY23]. Dabei haben KI-Methoden schon wesentlich länger eine Rolle im Alltag der Menschen eingenommen und auch der Einsatz von KI in produzierenden Unternehmen wird zunehmend größer [JAVA23, PART24, ROCK24]. Die wichtigste Voraussetzung für ein gut funktionierendes KI-Modell ist eine hinreichend große Datenmenge mit hoher Datenqualität, welche anhand unterschiedlicher Faktoren bewertet werden kann, wie in [ASKH13] beschrieben.

Auch wenn schon in vielen Arbeiten die Anwendung von KI-Methoden in der Drahtfunkenerosion behandelt wurde, konnten noch keine validen Modelle entwickelt werden, die auf Basis ausreichend großer Datenmengen trainiert wurden und auch bei veränderten Prozessbedingungen ihre Gültigkeit behalten. Daher wird in dieser Arbeit zunächst ein System entwickelt und implementiert, mit dem sich kontinuierlich physikalische Prozessdaten aufzeichnen lassen. Durch eine Datenverarbeitung in Echtzeit wird ein Speichern der hohen Datenmengen ermöglicht. Dabei wird kontrolliert, dass durch die Reduktion der Datenmenge keine relevanten Informationen verloren gehen, sondern im Gegenteil, die Informationsdichte erhöht wird. In der Praxis werden beim Drahterodieren in der Regel ein Hauptschnitt und ein oder mehrere Nachschnitte nacheinander ausgeführt, um die Genauigkeit und Oberflächenqualität zu erreichen. Da der Hauptschnitt einen erheblichen Einfluss auf die Produktivität und Konturgenauigkeit hat, wird in dieser Arbeit die Hauptschnittbearbeitung untersucht.

Basierend auf den Daten werden KI-Modelle entwickelt, die sowohl quantitative Prognosen bezüglich der Bauteilqualität als auch qualitative Prognosen bezüglich der Prozessperformance ermöglichen. Dies wird in Regressions- und Klassifikationsmodellen unter Anwendung verschiedener KI-Methoden realisiert. Dazu werden die relevanten Input- und Output-Parameter zunächst systematisch identifiziert und bewertet. Nachfolgend werden unter definierten Prozessbedingungen eine hinreichend hohe Anzahl an Experimenten durchgeführt und Daten erzeugt, um die Modelle zu trainieren und zu testen. Abschließend werden die Erkenntnisse für die Entwicklung eines DT in einem industriellen Umfeld übertragen.

## 2 State of the Art

Increasing use of wire Electrical Discharge Machining (EDM) as an alternative manufacturing process for high-cost products in tool and die as well as aerospace industry require the integration of this technology into a networked production in the context of Industry 4.0. For this purpose, the process must be digitized. The following section therefore examines recent research about digitalization of wire EDM.

First, the fundamentals of EDM are introduced. Second, the wire EDM process variant is detailed and studies dealing with the use of data are presented. In addition to statistical analysis the use of machine learning in wire EDM is focused. Thereto, the fundamentals of machine learning methods are described and use cases in wire EDM are examined. Finally, a conclusion summarizes this chapter, and a research deficit is pointed out.

### 2.1 Fundamentals of Wire EDM

#### *Physical Principles*

Non-mechanical subtractive manufacturing processes are divided substantially into thermal, chemical, and electrochemical erosion based on their removal principle. Electrical discharge machining is a manufacturing process with an essentially thermal operating principle, and is therefore classified as such in DIN 8590 [DIN03, KLOC07]. EDM has established itself as one of the key technologies, especially in the machining of high-strength materials, compared to conventional manufacturing processes. It is mainly used in tool and die making as well as in the aerospace industry [KLOC13, HENS17, WELL15].

The removal mechanism in EDM is based on the conversion of electrical energy into thermal energy. This principle lays the fundamental advantage of EDM over conventional manufacturing processes. Materials can be machined regardless of their thermo-mechanical properties like hardness or high temperature strength [KLOC07, MAYR16, KUNI05]. The electro-thermal machining process in EDM is only coupled to a minimum electrical conductivity of the materials. According to various investigations the minimum required conductivity is approximately  $\kappa = 10 \text{ S/m}$  [BRAN10, PANT90]. This even enables the processing of ceramic materials that are doped with a conductive phase [OLIV23].

During EDM, the workpiece electrode and tool electrode are immersed in a non-conductive liquid known as the dielectric. An electrical potential difference, generated by a generator, exists between these two electrodes, which are not in direct contact. They are separated by the working gap, filled with the dielectric, which surrounds both electrodes and serves to electrically insulate them from each other [MOEL10]. Various liquids such as deionized water, aqueous solutions, organic solutions, or hydrocarbon-based dielectrics are suitable for EDM [HO03, KLIN14, KLOC07, KUNI05].

The electrical discharge generates a localized, high-energy plasma channel. This is achieved by ionizing the working gap until the dielectric strength is exceeded. Dielectric

strength denotes the maximum electric field a material can withstand without experiencing a decline in insulating efficacy within its volume. The voltage that leads to an electrical breakdown is also called breakdown voltage. The corresponding field strength is defined as the breakdown field strength, which in turn is often referred to as the dielectric strength [HOFM13]. While researching the exact physical phenomenon of the discharge process, different explanations arose based on the literature but has not been conclusively clarified yet [BERO93, HOCK67, WATS85]. However, there is an agreement that the electrical discharge mechanism occurs in three different phases which are defined as “plasma channel formation”, “discharge phase” and “end of pulse” [KLOC07].

During the process, discharges lead to material removal of both surfaces. However, EDM is still economical because of the different rates of material removal on the electrodes, resulting from the different distribution of the discharge energies [HENS84, SCHN21]. Since the removal rate of a single discharge is very small, the discharge process is repeated at a high frequency up to millions of discharges per second, so the geometry of the tool electrode is reproduced in the workpiece electrode. This creates a surface characterized by craters, which determine the quality of the surface in addition to the shape accuracy due to the volume removed [KLIN17].

### ***Wire Electrical Discharge Machining***

Various configurations for the EDM process have been innovated to effectively manage the machining of hard materials featuring complex geometries and precise tolerances [VDI94]. One of these is sinking EDM finding extensive application in the tool and die making industry and turbomachinery manufacturing, particularly with the use of high-strength materials such as tool steels, nickel-based alloys, and titanium alloys [HOLS18, KLOC07, KUNI05].

Another configuration is wire EDM with material removal mechanism very similar to that of sinking EDM. Both processes involve the removal effect produced by electrical discharges. In wire EDM, a wire is used as an electrode and ever since the commercial introduction in the early 1970s, the achievable machining speeds and surface qualities have rapidly increased [YAN96]. The high degree of flexibility offered by the possibility of relative movement between the tool and the workpiece means that prisms and apertures of any cylindrical or conical shape can be produced with maximum precision using this process variant [KLOC07].

As a result, wire EDM is an alternative manufacturing process that is often used for high-value products. As the demand for materials with high thermo-mechanical strength grows, wire EDM is increasingly being used in a wide range of applications, such as tool and die making and the aerospace industry. The manufacturing share in the tool and die industry has already increased to nearly 25% in 2017 [BOOS18]. In addition, an increasing number of studies show the potential of using wire EDM to produce fir tree slots in turbine disks. The basic technological feasibility showed that wire EDM can meet the requirements for fir tree slots [WELL15, BERG20d]. A comparison of different machining technologies showed the technological and economic

advantages of wire EDM [HEID21, KÜPP22a]. In addition, special variants such as wire EDM turning [BERG20a, QU02, WEIN12, WEIN13] are becoming important and are used not only for machining rotationally symmetrical components but are also increasingly applied for dressing grinding wheels [KLIN09].

Ensuring good gap conditions is key for a productive and precise process, hence the dielectric fluid is continuously fed to the machining zone [KLOC07, KUNI05]. However, wire EDM processes are commonly carried out on workpieces that are totally submerged in the dielectric fluid. This method promotes process temperature stabilization. Moreover, it also improves flushing, especially in cases where the workpiece has varying thicknesses [HO03]. The flushing is of the utmost importance for the process performance evaluation. On the one hand, the removal of debris and decontamination of the working gap ensures optimal conditions for igniting discharges. Worsened flushing can lead to poor removal of debris resulting in short circuits, a local accumulation of discharges and finally to a wire break. On the other hand, it can lead to wire vibrations and wire lag caused by wire deflection. For this reason, many studies have dealt with flushing both experimentally and simulatively [BERG18a, EBIS18, FUJI12, IWA120, KIMU22, OKAD15, OKAD09].

Figure 2.1 shows a schematic of a wire EDM machine. The workpiece is securely held in place on the machine bench using an appropriate clamping system to prevent any slippage during the machining process. The fresh roll of wire is in the wire storage compartment. From there, it is fed through wire guides, through the upper nozzle and to the workpiece. From the workpiece, the used wire passes through the lower nozzle and wire guides to a separate wire storage. The upper and lower wire guides can be moved relative to each other. The lower wire guide can be moved along the illustrated x- and y-axes and the upper wire guide can be moved along the u- and v-axes. This feature allows the guides to achieve a wide range of contours, resulting in a high degree of process flexibility. In addition, the upper guide can be moved along the z-axis, making it possible to process workpieces with different heights while ensuring good flushing conditions [KLOC07].

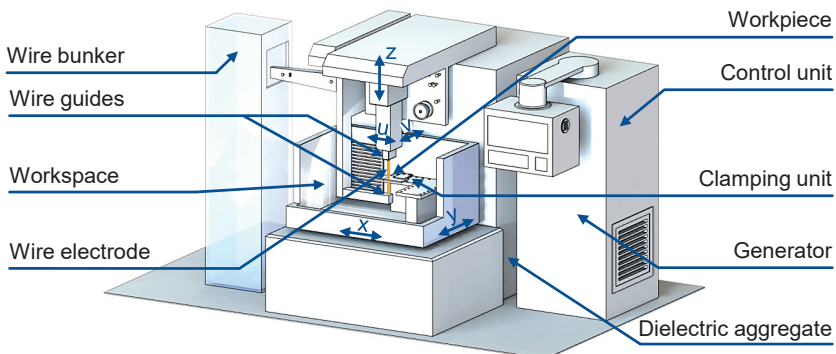


Figure 2.1: Schematic of a wire EDM machine according to [HENS17]



In wire EDM, two primary dielectric groups are utilized: deionized water and hydrocarbon-based (CH-based) dielectrics. CH-based dielectrics allow low discharge energies, improving surface quality, but are less common in high productivity scenarios. Deionized water is predominantly used due to its cooling and flushing capabilities, enabling higher cutting rates, despite residual conductivity leading to corrosion and larger working gaps. Dielectric units supply the working gap, equipped with pumps, filters, and ion exchangers to maintain electrical conductivity and cool the water [KLOC07, OLIV23].

The choice of wire electrode significantly influences productivity and machining outcomes. Initially, copper wires were used, but brass electrodes (CuZn37) proved more efficient due to lower conductivity, leading to faster plasma channel formation [HENS84]. The presence of zinc components in brass electrodes promotes oxide layer formation, preventing particle adhesion on the workpiece surface. Wires with a copper core and zinc-rich cover layer are now common, combining copper's conductivity with zinc's ignition properties [HENS17, KLOC07, WELL15]. Quantitative analysis by Welschhof et al. [WELS22] of discharge energy and removal volume for various wire electrodes reveals that coated wires yield significantly higher energy-specific removal. However, the small cross-section of wire electrodes limits their thermal and mechanical strength.

The increase of the cutting rate by using coated wires has been shown in several studies [KUNI05, SCHA04, WELL15]. In addition to the core material and coating, the diameter of the wire electrode has a significant impact on the process [SCHA04, WELL15]. Coatings and the wire diameter influence electrical resistance and thus the gap contamination. Hada et al. [HADA13] investigated the impedances of the wire and the workpiece using electromagnetic field analysis. It was discovered that the resistance is more dominant than the reactance in the impedance. It was also shown that the total resistance is mainly determined by the wire resistance. This resistance decreases as the diameter of the wire increases. Reduced resistance allows for higher currents, resulting in higher discharge energy. In addition, a larger diameter allows for greater wear of the wire and creates a larger gap. Furthermore, the expanded shell surface reduces the probability of local accumulation of discharges, which could lead to wire breaks [WANG23]. The limitation of the wire thickness is only determined by the geometry to be produced. To date, there are no validated studies that address with the maximum thickness of wire electrodes.

Currently, only high-performance wires with a maximum diameter of  $d = 0.35$  mm are commonly used in the industry. Küpper et al. [KÜPP21b, KÜPP24] showed that the use of brass and coated wire electrodes with a diameter of  $d = 0.4$  mm not only achieves the highest possible cutting rates, but also reduces the machining costs, considering the wire consumption, without reducing the machined surface quality. These results show the potential for wire electrodes with larger diameters and will be focused on in the future to increase the productivity.

Evaluation of main cut's quality can be achieved by considering the curvature of machined gap as geometrical feature, see Figure 2.2 [SIEG94]. The extent of these quality

characteristics depends on the discharge and flushing conditions as well as the wire properties such as material, diameter and pre-tension. These factors interact strongly with each other, so a worsened flushing can lead to an accumulation of discharges or wire lag that all result in a produced curvature [KLOC07, PURI03]. The causes and effects of different forces acting on the wire throughout the process and finally leading to wire lag have been discussed in many studies, e.g. [CHEN15, COND16, COND18a, DEKE89, MURP00, OBAR95, OKAD15, TOMU09].

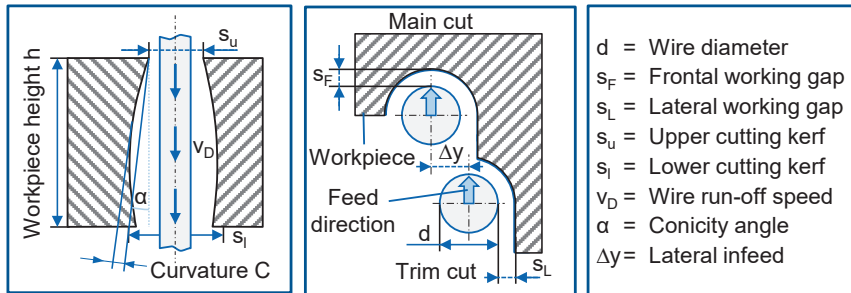


Figure 2.2: Geometrical dimensions of the working gap in wire EDM [KLOC07]

### Electrical Process Parameters in Wire EDM

As the production conditions in EDM are influenced by many different factors (temperature, machine design, material thickness...), the process must be specifically designed for different conditions. Therefore, manufacturers of modern wire EDM machines offer standard machining technologies, which are adapted to different basic conditions such as workpiece height and material, but also to the desired surface quality. The machining parameters adapted for an individual process are summarized by the term "machining technology" [KLOC07].

An optimal EDM process requires the selection of an appropriate set of machining parameters. Among these parameters, some of the most important parameters for identification and evaluation are described in Figure 2.3 according to [KLOC07]. Two successive discharge pulses are shown schematically. As pulse generator initiates a first pulse, the voltage then rises abruptly and remains constant throughout the so-called ignition delay time  $t_d$ . The voltage drops again suddenly as soon as the current begins to flow through the plasma channel. The current then rises steadily and the electrical discharge takes place [KLOC07].

The discharge duration  $t_e$  is the time during which the current flows through the working gap after breakdown. The so-called pulse duration  $t_i$  is the duration of the voltage pulses supplied to the working gap. It is the sum of the ignition delay time  $t_d$  and the discharge duration  $t_e$  [KLOC07].

The current flow ends as soon as the plasma channel breaks down. At the same time, the voltage drops back to its initial level. Before the next discharge is initiated, the working gap needs to be deionized as well be flushed of debris from the previous

discharge. The time during which this occurs, is called pulse interval time  $t_0$  and it is defined as the time between two successive voltage pulses. Therefore, one complete cycle is composed of one pulse  $t_i$  and a pulse interval time  $t_0$ . This duration is called the pulse cycle time  $t_p$  [KLOC07].

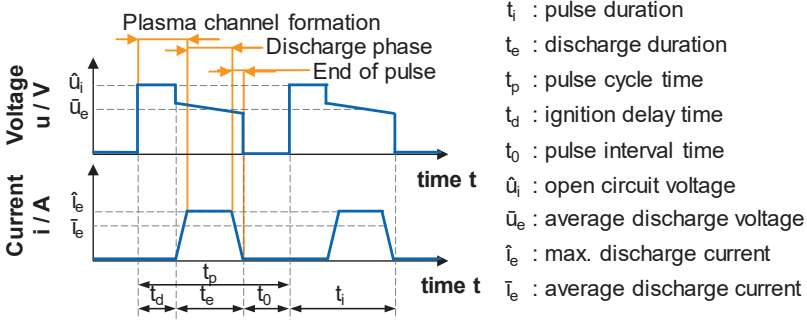


Figure 2.3: Schematic current and voltage curves in EDM [KLOC07]

For the classification of the periodic sequence of discharge pulses, further process relevant parameters are defined [KLOC07]. These parameters include the pulse frequency  $f_p$ , the effective pulse frequency  $f_e$  and the frequency ratio  $\lambda$ . The pulse frequency describes the number of voltage pulses built up per unit time. A typical EDM process consists of a mixture of normal discharges and so-called abnormal discharges. These abnormal discharges will be discussed in more detail in the following. In contrast to the pulse frequency  $f_p$ , the effective pulse frequency  $f_e$  considers only the number of ignited discharges occurring per unit time. The relationship between the effective pulse frequency and the pulse frequency is called the frequency ratio  $\lambda$  [KLOC07].

Of course, the characteristics of a discharge are determined not only by its duration but also by the corresponding current and voltage values during the discharge. These electrical parameters are differentiated between maximum and averaged values, as they are highly time dependent. During the plasma channel formation phase, the maximum attained voltage is called the open circuit voltage  $\hat{u}_i$ . This open circuit voltage supplied by the generator can directly be preset. Among others, this parameter is responsible for the gap width at which discharges are ignited. After the ignition of the discharge, the maximum discharge voltage  $\hat{u}_e$  occurs. However, this voltage drops throughout the discharge and hence the arithmetic average discharge voltage  $\bar{u}_e$  is often used [KLOC07].

As opposed to the course of the voltage, the current reaches its highest value at the beginning of the discharge phase. This value is characterized as the maximum discharge current  $\hat{i}_e$  and is limited by the performance of the generator. Analogous to the average discharge voltage, the discharge current rises and falls during the discharge, thereto the average discharge current  $\bar{i}_e$  is defined. The discharge energy  $W_e$ , supplied by the electric energy to the working gap during a discharge, can be obtained from the time integral of the discharge current and voltage or as a first approximation as the

product of the discharge duration and average electrical parameters. The material removal per discharge and the resulting surface modification are thus linked to the discharge energy which is defined as follows [KLOC07]:

$$W_e = \int_{t_e} u_e(t) \cdot i_e(t) dt \approx \bar{u}_e \cdot \bar{i}_e \cdot t_e \quad (2.1)$$

The discharge energy was taken into consideration for many investigations. A high discharge energy also generates a high removal volume, but also results in a high heat input into the workpiece [LUO95]. This depends on many factors such as the workpiece material [LIAO04b, LIAO04a]. However, the individual discharge parameters can also produce different results with the same energy [MARA20].

The feed rate is the relative velocity between the workpiece and the wire electrode in the cutting direction. By the product of the feed rate  $v_f$  and the workpiece height  $h$  the cutting rate  $V_w$  can be obtained, which is another important parameter as an assessment characteristic for the removal efficiency. It is calculated as follows [KLOC07]:

$$V_w = v_f \cdot h \quad (2.2)$$

It is controlled by the feed control system for accurately following the wire movement to accommodate material removal, wear and gap conditions. Its primary goal is to prevent short circuits, incorrect discharges, or open-circuit pulses. The ignition delay time  $t_d$ , proportional to the working gap, serves as the controlled variable. This parameter is determined either through voltage curve analysis using comparators or by evaluating changes in voltage and current.

The aforementioned process parameters result from a large number of factors influencing the EDM process which can be classified in groups according to [KLOC07] considering the workpiece and tool characteristics, the generator and machine as well as the environment. The generator is a crucial component of wire EDM machines, responsible for supplying electrical energy with the required waveform for the machining process [GINZ02, KUNI05]. Generators significantly impact both the quality of the final products and the productivity of the machining operation. Two main types of generators exist: relaxation and pulse generators. Among these, the pulse generator has gained widespread acceptance over the relaxation generator due to its advantages. Pulse generators allow for pre-setting of essential electrical pulse parameters. This wide range of setting parameters enables the realization of various machining tasks, contributing to the versatility and efficiency of wire EDM operations [KLOC07, KUNI05].

The control system is a key part of the wire EDM process, continuously monitoring and adjusting process parameters to match conditions within the working gap. This capability facilitates unattended multi-shift machining of workpieces [KLOC07]. Two main control systems are distinguished based on process parameters: iso-frequency and iso-energetic pulse control. The iso-frequency system maintains constant pulse duration  $t_i$  and pulse interval time  $t_o$ , whereas the iso-energetic system keeps discharge duration  $t_e$  and pulse interval time  $t_o$  constant [KLOC07]. Additionally, the machine control system allows for the implementation of various process modifications aimed at

achieving different machining objectives. These objectives include high-speed cutting, fine cutting, and conical cutting. During high-speed cutting, technologies are utilized to achieve high cutting rates, albeit with secondary importance placed on surface quality. This process subjects the wire to high thermal loads due to the transmission of high pulse energies. The main cut or roughing cut and the first trim cut primarily establish desired contours, while a secondary trim cut is employed to enhance surface quality. Achieving maximum surface quality may necessitate multiple trim cuts, with the discharge energy and lateral infeed reduced with each subsequent cut. If conical cuts are made on components, such as in the production of workpieces with conical recesses or clearance angles on cutting tools, a process variant called taper cutting can be used. By overlapping the upper and lower wire guides, taper angles of up to  $\alpha = 30^\circ$  can be achieved [HENS17, KLOC07].

### **Pulse Classification**

Beside process improvements, EDM machine manufacturers and operators still face certain challenges like electromagnetic interferences, wire breaks, geometrical inaccuracies, which till today, are not completely solved. Therefore, the further development of wire EDM machines lies primarily in the improvement of generator technology. For instance, modern generators can achieve pulse durations in the range  $t_p = 50 \text{ ns} - 1000 \text{ ns}$  and this under full control of the pulse shape, hence enabling cutting rates up to  $V_W = 500 \text{ mm}^2/\text{min}$  for the roughing process of steel materials to be attained [KLOC07].

To achieve zero-defect in wire EDM, an online process monitoring system is necessary for the detection and prevention of anomalies. Usually, process parameters like the average discharge current and average discharge voltage are used for monitoring purposes, as the parameters are directly linked to the realized material removal rate, surface roughness and geometrical accuracies [ÇPUN90, DAUW86]. Beside these parameters, the discharge type is also very important.

Discharge pulses can be generated with different shapes and there is no standardized shape that is applied by all machine manufacturers. For example, while modern GFMS machines generate sinusoidal pulses [BERG20d], the machine manufacturer Makino from Japan uses trapezoidal pulse shapes [BERG18b]. Clear advantages and disadvantages of each are not yet known, but Li et al. [LI16] identified differences between rectangular waveform and triangular in their studies. The comparison experiment found that rectangular waveforms excelled in processing speed and cutting efficiency over triangular waveforms, while triangular waveforms produced superior surface quality. Pulse groups of narrow triangular waveforms were effective for achieving both processing speed and surface quality in fine machining. Additionally, employing a dual waveform strategy, utilizing rectangular for rough cutting and triangular for trim cutting, demonstrated favorable processing outcomes according to experimental results.

Klocke et al. [KLOC07] categorized discharge pulses into five groups, as depicted in Figure 2.4, aligning closely with the classification outlined by Kunieda et al. [KUNI05]. These diverse pulse shapes exhibit specific current and voltage characteristics based

on the generator switching pattern. An open circuit pulse occurs when voltage is applied, but the gap between the tool (T) and workpiece (W) is too large or the conductivity of the working medium is insufficient, resulting in no discharge as shown in Figure 2.4 (a). Delayed ignition is comparable to open circuit pulse but with a longer ignition delay time, leading to minimal material removal, see Figure 2.4 (b). Discharge pulse describes ideal material removal when the workpiece and electrode are at an optimum distance, see Figure 2.4 (c). Abnormal discharges occur when the distance between the workpiece and tool is insufficient, as illustrated in Figure 2.4 (d), causing significant tool wear and potential wire break. Short circuit pulses occur when electrical contact is established between the workpiece and tool, causing no material removal but risking mechanical damage to the electrode or machine components, as shown in Figure 2.4 (e). The electrical contact does not necessarily have to be caused by contact between the electrode and the tool but can also be caused by particle bridges. These discharge types are mainly applicable to sinking EDM and represent one method of classifying discharge phenomena [KLOC07].

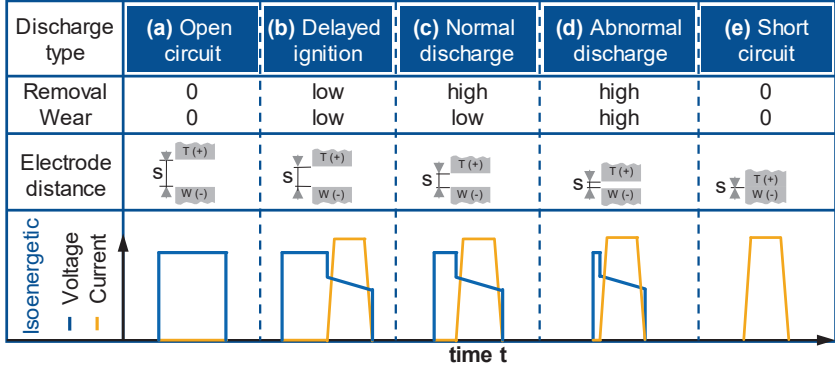


Figure 2.4: Schematic of different discharge types [KLOC07]

However, discharge types have been investigated in various works. Dekeyser et al. [DEKE88] developed a so-called ‘EDM pulse discriminating system’ which detected up to 13 different discharge forms based on the current and voltage signals. Ginzel [GINZ02] presented subdivisions of the discharge forms, some of which differentiate between 15 various types. There is no generally valid definition for different types of discharges in wire EDM. For this reason, a classification of the discharge forms must be specified depending on the generator technology.

2.2 Use of Data in Wire EDM

The use of data has long been applied to optimize EDM processes. Both simulation and process data are used to make correlations or develop models to describe or improve the EDM process. The concept for using data in EDM and the approaches that combine both simulations and process data to develop Digital Twins are presented in [GUO23, HOLS19]. Such Digital Twins in wire EDM by combining physical models and real process data have not been realized yet. However, Digital Twins enable real-time

monitoring and automation of the EDM process. These developments are necessary in order to integrate the process into networked adaptive production in the context of Industry 4.0 [KÜPP22b].

Using simulation data or process data to develop models for process evaluation have different challenges. While simulations are highly complex in terms of their exact physical description, the acquisition and evaluation of process data is a major challenge due to the high frequency process dynamics in EDM. This is also the reason why, on the one hand, most EDM simulations have specific boundary conditions and are not generic. On the other hand, due to discharge frequency, no continuously recorded process data was employed over a longer processing period to apply it for statistical or data-driven models. In this chapter, several studies are presented that deal with the use of process data to optimize EDM, particularly the wire EDM process. By analyzing mainly electrical parameters the EDM process is evaluated regarding its performance and quality. Especially, the correlation of process data with the occurrence of wire breaks, the workpiece quality and optimized machining parameters are focused on. However, the correlation analyses are conducted with process data collected in stationary conditions respectively quasi-stationary conditions and do not consider changing process conditions or longer processing periods.

### ***Using Data to Prevent Wire Break***

Process control and optimization are aimed at either increasing the cutting rate or improving the surface quality, depending on the selection of the setting variables. In particular, the control must ensure the stability of the process. Unstable conditions reduce the removal rate and can lead to wire breaks and thus limit the process productivity, worsening the surface quality of the workpiece and impairing manufacturing accuracy. Most relevant examples can be found in [CABA08b, LIAO97b, RAJU91, RAJU93, SAHA04].

Wire break is the most critical condition in wire EDM, as it leads directly to process interruption. Gamage et al. [GAMA16] analyzed the effects of wire breaks on the process energy utilization in wire EDM. The event can cause a significant energy wastage and the energy consumption is dependent on the machine tool control algorithm's ability to restore machining. An environmental impact study indicates a substantial 48% increase in the impact value of energy usage due to wire failure, emphasizing the importance of wire material despite the primary focus on process energy, ultimately highlighting the adverse effects of wire failures on production economics.

Various reasons for wire break are assumed, which is why many studies have dealt with finding the causes experimentally and through simulation [ARUN01]. The study by Saha et al. [SAHA04] utilizes a spatial heat distribution profile of the wire at any moment, examining points along the wire's trajectory through various heat zones. Employing a finite element model and optimization algorithm, the research concludes that the critical factor leading to wire break is the amount of generated heat.

Wang et al. [WANG23] developed a comprehensive thermal model incorporating latent heat and flushing efficiency through the observation of wire discharges and finite element method simulations. The model facilitated the simulation of wire craters. The heat partition ratio to the wire was determined as 47% through inverse fitting based on simulation and experimental results. In a wire break experiment, it was observed that 34% of discharges leading to break occurred within a 2 mm range, resulting in a minimum remaining wire cross-sectional area of 42% compared to the original wire.

Okada et al. [OKAD15] analyzed the influence of flushing conditions on wire breaks, which represents a typical cause for wire breaks in application. Besides experiments, simulations were conducted to numerically analyze the flow fields and debris residence time in the kerf, hydrodynamic stress distributions acting on the wire and wire deflections.

Fedorov et al. [FEDO18] investigated the impact of the Rehbinder effect, electrical discharge and wire tension on wire breaks. This is the first study considering the Rehbinder effect, which refers to alterations in the mechanical characteristics of solids, such as a reduction in strength or strain values, attributed to a decrease in surface interfacial energy. These changes occur during physicochemical processes at the interface between solids and liquids [TRAS09]. Following the conducted studies, it was established that the Rehbinder effect, tension force, and erosive damage to the wire do not exert a significant influence on its break.

Various factors can lead to wire breaks, but the cause cannot be clearly determined physically. These include the accumulation of discharges, especially short circuits, inefficient particle removal and other stochastic phenomena during the wire EDM process [CABA08b, HAN08a, LIAO97b, OKAD15, WANG23]. Different approaches and parameters were used to prevent wire breaks by analyzing process data. In the following some of the studies are presented.

Kinoshita et al. [KINO82] presented one of the earliest investigations into the detection of wire breaks using electrical signals. Based on their experimental findings, the authors discovered that there is an increase in the pulse frequency immediately before a wire break. Following on from this, they developed a system that recorded the pulse frequency in real time and switched off the power supply when it increased. The process was only continued when the working gap was completely deionized. However, according to recent research, this method is considered critical, as switching off the power supply causes a considerable loss of processing speed [YAN96].

In addition, Dekeyser et al. [DEKE85] found in their research work that the pulse frequency depends on a variety of process influences and is therefore not a reliable factor for evaluating and controlling the stochastic wire EDM process. This finding was confirmed by Rajurkar et al. [RAJU91]. Their method is based on the investigations of Kinoshita et al. [KINO82]. The pulse frequency was also monitored during the series of experiments. However, the pulse interval time was used to control the pulse frequency and thus to induce wire breaks in a targeted manner. No deviation in the frequency at high pulse frequencies before the wire break was determined. As a result,



contrary to the findings of Kinoshita et al. [KINO82], they described the change in pulse frequency as the cause and not as an indicator of a wire break [RAJU91].

Dekeyser et al. [DEKE88] used a different approach to investigate process stability. A system for differentiating pulses was developed with which 13 various forms of discharge could be distinguished. Wire breaks were generated by increasing the discharge frequency. It was shown that certain pulse shapes of the investigated discharges influence a wire break. Watanabe et al. [WATA90] reduced the number of discharge forms in their work to the known forms according to [KUNI05] into normal discharges, abnormal discharges and short circuits. A correlation was found between the discharge forms and the stability of the EDM process.

Since most studies support the theory that a local concentration of discharges in particular causes wire breaks, Shoda et al. [SHOD92] developed an adaptive control system that utilizes online detection of discharge locations to diminish discharge concentration at specific points on the wire electrode, consequently reducing the likelihood of wire break.

Obara et al. [OBAR97] compared three gap detecting signals: the ignition delay time, the discharge voltage and a radio signal as a function of the local position of the discharge in order to detect wire breaks at an early stage. In their results, they were able to demonstrate a decrease in the discharge voltage before wire breaks. In further studies the same authors proposed a new detecting method dividing these signals into groups according to discharge locations. This method clarifies an abnormal gap state just before the wire break [OBAR98].

Rajurkar et al. [RAJU93] conducted research that involved the development of a monitoring system for wire EDM. This system compared discharge frequencies with a database containing experimental evaluations of the thermal load capacities of the wire electrode, alongside corresponding maximum discharge frequencies. An algorithm was employed to assess a control strategy aimed at preventing wire break. However, the direct correlation between discharge frequency, removal rate and the efficiency of the wire EDM process hindered the effectiveness of this approach in facilitating early detection of wire break.

Based on the findings, several fuzzy systems were established. Fuzzy logic is described as a summary of mathematical rules for the representation of knowledge, which is based on the degrees of membership and not on a sharp membership as in classical binary logic. It incorporates fuzzy logic, which allows for imprecision and uncertainty, enabling the system to handle information that is not strictly binary and to better emulate human reasoning in complex and ambiguous situations [STYC17].

Yan and Liao [YAN96] introduced a self-learning fuzzy controller aimed at maintaining the discharge frequency at a safety threshold to prevent wire breaks. Yan et al. [YAN98] conducted investigations on the control of the EDM process by analyzing discharge frequency and the proportion of abnormal discharges. Two types of adaptive control systems were developed, with the first relying on a simple algorithm utilizing a

developed database to control the splitting state. This system, while applicable to various wire EDM scenarios, has limitations in memory capacity and inability to respond to unexpected disturbances. The second type of adaptive control system incorporated digital control technologies, model-based control and fuzzy systems. A novel monitoring and adaptive control system based on fuzzy logic was proposed to optimize the process. By regulating feed rate and discharge frequency, a more stable EDM process with reduced wire break risk was achieved. Different discharge forms, such as normal, arc discharges and short circuit, were detected and variables like the ratio of the discharge types were calculated. These variables were correlated with wire break probability, removal rate and surface quality.

Liao et al. [LIAO97b] observed two phenomena preceding wire break: a sudden increase in discharges lasting between  $t = 50 \text{ ms} - 2 \text{ s}$  and a rise in the proportion of abnormal discharges exceeding 50%, continuing until  $t = 60 \text{ s}$  when the wire breaks [YAN98]. To address these findings, a multivariable fuzzy controller was developed, adjusting feed rate and pulse interval time based on the proportion of abnormal discharges and discharge frequency for optimized wire EDM.

In further studies Yan et al. [YAN99] provided a detailed design of a fuzzy controller specifically for gap voltage control, aiming to enhance productivity and machining stability in the wire EDM process. Liao and Woo [LIAO00] developed a fuzzy logic control system, incorporating an online pulse discriminating and control device, to achieve high cutting speeds and ensure stable machining conditions. Despite the successful application of fuzzy logic control in adaptive wire EDM processes and its versatility across various machining conditions, these systems may encounter challenges in responding appropriately to unexpected disturbances, such as machining a stair-shaped workpiece. This was mainly due to the challenge of recording and analyzing process data at high frequency in real time. This could be realized in the beginning of the 2000s by the further development of measurement technologies and thus also offered new possibilities for using data.

Kwon et al. [KWON06] focused on the implementation and examination of real-time energy monitoring during the transient state of the wire EDM process. Although discharge frequency information has been employed for process control to enhance stability and efficiency, experimental results reveal limitations and inadequacies in this approach. Instead of relying on discharge frequency monitoring, the paper suggests the utilization of a real-time instantaneous energy monitoring system for a more precise interpretation of the wire EDM process state.

Despite all this research, wire breaks remain a challenge even with the most advanced wire EDM machines, particularly when machining components with varying heights, which are common in practice. Although Xu et al. [XU10] have presented an approach for an adapted 3D G-code considering workpiece heights, the basis for controlling the continuous process with changing process conditions is still missing.

### ***Process Monitoring with Continuously Recorded Data***

Lee et al. [LEE07] proposed a control system aimed at enhancing the efficiency of wire EDM processes when machining workpieces with varying thicknesses. It utilizes the abnormal ratio  $R_{ab}$  as a controlled variable, allowing temporary reduction during changes in cutting thickness. A gain self-tuning fuzzy control algorithm ensures stability and suppresses transient conditions. A grey predictor compensates for time-delayed  $R_{ab}$  caused by data processing. Experimental results show that optimizing  $R_{ab}$  can significantly improve cutting speed.

Cabanes et al. [CABA08b] investigated the possibility of online detection of unstable process states and wire breaks with higher frequencies for longer measure times. First, an acquisition system was developed that measures and records the current and voltage signals in real time. Subsequently, test conditions were defined with which stable and unstable process states can be set. A stable process is ensured by performing a straight cut under the standard settings of the machining technology. Unstable conditions are created by poor flushing conditions, machining complex geometries and varying the unloading frequency. Next the most important parameters were selected on the findings. In preliminary investigations, it was found that the discharge energy increases sharply before wire breaks. In addition, there are strong fluctuations and an increase in the maximum discharge current and the ignition delay time. Reference values for the parameters were initially defined for the further course of the investigations. These were chosen depending on the process parameters of stable machining. After selecting a suitable sampling rate, heuristic rules for predicting wire breaks are formulated. The rules are not described in detail here. With this system, wire breaks can be detected up to  $t = 500$  ms before they occur.

In a similar way, a system was developed that characterizes wire breaks using the discharge energy, the maximum discharge current and the proportions of abnormal discharges and short circuits [CABA08a]. To bring the EDM process to an unstable state, the flushing conditions are also worsened here, or the discharge frequency is increased. The process parameters are also investigated when both operations are carried out simultaneously. In addition, different workpiece heights are examined. The process behavior before wire breaks was analyzed using an algorithm that reflects the proportions of over- or underruns of the individual reference process parameters.

The methods of Portillo et al. [PORT07, PORT09] can be regarded as more advanced approaches. The authors developed a virtual measuring system that was able to sample current and voltage signals with a frequency of up to  $f = 10$  MHz. In addition to the maximum discharge current, the discharge energy and the ignition delay time, non-electrical indicators such as the workpiece height and the influence of flushing were investigated. Based on this, a three-stage alarm system was developed that evaluated the process in real time, classified it into one of the three stages and then controlled it accordingly. The three levels represented the risk of wire break. The study conducted tests involving wire break and wire stability. Wire stability tests established a reference value, while tests with wire break determined critical parameter values. Tests were

performed at workpiece heights of 50 mm and 100 mm, with results stored in a database. When a parameter deviated from its reference value, the diagnostic system triggered alarms based on wire break risk. Depending on alarm level and critical parameters, one of four algorithms initiated predefined countermeasures.

Schwade conducted an automated signal analysis in sinking as well as in wire EDM to optimize the machining technology for machining magnesium in medical applications [SCHW17]. In addition to examining the impact of individual electrical variables on process performance, the distribution of different discharge types was also taken into account in this study.

Even though the study conducted by Caggiano et al. [CAGG20] focuses on die sinking EDM, it illustrates the utilization of continuously recorded data for process monitoring through signal processing and statistical analysis. The research involved real-time acquisition of data related to eight distinct process parameters, encompassing variables such as the frontal working gap, average discharge voltage, pulse frequency considering various discharge types and more. The parameters were observed under both optimal and suboptimal machining conditions. The acquired process signals are segmented based on the frontal working gap, recognized as the most representative signal of EDM progression, to retain pertinent information. Each segment corresponding to a single slot undergoes statistical feature extraction, including mean value, variance, skewness, and kurtosis. This results in a dataset comprising 28 features, representing the four statistical parameters for each of the seven additional acquired signals. An anomaly detection approach is employed, utilizing machining data under standard conditions as the training set. Subsequently, the system is tested using a dataset of induced degraded machining signals, employing the Six Sigma approach. This approach involves calculating the mean value  $\mu$  and standard deviation  $\sigma$  during the training phase, and a range of six sigma is established to identify anomalies – any data point falling outside this range is flagged as anomalous. The authors assert that their methodology yields excellent results in anomaly detection based on this comprehensive approach.

Abhilash et al. [ABHI21b] addressed a similar approach using electrical process data through measuring the current and voltage signals. The discharge energies, pulse frequency and the pulse proportion considering the pulse classification were extracted from the recorded data to evaluate the process and forecast unstable scenarios. Furthermore, this evaluation is supposed to be used for an adaptive control and adjust these input parameters. In total 36 different setups with four input parameters were varied for the experiments. Since the setup is not able to record the high frequency process data continuously, the results only are representative for constant process conditions and the investigated parameter space.

Boccadoro et al. [BOCC18, BOCC20] presented the basis for using continuously recorded data in wire EDM by implementing a location sensor in an industrial wire EDM machine. By measuring the two currents flowing to the wire through upper and lower feeding path separately, the recording of spatially resolved single discharges could be

realized. A protection system is introduced which ensures that the number of discharges at specific workpiece heights is limited by thresholds. On the one hand, this approach should be able to prevent wire breaks, as a local accumulation of discharges can be detected. On the other hand, a correlation between the discharge distribution along the workpiece height and the component curvature should be able to be identified. However, the investigations do not address the exact frequency at which discharges are continuously recorded. The illustrated values are averaged. Furthermore, no distinction is made between the discharge types during recording, only normal discharges are recorded.

Based on this discharge location tracker, a simulation of the electrode in wire EDM was performed [DICA20]. A real-time numerical integration approach to model the transient behavior of wire thermal dynamics and wear using Finite Element Method (FEM), Finite Differences and Euler numerical methods was conducted. By integrating data on single discharge position and energy obtained from discharge location tracker with the wear model and real-time computations, the method enables realistic modeling and monitoring of wire condition across various part complexities. The simulation yields valuable insights into enhancing process control efficiency and validates the distribution of discharges as an effective indicator for preventing wire break strategies in wire EDM operations [DICA20]. However, the research does not consider the distribution of different discharge types which significantly affects the generated discharge energy. Furthermore, only a strong simplification was considered for modeling the thermal load [BANE93]. The actual energy dissipation required for the temperature profile of the electrode in wire EDM is still not known. Schneider [SCHN21] has so far presented the most extensive work on the energy dissipation in EDM and gained significant new insights. But even with comprehensive investigations in die sinking EDM, he was only able to provide a range for the dissipation of energy in the various areas, which differs greatly depending on various process boundary conditions and assumptions. This once again underlines the challenge of transferring complex simulation models to other boundary conditions.

Conde et al. [COND18a] analyzed the correlation between the produced workpiece curvature due to wire deformation as well as vibration and the distribution of different pulse types. Analysis of discharge patterns reveals correlations between machining accuracy and discharge quality. Results indicate a substantial increase in wire deformation, up to 45%, when cutting circular interpolations with a radius of 0.8 mm compared to straight cuts on similar thickness parts. Additionally, a relationship is established between wire lag and discharge characteristics, indicating a shift in discharge types with increasing radii, thereby impacting machining precision. Similar observations were made by Guo et al. [GUO03] in their simulation and analysis of electrode fluctuations in wire EDM. The findings demonstrate that attaining an optimal equilibrium among discharge energy, discharge frequency, wire tension, and wire span results in a notably more uniform distribution of discharge points across the wire length.

### **Parameter Optimization**

Ahmed et al. [AHME17] addressed common defects like surface lines, surface roughness and a white layer. Approaches are proposed individually for each type. Before machining, selecting optimal process parameter values is recommended and during machining, monitoring conditions to predict and prevent defects are essential. A combined online-offline fuzzy-nets approach for addressing these issues is recommended. Notably, the paper introduces a novel method for preventing surface lines in wire EDM, involving high frequency sensing, a new algorithm for detecting consecutive short circuits, and proactive pulse-off time adjustment through an adaptive fuzzy nets system, as validated experimentally.

A study by Goya et al. [GOYA22] deals with the optimization of a technology under consideration of the cutting speed and the formation of the white surface layer. A methodology was developed that uses Multi-Objective Particle Swarm Optimization (MOPSO) [SHAM22, WANG18b] to adapt the technology parameters for machining an AZ31 alloy.

Besides there are several studies using Single Objective Taguchi Methods and Multi-Objective Optimization Methods to correlate process parameters with the process performance. For example, by applying these statistical methods optimized machining setting parameters might be identified to produce an aimed surface roughness and kerf width [DURA13, LODH14]. Other works also included the prediction of material removal and considered chemical compositions of materials as an influence parameter [THAN19, UGRA15].

In conclusion, the use of process data in wire EDM is able to identify clear correlations between process parameters and the process performance. Therefore, analysis of process data can be exploited for process monitoring, development, and optimization. It was even possible to implement process control based on these correlations, but this was grounded on heuristic and empirical models. The further development of wire EDM machines, particularly the generators, means that even shorter pulses can be ignited and controlled. As a result, process is even more dynamic at higher discharge frequencies, which, due to its stochastic nature, can no longer be described with sufficient accuracy by evaluating process data using only statistical methods. Especially, the use of continuously recorded process data to consider process changes during machining results in large amounts of data and requires advanced analysis methods.

## **2.3 Machine Learning Methods**

Nowadays the modern manufacturing technologies are facing great challenges because of the increasing demands of productivity and quality. To meet these increasing demands, data collection, monitoring and analysis tasks play an increasingly important role in the machining process. This would inevitably lead to continuous generation of huge amounts of data. The system should be able to react fast to the input data and learn useful information from it, as the data stream is usually too large to be cached for later analysis and the raw data needs processing to become useful information. This

processing of large amounts of data is nowadays usually done with the help of Artificial Intelligence (AI) [FRAU18].

Although AI has been applied for years, there is still not a unified definition of it. But it is generally agreed that AI is the ability of digital computers to solve tasks normally associated with higher intellectual processing abilities of humans or to be developed to do things at which, at this moment, people are better. For example, monitoring large amounts of data, finding patterns and new insights, predicting and interpreting unstructured data as well as interacting with the physical environment. In recent years, artificial intelligence has developed more in the direction of machine learning, since humans are still far superior to computers in terms of learning ability, a particular strength of human intelligence which enables people to adapt to the most varied environmental conditions and to change our behavior accordingly. So according to the definition, machine learning is a central sub-area of AI [ERTE16].

In general, machine learning encompasses methods that are to recognize relationships in existing data sets using learning processes and make predictions basing on the patterns [MURP12]. The approach of Mitchell is often used, the basic concept of the machine learning process as “a computer program is said to learn from experience  $E$  with respect to some class of tasks  $T$  and performance measure  $P$ , if its performance at tasks in  $T$ , as measured by  $P$ , improves with experience  $E$ ”. To put it more simply: the ability of a machine or software to learn to do certain tasks is trained based on experiences respectively data [MITC13]. For this purpose, machine learning methods can mainly be divided into two different types. They are displayed in Figure 2.5 and explained in detail in the following [BADI20, BISH06, MURP12, RICH19].

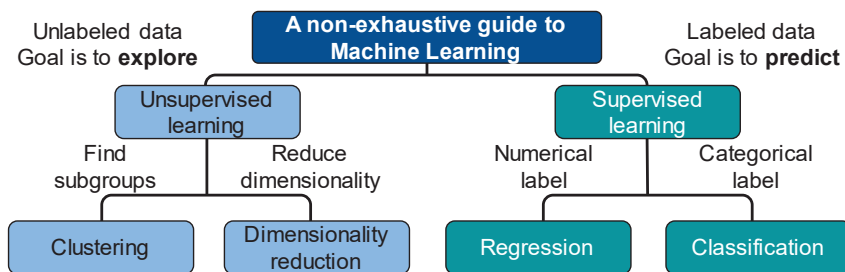


Figure 2.5: Overview of main machine learning (ML) algorithms according to [BADI20]

### Unsupervised Machine Learning

Unsupervised machine learning algorithms use a set of unlabeled data. The algorithm detects hidden structures and patterns within the data set without a result being defined in advance. A method variant of unsupervised learning is the principal component analysis. This variant enables a reduction of the attributes. Linear combinations are used to combine existing attributes into new attributes known as principal components. The group of anomaly detection also belongs to the unsupervised machine learning

methods. This variant makes it possible to recognize outliers within the data records [AUST21, BADI20, BISH06].

Another method variant of unsupervised learning is the cluster analysis. It is a frequently used example of unsupervised learning. The data is automatically divided into groups with similar characteristics. The individual clusters are only interpreted afterwards by the user. This procedure can be used to discover hidden correlations within large data packages [AUST21, BUXM21, FROC21].

However, clustering analysis is usually accompanied with three main challenges, which are first defining a unit to measure the similarity and hence judge the closeness or relatedness between different elements; second applying an efficient algorithm to discover and group these similar elements in clusters in an unsupervised manner and third derive descriptions that can characterize the elements of a cluster in a precise and concise manner [AHMA07, LARO14, WARR05]. Clustering is the most frequently used unsupervised ML algorithm and is also employed in exploratory data analysis to find similar entities or hidden patterns. Generally, clustering algorithms try to group data points in clusters that are as different as possible from one another while keeping intra-cluster data points as similar as possible [BISH06].

In clustering tasks, unlike classification tasks where the number of classes is known, determining the appropriate number of clusters is challenging and crucial for evaluating clustering algorithms [JIAW12, LIU11]. The number of clusters not only influences algorithmic choices but also affects the granularity and accuracy of cluster analysis. This hyperparameter balances compressibility and accuracy, where compressibility is maximized by considering the entire dataset as one cluster, while accuracy improves when each data point is treated as a separate cluster. However, the latter approach lacks data aggregation. Effective methods for determining the optimal number of clusters and evaluating cluster quality are the Elbow Method and more commonly used the *F1-score* [JIAW12, LIPT14].

### ***Supervised Machine Learning***

In supervised machine learning, correlations between input data  $X$  and one or more resulting target variables  $Y$  are examined. These target variables can be a numeric value or a class. Ideally, the relationship can be represented by a function  $Y = f^*(X)$  with  $f^*: X \rightarrow Y$ . For this purpose,  $n \in \mathbb{N}$  data with information about the input parameters and the associated target variables  $Y$  are collected. This data set can be used to train a model that can identify the relationships between the input parameters and the resulting target variables. A key challenge in model selection is that minimizing empirical risk does not guarantee generalizability, and the expected risk of an estimate is not directly accessible. One solution is to use a second dataset with known target values, called a validation dataset. The idea is to ensure generalizability by using data for validation or testing that has not yet been processed by the algorithm. This approach helps to detect and avoid overfitting. It should be noted that validation and test data differ in their function and have a different meaning in the field of data science than in classical engineering.



The data sets are defined as follows according to [PLAU21]. The *training data set* is a sample of pre-classified or pre-evaluated training examples, on the basis of which a machine learning process determines the parameters of a model (by minimizing the training error). The *validation data set* is a sample of pre-classified or pre-assessed test examples used for model selection: The test error is estimated using this data set to determine the optimal hyperparameters. The *test data set* is a sample of test examples, which are also used to estimate the test error in order to assess the quality of the final classifier or the regression model [PLAU21].

A typical workflow for implementing and testing a supervised learning method is done in four steps according to [PLAU21]. First, the entire dataset is partitioned, usually through random selection, into a training set, a validation set, and a test set. A common split is 70% for training and 15% each for validation and test sets. Second, model parameters are determined for a selection of hyperparameters. Hyperparameter selection can be done manually (grid search) or randomly (random search). Third, for each set of hyperparameters, the average loss is calculated using the validation set. Additional metrics may be used for evaluation. In practice, factors like processing speed and memory requirements can also be important. Finally, the model or hyperparameters that perform best in the validation step are selected and finally evaluated using the test set. In practice, the distinction between validation and test sets may not be strict. However, it is crucial that the training set does not overlap with the validation/test set to ensure proper evaluation [PLAU21].

Supervised machine learning is mainly divided into regression and classification. The main difference between these approaches lies in the type of output variable being predicted. Regression deals with predicting continuous numerical values, while classification deals with predicting discrete categories or classes. Both regression and classification are fundamental tasks in supervised learning, where the model learns from labeled data. Artificial Neural Networks represent a common method that can be employed for both different tasks and have gained immense importance in the past 15 years. They can be used where large or enormous amounts of training data are available [BADI20, BISH06, MURP12, PLAU21].

The basic idea behind Artificial Neural Networks (ANN) is based on the way the human brain works. Thus, ANNs consist of nodes and edges that act as a kind of neurons and synapses. The nodes (units) act as processing units and are connected by weighted edges to pass on information. The ANN can be divided into three layers. The first layer consists of the input units. They contain the necessary input data. The information from the input units is passed on to the second layer via edges. This can consist of several layers and forms the inner area of the ANN. This is where the decisive functionality of the ANN is determined. There are no clear rules for the number of hidden layers to be applied and therefore a combination of empirical values and experiments is used as a guide. The number of nodes within the individual layers can also be varied. The output layer forms the conclusion of the ANN. This contains nodes with the corresponding target variables. The general structure of a neural network is depicted in Figure 2.6 [AUST21, MATZ21, MURP12, PLAU21, RICH19, STYC17].

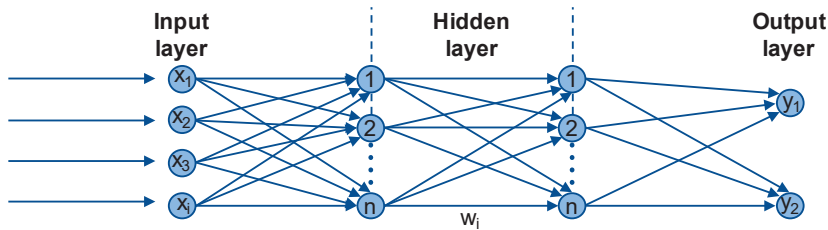


Figure 2.6: Structure of a neural network [MATZ21]

Various problems can be solved with an ANN. If classification problems are dealt with, the ANN has a node in the output layer for each possible class. The output values represent the probability or certainty that the class represented by the node applies. The class with the highest probability value is then assigned to the input data set. In this case, only one intermediate layer is usually required. A typical use case would be the classification of animal photos. Based on the pixels of the photo, the ANN determines the class assignment to the individual animal groups. For problems that have absolute numbers as target values, several intermediate layers are usually used. The result can be taken directly from the nodes of the output layer, which contain an absolute numerical value. For example, an ANN can make predictions about the surface roughness of a manufactured component [AUST21, MATZ21, MURP12, PLAU21, RICH19, STYC17].

In machine learning hyperparameters are configuration settings that are external to the model and cannot be directly learned from the data. But they need to be tuned and optimized to achieve optimal performance of the model [BISH06, MATZ21]. Especially, in hyperparameter optimization, overfitting presents a significant challenge. This phenomenon occurs when a learning algorithm fits the training dataset so precisely that it memorizes noise and idiosyncrasies within the data. Consequently, the performance of the algorithm decreases when tested on an unknown dataset. The amount of data used for the learning process plays a crucial role, with small datasets being more susceptible to overfitting than larger ones. However, even large datasets can be affected by overfitting, despite the complexity of the learning problem. Overfitting diminishes the generalization properties of the model, rendering its performance unreliable when applied to new measurements [GOOD16]. This creates a dilemma, as the goal of optimization algorithms is to find the best solution in parameter space based on a predefined objective function and available data. Underfitting is the opposite of overfitting in machine learning. It occurs when a model fails to capture the variability present in the data adequately [GOOD16]. For instance, if a linear classifier is trained on a dataset that follows a parabolic pattern, the resulting classifier will lack predictive power and fails to accurately represent the training data [JABB14, MURP12]. Solutions can be a different preparation of the data and its quantity, a larger number of training epochs and many other methods to avoid overfitting and underfitting [JABB14]. An epoch is determined by processing all training data during the training of ML models [PLAU21]. The goal is to find a balance where the model performs well on the training data but is

also able to react to new data. Figure 2.7 exemplarily presents schematically the different fits.

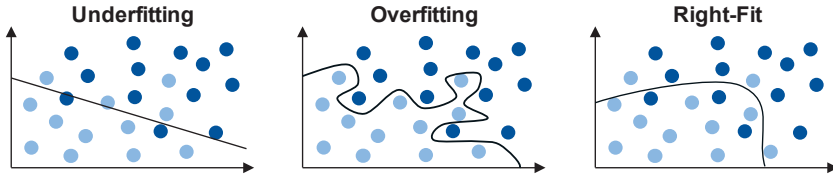


Figure 2.7: Presentation of different model fits according to [FERG22]

However, as the complexity of tasks increases, the limitations of traditional neural networks become apparent. Deep neural networks or deep learning can model a large number of model parameters in the range of  $10^4$  to  $10^{11}$  in order to learn highly individual classifiers and regression functions from training data, while maintaining a high degree of generalizability [PLAU21]. Therefore, deep learning represents a significant evolution in neural network architecture, characterized by the incorporation of multiple hidden layers. Unlike shallow neural networks, which may have one or two hidden layers, deep neural networks can have tens or even hundreds of layers. This depth allows these networks to automatically learn hierarchical features and representations, capturing intricate patterns in the input data. The specific threshold for the number of hidden layers that qualifies a model as "deep" can vary [MURP12]. What's more important than the exact number of layers is the idea that the architecture is deep enough to capture complex patterns and abstractions in the data. It is essential to note that the field of deep learning is dynamic and advancements in architecture and training techniques continue to evolve. Through a process of forward propagation and backpropagation, these networks are trained on large datasets to learn representations of the data that enable them to perform tasks such as classification, regression, clustering, and generative modeling. Deep Learning has demonstrated remarkable success in various domains, including computer vision, natural language processing, speech recognition, and reinforcement learning, often achieving state-of-the-art performance in complex tasks [GOOD16, MURP12, SWAM17].

## 2.4 Machine Learning in Wire EDM

After the use of data in wire EDM has been reviewed and different machine learning models have been presented in detail, the following section provides an overview of the work that has used the machine learning approach in EDM. The potential and the weakness of applying these methods in EDM, especially wire EDM, is highlighted. This is because most of the work in this field of research has two major deficits. Firstly, in most studies only the correlation between the discrete machine setting variables and the process evaluation variables was determined. The number of input parameters for the system and their variation options were kept so low that these relationships can be mapped sufficiently well with statistical models described in Chapter 2.2. Furthermore, the biggest weakness in the presented studies applying machine learning methods in EDM is the insufficient amount of training and test data as well as the data quality.

Data quality can be evaluated by various factors such as completeness, consistency, validity, uniqueness, correctness and actuality [ASKH13]. The typical amount of necessary data is not generated in almost any work to fulfill the required criterion and to develop such models with valid significance. On the contrary, in most cases the hyperparameter optimizations show a classic overfitting of the models, which leads to improbably high prediction accuracies of the models and does not provide a valid statement to the original problem [MURP12]. Finally, the validity of the studies is examined and a general research deficit for the underlying work is discussed.

### ***Using Discretely Recorded Data***

The first studies dealing with the application of machine learning in EDM have already taken place back in the 1990s. In their studies, Tarnq et al. [TARN95] developed a neural network to map the relationship between process parameters and process performance. Similar works were conducted by Spedding et al. [SPED97] to model the correlation between some electrical and mechanical parameters and the surface roughness, waviness as well as the cutting speed. However, only discrete machine settings were used for the model and a low number of training data.

Also, many current studies have enormous data weaknesses, both in terms of their quality and even more so in the quantity of data used. For example, an attempt was made to train a classical ANN model that predicts the surface roughness, the accuracy, the material removal and wire wear on the basis of only 27 test series with four input parameters [GURU17]. Unsurprisingly, overfitting in models with limited data and hyperparameter optimization often results in accuracies approaching 100%, highlighting the lack of data-based validity and technological interpretability in such studies.

The work of Ugrasen et al. [UGRA14] can be mentioned here as another study that leads to unrealistic model accuracies due to a lack of data and overfitting. Even though the use of a neural network for mapping complex content offers a promising solution, the results show the problems in this subject area. The parameters discharge duration, pulse interval time, discharge current and feed rate were used as input parameters to predict the quality and productivity of the wire EDM process. These were each set to four different levels when generating training data. A backpropagation algorithm was used to train the model. With only a few data for training, the surface roughness, the material removal rate and the geometrical deviation could be predicted with an unrealistic accuracy. In further studies, similar models were used to improve the removal rate and surface roughness as well to predict the accuracy and electrode wear e.g.: [BAHL20, CHOU18, MING15, SAHA22a, SAHA22b, SUDH22a, SURY17, ULAS20, THAN19].

Other studies [CHEN10, MAJU15, TARN95] combined the use of ANN with evolutionary algorithms such as Simulated Annealing, Genetic Algorithm (GA) or Particle Swarm Optimization (PSO) to correlate process input parameters and process performance. Simulated annealing and Particle Swarm Optimization differ in their inspiration and approach. Simulated annealing, inspired by metallurgical processes, uses a probabilistic method to explore solutions gradually, accepting suboptimal solutions with decreasing

probability [KIRK83]. In contrast, Particle Swarm Optimization is inspired by social organisms' collective behavior, utilizing particles in a multidimensional space that adjust positions based on individual and swarm experiences. PSO emphasizes cooperation among particles for efficient exploration and convergence [GAD22]. The key distinction lies in their exploration strategies and the mechanisms used for solution refinement.

More complex methods, such as the use of Adaptive Neuro-Fuzzy Inference Systems (ANFIS), have already been applied in some studies [ABHI20a, ÇAYD09, GOYA21, MAHE15, NARE20, SAHA23, SING20]. This system is a hybrid machine learning model that combines fuzzy logic and neural networks. ANFIS aims to adaptively model complex systems by learning from data. Clustering techniques can be used as a pre-processing step or in conjunction with ANFIS in certain scenarios [JANG93].

The studies using the ANFIS approach have different goals. For example, Abhilash et al. [ABHI20a] investigated the correlation between mean gap voltage variation and wire break occurrences. The mean gap voltage variation  $\Delta V_m$  is considered as an indicator of instabilities in the working gap, identified as a primary cause for wire breaks and suboptimal part quality. It is calculated as the difference between servo voltage and mean gap voltage. The experimental design involves only 31 experiments based on a central composite design (CCD) of response surface methodology (RSM), with pulse on time, pulse off time, servo voltage and wire feed rate as input parameters. The ANFIS model demonstrates high accuracy in predicting  $\Delta V_m$ , nevertheless the results must be questioned due to the small amount of data.

Caydas et al. [ÇAYD09] used the approach to predict the surface roughness and the thickness of the white surface layer. For this purpose, they used an ANFIS model, which can be trained very efficiently. The pulse duration, the open-circuit voltage, the dielectric flushing pressure and the wire feed speed were used as input parameters.

Maher et al. [MAHE15] also used the hybrid ANFIS model to make predictions about the effects of varying discharge durations, pulse currents and different wire tensions on the cutting speed, surface roughness and the heat-affected zone. A functional model was also created here. The deviation of the predicted values from the actual measured values is less than 4.2% on average. However, the authors make no attempt to address the interpretability of this result.

Similar approaches to machine learning techniques were conducted by Venkatarao et al. [VENK23] to optimize the development of sustainable production processes and reduce energy consumption. They used a hybrid optimization approach; the so-called Hybrid Teaching and Learning-Based Optimization (HTLBO). This method was developed to perform multi-criteria optimizations. Teaching–Learning-Based Optimization (TLBO) is a nature-inspired optimization and simulates the teaching and learning process in a classroom setting to iteratively improve a population of solutions for an optimization problem. The algorithm designates one solution as the teacher, considered the best, and others as students. During the learning phase, students adjust their positions based on the teacher's influence, aiming to converge towards an optimal solution. TLBO is known for its simplicity and efficiency in solving various optimization

problems across different domains [RAO11]. With this methodology the kerf width (KW), the material removal, the surface roughness as well as the power consumption (PC) were optimized resulting in specific working conditions.

Rahu et al. [RAHU23] used a Particle Swarm Optimization with a regression model based on the TOPSIS method (Technique for Order of Preference by Similarity to Ideal Solution) to find optimal process parameters for machining shape memory alloys. TOPSIS is a multi-criteria decision-making method used to determine the best alternative from a set of options. It evaluates alternatives based on their proximity to an ideal solution while considering multiple criteria [HWAN81, OLSO04]. In the study, a CNN model is employed to classify SEM images based on the material removal rate, utilizing pixel intensity histograms.

Drzajic et al. [DRZA22] developed an integrated autonomous system to execute the responsibilities of a virtual machine tool operator. Bayesian Optimization (BO) employing Gaussian Processes (GP) is applied for model-based adaption [TULL93]. The system's functionalities are showcased across various contexts through case studies involving EDM processes. Multi objective optimization is performed, and prior knowledge of existing optimization session is transferred to a new one to decrease the number of required experiments. This approach really is a methodical way of systematically developing technologies based on knowledge and data. However, the use of machine settings limits the application to the continuous process with unchanging machining conditions.

In other studies, attempts were also made to map the relationship between the machine settings and process performance, but even with the use of such complex methods, the results do not offer any new value compared to empirically and simulatively determined findings, as the quantity and quality of data is not high here either.

In addition to models for predicting quantitative values for cutting rates or surface criteria parameters, there is also the approach of evaluating the process using classifications. Abhilash et al. [ABHI21a] used classification models to indirectly evaluate the wire EDM finishing process. For this purpose, an attempt was made to use surface images to train a model that recognizes micro-defects that can be traced back to similar parameter settings and suggests an optimization of the parameters on this basis to improve the surface. The approach is interesting as it considers the quality after finishing, but the generation of images is associated with an enormous effort and is reflected here by the small number of 27 surface images used.

An equal concept was chosen to map the wire wear and thus predict the wire break [ABHI22b]. Again, a very small data set of only 18 trials with five input parameters was used for training and testing. To predict wire breaks, process signals were employed, and the model was extended by a statistical discharge pulse analysis. However, it offers no added value compared to the work on this topic presented in Chapter 2.2.

Workpiece images as input parameters were also employed to evaluate the process quality, but in sinking EDM [SAEE21]. In this study, deep neural networks were applied

to obtain the surface roughness and defect detection. A deep learning model was developed by using different types of neural networks.

In further investigations, the analysis of the different pulse types was extended by training machine learning-based classification models [ABHI22c]. Different methods such as decision tree, Naive Bayes, Support Vector Machine (SVM), K-Nearest Neighbor, and ANN were used. The ANN showed the highest accuracy of over 98% for classifying pulses into the four discharge types presented: normal, arc, short and open. Same approach was used by Zhang et al. [ZHAN15] for a pulse classification and yielded in similar results. However, the detection of different discharge types can also be realized by a simple signal analysis [BERG18b, OßWA18].

In another research the challenge of optimizing wire EDM process setting parameters is addressed, where manual adjustments failed to achieve optimal conditions [ABHI20b]. An ANN-based classification model to predict process events based on setting variables, classifying events into wire breaks, "sparks absence" (indicating inadequate processing conditions) and normal conditions is introduced. The input variables pulse-on time, pulse-off time, control voltage, and wire feed speed were utilized for classification. The neural network, featuring four input variables and three output categories, incorporated a central structure with 10 hidden layers. Optimal hidden layer determination involved experimenting with layer counts from 1 to 15, adopting the configuration with the best results. Backpropagation model measured quality using the cross-entropy loss function, terminating training after six consecutive iterations without a decrease in the error. Evaluation using a confusion matrix revealed a noteworthy alignment between target classes and algorithmic classification results. However, the work reveals two major weaknesses. Firstly, the basic categorization of the process events, in particular the description of "spark absence", is not comprehensible. Open-circuit pulses lead to slower machining, see Figure 2.4. But on the one hand this is only caused by a disproportionately high frequency and on the other hand this type of characteristic discharge is no longer present in modern wire EDM machines [BERG18b]. The determination of this process condition in the study is not explained. Secondly, this model is limited to a narrow parameter space and the extensibility to other process conditions is not given by the training with discrete parameters.

This work was expanded increasing the quality of data and methods while aiming the same goal [ABHI22c]. First, the total number of experiments was increased up to 108. Second, in addition to machine setting parameters physical process parameters were recorded and used for training. However, only discrete data was recorded here, where, for example, a value for the short circuit ratio is used for a test. This increased the total amount of data, but there is still too little data to generate ANN models with high significance. Secondly, discrete data does not represent the continuous process accurately enough to train machine learning models.

### ***Using Continuously Recorded Process Data***

As the wire EDM process is very slow and experiments are associated with time-consuming processing and slicing, only a small number of experiments is usually carried out. However, a statistically based reduction in the number of experiments using classic Design of Experiments (DOE) or Taguchi methods does not allow machine learning models to be trained with a reduced amount of data. On the contrary, these preliminary considerations are a prerequisite for generating data that is important for the process description under the most relevant process conditions possible. Based on such experiments, however, it is essential for the application of machine learning methods for process evaluation in wire EDM that continuous process data is used. Works that at least used real process data with different quantity for various purposes are presented below.

Huang et al. [HUAN18] conducted a study utilizing real process data and a Support Vector Machine (SVM) approach to determine real-time workpiece height in wire EDM. Preliminary investigations identified suitable input parameters, exploring the influence of various factors on machining states. Changes in machining conditions were observed by altering frequencies and feed rates, with some parameters proving influential. Pulse intervals and programmed feed rates were key factors, forming input parameters for the SVM model. Training data were generated by cutting stepped workpieces of different thicknesses and tests demonstrated the model ability to accurately predict workpiece height, with a maximum deviation of 2 mm.

Liao et al. [LIAO02] also aimed to estimate the workpiece height by using machine learning based on electrical process signals. They divided the discharges into different types, collected and analyzed them. The total discharge frequency, normal discharge and abnormal discharge ratio are used as input parameters for the neural network with an 8-9-2 topology and backpropagation. Utilizing the real-time estimation of the workpiece height, a rule-based approach is suggested for dynamically adjusting parameters. This strategy aims to ensure stable machining conditions and enhance overall machining efficiency. However, a correction approach for the thickness identification coefficient was introduced, aiming to enhance the accuracy of estimating workpiece height [LIAO13]. Experimental findings confirm the feasibility of achieving precise online estimation of workpiece height, with an estimation error below 1 mm and a processing time within one second. It must be considered that determining the workpiece height can also be realized by simple signal analyses and that the accuracy does not offer any advantages over the conventional methods presented in Chapter 2.2.

Portillo et al. [PORT08a, PORT08b] presented a model for interpolating instability trends in wire EDM using an Elman-based Layer Recurrent Neural Network (LRNN). An LRNN is a Recurrent Neural Network architecture that includes an Elman layer. This design, featuring recurrent connections, preserves context information across sequential inputs, making it well-suited for tasks involving temporal dependencies and sequential data processing [DING08]. Various types of degraded behaviors in workpieces of two common thicknesses (50 and 100 mm) were identified. While the



identified degraded behaviors were consistent across the studied workpiece thicknesses, the thresholds for detection varied. Consequently, the study aims to develop a single empirical model capable of detecting process degradation across different workpiece thicknesses. A comparative analysis is conducted to determine the optimal ANN configuration, followed by the implementation of a strategy to detect degraded conditions in different workpiece thicknesses. However, it must be noted that the accuracy of the model depends primarily on how the corresponding unstable states are defined. After all, these are designed heuristically, and the classification is particularly linked to the occurrence of wire breaks. A prediction with the model approx. 50 to 250 ms before a wire break is not yet a significant improvement on previous statistical analyses presented in Chapter 2.2.

Same method was applied by Conde et al. [COND18b] to predict the accuracy of components produced by wire EDM. An algorithm, combining LRNN with Simulated Annealing optimization, corrects deviations in machined parts. The proposed solution significantly reduces average deviation by up to 80% and decreases the Coefficient of Variation (CV) by 43%, especially effective in scenarios with substantial wire deformation. Importantly, the solution is easily implementable on existing wire EDM machines.

Wang et al. [WANG18a] introduced a novel approach to tolerance monitoring using unsupervised machine learning techniques for the manufacture of fir tree slots where component tolerances are subject to stringent requirements. Specifically, k-means and hierarchical clustering were investigated to avoid time-consuming experiments for establishing threshold values of the monitoring variable. The potential use of distribution ionization time was explored through preliminary experiments [WANG19b]. Efficiency in classifying regions based on wire infeed was observed in hierarchical clustering of ignition delay time distribution curves. Additional features extracted from these curves, notably average and kurtosis, demonstrated high Pearson correlation coefficients. Employing k-means with these features exhibited agreement with wire infeed. The proposed technique underwent validation through wire EDM of an actual fir tree slot geometry under industrial conditions. Clustering results (using hierarchical clustering) were compared with deviations measured using a Coordinate Measuring Machine (CMM).

Same authors employed a supervised machine learning approach, specifically a deep neural network, to establish a direct relationship between machining process data and tolerance defects [WANG19a]. They created extensive training datasets by varying machining parameters to produce again fir tree slots. The training data included variations in the lateral working gap (wire infeed) and the corresponding ignition delay times. Data collection involved an online recording application capturing ignition delay times of single discharges at a sample rate of 5 ms. Discharges were labeled based on their ignition delay times and categorized alongside the lateral working gaps. The dataset comprised ignition delay times as input and lateral gap as target parameters. The trained deep neural model demonstrated high accuracy in predicting the lateral gap during machining experiments, considering wire vibration uncertainties. Subsequently,

the model was utilized to predict defects in the first trim cut. Predictions of expected tolerances were compared to actual cut geometry measured using CMM, showing a high correlation. To validate their model, they imposed more stringent tolerance requirements, enabling a comprehensive assessment of component quality. However, this validation process was limited to finishing processes and involved straightforward gap voltage analysis at a low sample rate, focusing on a small number of continuous discharges for effective monitoring.

In another study, deep learning techniques were applied to predict an unexpected event like a change in the machining height for the main cut [SANC18]. The approach showed good results, but only 567 labelled examples for each category were used, which is considerably less than the recommended 5000 for the used technique [GOOD16].

Caggiano et al. [CAGG16] trained a neural network with different structures to figure out the relationship between surface defects or marks and different groups of pulses, average discharge energy, average discharge current pulse, discharge frequency and open circuit ratio as input parameters. Relevant signal features were extracted from the voltage and current signals to construct sensor fusion pattern vectors. This approach was presented in detail by the same authors in [CAGG15]. Based on this the correlation vectors calculated for different time intervals are used to predict quality output, which is 0 or 1 representing if it has lines and defect marks. In the end, it was concluded that the open-circuit ratio does not contribute to the identification of lines and marks.

Finally, several reviews summarize studies dealing with machine learning in EDM which did not reveal any significant new findings or also demand critical interpretations of the presented results [KIM18, GUO23, MOHD07, SUDH22b, WEIC19].

Table 2.1 summarizes the literature review on applying machine learning to wire EDM, considering the critical aspects of the used data and model validity. In most publications the black box approach was applied by using only discrete machine setting parameters (MSP). This approach requires large amount of data with high quality to develop generic models, which are not only applicable under defined machining conditions. It can be concluded that very few publications have briefly dealt with the use of continuously recorded process data including physical knowledge like the electrical process parameters (EPP) or discharge distribution.

Table 2.1: Overview of studies in the field of machine learning in EDM

Used data	Author	ML method	Input parameter	Output parameter	Data quality	Model validity
Discrete process data	[BAHL20] [CHOU18] [GURU17] [MING15] [SAHA22] [SPED97] [SUDH22] [SURY17] [THAN19] [ULAS20] [UGRA14] [TARN95] [CHEN10] [MAJU15]	ANN & SA/GA/PSO	Various Machine Setting Parameter (MSP)	Various productivity and quality parameter ( $v_f$ , MRR, Ra, Wa, WW, ...)	○	○
	[ABHI20b] [CAYD09] [GOYA21] [MAHE15] [NARE20] [SAHA23] [SING20]	ANFIS	Various MSP	Various productivity and quality parameter (Wire break risk, WL, HAZ,...)	○	○
	[VENK23]	HTLBO	5 MSP	KW, MRR, Ra, PC	○	○
	[RAHU23]	TOPSIS	5 MSP	MRR & Ra	○	○
	[DRZA22]	BO & GP	4 MSP	MRR	◐	●
	[ABHI20a] [ABHI21a] [ABHI22a] [ABHI22b] [ABHI22c] [ZHAN15]	Various classification methods	Various MSP	Wire break risk, pulse classification, surface defects	○	◐
Continuous process data	[HUAN18] [LIAO02] [LIAO13]	SVM & ANN	Various EPP	Workpiece height estimation	◐	●
	[PORT08a] [PORT08b] [COND18b]	LRNN	$W_e, i_e$	Wire break risk	○	◐
	[WANG18a] [WANG19a] [SANC18]	Clustering, deep learning	Discharge type ( $t_d$ )	Geom. Deviation, $\Delta h$	◐	●
	[CAGG16]	ANN	EPP	Defects	○	◐
	Good ● Adequate ◐ Weak ○					

## 2.5 Summary and Conclusions

Wire electrical discharge machining (wire EDM) is a pivotal technique employed in the fabrication of intricate geometric features in high-strength materials. The mechanism behind material removal in EDM is primarily attributed to thermal loading induced by electrical discharges. This characteristic allows for manufacturing irrespective of the mechanical strength of the material being machined. The use of new control strategies, new wire electrodes and the design of optimized mechanical parameters, such as wire tension or flushing pressure, has significantly increased the productivity and quality of the process and thus expanded the areas of application of wire EDM in production technology. This was reinforced due to the advancements of machine generators, which allow individual discharges to be controlled with increasing precision.

Extensive research has dealt with the use of data to evaluate the wire EDM process, especially, the occurrence of wire breaks. Nevertheless, even when adaptive rules are utilized, they are designed heuristically. The rules or fuzzy logic are usually based on simplified statistical models, such as empirically determined correlations between process data and process evaluation variables. These models or correlations are limited by the boundary conditions under which they were determined. Due to the high discharge frequencies, the acquisition of continuous process data is a challenging task. A great deal of previous research into process evaluation has focused mainly on the analysis of process data, independently applying statistical methods or machine learning methods. A method or system for recording continuous process data with the latest measurement technology has not yet been implemented. For this reason, previous work has considered process data that could only be recorded over a short period of time. However, these only represent a stationary or quasi-stationary process state.

In the context of Industry 4.0, data-driven models are required and seen as an enabler for monitoring and process development through inherent process signals. Based on the literature review, there is no data-driven model that can evaluate the continuous process based on physical process data recorded in real time and is not limited to constant process conditions.



### 3 Objective and Tasks

In most applications, wire EDM is used as one of the final steps in the process chain, which makes an investigation of monitoring and automation of the process a promising approach to acquire practical improvements which even may allow to generate a report with respect to the machined quality. Using the approach of implementing a Digital Twin, could achieve the integration in a networked adaptive production in the context of Industry 4.0. The use of process data in wire EDM represents a major challenge for the digitalization of the process due to its high frequency and stochastic behavior.

Based on the presented state of the art, it is evident that the utilization of process data in wire EDM is inadequately investigated. The described studies do not consider changing process conditions. Neither the data-driven models are based on physical quantities, nor they were provided with a sufficient amount of high-quality data. A data-driven methodology for process design and process monitoring in industrial application is also not given yet, especially, not for applying the main cut. Since productivity and contour accuracy are largely determined by the main cut [HEID21, KÜPP24, WELL15], this work examines main cut machining.

Therefore, this thesis addresses the need for research through the discussion of the following research hypothesis:

*The process performance and product quality in wire EDM can be evaluated using machine learning methods based on continuously recorded electrical process data.*

The hypothesis is investigated by answering the following research questions:

1. Can the high-frequency process parameters be recorded in a continuous process and reduced to their relevant information?
2. Which evaluation criteria are crucial applying the main cut and how do they correlate with process data?
3. Can a regression model evaluate the produced workpiece quality based on process data for changed process conditions and enable a Digital Twin representing the machined curvature in real time?
4. Can a classification model evaluate the process productivity based on process data for different technology setups?

The aim of this thesis is the development of data-driven models to evaluate the continuous wire EDM process based on physical process parameters. The conceptual approach of the work is illustrated in Figure 3.1. The procedure outlined here roughly covers the most important points for applying machine learning to a defined problem [MATZ21, SWAM17]. The procedure is based on the formulated research questions and is carried out in the following steps considering all important aspects [VIEI20].

A sufficient amount of high-quality has to be ensured by data acquisition and processing of process and product data. Because of the process-related high amount of data due to millions of discharges in the single-digit microsecond range and the

stochastically process behavior in wire EDM, the data acquisition is a challenging step for this process and has not been implemented in other works or industry yet. Therefore, in chapter 4, a data acquisition system is developed to record, and store spatially resolved and characterized single discharges in the continuous process. The data is reduced in two steps without any loss of relevant information to minimize the necessary storage capacity to ensure recording unlimited process data. In the first step, only characteristic discharge parameters are recorded by signal processing of the raw data in real time. Then, based on clustering analysis the maximum time interval is determined to average data without losing relevant information and increase information density. These data can be used to map the spatially resolved process energy.

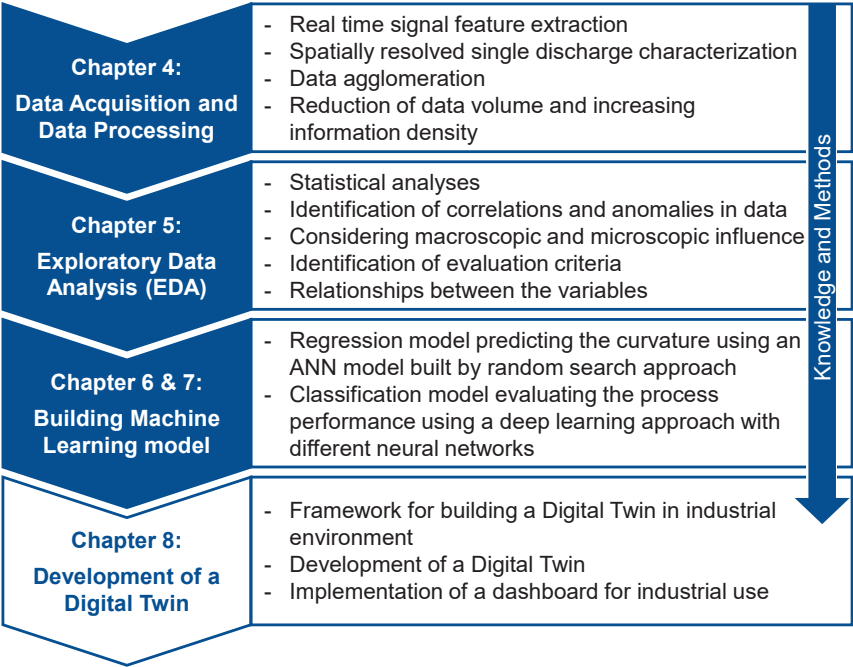


Figure 3.1: Procedure for the development of data-driven models to evaluate the wire EDM process

Exploratory analysis is then used in chapter 5 to identify evaluation parameters for the main cut process and to investigate the first characteristic process parameters. For this purpose, different experimental setups are examined. Different process parameters are analyzed for the evaluation of the productivity regarding the cutting rate and the occurrence of wire breaks. After that the influence of varied process conditions on the produced workpiece quality considering macroscopic as well as microscopic changes is investigated. Here the relevance of quality evaluation criteria is determined.

In Chapter 6, a regression model is developed to predict quantitatively the produced geometrical deviation based on only electrical process data. For this purpose, process

influence parameters are categorized causing geometrical deviation in form of workpiece curvature. After the data generation under defined process conditions, the data is processed and various input parameters for the machine learning models are identified by feature engineering. For the regression model neural networks are used and the model architecture is determined. Next the data is split into training, validation, and test data sets. Finally, the model is trained and tested with different data sets to evaluate the model performance.

In chapter 7, a classification model is built to differentiate between varied machine parameter setups based on process data and categorize them into defined productivity level. Here a deep learning approach is applied for which feature engineering is not needed. Building sub models, the different aspects affecting the productivity are classified considering speed, stability, and part quality. For this purpose, many technology variants are examined with changing machine setting parameters. The model architecture is built based on data sets with similar process conditions, here with the same workpiece height and changing machine setting parameters. To evaluate the transferability of the models, the testing is conducted with strongly changed process conditions such as changed workpiece height.

Finally, this thesis demonstrates how this approach, and the results can be utilized in an industrial environment. Thereto, the recorded and pre-processed data is streamed to a cloud of an AI software provider to analyze it with advanced machine learning techniques. The results then are transferred to a digitized manufacturing dashboard of an end user using the wire EDM machine.





## 4 Data Acquisition and Processing in Wire EDM

In the first part of this chapter, a short description of the used hardware and software for the experiments is presented, including the technical description of the devices. Once the problem has been defined, it is necessary to collect high quality data in order to develop a machine learning model. For this purpose, different measurement methodologies are described for the acquisition of specific discharge energies and electrical signals in the continuous wire EDM process. A methodology for the detection of spatially resolved process parameters is explained and validated. Finally, it is demonstrated that the agglomeration of data ensures no loss of information in the data processing step. For all experiments, a standard steel technology regarding to specific machining workpiece height was applied using the  $d = 0.25$  mm brass wire bercocut pro 900 by bedra [BERK24a]. Unless otherwise described, a workpiece height of  $h = 40$  mm was always used.

### 4.1 Offline Measurement of Single Discharge Energies

In the course of this work, all experiments were performed on a wire EDM machine from Makino. The U6 H.E.A.T. series machine, shown in Figure 4.1, offers a compromise between a high machining speed and a high manufacturing quality of the machined workpieces, while at the same time keeping wire consumption low. Due to the achievable high flushing pressure, it is possible to perform very short cycle times during roughing. Deionized water is used as working medium [MAKI24].


	Electrical parameters	
	Discharge current setting levels	35
	Discharge duration setting levels	200
	Open circuit voltage setting levels	60
	Pulse interval time setting levels	200
Accuracy		
Positioning accuracy / $\mu\text{m}$		1.5
Repeatability / $\mu\text{m}$		1.0

Figure 4.1: Makino U.6 H.E.A.T. and technical data [MAKI23a]

The isoenergetic pulse control generator of the machine supplies a constant energy per discharge type. This energy is mainly specified by the machining technology. While the machining technology parameters are stipulated by the machine manufacturer, these values are confidential, as they are considered core competencies. However, the energy values for the different technologies per discharge type can be computed from the electrical signals of the discharges using equation (2.1). To determine the energy per discharge, an offline measurement setup was examined, and a signal analysis was conducted [BERG18b].

High-frequency measurement technology by Tektronix was selected to measure the current and voltage signals of the wire EDM process. The modern equipment ensures the capability to handle high frequency measurements. The voltage signal is recorded with a THDP0200 high-voltage differential probe. According to the manufacturer, this device has a bandwidth of up to  $f_{\text{voltage}} = 200$  MHz and can be applied in conjunction with any oscilloscope. In addition, voltages in the range of  $u = \pm 1500$  V can be sampled [TEKT23a]. To measure the voltage, the probe is tapped between the upper wire guide head and the sample or the machine table.

The voltage signal is forwarded to a DPO7104C digital storage oscilloscope and can be displayed in real time. It has a bandwidth of  $f_{\text{oscilloscope}} = 1$  GHz and can store up to 125 million data points [TEKT18]. In parallel, a current signal is fed into the storage oscilloscope via a second channel. The current was recorded with a measuring system consisting of a TCP303 current probe and an associated TCPA300 amplifier. The total current through the workpiece can be measured using a specific clamping device and a toroid with a cable wound around it. The current probe is clamped to the cable of the toroid. From the current probe head, the signal is first passed on to the amplifier and then to the oscilloscope. The amplifier ensures that the measuring system covers a large current measuring range. This combination of current probe and amplifier covers a current measurement range between  $i = 5$  mA and 150 A. The bandwidth of the current measuring system is  $f_{\text{current}} = 15$  MHz [TEKT23b].

According to the manufacturer's specifications, the measuring equipment covers the resulting current and voltage ranges on a wire EDM machine. It must also be verified that the resolution of the measuring equipment is sufficiently high. According to the Nyquist-Shannon sampling theorem, the sampling frequency (also known as the Shannon frequency) must be at least twice as high as the maximum frequency occurring in the signal in order to ensure lossless measurement [ABEL09]. In the tests, the sampling frequency corresponds to the smallest bandwidth of the individual measuring devices. This means that the bandwidth of the discharge measuring system sets the maximum limit frequency of the signal to  $f_{\text{measure}} = 7.5$  MHz. The lowest signal characteristic is a short circuit and has a discharge duration of at least  $t_e = 0.5$   $\mu$ s. This means that the highest frequency appearing in the signal is  $f_{\text{max}} = 1$  MHz and the Nyquist-Shannon sampling theorem is thus fulfilled.

The storage oscilloscope can save and reproduce the fed signals at specified intervals. Various settings can be configured on the device for saving the data. The recording of a signal is determined by the set time span and the sampling frequency. In addition, the time or event at which data should be recorded can be specified. The oscilloscope offers various trigger options and for this purpose characteristics in the signal can be selected. Two different trigger events were used for data recording in the tests. For recordings during the cut that do not lead to wire breaks, an edge detection as a single event is selected as trigger type. Figure 4.2 shows a screenshot of the storage oscilloscope when edge detection was applied. After manual confirmation by the operator, data recording is started when a rising or falling edge exceeds or falls below a value according to the settings. Here, the edge voltage that reaches or exceeds the

value of  $u \geq 18$  V was chosen to stir a discrete recording in the continuous process. At least five recordings were conducted for each setting in different process technologies to determine the electrical process parameters such as discharge energies. The measurements were carried out with a sample rate of the oscilloscope  $f_{\text{oscilloscope}} = 200$  MHz and a recording time of  $t = 200$  ms resulting in 40 million data points for the current and voltage signal.

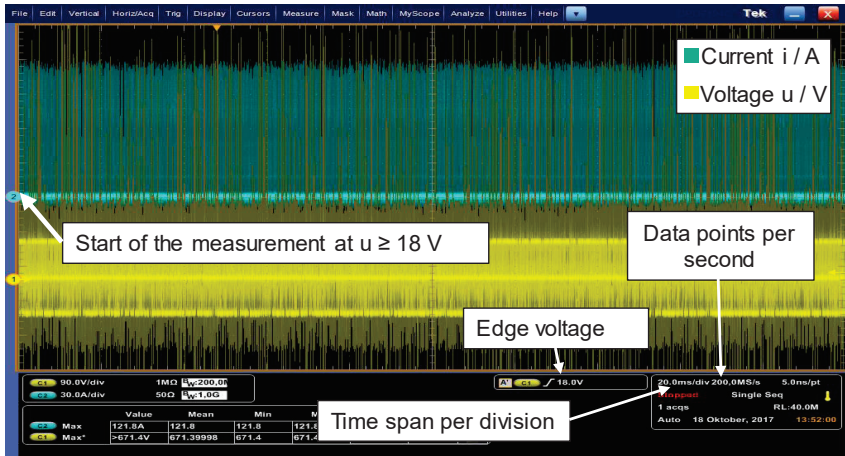


Figure 4.2: Trigger concept - edge detection

In the following the signal analysis of the recorded current and voltage raw data is explained. An analysis algorithm in Matlab is developed to extract process parameters from the current and voltage signals. Matlab is widely used for numerical computation, data analysis, visualization, and algorithm development. Its strength lies in its ability to perform calculations with matrices. This capability is particularly advantageous for evaluating wire EDM data, where large matrices are common due to the high number of discharges.

First, the current and voltage signals are read in and saved as vectors. Then, the signals are filtered to remove the noise since noise in signals can lead to problems in the feature extraction of data records [STEA18]. A low-pass filter and a moving average filter are used for filtering. The cut-off frequency and the order of the filters as well as the group delay were determined by a Fast Fourier Transformation (FFT) and by test runs.

Once the raw signals have been prepared, the signals systematically run through loops under defined conditions. The procedure is exemplarily explained by analyzing the current signal. First, all discharges are determined. To achieve this, the program checks the current signal and uses a logical operation to create a new vector of the same length as the current signal vector. This new vector consists only of two distinct entries (0 and 1) indicating whether the comparison operation is fulfilled. For this purpose, the loop checks which data points of the current exceed a specific value, e.g.  $i \geq 50$  A. For

illustrative purposes only, the value 150 is entered in the logical vector for each point where this condition is met, otherwise a zero is inserted. Figure 4.3 depicts a section of the current signal and the logical vector. As shown in the diagram, a value is entered in the logic vector for each position  $i \geq 50$  A. The red circles in the diagram show the point at which the current assumes the value  $i = 50$  A. Based on the created vector, the exact start and end points of the individual discharges can now be determined using new conditions. This is done by iteratively increasing and reducing until the lines of the logical vector reach the corresponding current values of  $i = 0$  A. The results of these loops in Figure 4.3 show the precise detection of the start and end of a single discharge.

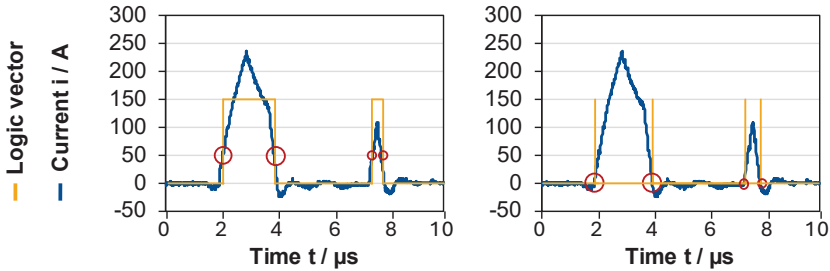


Figure 4.3: Detection of the exact start and end point of a discharge

With the same approach, the ignition delay time or the build-up of the open-circuit voltage can be detected. By the determination of these discharge characteristics, the current and voltage parameters can be calculated individually for every single discharge. With this methodology, an automated analysis of process parameters could be realized.

Based on this, different discharge types were identified. Figure 4.4 shows the current and voltage signals of different discharge types occurring on the used wire EDM machine applying a main cut. The extracted process parameters are shown in the diagram (a), which represents the signal of a normal discharge, following a pattern similar to normal discharges as described above [HENS17, KLOC07, KUNI05]. Initially, an open-circuit voltage is established, typically set by technology-specific variables. In a normal discharge on this machine, the open circuit voltage reaches around  $\hat{u}_i = 100$  V. However, in the discussed experiments, at least a  $\hat{u}_i \geq 70$  V is required. This voltage is sustained for a brief period before abruptly dropping to a very low value, initiated by the generator controller. Subsequently, the generator's power stage switches from low voltage to higher levels, causing the discharge current to increase. The specific current profile during discharge is influenced by processing technology settings, with the maximum discharge current typically exceeding  $\hat{i}_e \geq 300$  A.

The abnormal discharge depicted in the diagram (b) on the right reaches the same energy level of a normal discharge. This means that the power stage of the generator is also ignited here. However, it does not correspond exactly to a normal discharge, as a lower open-circuit voltage is built up during the ignition delay time. Consequently,

any discharge with an open-circuit voltage of  $\hat{u}_i < 70$  V was here defined as an abnormal discharge.

The abnormal discharge drawn in the diagram (c) differs from a normal discharge both in the ignition delay time and energy. The open-circuit voltage is usually even lower than that of the previously described abnormal discharge. This value is so low that the machine does not switch on the power stage of the generator. This results in significantly lower discharge energies. The maximum discharge current measured for this type of abnormal discharge does not exceed the value of  $\hat{i}_e = 300$  A and for the most part is even much lower at approx.  $\hat{i}_e \approx 200$  A.

The short circuit is displayed in the diagram (d). No open-circuit voltage is built up. In addition, no power stage is ignited here due to the low open-circuit voltage. The discharge energy corresponds to the energy level of the abnormal discharge in (c) without ignition of the power stage.

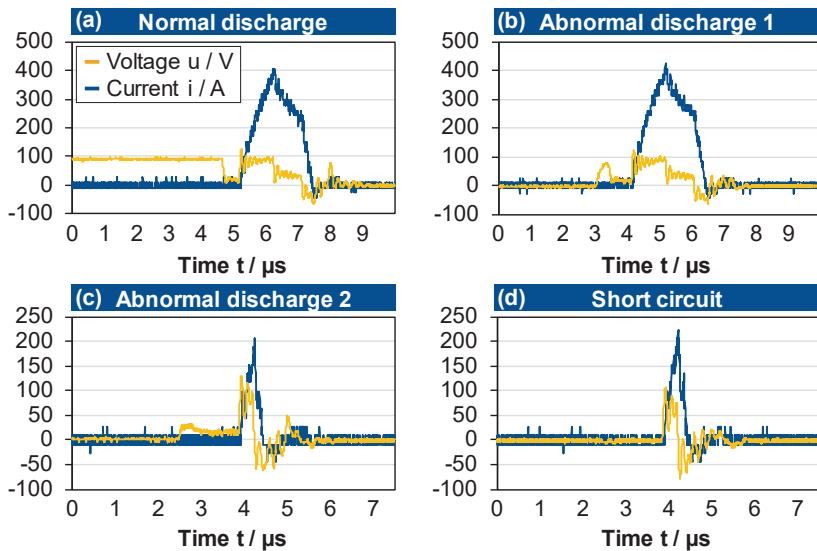


Figure 4.4: Different forms of discharges on the wire EDM machine

The effects of the individual discharges in terms of material removal and wear on the workpiece and electrode have already been explained in chapter 2.1. While a normal discharge leads to the greatest material removal, abnormal discharges and short circuits reduce the productivity of wire EDM, especially, considering the discharge energy. In addition, abnormal discharges respectively short circuits increase wear on the wire electrode, which can lead to wire breaks. It is therefore essential to evaluate the distribution of different discharge types in order to assess the process performance in wire EDM. The analysis of various experiments has shown that the described abnormal discharge types (b) and (c) can be neglected for the further consideration in this work. The proportion of these specific discharge types is negligible. Figure 4.5 shows the

distribution of the different types for operations with different pulse interval times. Instead, an energy-based differentiation of the discharges is considered.

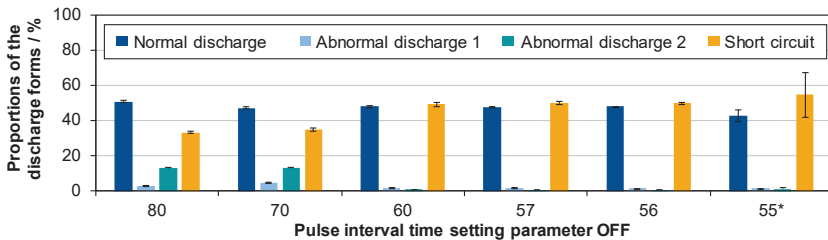


Figure 4.5: Distribution of discharge types for decreasing pulse interval time

## 4.2 Online Measurement of Process Parameters

Even though comprehensive analysis of single discharges has been conducted, for the evaluation of the continuous process, consecutive discharges have to be considered [KUNI05]. However, due to the high discharge frequency in the wire EDM process, an analysis of electrical process parameters is limited by the duration of the measurement [BERG18b]. In most other investigations, the same approach was used like described above. Raw data of the current and voltage signals are measured with a high sample rate and saved on a storage oscilloscope. The characteristic process parameters are subsequently determined offline.

A methodology was developed to characterize single discharges in the continuous wire EDM process without saving the raw signal data implementing a real time capable system to extract features. The system is equipped with a digitizer and a Field Programmable Gate Array (FPGA). FPGAs are part of the broad category of programmable logic components. They consist of a matrix of configurable logic blocks, which can be either combinational or sequential, interconnected through a reprogrammable interconnection network. Memory cells within the FPGA control both the logic blocks and the connections, enabling the component to meet specific application requirements [MONM07].

The FPGA system FlexRIO from National Instruments was used to analyze the high-frequency signals in real time. FlexRIO systems combine powerful analog-to-digital converters, digital-to-analog converters or high-speed serial connectivity with an FPGA for user-defined signal processing [NATI24b]. The two devices are connected to each other via high-speed interfaces. The NI 5733 adapter module for the FlexRIO with two channels, a bandwidth of 120 MS/s and a 16-bit digitizer was employed for the experiments. It is able to process analog data in real time using its high-performance A/D converters and transmit it to the FPGA [NATI24a]. Finally, the calculated parameters are transferred to a conventional PC.

The raw data was evaluated directly in real time on the FPGA. This eliminates the need to save the raw data. Only the characterizing process parameters need to be saved and are identified by a signal feature extraction. The same approach as used for offline

measurement was applied to detect the discharges via the FPGA. Thereto, the current signal is sufficient to determine discharges. Based on the isoenergetic working principle of the generator only two different discharge types were distinguished. The current signal of a normal discharge and a short circuit are plotted in Figure 4.4. The maximum discharge current, the average discharge current or the discharge duration can be used to distinguish between discharge types. For the investigations in this thesis, the discharge duration was used to differentiate and evaluate the discharges. In preliminary tests, this showed a clearer distinction between normal discharges and short circuits than an assessment based on the discharge current parameters. The duration of a normal discharge is in the range of  $t_{e,n} = 2 \mu\text{s}$ , whereas the discharge duration of a short circuit is in the range of  $t_{e,s} = 0.7 \mu\text{s}$ .

The functionality of the program code for signal feature extraction is presented below. The LabView program from National Instruments is employed for this purpose. This is a graphical development environment that is applied for test, measurement, control, and regulation systems [ELLI07, NATI24c]. The finished program code is compiled and can be stored in the configuration memory of the FPGA. Function blocks are called Virtual Instruments (VIs) in LabVIEW. The VIs often have several subprograms, which are called SubVIs. The program for the acquisition or processing of electrical signals consists of two VIs, each with several SubVIs.

The system processes input data by first scaling and transmitting it to an FPGA. A First In First Out (FIFO) queue ensures ordered data exchange, temporarily holding measured values to prevent computer overload before transferring them to the MainVI at a 20 Hz rate for further processing and saving. The MainVI sets discharge start and end points based on specified limits, adjusting for the digitizer's output. Shift Registers (SR) dynamically store parameters. One SR counts samples and identifies discharge initiation by comparing current values against a threshold. Discharge characteristics are calculated using additional SRs, which count samples and sum current values during a discharge, adjusting for the detection of discharge ends. The system converts these calculations into time and current units, assessing discharge type based on duration and summarizing the proportion of normal discharges. User-friendly GUI allows for easy adjustments and monitoring. The system efficiently stores unlimited discharge data, requiring 15 MB per minute storage space compared to 3 GB per minute storing raw signal data, significantly reducing storage demands.

### **Validation of the FPGA System**

To validate the FPGA system, tests were conducted comparing it with offline measurements using a storage oscilloscope. Based on the observations, iterative modifications of the algorithm were made to optimize the feature extraction. But first a possible influence of the set sampling frequency on the accuracy of the measurement was analyzed. It was set to  $f = 40 \text{ MS/s}$  for previous tests. In order to determine the quantitative influence, the current signal was sampled once at  $f = 40 \text{ MS/s}$  and once at  $f = 60 \text{ MS/s}$ . To validate the results, the discharge durations are compared as a histogram in Figure 4.6. There are hardly any differences between the two sampling frequencies and the



discharge durations differ by less than one percent. Only the resolution of the measured values was improved negligibly small.

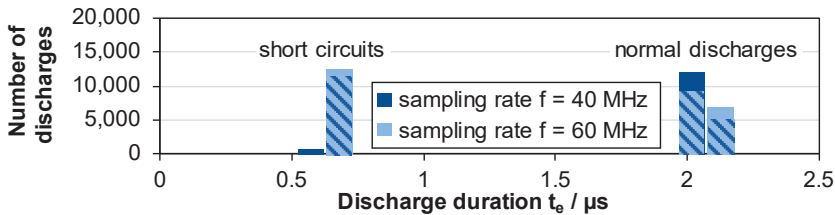


Figure 4.6: Comparison of discharge duration using different sampling frequency

The accuracy of the calculated current parameters is exemplarily illustrated in Figure 4.7, where the average discharge currents of both measurements are displayed in a histogram. While the average discharge current of normal discharges can be determined with the FPGA system with a deviation less than 1%, the current parameter of short circuits deviates by approx. 20%. Possible source of error is incorrect attenuation of the current signal due to the impedances of measurement devices and has to be considered in further analyses.

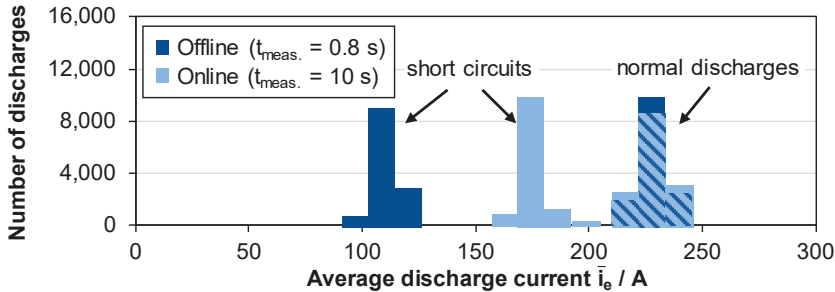


Figure 4.7: Average discharge current of offline and online measurements

Discharge durations between online and offline measurements were compared by conducting measurements with both systems under identical conditions, investigating over 50,000 discharges for each setup. Figure 4.8 depicts a histogram illustrating the distribution of discharge durations for both online and offline evaluations.

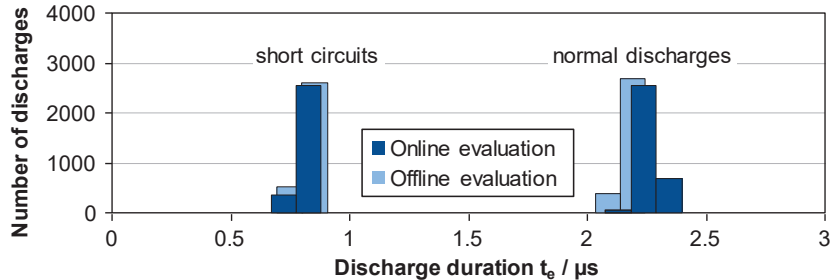
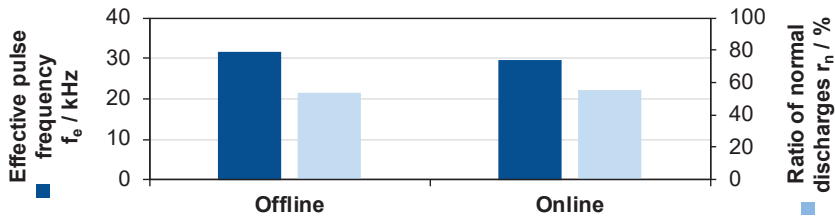


Figure 4.8: Offline and online evaluations of the discharge duration  $t_e$  [KÜPP20]

The histogram is presented with a specific number of categories but without a threshold. The various analysis methods demonstrate a significant correspondence in discharge duration, particularly for short circuits between  $t_{e,s} = 0.5$  and  $1 \mu\text{s}$  and for normal discharges, exhibiting a high consistency with deviations less than 5%.

The subsequent section demonstrates the ability to detect and accurately classify all discharges as either normal or short circuits. Figure 4.9 illustrates the effective pulse frequency  $f_e$  and the ratio of normal discharges  $r_n$  for both online and offline measurements. Each measurement involved analyzing again over 50,000 discharges. While online measurements were conducted continuously during the process, offline evaluations required multiple measurements with subsequent averaging of values. The effective pulse frequency  $f_e$  exhibits a deviation of less than 5% between the two systems, likely attributable to variations in measuring durations. Regarding the classification of discharge types, the values differ by less than 2%.

Figure 4.9: Online and offline evaluations of effective pulse frequency  $f_e$  and ratio of normal discharges  $r_n$  [KÜPP20]

These results indicate a high level of consistency between the two methods, thereby validating the efficacy of the online system. Nevertheless, single discharge energies cannot be determined with high accuracy using the FPGA system. For constant machine settings, the discharge energies are also constant and only two different values occur because of the isoenergetic generator. Therefore, a combination of the offline discharge energy calculation, as described in chapter 4.1, and the described online measurement was applied for further data acquisition.

### 4.3 Online Measurement of Spatially Resolved Single Discharges

By the presented FPGA system, process data can be recorded continuously without any limit of the process time. Therefore, changing process conditions can be captured and high amount of process data are ensured. To increase the quality of the process data and extend the information density, the characterization of single discharges is not only time but also spatially resolved.

#### 4.3.1 Measurement Setup

Several studies investigated the localization of discharges in sinking EDM [HAN08b, KOB99, KUN90, LI97, KUN91]. The localization of discharges over the workpiece height in wire EDM were initially analyzed for only short periods using different process

signals considering current and voltage signals [HAN04, HASH09, OBAR98, RAJU94, RAJU97, SHOD92] or even acoustic emission signals [SMIT13]. In addition to detecting the discharge position, initial attempts have already been made to ignite the discharges in a controlled manner at specific positions [KUNI01].

Findings by Hada and Kunieda [HADA12] revealed that, even with identical pulse conditions, thicker workpieces yielded higher discharge currents. Consistency between analytical and experimental outcomes suggests the feasibility of in-process workpiece thickness measurement based on monitored discharge currents. The current signals were used to measure discharges considering the localization in a continuous process [BOCC18, BOCC20, DICA20]. However, the different discharge types are not considered by localizing the discharges. Due to the various energy of different discharge types, the distinction in detection is necessary to determine the spatially resolved process energy and thus represents the need for a method to characterize spatially resolved discharges.

The discharge position is determined using two current probes. Based on the several findings, the currents of the upper and lower wire head are measured separately for the localization of single discharges along the workpiece height [LI97, KOB99, HAN08b, HAN04, OBAR98, SHOD92, BOCC18]. These are each connected to the current line of the upper and lower wire head via a toroidal transformer. The measurement setup is shown in Figure 4.10 and is based on the FPGA measurement chain described in chapter 4.2, except that two current clamps are used instead of just one.

The total current  $i_{total}$  is supplied via workpiece, see Figure 4.10. As soon as the dielectric strength of the working medium is overcome and a discharge occurs, the total current splits and flows via the wire electrode. The current flows through the connection between the wire electrode and the wire heads via the power cables to the ground point of the machine. Depending on the position of the discharge on the workpiece, different distances or path lengths to the earth point result for the current  $i$  flowing upwards or downwards along the wire electrode. As a result, the total current is distributed unevenly to the upper or lower wire head. This can be explained with the help of Ohm's law and the resistance  $R$  of a current-carrying conductor with a constant cross-sectional area [WEI15]:

$$u = R \cdot i \Leftrightarrow i = \frac{u}{R} \quad (4.1)$$

$$R = \rho \frac{l}{A} \quad (4.2)$$

The path length from the discharge position to the machine's earth point is represented by the length  $l$  in equation 4.2. As soon as different path lengths to the earth point occur due to an off-center discharge position, different resistances  $R$  result for the current flow. Based on Ohm's law in Formula 4.1, for a constant voltage and unequal resistances, different current strengths  $i_{upper}$  and  $i_{lower}$  result at the upper and lower wire head.

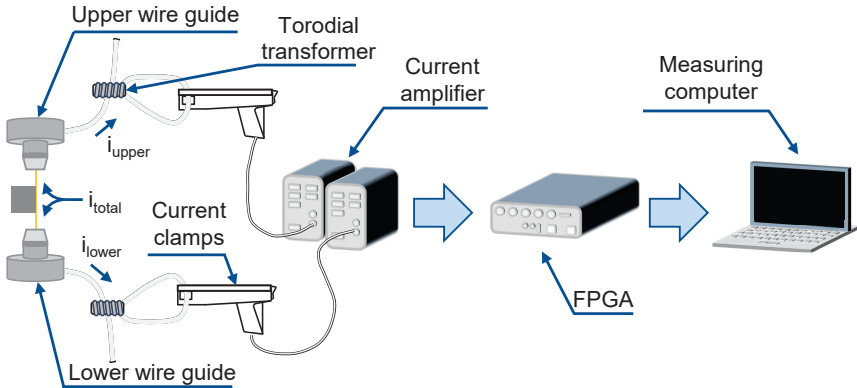


Figure 4.10: Measurement setup for determining the discharge position [KÜPP21a]

Based on the measurement setup and the physical principles, the method for the spatially resolved characterization of single discharges is described in [KÜPP21a]. Therefore, the determination of the difference in the current signal during a discharge can be attributed to the discharge position. In Figure 4.11, the upper, lower, and total current signals for the different discharge types are depicted. The difference in current of the upper and lower wire head between two discharges is independent of the workpiece or the tool material and can thus be used generically to detect the discharge position [HAN04, OBAR98, SHOD92]. To determine the discharge position using the current difference, the differentials are plotted as a frequency distribution in the form of histograms with constant bins, which are defined by a uniform width. Binning in data science can be useful when dealing with numerical data, as it can help to understand certain trends or distributions [SUCK20].

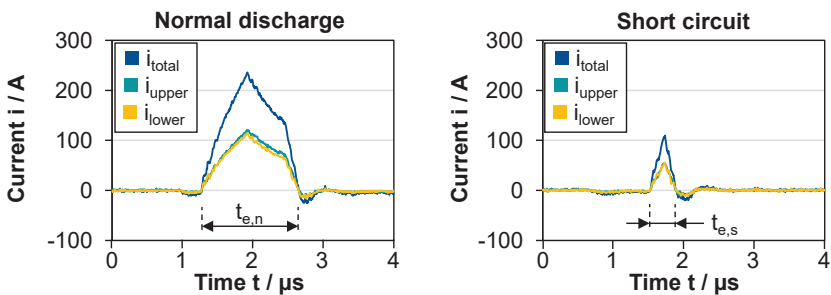


Figure 4.11: Upper and lower current of a normal discharge and a short circuit [KÜPP21a]

The following investigations examine how well the discharge distribution along the workpiece height can be determined and visualized. The average discharge current and the maximum discharge current were calculated for both measured current signals in real time. In first experiments, the measurement capability of the FPGA for this purpose was examined. After that, the deviations between the difference of the maximum

and average current must be obtained to define the best performing indicator. This is done by evaluating the variance of the frequency distribution of the maximum discharge current and the average discharge current.

### 4.3.2 Adaption and Validation of the Measurement Setup

As described in chapter 4.2, the determination of the current values can only be realized with small deviations compared to the high-frequency measurement using a storage oscilloscope, which enables the most accurate measurement. To validate the FPGA, the number of discharges with the corresponding current difference  $\Delta i_e$  is plotted in Figure 4.12. This was carried out for both the FPGA measurement and the oscilloscope reference measurement. The class width resulted on the one hand from the distance between the minimum and maximum current difference and on the other hand from the selected resolution. The resolution or the number of classes  $n_b$  can be set in advance in the algorithm. It is important to ensure that the resolution is not set too low, otherwise the class width will be so large that outliers will no longer be weighted. This reduces the significance of the processed data.

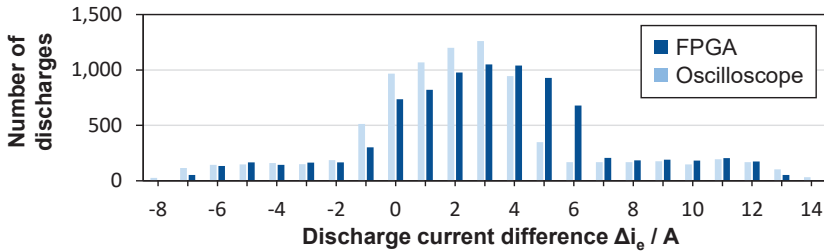


Figure 4.12: Current differences determined with the FPGA and oscilloscope

It can be seen from the data in Figure 4.12 that the discharge distribution of the oscilloscope measurement strongly resembles a classical normal distribution. What is striking in this chart is the shift of FPGA measurement towards bigger current differences. The mode of the two measurements is  $\bar{x}_M = 3$  A. The mode  $\bar{x}_M$  is an important measure of position that indicates which characteristic occurs most frequently in a data set [FAHR16].

The difference in the discharge distributions can be explained by the shift of the current zero line. The FPGA is able to detect voltage signals in the range from  $u = -1$  V to  $+1$  V. These voltage values are converted into so-called bits and are mapped to a total range of  $2^{16}$  bits. The total number of bits results in the possible mapping spectrum of the FPGA. To determine the current values precisely, the current zero line must run exactly along the center line of the mapping range, i.e. at  $2^{15}$  or 32768 bits. The correction of the current consists of two steps. First, the difference between the zero line of the current and the center line of the spectrum must be determined and corrected. This correction is described by the factor  $K_S$ . To determine  $K_S$ , the upper and lower currents were recorded with the FPGA, analogous to the previous measurement setup. The data was then analyzed using the DIAdem software from National Instruments.

DIAdem is a data management software for combining, analyzing, evaluating and logging measured values very easily without the necessity of programming [NATI20c].

A section illustrating the DIAdem evaluation is shown in Figure 4.13. The current signals of the raw data sets are plotted over the measurement duration  $t_{\text{measure}}$ . Two normal discharges and one short circuit are shown in the diagram. The type of discharge can be distinguished by the height of the peaks. The magnification of the signal shows that the zero line of the current signal (yellow line) is shifted upwards by a factor of  $K_S$  relative to the center line (grey line). The correction factor results from the bit difference between the two lines at  $K_S = 192$  bits. Due to the oscillating signal fluctuations in the single-digit bit range along the center line, errors occur in the determination of the average discharge current. These signal fluctuations can be seen in the magnified section of the previous Figure 4.13.

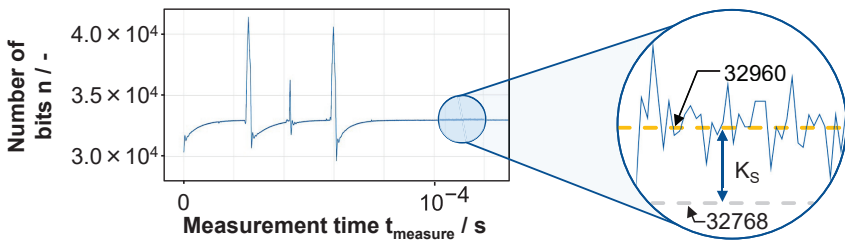


Figure 4.13: Determination of the correction factor  $K_S$

The diagram in Figure 4.14 shows a characteristic normal discharge from the DIAdem evaluation and demonstrates the increase of signal fluctuations especially just before the discharge. After the discharge, the current drops significantly. The average discharge current is determined based on the area that forms between the center line and the signal contour. The limit values of the area along the X-axis are determined by the number of passes of the signal at the center line. As a result of the signal noise, the limit value on the left-hand side is determined incorrectly. This causes the area between the center line and the signal to be calculated incorrectly, resulting in a falsification of the average discharge current.

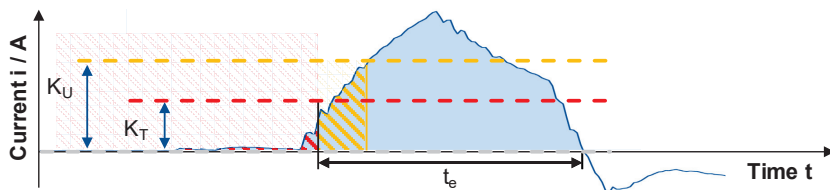


Figure 4.14: Schematic representation of the recursive limit value  $K_T$

To counteract this situation, in a second step of the current correction the factor limit value  $K_T$  was defined. It is presented as a red line in Figure 4.14. The distance between this limit value and the center line is described by the factor  $K_T$ . As soon as a measurement is started, the LabVIEW program begins to record the signal curve. If the

current signal rises above the  $K_U$  value specified in the user interface, the program detects a discharge. This discharge is recorded until the current signal falls below the center line again (light blue area). The area under the discharge is then recursively supplemented by the yellow shaded area. The discharge duration of the discharge thus results from the right-sided passage of the signal at the center line and the left-sided perpendicular of the signal intersection with the correction factor  $K_T$ . On the one hand, this ensures that not every signal fluctuation is recorded as a discharge and, on the other hand, exact recording of the discharges.

The correction factor  $K_T$  was determined experimentally. A total of six measurements ( $K_T = 0 - 5$ ) were recorded for this purpose. During the series of measurements, the correction factor  $K_T$  was gradually increased before each measurement. In Figure 4.15 the recorded number of normal discharges over the average discharge current  $\bar{i}_e$  for three of the six correction factors are plotted in the histogram.

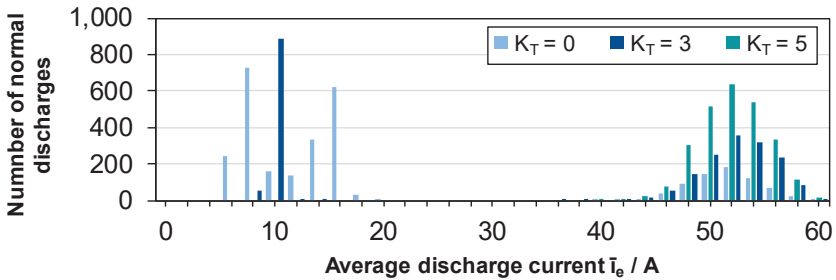


Figure 4.15: Determination of the correction factor  $K_T$  of the recursive loop

An accumulation and shift of the discharge distributions to the higher discharge values can be detected as the correction factor increases. This is consistent with the situation described above. With a correction factor  $K_T = 0$ , discharges that by definition do not represent a discharge as such are incorrectly assigned to the normal discharges. In Figure 4.15, this can be seen by the light blue bins in the left-hand diagram area. With the correction factor  $K_T = 3$ , shown in dark blue, the incorrectly allocated discharges in the range of  $\bar{i}_e = 6 \text{ A} - 18 \text{ A}$  decrease significantly. However, the discharges in the left-hand diagram area only disappear from a correction factor of  $K_T = 5$ , see red marked discharge distribution. An increase in the correction factor  $K_T$  did not result in any further improvement.

As mentioned, in addition to the average discharge current  $\bar{i}_e$ , the maximum discharge current  $\hat{i}_e$  can also be employed as an evaluation parameter. The advantage of the maximum discharge current lies in the fact that it is determined based on the highest level of the discharge current profile and therefore remains unaffected by signal noise around the center line. However, it must be checked whether the maximum discharge current is sufficiently accurate to determine the position of the discharge location. For this purpose, the number of normal discharges and short circuits from a total of five measurements were compared with each other. The results of the comparative measurements are shown in the histograms in Figure 4.16.

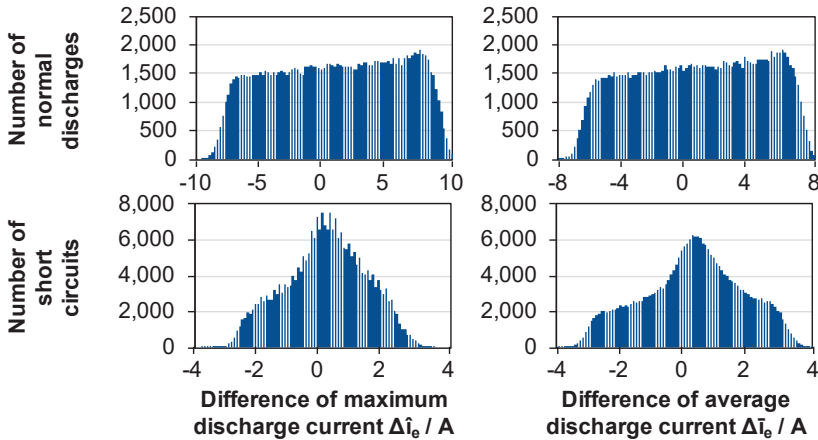


Figure 4.16: Comparison of the maximum and average discharge current [KÜPP21a]

It can be stated that the evaluations of the average and maximum discharge currents show comparable results. The values of normal discharges show slight differences in the width of the discharge distribution. The maximum discharge currents of short circuits show more isolated peaks. This can be attributed to the lower current values of the maximum discharge current. The lower currents result in smaller absolute current differences and thus the impact of signal fluctuations increases. Therefore, the average discharge current was used for the measurement, despite the greater computational effort involved.

In summary, it can be said that the capability of the online measurement system could be demonstrated based on the validation tests of the individual measuring devices. The deviation of the FPGA from the storage oscilloscope is less than 5% and can be attributed to signal noise and the input impedances of the individual measuring devices. This means that a real-time calculation of the current differences can be carried out with sufficient accuracy using the FPGA system.

#### 4.3.3 Correlation of Discharge Current and Discharge Position

The following description of the procedure for correlating the discharge current with discharge position was also presented by the author in [KÜPP21a]. Even though, the averaged discharge current is used and represents a statistically safer variant, since more values are considered; the measurement uncertainty is still an issue. As mentioned before, the histograms are formed with constant bins. Thereby, the limits are defined by the calculated current differences. Depending on how many classes are specified and how small the value range of the current difference is, the measurement errors at the boundaries can lead to distorted results. It can be assumed that outliers will always be measured. In order, to eliminate these errors, data processing is conducted before forming the final histogram. Based on the investigations a minimum number of bins is recommended, which is at least as large as the workpiece height in millimeter. The procedure for the formation of histograms is exemplary shown in Figure



4.17. With the specification of the number of classes, the width and the boundaries are formed based on the data. In this example, five bins are chosen. The classes at the margins contain measurement errors, which induce the value areas and limits of the bins. A minimum number of discharges is defined, which each bin must contain, otherwise the data points of the bin are deleted. Subsequent, a new histogram is formed with the same number of bins but new limits and adapted boundaries. This procedure can be repeated iteratively to minimize the measurement error.

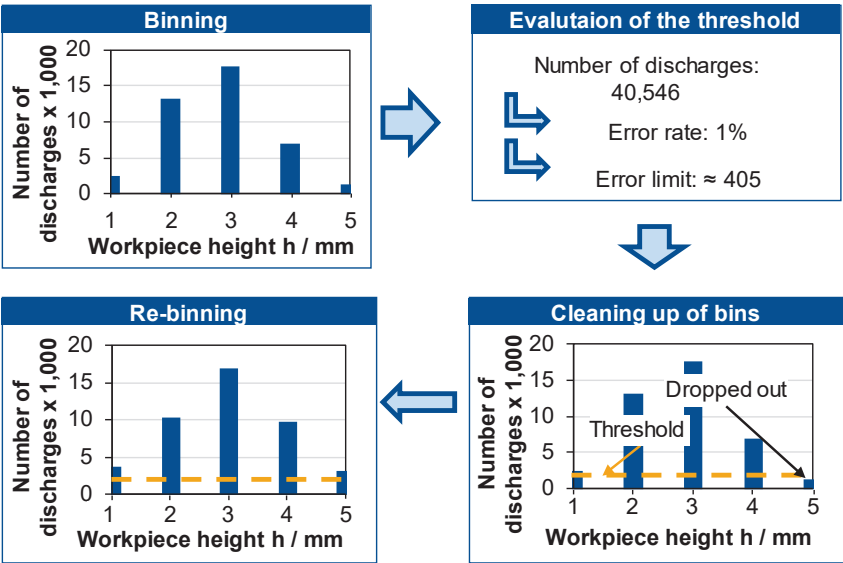


Figure 4.17: Methodology for the formation of the histograms [KÜPP21a]

4.3.4 Influence of the Workpiece Position and Workpiece Height

In order to determine the relationship between the discharge position and the current difference, the following experimental setup was conducted, see Figure 4.18. A workpiece with a height of  $h = 2$  mm was machined at varied positions of height  $z$ . The first sample was machined on the machine table at a height position  $z = 0$ . Then, shim plates of a thickness  $t = 1$  mm are successively placed underneath and the sample was machined each time up to a total height position of  $z = 40$  mm. For each position, the current difference was recorded.

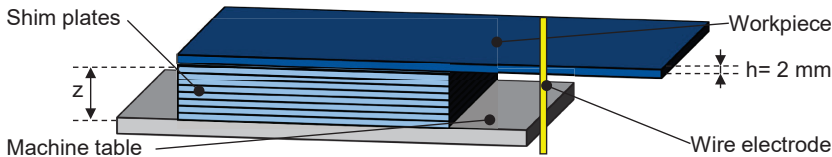


Figure 4.18: Experimental setup to determine the influence of the workpiece position [KÜPP21a]

In Figure 4.19 (a), some of the results are depicted in a histogram. A distinction of the current differences machined during varied height positions can be clearly seen in the histogram. The gaps between the individual data sets show that the current differences can be distinguished with the described method even with a height difference of less than  $\Delta z = 1$  mm.

However, the observation of individual frequency distributions clearly demonstrates that the frequencies are approximately normally distributed. The center of such a normal distribution is represented by the mode value. Since the number of discharges is highest in the center of the component, the mode can therefore represent the position of the center of the component  $z + h/2$  via the current difference  $\Delta i_e$ . For this reason, a mode analysis of all 21 component positions was carried out for a more detailed representation of the frequency distributions and plotted over the position  $p = z + h/2$ . As expected, there is a linear correlation between the discharge position and the current difference with a coefficient of determination of almost  $R^2 = 1$ . The distribution of the mode values is more uniform compared with the frequency distributions in Figure 4.19 (b). The individual workpiece positions show uniform distances in their current differences. Only the current difference of height  $z = 1$  mm is shifted to the left.

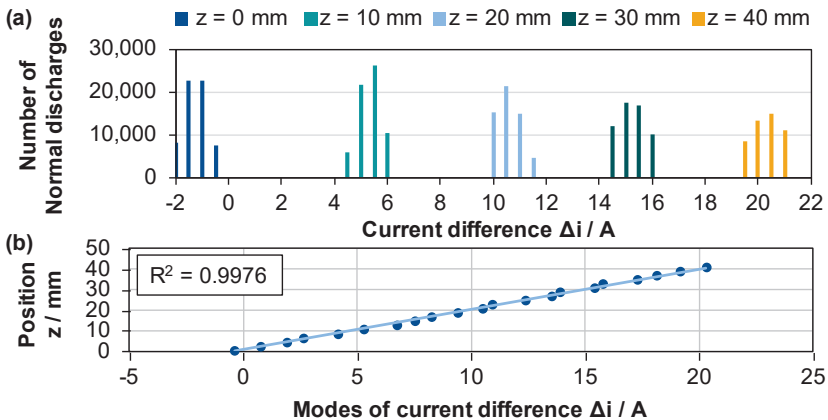


Figure 4.19: Distribution of normal discharges for different workpiece positions (a) and correlation between the workpiece position and calculated modes of discharge distribution (b) [KÜPP21a]

The corresponding, linearly interpolated straight line of the 21 component positions has the following equation:

$$z = 1.96 \cdot \Delta i + 1.02 \quad (4.1)$$

With a calculated slope of  $m = 1.96$ , the current difference is increased by the factor  $m^{-1} = 0.51$  A/mm over the position of the component. The position of the components can be determined to an accuracy of  $\Delta z = 0.71$  mm using the interpolated straight lines.

In this section, the distribution of current differences for different workpiece heights are evaluated. For this purpose, 10 experiments with varying workpiece heights from  $h = 5\text{ mm}$  to  $50\text{ mm}$  with  $\Delta h = 5\text{ mm}$  steps were machined. In Figure 4.20, the evaluated results of different workpiece heights are presented by plotting the distributions of normal discharges after the application of the described methodology. The number of bins for each data set equates to the workpiece height value. The depicted diagrams show good results, and the current difference can be converted directly into the workpiece height regarding the linear correlation.

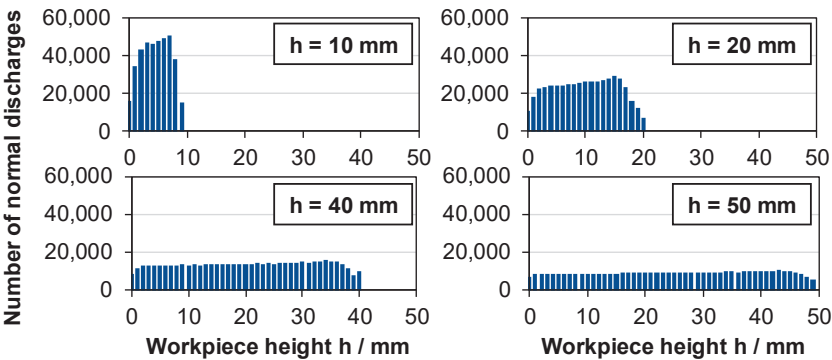


Figure 4.20: Discharge distribution dependent on workpiece height [KÜPP21a]

With the use of a specific component with recesses, it is proven that not only different workpiece heights are correctly mapped by the methodology and system, but also locations where no discharges ignite. The specimen and results are illustrated in Figure 4.21. The component has a height of  $h = 100\text{ mm}$  and six recesses with different thicknesses.

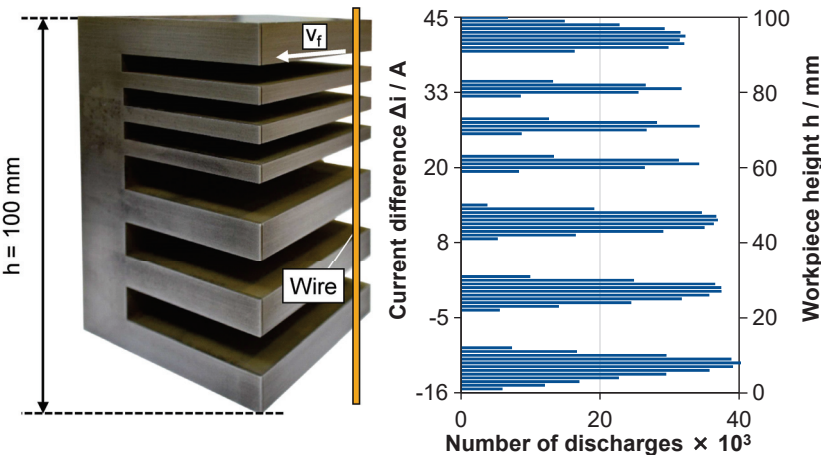


Figure 4.21: Visualization of workpiece geometry by process data [KÜPP21a]

The wire position is tracked using a program by Makino connected with a machine interface. By the recorded wire position, the electrical signals can be allocated on the workpiece and the cutting rates can be determined. Finally, the geometry can be visualized precisely by the system characterizing and recording every single discharge, see Figure 4.21. This visualization is real-time capable and can be realized during machining by implementing the methodology of histogram formation in the FPGA system.

#### 4.4 Data Agglomeration

Generally cleaning data by handling missing values, outliers and inconsistencies is necessary. While normalizing or standardizing numerical features are typical process steps in data processing, in this case especially data agglomeration is meaningful. This necessity arises not only due to the high data volumes, but also because of the operating principle of the process. Since the investigations of individual discharges show only microscopic material changes, the first step is to determine how much the data can be agglomerated without loss of information. This involves the accumulation of consecutive discharges over a period of time, causing not only a microscopic but also a macroscopic change in the workpiece. For example, a typical feed rate of  $v_f = 3 \text{ mm/min}$  and an effective pulse frequency of  $f_e = 50 \text{ kHz}$ , results in one million discharges for a cut length of only  $l = 1 \text{ mm}$  with a period of  $t = 20 \text{ s}$ . The purpose of this data is to provide information about the change in the workpiece, in terms of geometry, surface or subsurface layer. Therefore, the aim is to find longest possible time over which data can be agglomerated without losing relevant information. Machine learning-based approaches offer the possibility to quickly process the enormous data stream. In the following, it is shown how data can be systematically agglomerated with an evaluation of the conducted agglomeration. Unlike in other studies, the measurement and analyses are not restricted to specific sample rates. All single discharges are recorded and subsequently agglomerated.

For the evaluation of data agglomeration, a workpiece with different heights and varied nozzle distances was machined. In industrial applications, many components cause changing workpiece heights, nozzle distance and thus flushing conditions due to their geometry. The component had different heights from  $h_{min} = 5 \text{ mm}$  to  $h_{max} = 50 \text{ mm}$ , each with 5 mm steps. Figure 4.22 shows the staircase-shaped workpiece as well as the schematic top view of the clamped workpiece indicating the machined slot.

A test series composed of a total of ten straight cuts was performed. This consisted of one cut per step. For each step, machining parameters of the slot were recorded over a minimum time interval of  $t = 60 \text{ s}$ . To counterbalance any influence due to unstable or varying flushing conditions, machining parameters were recorded three times at different locations along the machined slot. For all the machined slots, the upper head and hence nozzle position was kept constant. The position of the upper head was kept at 8 mm over the highest step  $h_{max}$ . It should be emphasized that the change from one step to another involved not only changing the thickness of the workpiece, but also changing the flushing distance of the top nozzle, which are two different factors that affect wire EDM machining and, therefore, the machining parameters. While the

thickness reduces from  $h_{max}$  to  $h_{min}$ , the upper nozzle distance increases from  $a = 10\text{ mm}$  to  $55\text{ mm}$ . In Figure 4.22 an overview of the different setups is listed.

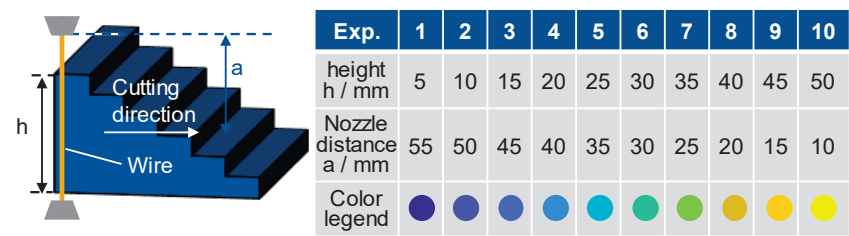


Figure 4.22: Staircase-shaped workpiece and clamping design

A medium carbon steel C45, typically used in various applications including mechanical engineering, automotive industry and tool making was machined. All tests were conducted with the  $d = 0.25\text{ mm}$  brass wire bercocut pro 900 by bedra [BERK24a]. In order to keep the machining efficiency high on one hand and to avoid wire break on the other hand, a standard machining technology for a workpiece with the average height  $\bar{h} = 25\text{ mm}$  was used. Data of the continuous process were recorded which included every single discharge and the corresponding label for the type of discharge, the time at which the discharge was ignited and the current difference for the spatial resolution of the single discharges as described above.

Based on the machining data, characteristic process parameters like the effective pulse frequency  $f_e$  and the ratio of normal discharges  $r_n$  were evaluated over specific time intervals. Starting with averaging time of  $\Delta t = 3\text{ ms}$  it was then increased iteratively by one millisecond until  $\Delta t = 350\text{ ms}$ . Agglomerations over  $\Delta t = 3\text{ ms}$  can cover approximately 25 to 150 consecutive discharges while  $\Delta t = 350\text{ ms}$  covers over 2,500 to 15,000 consecutive discharges, depending on the machining settings and the workpiece and wire materials. The goal was to find the agglomeration time interval which can be used to precisely describe and distinguish between these tests. Optimally, this time interval should be as large as possible to maximize information density, but small enough to detect relevant changes, whether in the workpiece or in the machining stability parameters. For example, early detection of deteriorating machining stability, usually a few hundred milliseconds in advance, can be used to prevent wire breaks [BERG18b, CABA08a]. This can serve as an upper limit for the agglomeration time interval depending on the purpose of the data use.

Figure 4.23 shows the agglomeration of the different processes averaged with various time intervals. The effective pulse frequencies are plotted against the corresponding ratio of normal discharges in different colors according to the legend in Figure 4.22. As it can be seen in the diagrams, machining of workpieces with smaller heights is characterized by high ratios of normal discharges resulting from the good flushing conditions, which enhances the deionization of the working gap and promotes rapid debris removal from this region. In isoenergetic pulse control systems employing a constant pulse interval time, higher ratios of normal discharges result in lower effective pulse

frequencies, as normal discharges typically endure about four times longer than short circuits. Furthermore, higher ratios of normal discharges achieve higher material removal rates since material removed by short circuits is negligible compared to that of normal discharges. However, this was only determined for single discharges according to the literature [KLOC07].

Contrary, lower ratios of normal discharges, here for the machining of higher workpieces, correspond to higher effective pulse frequencies. The stagnation area, region where debris accumulates and hence promotes short circuits, increases with the height of the workpiece. Thereupon, in general, the trend is a linear relationship between the workpiece height and the effective pulse frequency on the one hand and an inverse relationship between the workpiece and the ratio of normal discharges. However, an overlapping of the data points for a certain region can be observed.

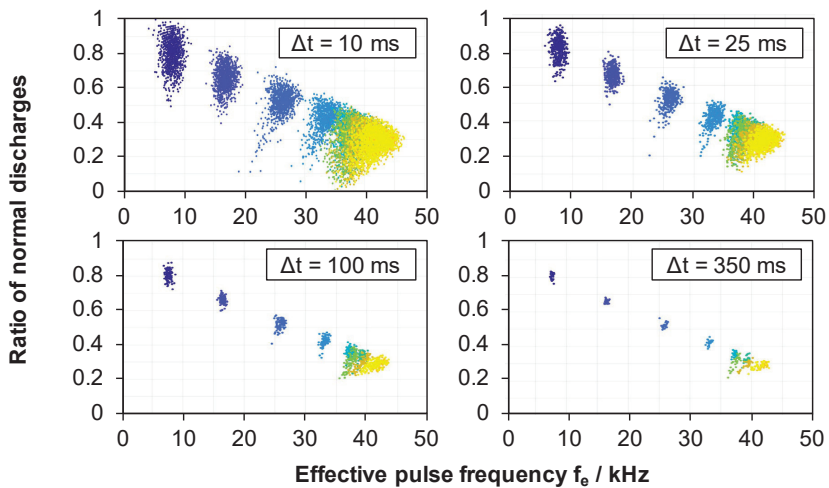


Figure 4.23: Ratio of normal discharges in correlation with effective pulse frequency for different averaging times

Subsequently, the ability of unsupervised machine learning methods to effectively distinguish the different processes when they are analyzed as a single data set for varying averaging times was investigated. Accordingly, the data records were divided into the same time intervals as before. This results approx. in 350 data sets of two features: ratio of normal discharges and the effective pulse frequency. Four unsupervised machine learning algorithms were used to cluster these data sets. As already discussed in chapter 2.3, clustering analysis is often used to group similar data points or find hidden patterns in data sets. Here, the clustering algorithm should sort the data points per test so that each cluster represents the data set of a specific test. The four different clustering algorithms used are k-means, hierarchical, spectral, and fuzzy c-means. The general approach of these algorithms, where the number of clusters must be defined a priori, is particularly suited for the desired task since the number of tests is known

and is the same for all data sets. A detailed description of the clustering algorithms used in this work is provided in the following.

### ***k*-means**

Among clustering algorithms, *k*-means is probably the most used owing to its simplicity. It aims to divide a dataset with  $n$  data points into  $k$  distinct, non-overlapping clusters. Each data point is assigned exclusively to one cluster, constituting “hard clustering”. The number of clusters  $k$  is defined a priori, and data points are randomly chosen as initial cluster centers. Subsequently, each data object  $x_i$  is assigned to the nearest center  $m_k$ , typically determined using Euclidean distance [NA10]. Data points are then allocated to the nearest cluster center, creating subsets (clusters)  $C_1, C_2, \dots, C_k$ . The centroid of each cluster is computed, and cluster center locations are updated accordingly. This process iterates until convergence or the fulfillment of termination criteria, ensuring optimal clustering. The most commonly used criterion is the sum of squared Euclidean distances between each data point  $x_i$  and the centroid  $m_k$  (cluster center) of the subset  $C_k$  containing  $x_i$ . This criterion, termed clustering error  $E$ , is dependent on the cluster centers  $C_1, \dots, C_k$  [LIKA03, SINA20]:

$$E(C_1, \dots, C_k) = \sum_{i=1}^n \sum_{j=1}^k I(x_i \in C_k) \|x_i - m_k\|^2 \quad (4.2)$$

where  $I(x_i, \dots, x_n) = 1$  if  $x_i, \dots, x_n$  is true and 0 otherwise.

Good clusters should have large between-cluster variation compared to the within-cluster variation. The main drawback of *k*-means algorithm is that it is sensitive to the initial positions of the cluster centers. Therefore, in order to obtain near optimal solutions with this algorithm, the data points are clustered several times with different initial positions of the cluster center and compared [AHMA07, ARTH07, WARR05].

### ***Hierarchical Clustering***

Hierarchical clustering is a method for constructing a hierarchy of clusters, organized in a tree-like structure either from top to bottom or bottom to top. Unlike *k*-means, it does not require a predetermined number of clusters. This technique can be agglomerative or divisive, forming clusters in a bottom-up or top-down manner, respectively. It generates a nested sequence of partitions, starting with a single encompassing cluster at the top and individual data points as singleton clusters at the bottom. Each level represents a different number of clusters, with clusters formed by combining or splitting clusters from adjacent levels. A dendrogram graphically displays the clustering result. Initially, each data point forms its own cluster, resulting in  $n$  clusters. Then, pairs of clusters with the highest similarity are iteratively merged, reducing the number of clusters by one until only one cluster remains [LUCZ16, RAN113].

The cluster's merging step is usually performed using either the so-called ‘single linkage method’, the ‘complete linkage method’ or the ‘average linkage method’. In single linkage, clusters merge based on the smallest distance between any two records, emphasizing similarity between the most similar records. Conversely, the complete

linkage method merges clusters based on the maximum distance between any two records, prioritizing similarity between the most dissimilar records. The average linkage method mitigates the impact of extreme values by computing the average distance between all pairs of records from different clusters [ŁUCZ16, RANI13].

Hierarchical clustering algorithms offer flexibility in distance or similarity functions and enable exploration of clusters at different levels of granularity through dendrogram visualization. Despite these advantages, hierarchical clustering is prone to the chain effect in single-linkage and sensitivity to outliers in complete-linkage methods. Additionally, it exhibits computational complexity that increases quadratically with data size, making it less efficient for large datasets compared to algorithms like k-means [BACH10, LARO14].

### ***Spectral Clustering***

Spectral clustering is a graph-based algorithm utilized for grouping data points into a predetermined number of clusters. It effectively reduces complex multidimensional datasets into groups of similar data points in lower dimensions, often employing simple algorithms like k-means for this purpose. This technique finds applications in various fields such as exploratory data analysis, computer vision, and speech processing [BACH04].

The spectral clustering process involves several key steps, beginning with the creation of an affinity matrix based on the similarity between data points, which is adjusted by a parameter. This matrix underpins the process by reflecting the relationships between data points. A diagonal matrix is then formed from the affinity matrix and used to generate a normalized affinity matrix, allowing for an accurate representation of data point relationships while adjusting for size differences. The next step involves finding the top  $k$  eigenvectors of this normalized matrix through eigenvalue decomposition, which serve as new dimensions that reveal the data's inherent structure. These eigenvectors are compiled into a matrix and renormalized to create a matrix, ensuring uniformity in the scale of data points and preserving the significance of each dimension. The renormalized data is then clustered into  $k$  groups using techniques like k-means, based on the spectral representation. Each data point is assigned to a cluster according to its position in the renormalized matrix, finalizing the spectral clustering process and organizing the data into distinct groups based on spectral characteristics [JIAW12]. While spectral clustering is effective for various data distributions, it is noted for its computational demands, particularly in handling large datasets due to the requirement for eigenvector calculation [ZELN04].

### ***Fuzzy C-Means Clustering***

In all the above-mentioned clustering algorithms, each data point can be assigned to one and only one cluster. This assignment rule or hard clustering is required in many applications. However, for some other purposes, this rigid assignment is often not desirable, instead clusters with flexible or "fuzzy" boundaries are needed, which is the main principle behind fuzzy clustering methods. A given data point can simultaneously



belong to a given fuzzy set to a certain degree and to another fuzzy set to a certain degree [BEZD81]. This degree is called the degree of membership, typically represented by a real-valued number in the interval  $[0, 1]$  [FREI02]. For a given set of data points,  $X = \{x_1, \dots, x_n\}$ , the fuzzy set  $S$  is a subset of  $X$  that allows each element in  $X$  to have a membership degree between 0 and 1 [BEZD81, JIAW12].

In Figure 4.24 the results of the clustering analysis for selected averaging time intervals are exemplary shown. Various cluster methods were examined separately to distinguish the data sets based on only knowing the total number of data sets. It can be observed that machining parameters that overlap are more difficult to be sorted, which is true for virtually any system, as clear distinction is hard to achieve. This is independent of the averaging time interval.

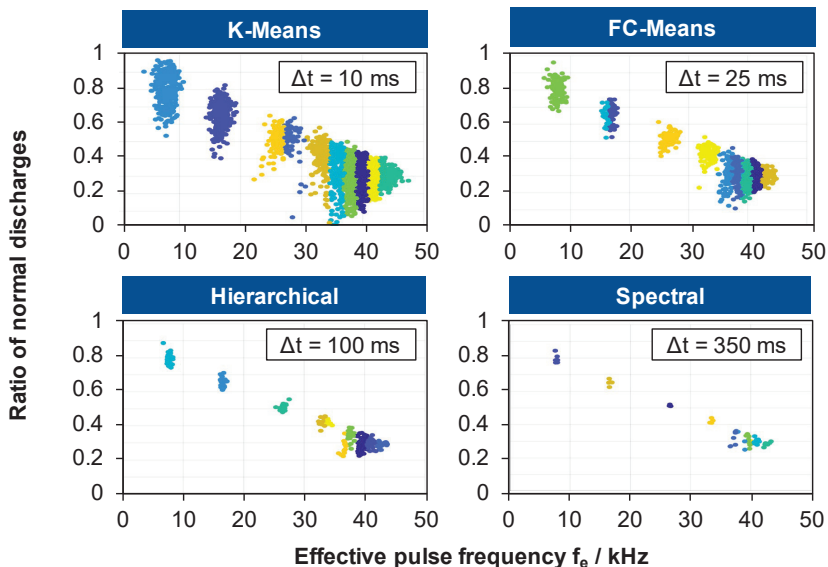


Figure 4.24: Overview of clustering results for different agglomeration time intervals

In order to evaluate the performance of each clustering method, the *F1-score* is determined. It is a performance metric which is crucial for evaluating the quality of machine learning models. The *F1-score*, defined as the harmonic mean of precision and recall, is commonly used in assessing clustering algorithms due to its ability to meet essential criteria [JIAW12]:

1. **Cluster homogeneity:** This criterion grades the purity of the clusters, which requires that the purer the resulting clusters are, the better is the clustering process.
2. **Cluster completeness:** This is analogue to cluster homogeneity and seeks to evaluate if data points of the same cluster, according to the ground truth, are assigned to the same cluster.

3. **Rag bag**: This criterion penalizes heterogeneous data points assigned to pure clusters more severely than those assigned to miscellaneous clusters, reflecting the challenge of merging dissimilar data points.
4. **Small cluster preservation**: Recognizing that splitting smaller clusters tends to generate noise, this criterion penalizes splitting smaller clusters more than larger ones.

However, computing the *F1-score* requires ground truth, representing the ideal clustering compared against the clustering results. Precision  $p$  measures the relevance of elements assigned to a cluster, while Recall  $r$  indicates how many data points of the same category are assigned to the same cluster. These parameters are derived from the confusion matrix, depicting the counts of different predictions made by the model as shown in Figure 4.25.

		Ground truth	
		A	B
Predicted Cluster	A	true positives ( $tp$ )	false positives ( $fp$ )
	B	false negatives ( $fn$ )	true negatives ( $tn$ )

Figure 4.25: Confusion matrix [TING10]

True positive and true negative outcomes indicate correct clustering assignments, while false positive and false negative outcomes represent incorrect assignments. Precision and recall can then be calculated using these results [LIPT14]:

$$p = \frac{tp}{tp + fp} \quad (4.3)$$

$$r = \frac{tp}{tp + fn} \quad (4.4)$$

Hence the *F1-score* given as the harmonic mean, which is the reciprocal of the average of the reciprocals, of precision and recall is given by [LIPT14]:

$$F1 = 2 \frac{p \cdot r}{p + r} = \frac{2 \cdot tp}{2 \cdot tp + fp + fn} \quad (4.5)$$

In Figure 4.26, the *F1-score* values of different clustering methods for varied averaging times from  $\Delta t = 0 - 350$  ms are presented. In general, the clustering methods show a better performance from an averaging from  $\Delta t = 50$  ms upwards. The results identified k-means and spectral as best performing clustering methods. Furthermore, different statistical measures were used but showed no improved clustering performance. These statistical measures include the mean values of the distribution of discharges, the standard deviation and the kurtosis of normal and abnormal discharges, etc.

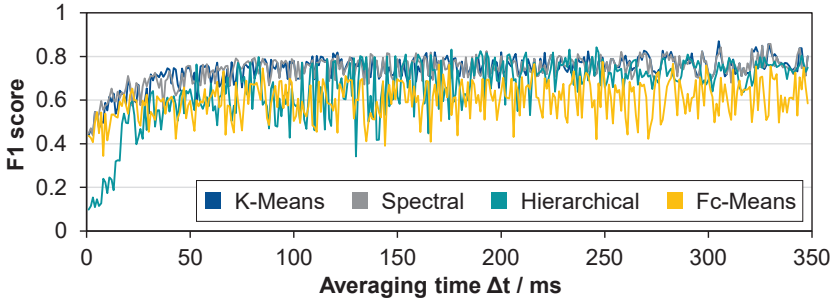


Figure 4.26: *F1-score* of different clustering methods for varied averaging time [KÜPP22b]

Characterization of the discharges along the cutting direction alone is not sufficient to evaluate process performances [KÜPP20]. Hence the spatial resolution of process parameters along the workpiece height is necessary. Previously, the agglomeration potential of process data with different averaging time without losing relevant information of the continuous wire EDM process was investigated. Under consideration of these findings, a data agglomeration approach was developed, as shown in Figure 4.27. In order to visualize these microscopic changes, the spatially resolved machining parameters were evaluated along the cutting length. Based on an analytical analysis, interval values from  $\Delta x = 0.05$  mm and  $\Delta z = 0.5$  mm were selected for most parts of the exploratory data analysis.

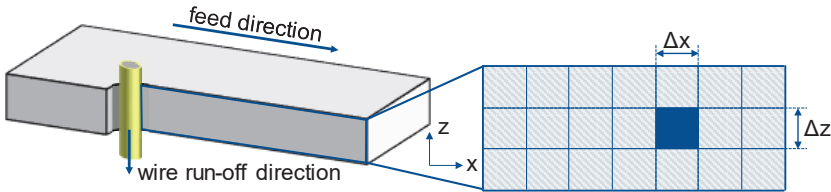


Figure 4.27: Area-dependent process data evaluation

With this, process parameters can be spatially resolved in such a way that locally induced anomalies could be identified. The wire tracing program from the machine manufacturer has a sampling rate of approximately  $s = 10$  Hz, returning the wire position on average every 100 ms, which is sufficient according to the previously performed investigations. With the typically low feed rates achieved in wire EDM, this time still represents only changes on the microscopic scale ( $\Delta l_{100\text{ ms}} \approx 0.005 - 0.008$  mm).

Figure 4.28 shows the spatially resolved characterization of single discharges representing the ratio of normal discharges and short circuits of the continuous wire EDM process machining a C45 steel material with a workpiece height of  $h = 50$  mm. The data were recorded for a cutting length of approximately  $l = 8$  mm.

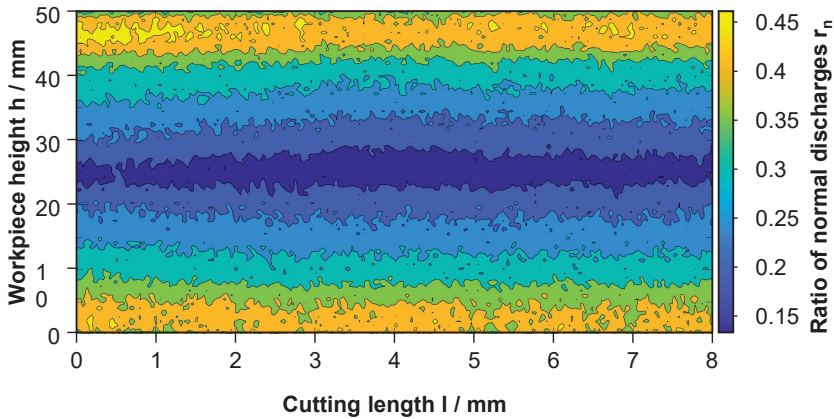


Figure 4.28: Spatially resolved ratio of normal discharges [KÜPP21a]

An optimal nozzle distance of  $a = 8$  mm was used which is recommended for the used technology. The process data recorded for the evaluation amounted to 766 MB for almost 14 million single discharges. Upon evaluation, the process data were only 1.5 MB, representing a compression factor of more than 500. The lowest ratio  $r_n$  is found in the middle of the component. This can be explained by the particle accumulation due to the flushing from the top and bottom of the working gap, which causes short circuits especially in the center of the workpiece [OKAD09, OKAD15].

Based on this information, the effective pulse frequency considering all discharges can be displayed in Figure 4.29. As a result of the discharge distribution in Figure 4.28 and due to the two times shorter discharge duration of short circuits and the missing ignition delay time, logically more short circuits than normal discharges take place at the same time.

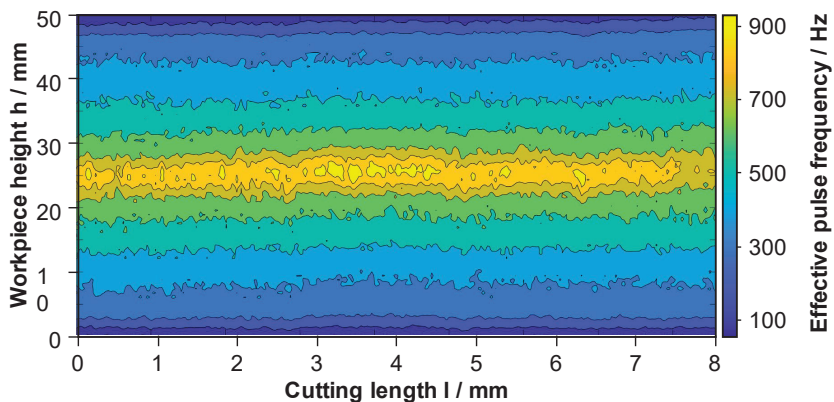


Figure 4.29: Spatially resolved effective pulse frequency

Due to the isoenergetic working principle of the generator in wire EDM, the discharge energies are constant for each type with unchanged input machine parameters [KÜPP20]. The discharge energy can be influenced by variations of the workpiece height. But this effect on the energy of a single discharge is negligibly small [HADA12], since here the mapping of the total process energy is to be represented.

To visualize the local discharge energy  $w_{local}$ , it is calculated in dependence of the number of all discharges  $n_d$ , the various discharge types  $r_n$  and  $r_s$ , the cutting coordinates, and the discharge position along the workpiece heights with following equations:

$$w_{local,n} = n_d \cdot r_n \cdot w_{e,n} \quad (4.6)$$

$$w_{local,s} = n_d \cdot r_s \cdot w_{e,s} \quad (4.7)$$

$$w_{local} = w_{local,n} + w_{local,s} \quad (4.8)$$

The energy of a normal discharge is two times higher compared to the energy of a short circuit. Figure 4.30 visualizes that even if short circuits have a substantially lower discharge energy compared to normal discharges, a concentrated energy input can take place considering the number and type of single discharges.

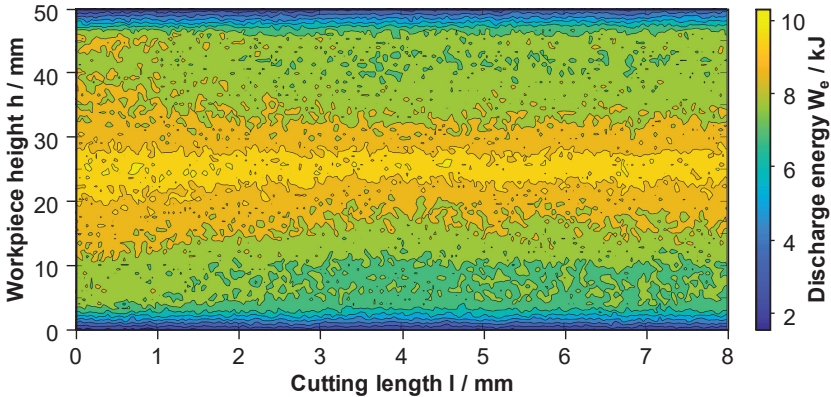


Figure 4.30: Spatially resolved generated discharge energy [KÜPP21a]

## 4.5 Summary and Conclusions

In this chapter, a methodology and system were developed to record spatially resolved single discharges in wire EDM considering the individual discharge type. For this purpose, first the approach for the determination of single discharge energies was introduced. Based on the described high-resolution measurements using a storage oscilloscope and conducting an offline feature extraction, the electrical parameters could be calculated precisely, and different discharge types were introduced. With an expanded feature extraction approach and the employment of more powerful measurement technology such as an FPGA, the recording of continuously measured discharges was realized. The system is capable to record time resolved single discharges considering

electrical parameters and the discharge type without saving any raw data. By combining these two approaches, the single discharge energies can be recorded for an unlimited measurement time, due to the isoenergetic working principle of the generator.

By expanding the FPGA system and introducing a methodology, single discharges could be recorded not only in time but also in spatial resolution. With the recorded process data, it is possible to digitally map the generated process energy along the workpiece height. The data acquisition system was optimized by conducting experiments and data analysis considering wire head and workpiece position as well as the workpiece height. Thereby, discharges can be detected with an inaccuracy of less than 1 mm in real time along the workpiece. The most important prerequisite for the development of data-driven models and the application of machine learning methods is thus fulfilled by the possibility of recording unlimited continuous process data with high quality as well as high information density.

An agglomeration approach was developed to reduce data volumes by averaging machining signals over specific time intervals. This method accumulates consecutive discharges within defined intervals. Various tests were conducted using a staircase-shaped workpiece with fixed nozzle positions, and machine parameters were averaged over different periods. Each test generated datasets based on these periods, which were then combined. Four different unsupervised machine learning algorithms were used to classify the data into ten groups, with k-means and spectral clustering yielding the best results. The effectiveness of these algorithms was evaluated using the *F1-score* metric. The results indicated that the overall clustering performance improved for time intervals longer than  $\Delta t = 50$  ms.



## 5 Analysis of Evaluation Criteria in Wire EDM

After the acquisition and collection of process data with high quality, preparation or processing of the recorded data was conducted. With the collected data, an analysis of the data follows the procedure illustrated in Figure 3.1. The data analysis is employed to obtain relevant information and useful knowledge through systematic organization, statistical processing and graphic presentation of data [PLAU21]. Initially, the aim is the determination of relevant evaluation variables for the main cut process. Based on this, the analyses should serve to understand the data and show first correlations between the data and the identified evaluation variables. Figure 5.1 shows an overview of the evaluation criteria that were examined and evaluated in this work. The findings described in chapter 2.2 were taken into account when selecting the parameters and the test design. Productivity was evaluated by the speed and process stability, which is determined by the occurrence of wire breaks. The quality parameters have different levels of detail and include the macroscopic influence of the process in the form of geometric deviations as well as microscopic changes in the form of surface roughness and the generated rim zone. Again, standard steel technologies were used for all experiments regarding the specific machining workpiece height.

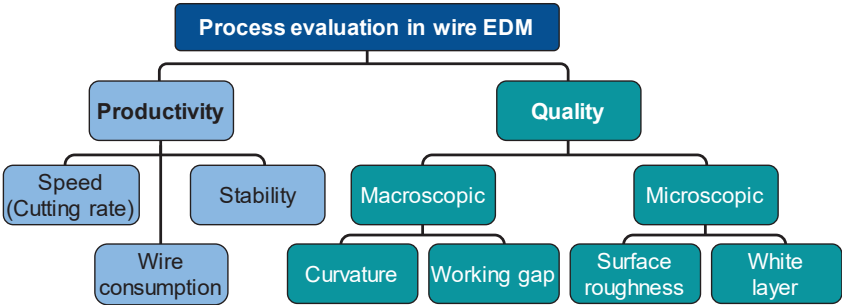


Figure 5.1: Overview of evaluation criteria in wire EDM

### 5.1 Exploratory Data Analysis for the Productivity

As mentioned in chapters 2.2 and 2.4, there are many studies that deal with the influence of process parameters on productivity, in particular the cutting rate. A correlation has been identified between increasing discharge energies and discharge frequencies with increasing removal rates. However, two aspects were not taken into account in the previous work. On the one hand, the relationship between the distribution of different discharge types and the removal rate has not been investigated. Secondly, no continuous process data have been analyzed to account for temporal changes in the data.

In the following, the results obtained by Küpper et al. [KÜPP20] are presented. To assess the performance of the continuous wire EDM process, the current signals and wire positions across various parameter configurations were recorded. The wire's position was monitored using a program by the machine manufacturer Makino interfaced with the machine. The recorded wire position allowed for the allocation of electrical



signals on the workpiece, enabling the determination of cutting rates. However, these analyses do not yet include the discharge position via the workpiece height, but only a continuous recording of characterized discharges.

The main objective was to investigate the impact of different discharge types and the effective pulse frequency  $f_e$  on the cutting rate  $V_w$  and the process stability with easy to record and handle process data considering single discharges. To achieve this, the pulse interval time  $t_0$  was varied to manipulate the number of discharges. A workpiece with a height of  $h = 10$  mm was utilized, fastened to the machine table with an optimal upper nozzle distance  $a = 8$  mm for the specific technology or parameter setting employed. The test geometry featured a cutting length  $l = 25$  mm. A reference specimen with a the standard pulse interval time of  $t_{0,ref} = 15$   $\mu$ s and turned on adaptive control was machined. Based on this technology, the adaptive control of the machine was initially switched off in order to prevent an increasing of  $t_0$  by the machine during the process. Subsequent tests were conducted with both standard and altered  $t_0$  settings. The pulse interval time was varied incrementally in steps of  $\Delta t_0 = 1$   $\mu$ s with adjustments made in both directions until wire breaks occurred while the adaptive control was switched off. Fourteen test series were conducted, with the standard pulse interval time set at  $t_{0,std} = 15$   $\mu$ s (without adaptive control). This value was incrementally increased to  $t_{0,19} = 19$   $\mu$ s and decreased to  $t_{0,wb} = 7$   $\mu$ s, leading to instances of wire breaks (wb). Each test series involved the evaluation of more than five million discharges [KÜPP20].

In order to determine initial findings using exploratory statistics, the process parameters that are directly influenced by the change in the pulse interval time were examined first. These are the pulse effective frequency, the proportion of normal discharges, the resulting generated process power and the cutting speed. In addition to statistical characteristic values over averaged time periods, Fourier analyses were also carried out. The averaging times were varied in order not to miss possible correlations. Figure 5.2 shows an example of the pulse effective frequency with different averaging times over a process. The strong smoothing caused by a longer averaging time is clearly visible, as are the strong fluctuations due to a short averaging time. The standard deviation of the discharge frequency at different averaging times depicted in Figure 5.3 confirms this observation.

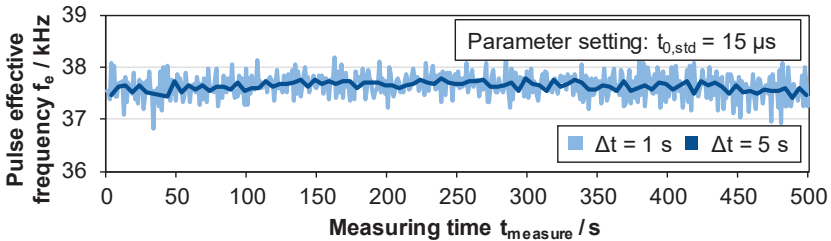


Figure 5.2: Pulse effective frequency  $f_e$  for averaging times  $\Delta t = 1$  s and  $\Delta t = 5$  s

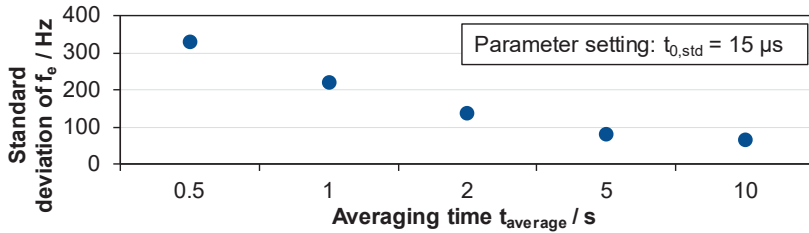


Figure 5.3: Standard deviations of  $f_e$  for different averaging times  $\Delta t$

In Figure 5.4 the correlation of the pulse interval time  $t_0$  and the pulse effective frequency  $f_e$  is depicted. The effective pulse frequency increases as expected as  $t_0$  is reduced, while the standard deviation of  $f_e$  also rises. A consistent frequency  $f_e$  signifies a stable process [KINO82, YAN96, YAN98], so the standard deviation of  $f_e$  serves as an indicator of process stability. However, these process data do not directly indicate why the pulse interval time of the standard technology has been set to  $t_0 = 15 \mu\text{s}$ .

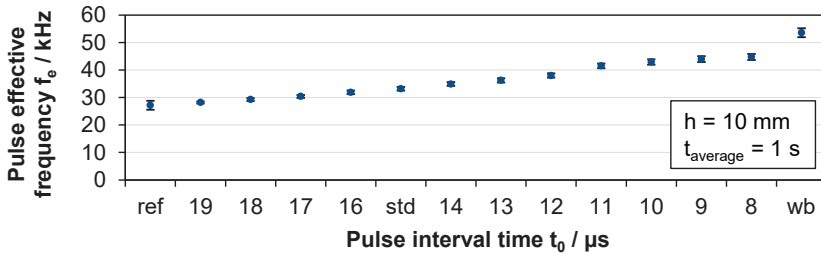


Figure 5.4: Averaged pulse effective frequency  $f_e$  for different pulse interval time  $t_0$

Analogous to the study by Kwon et al. [KWON06], Fast Fourier Transform (FFT) analysis were conducted. However, a Fourier analysis with additional high-pass and low-pass filtering to identify unstable frequencies did not lead to any meaningful results, as no dominant frequencies could be detected repeatedly in the process data using different averaging times.

Decreasing pulse interval times  $t_0$  cause poorer flushing conditions in the gap and the resulting worsened deionization of the working gap results in a higher number of short circuits respectively lower number of normal discharges [OKAD15]. A strong linear correlation between  $f_e$  and the power  $P$  as well as ratio of normal discharges  $r_n$  and  $P$  can be observed in Figure 5.5. For the calculation of the power, the respective energies of the ignited discharges were summed and averaged for the total duration of the test cut. The coefficients of determination  $R^2$  were calculated over  $R^2 = 0.9$  and the trend lines were displayed without the results of  $t_{0,\text{wb}}$ . Due to the negative correlation between  $f_e$  and  $r_n$ , the power increases by risen number of discharges. The growing number of short circuits has no negative impact on the amount of generated power. Contrary to the assumption that the highest possible number of normal discharges would result in a higher power, there is a range in which a growing power is achieved by an increase

in both normal discharges and short circuits. Due to the shorter pulse cycle time of short circuits, more discharges occur and generate more power [KÜPP20].

The results for  $t_{0,wb} = 7 \mu s$  stand out in this diagram. For this parameter setting wire breaks occurred. A significant increase of  $f_e$  by the risen ratio of short circuits, could be identified similar to other works immediate before wire breaks [BERG18b, CABA08b, CABA08a, PORT09]. An increasing amount of power could be observed in some studies [CABA08b, CABA08a, PORT09]. These effects can also be monitored in following experiments for a longer observation period. The normal discharge respectively short circuit ratio can be used to evaluate process stability. The critical threshold value of the proportion of short circuit is difficult to define but is in the same order of magnitude as already defined by Yan et al. [YAN98] at approx. 40%. However, not only a decrease in the ratio of normal discharges rate is provoked, but also the standard deviation of the measuring points increases simultaneously. This means that with a shorter pulse interval time, more short circuits occur, and they are also less homogeneously distributed over the process time. Such a less homogeneous distribution of the discharges can be an indication of a more unstable process. In addition, inhomogeneous discharge distributions potentially could imply that the process undergoes uneven removal [KÜPP20].

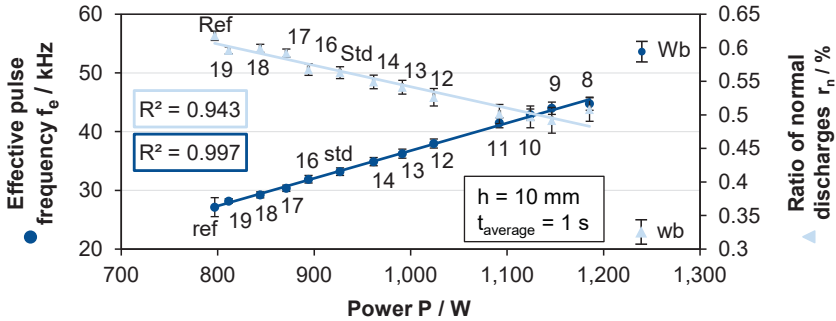


Figure 5.5: Effective pulse frequency  $f_e$  and ratio of normal discharges per second  $r_n$  as a function of power  $P$  for different pulse interval times [KÜPP20]

The generated discharge power has a significant effect on the cutting rate and should be considered in data analysis [KLOC07]. For this purpose, Figure 5.6 shows the interrelationship between the power and the cutting rates. The cutting rates are also averaged for the total duration of the test cut. What is striking out in this diagram is that the cutting rate reaches its maximum despite increasing power. From  $t_{0,12}$  the cutting rate does not increase any further. Thus, the results indicate a kind of limit for the necessary power to achieve the highest cutting rates. Since higher power could induce greater impact on the material and thus higher material removal on workpiece as well on the wire electrode, the aim is to machine with lowest possible power [KÜPP20].

The trend line in the diagram could also describe this correlation. While the coefficients of determination are not as high as before because of the high dispersion of the values, still a  $R^2 \approx 0.76$  can be calculated characterizing the polynomial function (except  $t_{0,wb}$ ).

Two clusters are formed respectively on the left and right side of the trend line. The short pulse interval times, which do not induce any increase of the cutting rates, are on the left side of the line. These clusters could be evaluation criteria for an optimal power and thus a specification for the effective pulse frequency and distribution of discharge types. However, there are still further studies to be carried out to verify this hypothesis [KÜPP20].

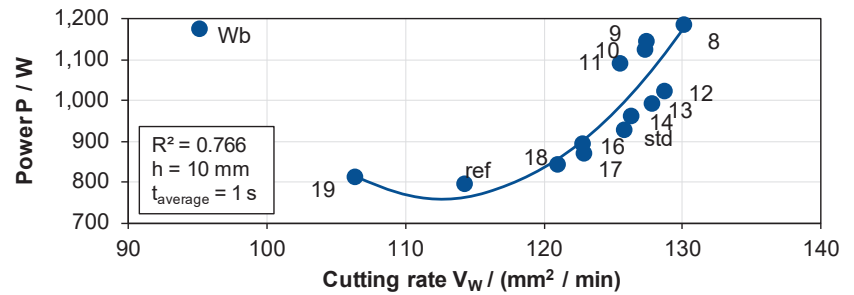


Figure 5.6: Power as a function of cutting rate for different pulse interval times [KÜPP20]

Beside the cutting rate, another criterion to evaluate the process performance or productivity is the process stability, which can also be defined by the probability of occurrence of wire breaks. In the following individual measurements of different pulse interval time settings are analyzed. The aim is to assess if there are features in the signal during machining without changing the parameter setting. Therefore, the generated power for every second was calculated for the whole cutting length. In Figure 5.7 diagrams with the generated power for  $t_{0,\text{ref}}$  and  $t_{0,\text{wb}}$  as a function of the effective pulse frequency are depicted. The reference test cut with the activated adaptive control produced a linear behavior between the generated power and the effective pulse frequency. Similar coefficients of determination are calculated for  $t_{0,\text{std}}$  with  $R^2 = 0.95$ . The analysis of test cutting with  $t_{0,\text{wb}}$  shows a high variance for the generated power and  $f_e$ , see Figure 5.7. The ratio of normal discharges  $r_n$  varies widely for shorter pulse interval times and causes different power for same number of discharges [KÜPP20].

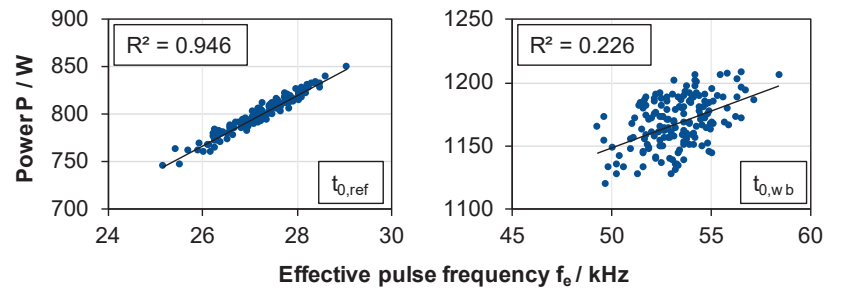


Figure 5.7: Power as a function of effective pulse frequency for  $t_{0,\text{ref}}$  and  $t_{0,\text{wb}}$  [KÜPP20]

Similar trends outcome in the diagrams in Figure 5.8. The diagrams highlight the different power values, which cause the same cutting rates. The variations are larger for shorter pulse interval times like  $t_{0,wb}$ . These differences could lead to various impacts on the material's surface. Especially, the power over such a trend line like in Figure 5.8 for  $t_{0,ref}$  could induce these effects. However, for a validation of this hypothesis, a spatially resolved characterization of single discharges is necessary [KÜPP20].

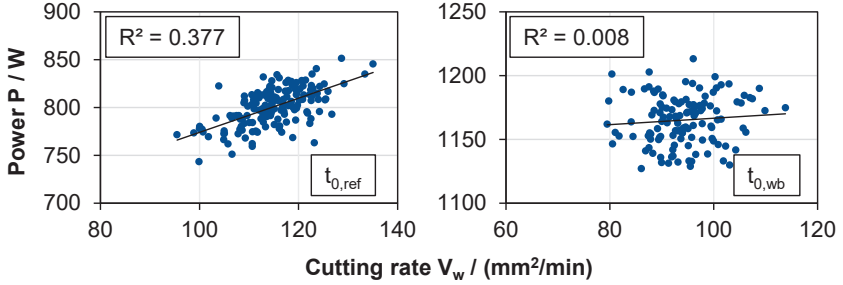


Figure 5.8: Power as a function of the cutting rates for  $t_{0,ref}$  and  $t_{0,wb}$  [KÜPP20]

The observations of an accumulation of short circuits immediately before a wire break have been made by many different studies [BERG18b, RAJU91, RAJU93, YAN98, WATA90, LIAO97a, KINO82]. To consider this phenomenon, in Figure 5.9 the accumulation for the different  $t_0$  settings is depicted. For each parameter setting, it is counted how often more than 100 consecutive short circuits occur. In addition, the maximal number of consecutive short circuits is shown on the right axis. Both values significantly rise for shorter  $t_0$  [KÜPP20].

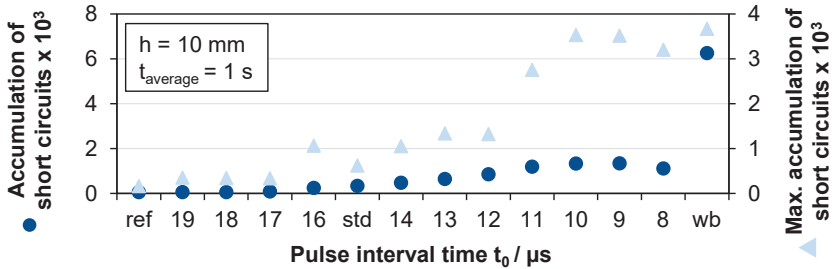


Figure 5.9: Accumulation of short circuits for different  $t_0$  [KÜPP20]

It is possible to determine each ignition delay time of the individual discharges during the process. The system stores the time at the start of each discharge  $t_i$ . It also measures the discharge duration  $t_e$ . The pulse interval time  $t_0$  is set on the machine for each sample and is therefore also known. Subtracting the time from two consecutive points at which a discharge has started gives the time interval between these two discharges. The discharge duration of the first discharge and the pulse interval time  $t_0$  are then subtracted from this time interval. The result is the ignition delay time  $t_d$  of the subsequent discharge calculated as follows:

$$t_d(t_{j+1}) = t_{j+1} - t_j - t_e(t_j) - t_0 \quad (5.1)$$

As expected, the evaluation of the ignition delay times with consideration of the discharge types provide a strong correlation between short ignition delay times (usually  $< 5 \mu\text{s}$ ) and short circuits and between long ignition delay times (usually  $> 15 \mu\text{s}$ ) and normal discharges, see Figure 5.10. When analyzing the characteristic, an increase in the ignition delay time can be determined for the parameter settings that lead to a wire break. In this diagram the rise of the standard deviation of the ignition delay time for the reduced pulse interval time  $t_{0,s}$  immediately before a wire break is depicted. Nevertheless, there are no significant trends which could precisely predict a wire break or be representative as an indicator of the process stability.

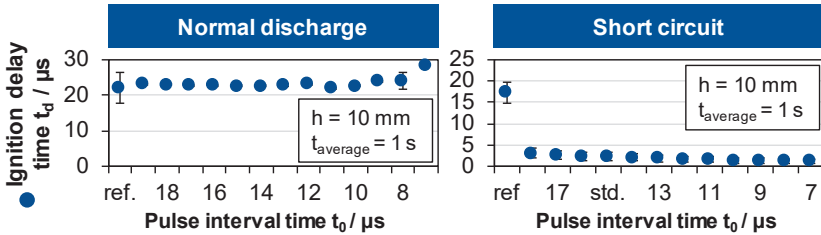


Figure 5.10: Averaged ignition delay times for normal discharges and short circuits

## 5.2 Exploratory Data Analysis for the Workpiece Quality

As already described, the produced product quality can be categorized in terms of its level of detail. The first step is to discuss which quality categories play a significant role after the main cut and should be considered for this processing step. For this purpose, both macroscopic and microscopic changes were examined. Possible correlations between the electrical process data and the corresponding quality categories were visualized. Experiments and the exploratory analysis of the process data are presented below. Due to the large amount of data and the fact that this was the first time that real process data from the continuous process was recorded and analyzed over a longer period of time, different test conditions were deliberately defined for data generation. This should ensure that the data analyses and the subsequent data-driven models are as generic as possible for the use in evaluating the wire EDM process.

### 5.2.1 Macroscopic Influence – Geometrical Deviation

There are two geometrical features produced by the main cut which are relevant. One is the straightness over the workpiece height. The other is the generated working gap which defines the offset value for specific machining conditions [KLOC07]. Both features were examined in different experiments to identify relevant features which are necessary to monitor or predict after the main cut in order to compensate possible deviations using the trim cuts.

Since only straight cuts were initially considered in this work, the focus was particularly on the straightness of the components over the workpiece height. While in most applications the main cut is not the last process step and trim cuts define the final

geometrical accuracy, it is however important to determine deviations after main cut to consider it for further machining steps. In addition, there are machining technologies which aim to ensure geometrical accuracies with tolerances under  $10\text{ }\mu\text{m}$  or even  $5\text{ }\mu\text{m}$  even after the main cut.

Several experiments with different workpiece heights and various flushing conditions were examined to investigate the influence of a produced curvature after the main cut. Depending on the conditions, especially, the size of the curvature, the first trim cut cannot compensate the deviation and thus the standard geometrical accuracy cannot be met. This can be illustrated briefly by Figure 5.11. Exemplary, two different machined workpiece heights with  $h = 120\text{ mm}$  and  $h = 200\text{ mm}$  were machined under modified process influencing variables. In each case, reference specimens were produced under optimum conditions respectively standard technologies and specimens with various nozzle distances and thus changed flushing conditions. Under degraded conditions, a curvature was produced that could not be fully compensated by a further trim cut. The reference values named  $\text{Standard}_{120}$  and  $\text{Standard}_{200}$  were manufactured with a standard machining technology and show that curvature values around  $C = 5\text{ }\mu\text{m}$  or even under can be achieved, while changed flushing conditions cause significant deviations which are not compensable [KÜPP23].

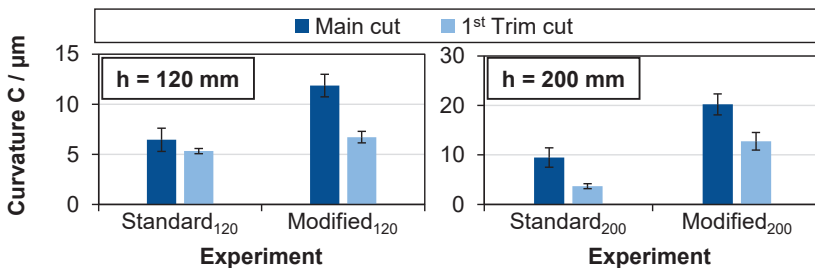


Figure 5.11: Geometrical deviation after the main cut and the trim cut [KÜPP23]

This was also observed in the studies by Bergs et al. [BERG20d] which investigated the effect of changing flushing conditions on the automated machining of fir tree slots. There, the tolerance for the straightness produced could no longer be maintained after changing the flushing conditions due to the use of a rotary axis. This observation supports the statement that predicting the contour deviation after the main cut and adjusting the trim cuts are necessary to still meet the requirements.

Based on this knowledge, experiments were designed and systematically conducted to correlate the recorded process data with the measured curvatures. The focus here was on investigating geometric deviations caused by changing flushing conditions. In this way, such deviations are ultimately generated in practical applications and would therefore also be relevant for process monitoring. In order to realize this, the correlation between process parameters like the spatial resolution of the discharge energy and the amount of material removal needs to be formulated. Several studies indicate a correlation between the amount of removal by different discharge energies and

discharge types [KLIN16, SHAH16]. However, these effects have not been studied for consecutive discharges in wire EDM, especially for the continuous process. Thereto, it is shown, how this knowledge can be extrapolated to the continuous process and how big the impact of discharge energy considering discharge types on the process is. By agglomeration of data and determining the distribution of discharge types, the material removal should be reproduced qualitatively. From the spatially resolved discharge energy illustrated in Figure 4.30, energy levels five times greater at the middle of the workpiece compared to edges can be observed and can have a relevant impact on the produced quality. For this purpose, experiments were conducted machining steel C45 with a workpiece height of  $h = 40\text{ mm}$  and a cutting length of  $l = 5\text{ mm}$  and varying nozzle distances in order to reproduce industrial machining of workpieces with altering heights, often ranging from optimal to poor flushing conditions. In addition, to the analyzed data the produced curvature of workpiece was determined by tactile measurements.

Figure 5.12 shows an overview of the experiments performed with the different machining setups and the realized cutting rates  $V_w$ . The highest cutting rate is achieved with the optimal flushing conditions as debris exclusion from the working gap is more effective. With higher nozzle distances, the dielectric enters the working gap with comparatively lower pressure and consequently resulting in lower debris exclusion from the working gap [KIMU22, OKAD09, OKAD15]. Even though setup B represents the mirrored condition of setup D, the feed rate of setup D however is considerably low. At a first glance, this may suggest that the lower nozzle distance with respect to the wire run is more determinant. Also, there is a considerable jump of the cutting rate from the symmetric flushing condition with  $a = 10\text{ mm}$  to that with  $a = 50\text{ mm}$ . This halving of the speed clearly shows the importance of flushing and its appropriate setting during machining, as it can result to doubling of machining time. Therefore, the optimal setup of a workpiece, even one with a varying height, is crucial for the machining times and hence costs.

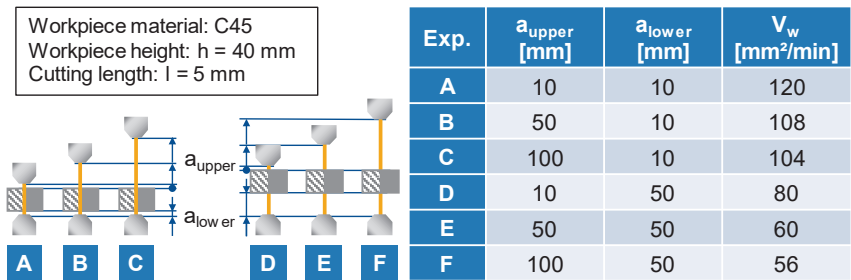


Figure 5.12: Overview of nozzle distance and cutting rate

Figure 5.13 shows the resulting machined profile for two different experiments. The MarSurf XC basic tactile profile measuring instrument was employed which is designed for simple and basic contour measuring tasks and has a resolution of  $1\text{ }\mu\text{m}$  [MAHR19]. The parameter C describing the maximum total height of the waviness of the profiles



was recorded for each experiment. This parameters does not consider the surface roughness as this is filtered out [DIN22]. While the profile in the case of experiment A shows no specific pattern, that of experiment D shows a distinctive curvature. Experiment A to C all achieved a similar profile while experiment D to F all produced a curvature. For the investigations in this work, no explicit distinction was made between concave or convex profile curvatures, but this was always defined as curvature.

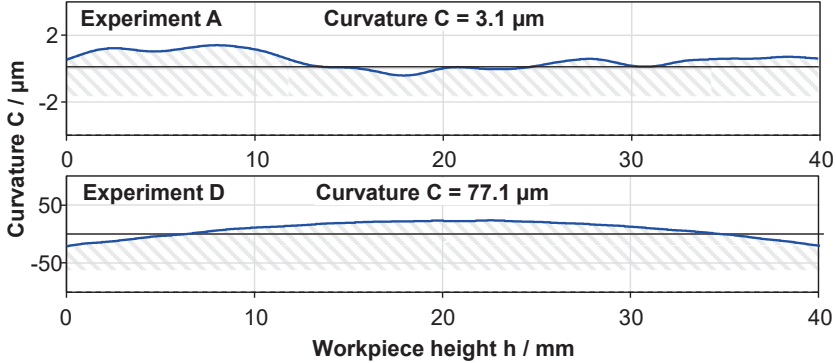


Figure 5.13: Measurement profiles of experiments A and D

In order to analyze the resulting machined profiles, the discharge energy distributions which can be determined from the discharge distribution were evaluated. A simplistic model to calculate these process parameters was derived by observing this in two dimensions as shown in Figure 4.30. The calculation is done by summing the energy per discharge for all discharge types over the height of the workpiece. The discharge distribution is also plotted. For better comparison, only the discharge and energy distribution for a machining length of  $l = 1$  mm with the respective setup A-F is shown in Figure 5.14.

As can be seen in the plots, the energy intensities and the number of discharges increase overall from setup A to setup F, which initially contrasts with the decreasing feed rate listed in Figure 5.12. Characteristic peaks for the short circuit and energy distribution for experiments D to F can be observed. The energy peaks are located in regions where short circuits are mostly ignited. As already mentioned, this can be caused by particle accumulation due to the poor flushing process, which causes short circuits especially in the center of the workpiece [OKAD09, OKAD15]. Since the dielectric is flushed into the working gap from the top and bottom nozzles, decontamination is most likely to be achieved at the gap entrances.

A possible explanation for the decreasing speed can be referred to the energy dissipation in the working gap. It is known that only a proportion of the discharge energy is absorbed by the workpiece. Other proportions of discharge energy is absorbed by the dielectric, the tool and debris a portion of the this energy [SCHN21, ZEIS17]. Analogically, the rise of short circuits can be rooted to the high accumulation of debris which in turn favor the ignition of further short circuits and disfavors the ignition of normal

discharges. It was shown by Kunieda et al. that the gap width increases as a function of the particle concentration [KUNI95, KUNI99]. Even the influence of the electric field on the particles and their movement in the working gap was investigated [KUNI97]. An increased particle concentration increases the risk of particle bridges forming and increasing the gap width. A larger gap width and the rise of short circuits leads to a reduction of the speed [KLOC07, WELL15]. Furthermore, a larger gap can degrade imaging accuracy.

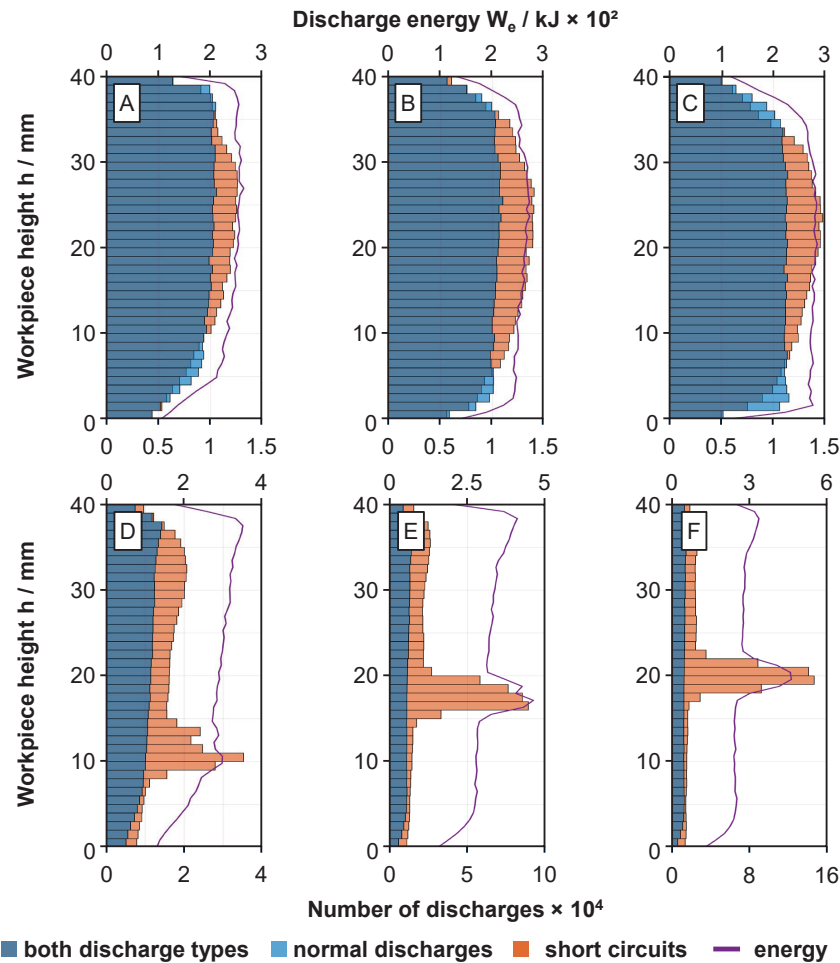


Figure 5.14: Spatially resolved discharge energy and distribution of normal discharges and short circuits [KÜPP22b]

On the contrary, experiments A to C show a relatively uniform distribution for both the energy and the discharge distribution. Furthermore, a surprising asymmetric relationship between the discharge distribution and the nozzles distances can be observed. While this distribution is insensitive to the lower nozzle distance of  $a_{lower} = 10$  mm, the opposite is true when the lower nozzle distance is  $a_{lower} = 50$  mm. An explanation to this phenomenon cannot be easily formulated. It could be a machine-based error resulting in unstable machining conditions, which has to be considered in further tests. Nevertheless, this proves the necessity of an online monitoring system being able to detect unstable machining conditions early enough which will enable machine operators to take adequate counter measures.

In order to correlate the resulting curvature to the process data, the distribution of both discharge types was analyzed. As can be seen in the plots, the discharge distributions are not always normally distributed, so the kurtosis and skewness were used. The kurtosis is a statistical measure used to quantify how heavily the tails of a distribution differ from the tails of a normal distribution. Data sets with high kurtosis tend to have heavy tails, or outliers. Data sets with low kurtosis tend to have light tails, or lack of outliers. Additionally, the skewness is calculated, which indicates the symmetry of the distribution. The skewness for a normal distribution is zero and any symmetric data should have a skewness near zero. Negative values for the skewness indicate data that are skewed left and positive values for the skewness indicate data that are skewed right [FAHR16].

The kurtosis is calculated as follows [FAHR16]:

$$K = \frac{1}{n} \frac{\sum_{i=1}^n (x_i - \bar{x})^4}{s^4} \quad (5.2)$$

The skewness is calculated as follows [FAHR16]:

$$\gamma = \frac{1}{n} \frac{\sum_{i=1}^n (x_i - \bar{x})^3}{s^3} \quad (5.3)$$

In both equations,  $n$  represents the total number of elements in the dataset,  $\bar{x}$  is the mean value, and  $s$  is the standard deviation. Both parameters determine how well a data set follows a normal distribution but with different focuses. The kurtosis and skewness of both normal discharges and short circuits were calculated. For example, the evaluation of the kurtosis for normal discharges and short circuits for different tests are depicted in Figure 5.15.

For this, the number of bins was set to  $n_{bins} = 100$ . It was observed that the kurtosis stabilizes above a number of bins that is twice the height of the workpiece. Values below this have led to large fluctuations in the values. As it can be seen in Figure 5.15, the kurtosis of normal discharges shows a positive trend with respect to the curvature of experiments D to F such that when the curvature increases, the kurtosis also rises.

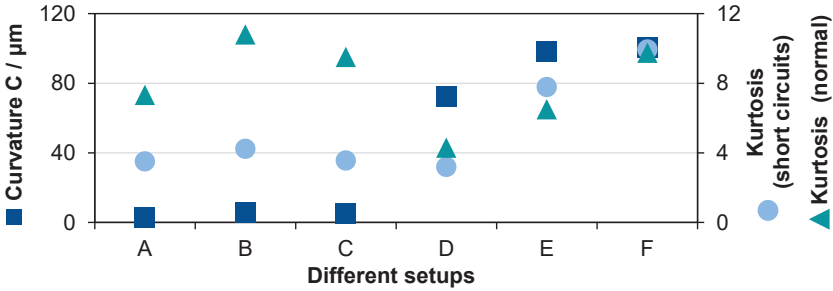


Figure 5.15: Correlation between the curvature and kurtosis of normal discharge and short circuit distribution [KÜPP22b]

However, this trend is not consistent with experiments A to C and does not describe any generic trend that correlates the curvature and the process data. The kurtosis of short circuits shows a similar behavior and can hence not be used in a generic manner. A related observation has been made when analyzing the skewness of the discharge distribution [KÜPP22b].

In order to correlate the curvature with the process data, the parameter  $e_{max}$  was formulated and defined by the ratio of the maximum counts of short circuits to the related counts of normal discharges at the same position when these discharges are discretized. This definition is graphically described in Figure 5.16 [KÜPP22b].

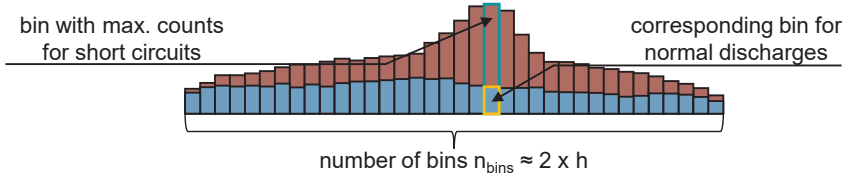


Figure 5.16: Formulation and presentation of  $e_{max}$  [KÜPP22b]

Its formulation is only based on empirical observations and is calculated as follows:

$$e_{max} = \frac{\text{max. number of short circuits } (x,y,z)}{\text{max. number of normal discharges } (x,y,z)} \quad (5.4)$$

Additionally, the dependence on the number of bins was also analyzed. Figure 5.17 displays the  $e_{max}$  results for the setups and its dependence on the number of bins. As can be seen, the values of  $e_{max}$  fluctuate greatly for lower numbers of bins, that is, for a number of bins less than the height of the workpiece. In contrast, these values tend to be more stable for bin sizes  $n_{bins} = 2 \times \text{workpiece height } h$ . This is also true for setups with much lower ranges of  $e_{max}$  [KÜPP22b].

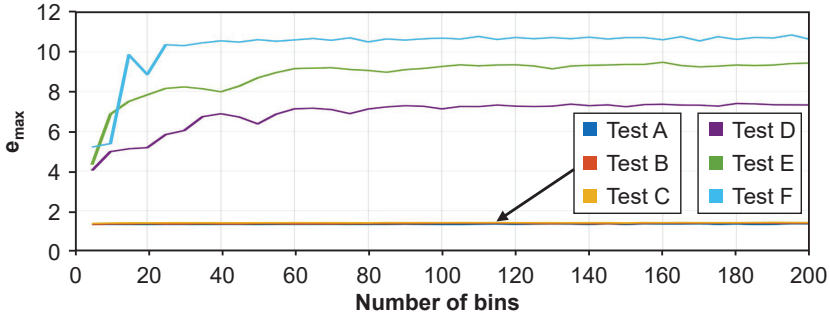


Figure 5.17: Dependence of  $e_{max}$  on the number of bins [KÜPP22b]

Using  $n_{bins} = 100$  the  $e_{max}$  parameters for the process were evaluated and plotted as shown in Figure 5.18. The resulting curvature by the different setups are also plotted. From the diagram the  $e_{max}$  for experiment A to C have very low values. However, these values increase for experiments D through F and correspond to experiments that produced high curvatures. This indicates a high correlation between the curvature and the  $e_{max}$  parameter [KÜPP22b].

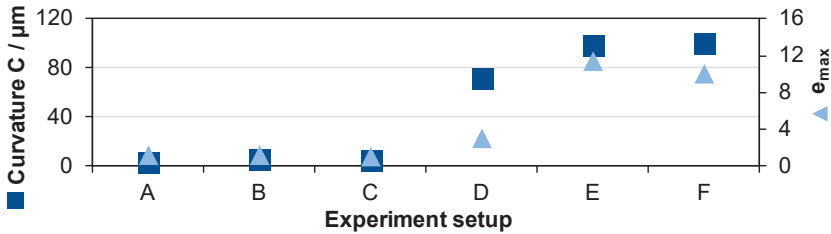


Figure 5.18: Correlation between analyzed process data and curvature [KÜPP22b]

The advantage of this parameter is the easy calculation, which simplifies the application for real-time process monitoring. Therefore, further experiments were conducted machining workpieces with heights of  $h = 40$  mm and  $h = 80$  mm. The flushing height was also varied ranging from  $a = 10$  mm to  $a = 200$  mm. The evaluation  $e_{max}$  was performed every 150 ms using the number of bins set to  $n_{bins} = 2 \times \text{workpiece height } h$ . The averaged value and the resulting standard deviation as error bar are plotted in Figure 5.19. While all the test series on the left side of the red line, where the nozzle distance was significantly increased, showed a distinctive curvature, all the tests on the right side, where only small changes of the nozzle distance have been changed, showed no characteristic curvature. Furthermore, the  $e_{max}$  evaluated from these curvature-free tests were not only small, but also very constant which can be seen from their very low standard deviation. In contrast, the tests with high curvatures returned high  $e_{max}$  values with high standard deviations. However, neither the  $e_{max}$  nor the standard deviation was proportional to the measured curvatures. Based on these observations, a threshold  $e_{max,th}$  for the formation of a curved profile could be approximated to  $e_{max,th} = 1.5$ , as shown by the dotted yellow line in Figure 5.19 [KÜPP22b].

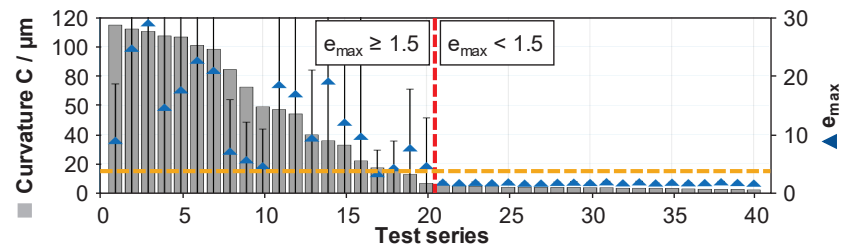


Figure 5.19: Detection of curvature during wire EDM [KÜPP22b]

Beside the straightness of the workpiece, the gap width was measured using the Zeiss Smartzoom 5 digital light microscope. Therefore, the specimens with a height of  $h = 10\text{ mm}$  machined in the experiments from chapter 5.1 were examined. The gap width varied by only about  $10\text{ }\mu\text{m}$  and is plotted in Figure 5.20. This does not represent a significant deviation but still a change of the gap width could lead to deterioration of the geometric accuracy and should be considered when applying the trim cut.

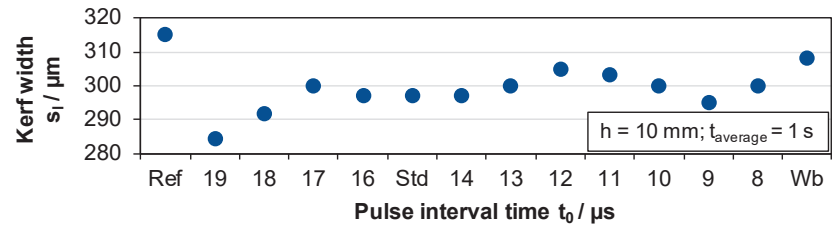


Figure 5.20: Generated gap width for different  $t_0$  [KÜPP20]

These results are also consistent with the observations made in the work of Bergs et al. [BERG18a]. Specimens also with a height of  $h = 10\text{ mm}$  were processed. The distance of the upper nozzle, the pulse interval time, the discharge current and the flushing pressure were changed. The individual parameter values were halved or doubled. While a halved discharge current significantly decreased the gap width due to reduced discharge energy and resulting smaller erosion craters, changing the other parameters does not demonstrate such a comparable influence on the gap.

### 5.2.2 Microscopic Influence – Surface Roughness

The surface roughness is in general determined by the trim cuts [HENS17, KLOC07]. This was also confirmed by the evaluation of the test specimens surface roughness examined in chapters 5.1 and 5.2. The surface roughness was measured according to DIN EN ISO 4288 [DIN98]. The average surface roughness  $R_a$  values of the specimens from chapter 5.2 are represented for the different settings in Figure 5.21.  $R_a$  is the arithmetic average of the absolute values of the roughness profile deviations from the surface within the evaluation length [DIN22]. No significant change in the surface roughness could be detected by a variation of the pulse effective frequency and the ratio of normal discharges [KÜPP20]. The standard deviation of the measurements was so small that they cannot be seen here at this resolution.

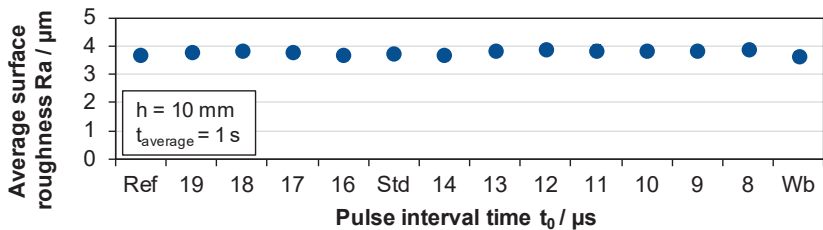


Figure 5.21: Average surface roughness using different  $t_0$  [KÜPP20]

For the described experiments in chapter 5.2 also the surface roughness was examined and the results for the  $R_a$  values are depicted in Figure 5.22. Here, also the surface roughness parameter  $R_z$  was measured. It is also known as the peak-to-valley height and represents the maximum height difference within the evaluation length [DIN22]. Overall, the roughness varies from  $R_a = 3.3 \mu\text{m}$  to  $R_a = 3.8 \mu\text{m}$  for the main cut. The values and their scatter are representative of typical roughness values after the main cut and show no significant differences between the different machining processes for either  $R_a$  or  $R_z$ . Instead, based on these results, it can be assumed that changing flushing conditions have no significant influence on the surface roughness. The surface roughness is mainly determined by the electrical parameters. It rises with increasing discharge energy, while the individual variables such as discharge current and discharge duration have different effects on the topography [KLIN17, LI13, MARA20]. The roughness is therefore largely determined by constant pre-process settings. Therefore, surface roughness was excluded as a quality factor for this work. However, it must be taken into account that surface roughness is important for future work that includes trim cut processing. As described in chapters 2.3 and 2.5, the monitoring of trim cuts could already be realized by using data of the continuous process [KLOC14b, WELL15].

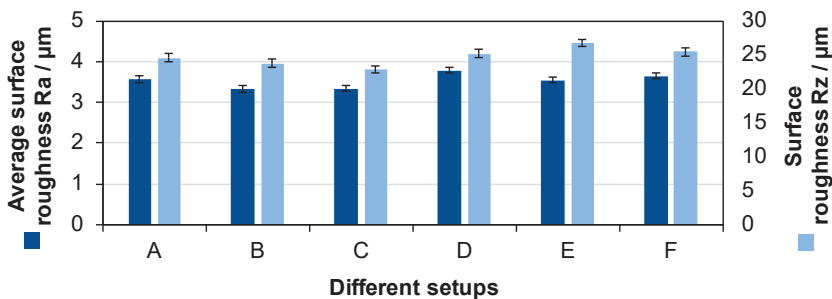


Figure 5.22: Surface roughness during various flushing conditions

5.2.3 Microscopic Influence – White Layer

As described the mechanism of material removal in EDM is primarily based on vaporization and melting induced by thermal energy input – at least for metals. A portion of the resulting melt pool is ejected by pressure gradients during and after discharge, leaving behind a white layer on the workpiece surface. The white layer (WL) consists

of re-solidified material, is characterized by the nanocrystalline microstructure and the susceptibility to cracking. Its thickness predominantly fluctuates based on discharge energy levels, with reduced energy resulting in thinner layers [KLOC16, LIU16b]. The heat-affected zone is located under the recast layer, also called white layer, where metallurgical changes occur due to phase transformations and high spatial temperature gradients, leading to residual stresses within the material [HESS22, LIU16a, MOHA21]. The resulting three-part subsurface layer is shown in Figure 5.23. The induced thermal state cannot be precisely determined but affects the material properties on the surface, persisting even after the process and amenable to analysis [KLOC07].

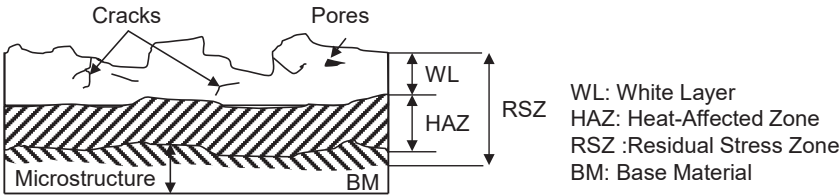


Figure 5.23: Schematic representation of the subsurface layer [KLOC07]

In order to determine the average depth of the white layer thickness (WLT), metallographic sections of the machined specimens were analyzed. A defined area of the sample was cut out. The section was then etched to generate the edge zone characteristic white color. Finally, images of these cross sections were taken using the Zeiss Smartzoom 5 digital light microscope. This microscope offers a wide range of image acquisition modes, and a 5x magnification objective was selected to capture the cross sections. Using the "stitching" function, up to 100 images of each sample were captured and automatically merged into a single image. The result is an image of the entire cross section with a length of about  $l = 20\text{ mm}$ , a resolution of over  $60,000 \times 1600$  pixels and a file size of up to 250 megabytes [ZEIS23].

Typically, several images with a length of approx.  $l = 0.25\text{ mm}$  are processed manually using image processing software to evaluate the white layer. First, the image is read in, and the pixel-millimeter ratio is determined using the measurement scale and then calculated. Finally, the average depth is obtained by dividing the white layer area by the width of the image. Figure 5.24 illustrates the manual evaluation of the white layer in the open-source software ImageJ.

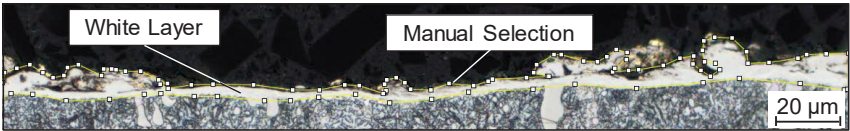


Figure 5.24: Manual evaluation of the white surface layer

In order to fully analyze the cross-sectional samples, an algorithm in Python was developed to automatize the analysis. Initially, the image is read in and aligned. The desired file and the two outer points of the contour are selected. These points can be used to determine the gradient of the sample in the image. Finally, 100 pixels above



and below the gradient line are selected to create a new image. This image is divided into several images of width  $dx$ . Then all the slices of the cross section are presented one after the other in the GUI. The contour of the white layer is detected using the Python library Open-CV (Open Source Computer Vision Library). The image is converted to grayscale using a threshold. The resulting binary image is then examined for contours using various algorithms. The results are depicted in Figure 5.25. Since the brightness varies within the images, the brightness and threshold for gray image generation can be changed for each image. By using the developed program, the evaluation time for the analysis of cross-sectional images could be significantly reduced, thus ensuring a large database for the evaluation of the white layer thickness. User-related measurement errors that can occur due to different approaches and accuracies when measuring surfaces can also be avoided.

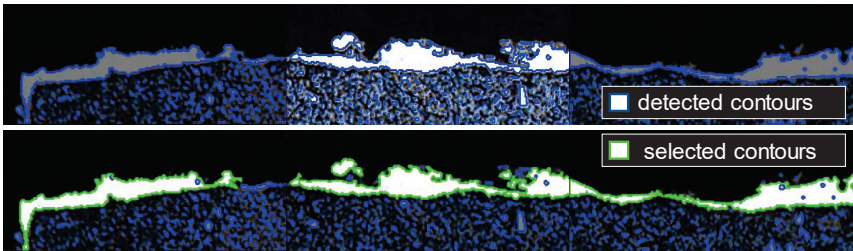


Figure 5.25: Semi-automated detection of the white layer thickness

In order to analyze the relationship between the produced white layer and the process data, the discharge energy distribution of different process settings was created. The calculated distributions were visualized in heat maps. Figure 5.26 first presents the energy distribution for machining a steel material with a height of  $h = 40$  mm and a cutting length of  $l = 32$  mm using a standard technology setting as a reference. The other examples display the energy distributions for modified machining technologies.

The standard technology test demonstrates a largely uniform energy distribution. In contrast, the second and fourth samples show a significantly higher energy input in the center of the sample. When using a technology with an increased discharge time, wire breakage occurred after a cut length of approximately 5 mm. The process was continued without changing the technology and the generated total energy after the wire break is higher than before.

The evaluation of the test with a reduced pulse interval time showed punctual high discharge energy accumulations. By changing the nozzle distance of the lower head to 50 mm and the upper head to 100 mm, in addition to the high energy input in the center of the specimen, very large fluctuations in the discharge energies occurred over the cutting length. In order to investigate the correlation of the discharge energy distribution with the produced white layer, cross sections in both transverse and longitudinal directions of different samples were taken at selected positions, see Figure 5.26.

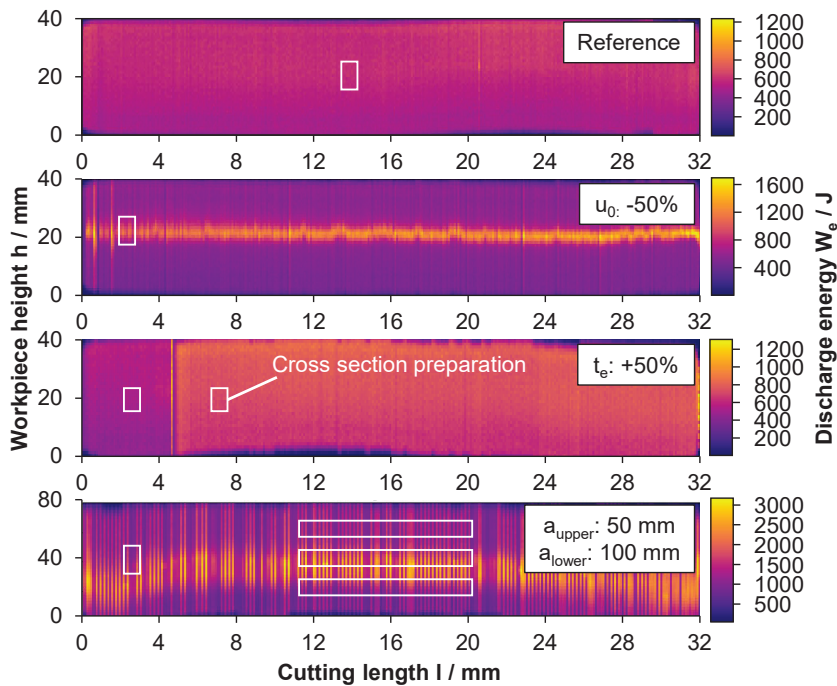


Figure 5.26: Distribution of spatially resolved discharge energy for different settings

After capturing the images with a light microscope, see Figure 5.27 showing some examples, the samples were analyzed using the previously described program for semi-automatic evaluation of the average thickness of the white surface layer.

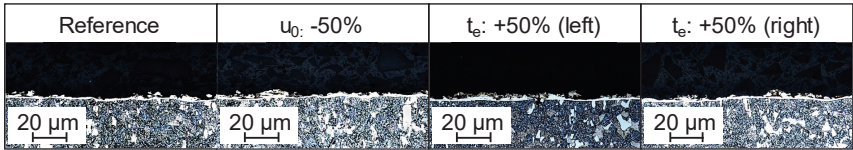


Figure 5.27: White layer analysis of X155CrVMo12-1 machined with different settings

The results are summarized in Figure 5.28. It has been observed that there is no significant correlation between the generated process energy and the white layer. Instead, the results are supported by studies in which a larger white layer is propagated with an increase in the set individual discharge energy [GOST12, LI13, MARA20]. This hypothesis was also examined in detail by Schneider [SCHN21] using different simulation approaches. While a very precise calculation of the energy dissipation was taken into account, assumptions were made to estimate the positional distance between two consecutive discharges.

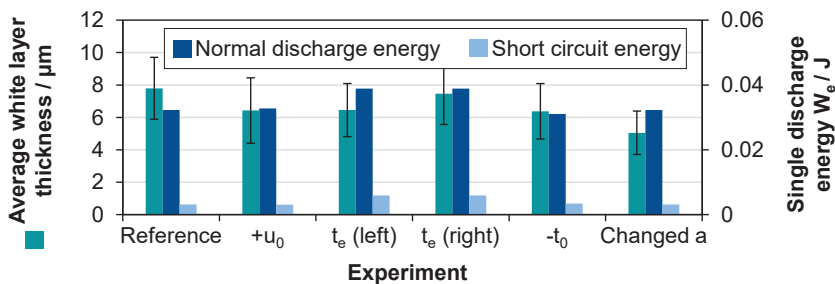


Figure 5.28: Comparison of the white layer and the discharge energy of individual discharges

To verify the hypothesis for wire EDM, the modes for the local and temporal distance of consecutive discharges are plotted in Figure 5.29. For the local distance  $\Delta z$ , the distribution along the height within the cutting path of  $l = 0.1 \text{ mm}$  was considered. For the temporal distance  $\Delta t$ , the ignition delay time  $t_d$  was determined from the data. Finally, a pulse interval time of typically  $t_0 = 10 \text{ }\mu\text{s}$  must be added to calculate the temporal distance of two consecutive discharges. This resulted in most frequent spatial distance of approx.  $\Delta z = 1 \text{ mm}$  and an average temporal distance of  $\Delta t = 15 \text{ }\mu\text{s}$ .

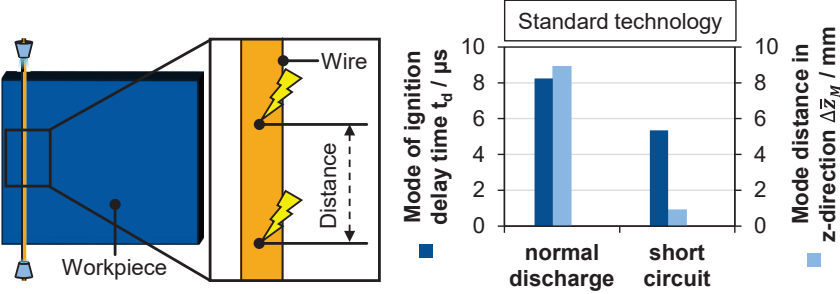


Figure 5.29: Distributions of local distance  $\Delta z$  along the workpiece height and  $t_d$

Considering typical discharge crater geometries, individual discharges typically do not overlap. A very simplified simulation model according to Schneider [SCHN21] illustrates that also no superposition of the generated temperature fields takes place at the determined distances, see Figure 5.30.

There, the worst case was assumed that 100% of the discharge energy is dissipated into the workpiece and no cooling takes place via the dielectric. Nevertheless, no superposition occurs at the measured values and Schneider's hypothesis which states that the surface modification is mainly determined by the individual discharge energy can also be confirmed for wire EDM. The white layer is also determined by constant pre-process settings. Therefore, the white layer thickness was also excluded as a quality factor for this work. However, as with roughness, this evaluation parameter must also be taken into account for further processing steps.

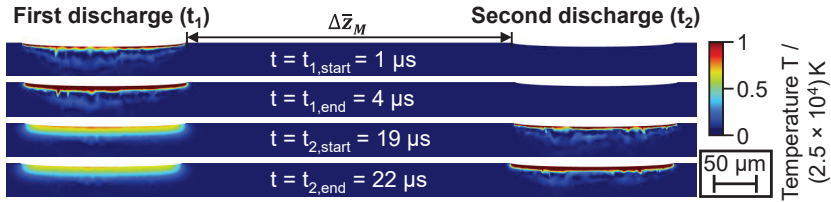


Figure 5.30: Temperature fields of consecutive discharges under determined local and temporal intervals

### 5.3 Summary and Conclusions

In this chapter, different evaluation criteria for the main cut regarding the process productivity and product quality were analyzed. The focus here was on analyzing the influence of changing machining conditions, in particular flushing. For this purpose, continuous process data was recorded to identify possible correlations with process productivity and quality. Statistical analysis was used to determine initial correlations and trends for evaluating productivity by analyzing the speed and occurrence of wire break using the process data. The observations were consistent with previous findings and new knowledge was also gained to understand the influences of discharge distribution and the cutting rate.

To evaluate product quality, macroscopic as well microscopic changes were considered. It was shown in Figure 5.11 that a change in the curvature was produced by changing process conditions which, depending on the extent, could not be compensated by trim cuts. First analyses indicated correlations between the curvature and the discharge distribution over the workpiece height. Thereby, statistical parameters as skewness and kurtosis for the different discharge types were calculated. Based on these findings, the parameter  $e_{max}$  was defined heuristically, which represents a relation between the distribution of normal discharges and short circuits defined in Figure 5.16. It resulted in good correlation with the produced curvature but is depending on the data resolution.

Microscopic changes in the workpiece in the form of surface roughness and white layer were not influenced by changing process conditions such as nozzle distance or workpiece height. These factors are mainly dependent on the single discharge energy, what could be demonstrated through the experimental results and some simulations based on the findings by Schneider [SCHN21]. Therefore, these criteria are not important to monitor in the continuous process because they are determined by defined pre-process setting parameters which impact the single discharge energy.



## 6 Regression Model for Quality Evaluation

Based on the results of the first statistical analyses, this chapter presents regression models to evaluate the produced quality in wire EDM by using continuously recorded process data. As displayed in chapter 5, the variables for evaluating the main cut process are initially limited to workpiece curvatures as a quality criterion. Using recorded process data and measured part geometry data, machine learning models are trained to represent the geometric deviation. The focus here is on predicting the generated curvature, which is to be determined with certain continuous values without measurement. For this purpose, tests were carried out in which the adjustable and non-adjustable process variables were varied separately, and the data was recorded. After data processing and feature engineering, the model architecture was selected while optimizing hyperparameters. Thereto, training and validation data was used. The chosen regression model was finally tested with unknown data and evaluated.

### 6.1 Data Processing

#### 6.1.1 Categorization of Process Influencing Parameters

A process evaluation can be used in EDM to monitor or control the process in real time or to develop as well as optimize a specific machining technology. In order to realize this with the help of a data-driven model, it is of great importance under which conditions the data for the analysis or modeling is generated. For the data basis, experiments were conducted which cover the challenges for an online monitoring system and for a technology development. Thereto, the process influencing parameters in wire EDM are distinguished in two categories: “adjustable” and “non-adjustable” parameters [KÜPP23].

Adjustable parameters are machine parameters, which are set before the beginning of machining. They are used to develop, adapt or optimize a specific machining technology. The configuration and selection of parameter values are made heuristically and mainly based on experience or on time-consuming experiments. This kind of parameters include for example the electrical parameters like discharge current, discharge voltage, and discharge duration as well as the pulse interval time and the open circuit voltage. In addition, mechanical machine parameters like wire tension, wire run-off speed or the flushing pressure belong to it, see Figure 6.1. The selected parameters for the experiments represent the most important ones for technology developments and have great impact on process performance [BERG18a, KLOC07, KUNI05]. They were chosen based on experience, research literature and machine manufacturer advice.

On the contrary, non-adjustable parameters are process influencing parameters, which are mainly defined by the workpiece. The process is influenced by the material of the workpiece and by its geometry. The workpiece geometry affects the process especially with changing machining heights. Machining technologies are optimized for specific machining heights with a defined nozzle distance. Changing heights in a workpiece have also a big impact on the flushing conditions due to changed nozzle distances

[FUJI12, KIMU22]. Wire EDM machines can only control such machining operations to a limited extent. These machining operations are usually associated with a loss of quality or productivity during machining [BERG18a, BERG20b, EBIS18, OKAD15]. To do this, the data generated by these parameters must be processed for process monitoring.

For the selection of the test boundary conditions, a survey was developed in cooperation with the WBA Aachener Werkzeugbau Akademie GmbH. The WBA is a leading partner for tool and die industry in the fields of consulting, digital solutions, training, and research. In a survey, companies from the tool and die industry were asked which process conditions particularly affect the wire EDM process in their production. The machining heights and the selection of nozzle distances were defined based on the results of the surveys in order to cover the requirements as close to the application as possible.

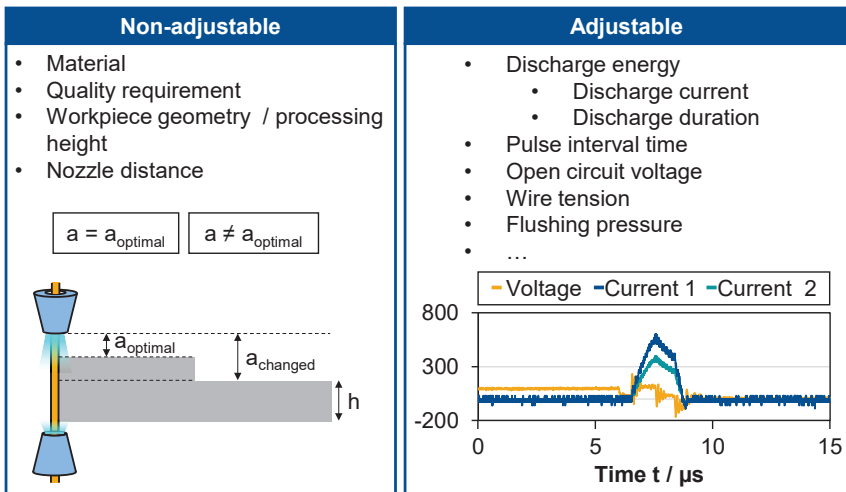


Figure 6.1: Classification of process influencing parameters in “non-adjustable” and “adjustable”

### 6.1.2 Data Generation and Preparation

For data generation, tests were carried out separately for the two categories. A tool steel X155CrVMo12-1 was chosen as the experimental material. The material is a high-alloy cold work steel which is used for high-performance cutting tools, milling cutters, broaches, and stamping tools. This steel is characterized by low residual stresses and ensures that there is no material-based distortion that would affect the measurement and evaluation of the produced curvature [BLEC18]. All tests were performed using the bercocut pro 900 brass wire by bedra with a diameter of  $d = 0.25$  mm, which represents a typical wire for the machined material [BERK24a]. In order to avoid the effect of material distortion, the parts were manufactured with a sufficient thickness.

This was tested in preliminary trials and set at a thickness  $t = 10$  mm. Three different machining heights were selected based on the conducted survey:  $h = 40, 80$  and  $120$  mm. As a reference, the standard machining technology was chosen dependent on the individual machining height which is specified by the technology database of the machine. The selected influencing parameters and the setting for each category are listed in Table 6.1. The adjustable parameters were increased and decreased by 50%. When the upper limit was reached before, it was increased to this maximum. All parameter selections were conducted for every workpiece height. In addition, each variation for the two categories was performed with each other. This results for example in 27 data sets of “non-adjustable parameter” variations.

Table 6.1: Changed process parameters for data generation

Adjustable process parameter			
Discharge current $i_e$ / A	standard	-50%	max.
Discharge duration $t_e$ / $\mu$ s	standard	-50%	+50%
Open circuit voltage $u_0$ / V	standard	-50%	+50%
Pulse interval time $t_0$ / $\mu$ s	standard	-50%	+50%
Wire tension $wt$ / N	standard	-50%	max.
Flushing pressure $p$ / MPa	standard	-50%	+50%
Wire run-off speed $v_D$ / (m/s)	standard	-50%	+50%
Non-adjustable process parameter			
Upper nozzle distance $a_{\text{upper}}$ / mm	10	50	100
Lower nozzle distance $a_{\text{lower}}$ / mm	10	50	100
Varied parameter for all experiments			
Workpiece height / mm	40	80	120

Workpieces with a length of minimum of 30 mm were machined and the curvatures were measured using a coordinate measuring machine (CMM) Prismo navigator by Zeiss [KÜPP23]. The curvatures of every specimen are measured every 1 mm, which means for every experiment setting there are in total 30 curvatures, see Figure 6.2. Due to the large number of measurements, there was also an attempt to automate data acquisition. The geometric parameters are output in a PDF file following a measurement. Therefore, an algorithm in Python was developed to automatically extract the required measurement data from the PDF files and save as a CSV-file.

For developing the machine learning models, more than 7.3 billion counted individual discharges, generated in over 40 hours machining time, were evaluated. This extensive processing time was necessary to generate a sufficiently large amount of data. Despite the signal processing and a strong data reduction, more than 200 GB of information was stored as binary file. Over 2400 contour measurements were performed to predict the curvature. This resulted in a total of over 800 data sets for adjustable process parameters and 1300 data sets for non-adjustable parameters. The models were



partly trained and validated separately with the different data and partly data from both categories were used together. A selection of the results is presented in the following.

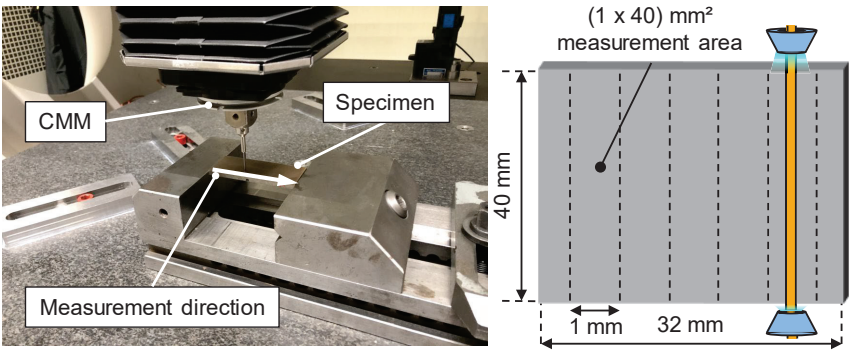


Figure 6.2: CMM measurement setup (left) and measurement procedure (right)

The results for the averaged curvature values considering all experiments with changed adjustable and non-adjustable parameters are plotted in Figure 6.3. Each bar was calculated using 30 measured curvature values. It is apparent from this table that larger curvatures are produced when machining higher components. Interestingly, a higher standard deviation was observed for the curvature produced during poor flushing conditions. This represents a first indication for process instability and confirms the importance of flushing conditions by the state of the art [BERG20d, KIMU22, KLOC07].

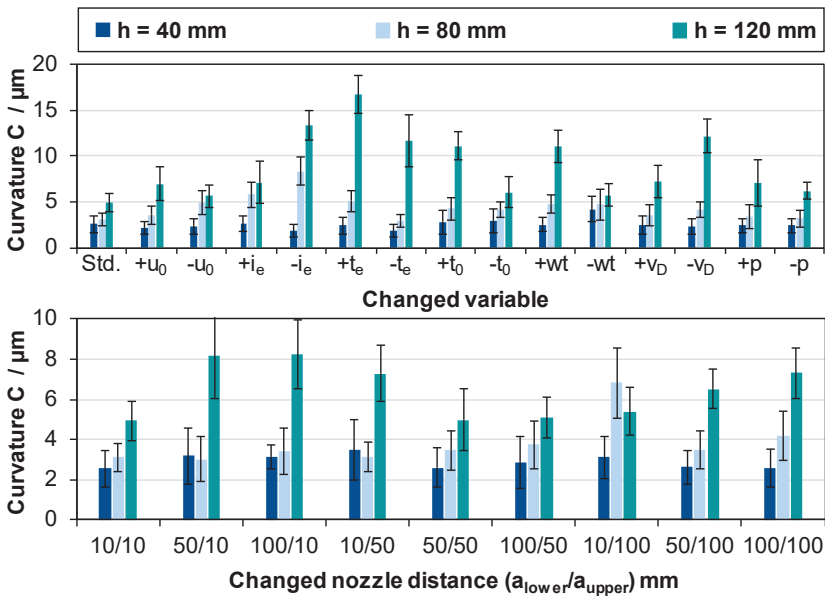


Figure 6.3: Curvatures machined with varied adjustable and non-adjustable parameters

Before training a model, it is essential to define which features are potential input parameters for a supervised machine learning model. Although after preprocessing, 3 GB sized data is compressed to about 1 MB files, there are still too many selectable features since adding more features increases the dimensionality and some tasks become exponentially more difficult as this number increases [GOOD16, BADI20]. Therefore, feature engineering is performed initially before selecting and training models to create meaningful features from existing data [PLAU21]. Various aspects are taken into consideration for this. Firstly, more input parameters are initially used, even if these increase the training times, to achieve the highest possible model performance. Nevertheless, a dimension reduction was carried out by feature selection to exclude the input parameters that do not generate any added value for the models. The averaging time or interval sizes were also factored in, which considers data-based changes but can also be used to represent physically interpretable results. Depending on the parameter, these are calculated with different local resolutions. Figure 6.4 illustrates how this resolution can take place in principle. For some parameters, only averaging over the total height is more meaningful. For example, it must be considered that the CMM measurements in the cutting direction were not only sensibly set to a distance of  $\delta_x = 1\text{ mm}$  from a metrological point of view, but that the recorded process data also allows such a compression ensuring no loss of relevant information. The division into grids in the  $\Delta x$  and  $\Delta z$  directions is very interesting, especially for the ratios of normal discharges and short circuit illustrated in Figure 6.4. In the following, the influence of the interval size on the characteristic values is examined and the calculation of the discharge type ratios is explained in more detail.

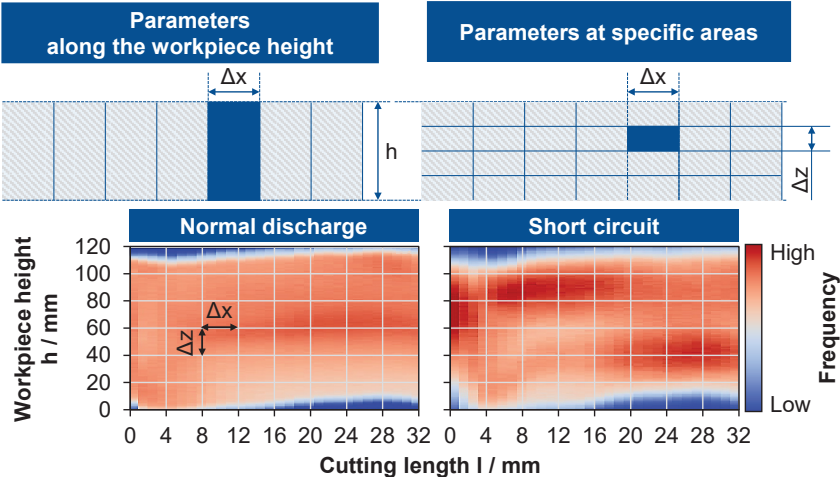


Figure 6.4: Data processing using different resolutions

### 6.1.3 Effect of Interval Sizes on Data

The processed data is summarized in matrices with input and output data. Table 6.2 shows an example of a data matrix. Each row characterizes here one millimeter of the

machined component and is given in total such as the number of discharges and energy  $W_e$  or as an average value such as  $f_e$  or  $r_n$ . As the individual discharges can also be assigned a position in the Z direction, the areas can also be compressed within the height.

Table 6.2: Example of a data matrix with measured and extracted features

$f_e$ [Hz]	Discharges $\times 10^6$	$r_n$	$\bar{I}_{e,normal}$ [A]	$\bar{I}_{e,short}$ [A]	$W_e$ [mJ]	$v_f$ [mm/min]	Curvature C [ $\mu$ m]
31411	3.85	0.41	121.5	46.6	67834	0.499	10.4
35844	4.78	0.45	103.1	43.2	86431	0.459	8.8
35907	4.78	0.43	101.8	42.8	86939	0.458	8.4

The selected interval size of one millimeter for the tests can be varied as required and is limited only by the sampling frequency of the position determination program. In this way it can be decided whether a more detailed resolution and thus smaller evaluation intervals should be used. This would increase the amount of data available. In addition, the influence of a lower resolution on the characteristic values is determined. If there are no major changes between large and small intervals, the resolution can be reduced, since a more detailed resolution does not provide any additional information, and the workload can be reduced due to the smaller area measurements.

Next, the number of discharges is observed to illustrate the effect of interval size. Intervals of size  $\Delta x = 0.25$  mm and  $\Delta x = 4$  mm are compared to the  $\Delta x = 1$  mm interval size used for the tests. The results are plotted in Figure 6.5 for  $l = 32$  mm of cutting length machining a workpiece with a height of  $h = 40$  mm using a standard steel technology. The number of discharges at  $\Delta x = 0.25$  mm and  $\Delta x = 4$  mm is scaled to allow comparison of the three curves. The scaling factor is set to  $S = 4$  or  $S = 0.25$ , so that the data points represent the discharges per millimeter. The data is shown here as lines without dots for clarity.

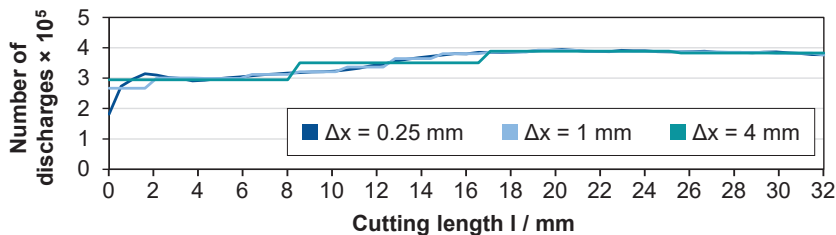


Figure 6.5: Influence of interval sizes on the number of discharges

In the range between  $l = 8$  mm to 16 mm, all three tests result in almost identical patterns. Here the number of discharges is at a constant level and not subject to large fluctuations. A higher resolution does not generate more information. In the front area, however, the number of discharges changes much more. While the curve with an interval size of  $\Delta x = 1$  mm still shows the fluctuations well, there are already significant deviations at an interval size of  $\Delta x = 4$  mm. The contour values associated with this

test in Figure 6.6 show that the values in the cut area in particular are subject to strong fluctuations. Therefore, evaluation with an interval size of  $\Delta x = 4$  mm is not recommended. Much better results can be obtained with an interval size of  $\Delta x = 1$  mm. Only slight deviations from the interval size  $\Delta x = 0.25$  mm can be observed here.

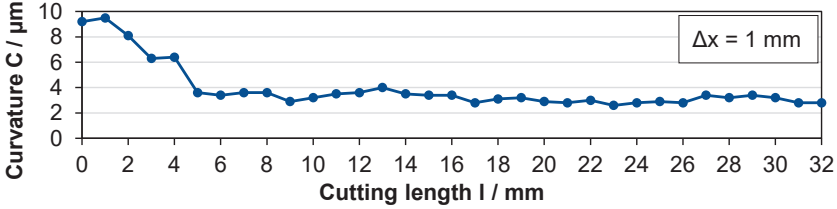


Figure 6.6: Curvature of a machined sample with an interval size of  $\Delta x = 1$  mm

For two reasons the interval size is left at  $\Delta x = 1$  mm for the following test series. First, the evaluation of curvature measurements revealed that deviation is constant during unchanged process condition which can also be seen in Figure 6.6 between the cutting length of  $l = 5 - 32$  mm. Second, the correlation of the measured process data with the determined surface properties is significantly more difficult with very small intervals and not useful in practice.

Beside the ratio of normal discharges to total discharges, discharge distribution characteristics in z-axis directions and many other features could be extracted from these data points. In the preprocessed file, the number of normal discharges and short circuits are recorded in every  $(\Delta x \cdot \Delta z)$  mm<sup>2</sup> square in x- and z-axis as a data point. All these squares with same x coordinate from 0 mm to the height of workpiece in z-axis together represent one curvature value. For example, to calculate the average ratio of normal discharges to total discharges for a specific cutting length interval  $\bar{r}_n(x_i)$ , all normal discharges are summed up and divided by sum-up total discharges in range of  $z_0 = 0$  mm to height of workpiece  $z_h$  in the same x position  $x_i$ , as equation 6.1 shows:

$$\bar{r}_n(x_i) = \frac{\sum_{j=0}^h n_{x_i, z_j, normal}}{\sum_{j=0}^h n_{x_i, z_j, total}} \quad (6.1)$$

With the same calculation the ratio of short circuits  $\bar{r}_s(x_i)$  is defined as follows:

$$\bar{r}_s(x_i) = \frac{\sum_{j=0}^h n_{x_i, z_j, short\ circuit}}{\sum_{j=0}^h n_{x_i, z_j, total}} \quad (6.2)$$

Figure 6.7 depicts an overview of the number of total discharges for an unstable process with a resolution of 1 mm  $\times$  1 mm considering cutting length and workpiece height. In order to explicitly analyze the correlation of the local ratio of normal discharges and short circuits with the curvature, new height-dependent characteristic values were created. As already explained, the local ratio of different discharge types is formed for each area on the workpiece surface. This results in a different number of values depending on the height and area division.

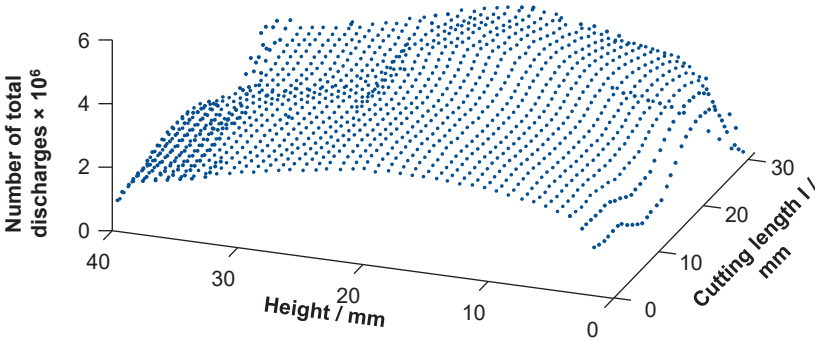


Figure 6.7: Plotted number of total discharges with a resolution of 1 mm × 1 mm

As the data set consists of different workpiece heights and the areas for  $\Delta z$  therefore varies, relevant features for the machine learning model may be lost as a result. For this reason, in addition to the determined statistical parameters of the median, arithmetic mean, standard deviation, variance, kurtosis, skewness and mode, new parameters  $k_i$  are introduced that are intended to put the discharge distribution of the upper, lower and middle areas of the workpiece height in relation to each other. The index  $i$  describes the underlying data (normal discharge, short circuit, all discharges) and the quantile ranges  $q$  dividing the data in different parts. A graphical representation of this calculation is illustrated in Figure 6.8.

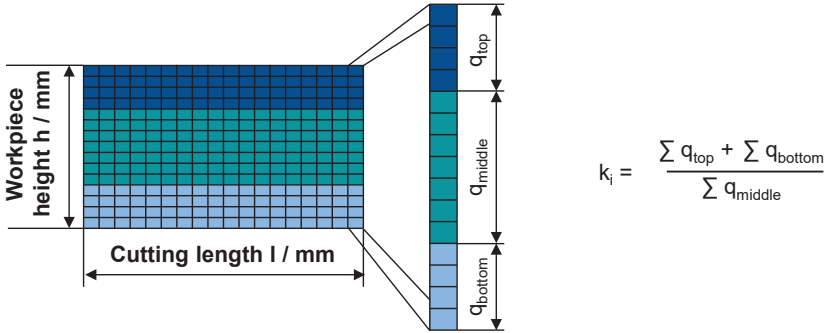


Figure 6.8: Calculation of the  $k$  and  $q$  values

It was also proven that no relevant information got lost by using the specified interval sizes for the calculation of the statistical variables. This can be illustrated briefly by Figure 6.9 representing the data of same experiments conducted before machining a workpiece height of . Three different widths of data are selected here:  $\Delta x = 0.2$  mm, 0.5 mm, and 1 mm. The comparison reveals that there are no significant differences in the data between these three widths, except for kurtoses of first 2 mm and last 2 mm, which show slight differences. This could occur due to the instability of the machining condition, especially at the entry and exit of the parts. Also it can be observed because of the poor flushing conditions particularly at these points

[OKAD15]. The result underlines again that the width of  $\Delta x = 1$  mm can well represent surface quality of certain small area. These analyses were performed for all relevant input parameters and the results are almost the same.

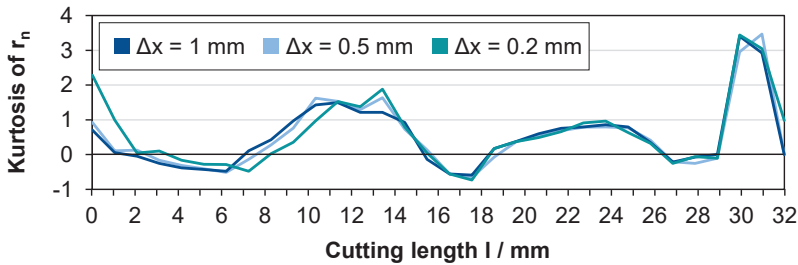


Figure 6.9: Kurtosis comparison of different data widths

Finally, an important and last step of data preparation is scaling. The data for training a machine learning or deep learning model can sometimes have large jumps in its value ranges. Moreover, data recorded in real experiments often contain outliers due to individual measurement errors or other interferences that cannot always be corrected, or for research reasons, are not always desired. Scaling reduces the effect of these influences. Used features can also have different ranges, for example, for heights  $h = 40$  and  $120$  mm, the skewness and kurtosis vary from  $K = -5$  to  $5$ , while the standard deviation can be more than  $\sigma = 10$ . If these parameters are directly fed into the model, parameters with higher values and ranges could have more influence on the network than others. To avoid this, the range of features need to be normalized. The “Standard Scaler” is used extensively; its functionality is based on a simple mathematical transformation. The data is presented as the quotient of the difference between the data point and the mean value and the standard deviation. The transformation is calculated as follows [PATR15, RAJU20]:

$$x' = \frac{x - \bar{x}}{\sigma} \quad (6.3)$$

$x$  is the original feature vector,  $\bar{x}$  is the mean value of  $x$ , and  $\sigma$  is the standard deviation. After the normalization, the average value of  $x'$  is zero and its standard deviation is one [PATR15, RAJU20].

## 6.2 Feature Engineering

Only information based on physical parameters were used to train the models. Input parameters such as the information of nozzle distance or knowledge about the changed variable for the respective datasets were intentionally not used for training the algorithms. A neural network can recognize and exploit obvious and unknown correlations. Since some input parameters have a simple formulaic relationship with other parameters, a supervised machine learning algorithm can learn these relationships independently. These types of parameters provide no additional information and can be neglected.

There are simple examples such as the feed rate and the cutting rate, which are formally defined by the multiplication of the workpiece height. Also, the number of different discharge types can be calculated with their ratio values and the number of total discharges. To ensure a recommended dimension reduction for the machine learning models, it is necessary to identify the main variables determining the data. For this purpose, Exploratory Data Analysis (EDA) has been conducted using descriptive statistics, visual data exploration and correlation analysis.

The machined workpiece height has a large influence on the generated curvature of the part. As can be seen in Figure 6.3 larger workpieces have a greater potential for curvature and therefore have a large influence on the target value used for the algorithm. In addition, the cutting speed is strongly dependent on the workpiece height. For this reason, the use of a parameter that differentiates between the various heights will be selected as an input parameter for the algorithm.

To do this, the curvature is plotted in a graph as a function of the number of discharges and process energy in Figure 6.10 (a) and (b). Clear clusters can be seen here that allow the data to be assigned to different workpiece heights. The graphs (c) and (d) indicate a certain correlation between the pulse effective frequency  $f_e$  and the ratio of normal discharges  $r_n$  with the produced curvature. As  $f_e$  increases and  $r_n$  decreases, the curvature  $C$  appears to be less pronounced.

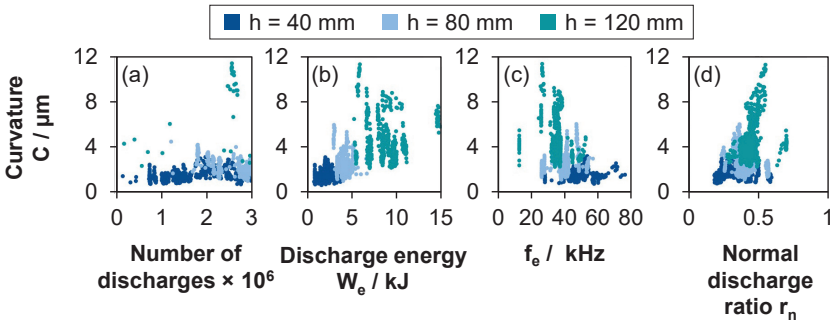


Figure 6.10: Curvature as a function of the total number of discharges (a), discharge energy (b), pulse effective frequency (c) and norm discharge ratio  $r_n$  (d)

Beside scatter plots, the relation between the process parameters has also been analyzed by visualizing various statistical parameters with the target value. As an example, kurtosis of the ratio of normal discharges and the generated curvature for the workpiece height of  $h = 120$  mm are plotted in Figure 6.11. This was carried out separately for a large number of parameters for the different workpiece heights.

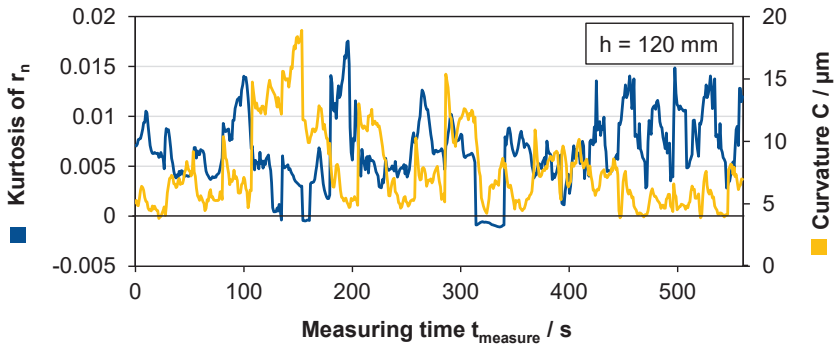


Figure 6.11: Kurtosis of the ratio of normal discharges  $r_n$  for  $h = 120$  mm workpiece heights

To systematically identify relevant input parameters, in addition to the evaluation based on technological knowledge and visual data exploration, correlation analyses were performed to determine the influence of process parameters on process performance. These analyses involve calculating correlation coefficients using three different methods, which ensures more robust and reliable analyses.

A measure of the strength of a linear relationship is the empirical correlation coefficient, also known as the Bravais-Pearson correlation coefficient  $r$ . It is assumed that characteristics are related, if the values are arranged in such a way that as the value of characteristic  $x$  increases, the value of characteristic  $y$  also tends to rise. The coefficient can be calculated by the following equation (6.4) [FAHR16]:

$$r = r_{XY} = \sum_{i=1}^n \frac{(x_i - \bar{x})(y_i - \bar{y})}{\sqrt{\sum_{i=1}^n (x_i - \bar{x})^2 \sum_{i=1}^n (y_i - \bar{y})^2}} \quad (6.4)$$

This correlation coefficient measures the strength of the linear relationship. Typical interpretations for  $r$  are:

- low correlation:  $|r| < 0.5$
- moderate correlation:  $0.5 \leq |r| < 0.8$
- high correlation:  $0.8 \leq |r|$

However, for systems that cannot be measured accurately, lower values may still indicate good correlations. It is important to note that this correlation coefficient cannot indicate non-linear correlations [FAHR16].

An alternative calculation of the correlation properties is the Spearman's method. This method replaces the data with their ranks. The rank describes the position a value would occupy if it was sorted by size. The advantage of the Spearman coefficient is that it can index not only linear but also non-linear relationships. Spearman's correlation coefficient is now obtained as the Bravais-Pearson correlation coefficient applied to the rank pairs and calculated by equation (6.5) [FAHR16]:



$$r_{SP} = \sum_{i=1}^n \frac{(rg(x_i) - rg(\bar{x}))(rg(y_i) - rg(\bar{y}))}{\sqrt{\sum_{i=1}^n (rg(x_i) - rg(\bar{x}))^2 \sum_{i=1}^n (rg(y_i) - rg(\bar{y}))^2}} \quad (6.5)$$

Kendall's calculation is another common method to quantify the correlation using only the ordinal scale level of the data. It is mainly used to compare the proportion of concordant and discordant data. It compares pairs  $X$  and  $Y$  of data. A pair is concordant if the observation that has a higher rank for  $X$  also has a higher rank for  $Y$ . Otherwise the pair is discordant. If the pair is neither concordant nor discordant, it is called tied. An advantage of calculating concordance measures is that, unlike correlation coefficients, probability-based measures can also be described in the population. Kendall's  $\tau_a$  is a concordance measure that relates the difference between concordant  $N_c$  and discordant  $N_d$  pairs to the number of pairs that can be formed from  $n$  observations [FAHR16]:

$$\tau_a = \frac{N_c - N_d}{n(n-1)/2} \quad (6.6)$$

Figure 6.12 presents exemplary the correlation and concordance measures of the three different calculation methods evaluating the relationship between the produced curvature and several process parameters. All three measures have a range from -1 to 1, where -1 indicates negative correlation or discordance, 1 indicates positive correlation or concordance, and 0 indicates no correlation or no concordance. Since only the magnitude of the correlation or concordance is of interest in this case, the values in this diagram are reported as absolute values. The results agree with the visual analysis. The statistical distribution of different discharge types over the workpiece height has a high influence on the produced curvature. Especially, the median of the ratio of normal discharges has a high correlation coefficient, whereas the ratio of normal discharges  $r_n$  and the factor  $e_{\max}$  do not result with same high correlation values. In addition, the k-factor correlates with the curvature with a quantile classification of 33%. A total of over 300 statistical variables were determined and evaluated using an automated feature extraction approach. This was carried out both separately and for all workpiece heights together.

For example, the Shannon Entropy for normal discharges and short circuits are plotted here. For a categorical characteristic with  $K$  possible values, it can be obtained that the relative frequencies  $f_1, \dots, f_K$  of the occurrence of each value by dividing the absolute frequencies  $n_1, \dots, n_K$  by the size of the sample  $n$ . The absolute frequencies always add up to  $n$ , the relative frequencies to one. The characteristic with the highest frequency, i.e. the maximum value for  $f_k$  or  $n_k$ , is the position parameter, which is known as the mode. In a bar chart, it corresponds to the highest column. The Shannon Entropy, on the other hand, is a measure of the extent to which all columns have a similar height. It measures the degree of uncertainty or randomness in the dataset. A higher entropy occurs when the data distribution is uniform, reflecting maximum unpredictability. Conversely, lower entropy indicates that some values are much more likely than others, showing predictability and less diversity in the dataset [MURP12, PLAU21].

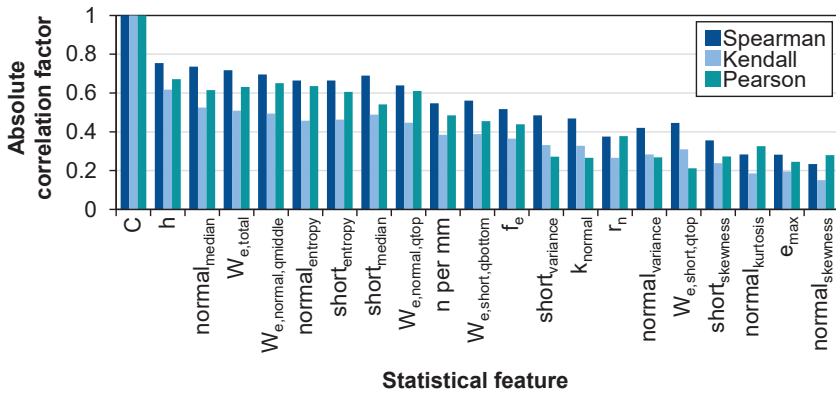


Figure 6.12: Correlation analyses of the curvature and determined statistical features

### 6.3 Regression Model Architecture

Chapter 5.3 already provided first insights into the generated data. There were no direct, linear correlations between the parameters and the surface contour to be predicted. With this level of complex correlations, the application of a supervised machine learning algorithm is appropriate [GOOD16, PLAU21]. The problem with the given input and output data and the number of input parameters is suitable for building a neural network. It enables independent learning of hidden correlations and can then make predictions based on new input data. The available data is divided into training, validation, and test data. The training dataset is used to train the model, the validation dataset is used to monitor the performance and optimize the hyperparameters, and the test dataset is used to evaluate the final performance of the model. Using separate datasets for these purposes helps to ensure that the model is well generalized and not overfitted [BISH06]. In this work, the proportion of training data is set to  $\alpha = 70\%$ . Thus, approx. 1500 training data sets and 600 validation and test data sets are available.

#### Functionality of Artificial Neural Networks

The general structure and basics of neural networks were presented in chapter 2.3 and illustrated in Figure 2.6. In artificial neural networks data is transported between the nodes via the weighted edges. The nodes of the previous layer are connected to the nodes of the subsequent layer by edges. If all nodes of layer  $A$  are connected to all nodes of the subsequent layer  $B$ , this is referred to as a fully connected layer. The weighting remains the same for each edge. In general, the significance of node information for the subsequent node is determined by the edge weighting. This information can be summarized in a simplified weighting matrix. The information of the units of each layer can be recorded in vectors. Bias is used for scaling in addition to the channel weights. These help to keep the value of the nodes within a certain interval or to increase their influence on the resulting outcome. They shift the values of the output up or down like the Y-intercept of a linear function [AUST21, MURP12, PLAU21].

Basically, there are two types of parameters in artificial neural networks. Parameters such as the weighting of the edges or the bias are continuously adjusted during the training phase. They only remain unchanged after the training phase. The initial values of these parameters are arbitrary. Hyperparameters, on the contrary, must be defined before the start of the test phase. They contain the structure and functionality of a neural network. Hyperparameters include the number of layers, the number of nodes per layer, the shape of the activation function within the nodes, the learning rate and the batch size [MATZ21]. The parameters remain unchanged throughout the lifetime of the neural network. The following section explains how the network is built in detail and how the model can be optimized by adapting hyperparameters [MURP12, RICH19, STYC17].

A feed forward neural network is the simplest form of artificial neural network and was employed here. It is based on a hypothesis space that consists of functions of the following form as:

$$f: \mathbb{R}^{D_0} \rightarrow \mathbb{R}^{D_L}, f(u) = (f_L \circ f_{L-1} \circ \dots \circ f_1)(u) \quad (6.7)$$

Every layer  $f_l$  for all  $l \in \{1, \dots, L\}$  is a function of following form as

$$f_l: \mathbb{R}^{D_{l-1}} \rightarrow \mathbb{R}^{D_l}, f_l(u) = \phi_l(w^{(l)} \cdot u + b^{(l)}) \quad (6.8)$$

with so-called activation functions  $\phi_l: \mathbb{R}^{D_l} \rightarrow \mathbb{R}^{D_l}$  and matrices of weights  $w^{(l)}$  in the format of  $D_l \times D_{l-1}$  and the offset vectors  $b^{(l)} \in \mathbb{R}^{D_l}$ . The component functions  $f_{11}, \dots, f_{lD_l}$  represent the neurons of the respective  $l$ -th layer, a certain function value represents an activation of the neuron. The first layer is the input layer, the last layer  $f_L$  represents the output layer and the middle layer where  $1 < l \leq L$  is called the hidden layer as shown in Figure 2.6. The number of layers determines the depth of the network and the number of neurons in each layer determines its width.

Each node corresponds to a neuron. Neurons in a given layer are linked to each neuron in the next layer by weights. The incoming information in a node is processed within a node by an activation function. The choice of activation function is pivotal in shaping the behavior and learning capabilities of a neural network. This mathematical function determines the output of a neuron based on its input, introducing non-linearity essential for capturing complex relationships. The variety of activation functions can be broadly categorized into two classes: piecewise linear and locally quadratic functions. Piecewise linear functions consist of one or more linear segments, while locally quadratic functions exhibit non-zero second-order derivatives [RSA20, SHAR20, YUEN21]. These distinctions are illustrated in Figure 6.13.

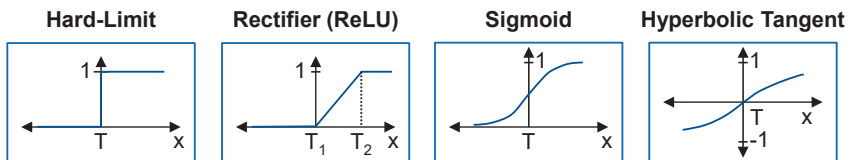


Figure 6.13: Various activation functions based on [MIRF22]

At its core, an activation function operates similar to a threshold function, activating the neuron once a certain threshold is surpassed. Linear activation functions simply transmit input to output, proportionally increasing with the input signal. Non-linear alternatives include the sigmoid function, bounded between 0 and 1, and the zero-centered hyperbolic tangent function (Tanh), ranging between -1 and 1. Other common activation functions include Rectified Linear Unit (ReLU), Gaussian Error Linear Units (GELU), and Sigmoid Weighted Linear Units (Swish), which lack output limitations in the positive range [RASA20, SHAR20, YUEN21].

In order to determine the model parameters weight and bias as quickly as possible, the algorithm does not adapt them individually, but all model parameters are optimized simultaneously during the training phase. During the forward pass, the input data is fed through the network, and predictions are made. Then, during the backward pass, the error between the predicted output and the true output is calculated.

Before the ANN delivers meaningful results, it must learn the relationship between the input and target variables. To do this, the model parameters weight and bias are optimized simultaneously during the training phase by using backpropagation. In a first step, arbitrary edge weights are defined. The untrained model propagates the values of the initial nodes from the training data. These are compared with the real measured results and the error is determined [MATZ21, WERB88]. This error between the predicted output values of the model  $\phi(u_i, w, b)$  and the corresponding correct output values  $y_i$  from the training data is calculated using the loss function  $E$ . The most common loss function is the Mean Squared Error (MSE) loss and is calculated considering the number of observations  $n$  as follows [MATZ21, WANG22]:

$$E = \frac{1}{n} \sum_{i=1}^n (y_i - \phi(u_i, w, b))^2 \quad (6.9)$$

MSE penalizes larger errors more than smaller ones because the differences are squared. The smaller the error  $E$ , the better the artificial neural network is adapted to the data set. How many data points are used for each optimization loop can be defined by the user as a so-called batch size. Batch sizes can range from just 1 data point to so-called "mini batches" (for example 10-100 data points) to a full data set in each optimization loop. The optimization of the model parameters by means of backpropagation takes place in the following six steps [GOOD16, MATZ21]:

1. For the first run all weights  $w$  and biases  $b$  are determined randomly and the error  $E$  is calculated for the first batch of data points.
2. Before the second run,  $w$  and  $b$  are changed slightly by random values  $\delta w$  and  $\delta b$ .
3. With the changed model parameters  $w$  and  $b$ , the error  $E$  is calculated for a new batch of data points.

4. Since the weightings of the connections to the subsequent layer are known, the influence of the individual neurons of the previous layer on the change in the error  $\delta E$  can be calculated. This is continued layer by layer up to the input layer (backpropagation).
5. Since it is now known what proportion of  $\delta E$  each neuron in the layer has, it is possible to calculate which ratios  $\frac{\delta E}{\delta w}$  and  $\frac{\delta E}{\delta b}$  exist between the change in the error  $\delta E$  and the change in the model parameters  $\delta w$  and  $\delta b$ .
6. The model parameters  $w$  and  $b$  are calculated and updated using the ratios  $\frac{\delta E}{\delta w}$  and  $\frac{\delta E}{\delta b}$  with the gradient descent or other optimization methods.

The algorithm repeats steps 3 to 6 until a pre-defined number of runs have been completed or the error  $E$  no longer improves. The backpropagation thus allows to assign the influence of the change in the error  $\delta E$  to each neuron. Since the changes in the weights  $\delta w$  and threshold values  $\delta b$  and the last optimization are known for each neuron at the same time, it is possible to calculate which positive or negative influence the change in all model parameters  $w$  and  $b$  had on the error  $E$  [MATZ21].

The gradient method is employed to minimize the model error. When the error measure reaches a satisfactory level, the backpropagation process can cease; otherwise, weight adjustments are computed. This involves partially deriving the error function, with respect to all connection weights. For each weight, the resulting direction indicates the steepest increase in the error function, guiding adjustments for optimal error reduction. Since the aim is error minimization, weights must be adjusted in the opposite direction of this increase, negating it accordingly. Additionally, these adjustments are scaled by a step size factor, known as the learning rate  $\eta_k$ , which determines the model responsiveness to error in each iteration. Another important parameter, the momentum, ensures convergence to a local optimum regardless of the starting point, known as global convergence. Exact line searches may result in a “zig-zag” behavior along the descent path due to the perpendicular relationship between consecutive gradient directions and search directions. To mitigate this, a momentum term  $(\theta_k - \theta_{k-1})$  where  $0 \leq \mu_k \leq 1$  controls the importance of the term, is suggested to reduce zig-zag behavior by adding inertia to the descent direction, promoting smoother convergence towards the optimum solution. One of the simplest algorithms for unconstrained optimization is gradient descent, also referred to as steepest descent and can be expressed as follows [ERB93, MURP12]:

$$\theta_{k+1} = \theta_k - \eta_k g_k + \mu_k (\theta_k - \theta_{k-1}) \quad (6.10)$$

These two important hyperparameters can be adaptively optimized during training using the Adaptive Moment Estimation (ADAM) algorithm. ADAM is an adaptive learning rate optimization algorithm that directly incorporates momentum as an estimate of the first-order moment of the gradient, using exponential weighting. Additionally, this method includes bias corrections for both the first order and second order moment

estimates to account for their initialization at the origin. This correction ensures more accurate moment estimates, particularly early in the procedure [KING14, ZHAN18b]. In this work, the ADAM algorithm was used for all models in combination with back-propagation.

## 6.4 Training the Regression Model

In the development of an artificial neural network, the identification of appropriate hyperparameters stands as a critical precursor to the model's subsequent performance. However, the abundance of hyperparameters poses a significant challenge in this regard. There are no clear rules for determination of hyperparameters. The predominant approach frequently employed involves a fusion of Grid Search and manual exploration [BERG12]. This typically involves experiments, wherein a multitude of potential hyperparameter variables are systematically combined to generate various model configurations. The outcomes of these experiments serve as a basis for model development. Should the performance of the leading model fall short of expectations, further grid experiments can be conducted to refine the model. Alternatively, the Random Search method presents an alternative approach to optimize hyperparameters. This method entails the development of a script that either randomly selects hyperparameters from a predefined list or generates numerical values utilizing a random number generator. In a study by Bergstra et al. [BERG12], the efficiency of Grid Search was compared to that of the Random Search method. The findings suggested that Random Search often proves to be a more efficient strategy, given that only a handful of hyperparameters significantly influence model performance across numerous datasets. Consequently, the Grid Search approach is rendered inefficient, as it expands considerable effort in less critical dimensions. In contrast, the Random Search method is frequently more adapted at navigating through larger, albeit less promising, configuration spaces [BERG12, FLOU09, LIAS19].

Therefore, the Random Search approach was performed. The parameters presented in Table 6.3 were tested. For the selection of data for training and validation, cross-validation was conducted. Cross-validation is a statistical technique for evaluating learning algorithms by dividing data into two segments: one for training the model and the other for validating it. The process involves successive rounds where training and validation sets interchange, ensuring that each data point is validated against the others. The most common form is k-fold cross-validation, with other variants being derived from it or involving repeated rounds of k-fold cross-validation. In k-fold cross-validation, data is divided into k equally sized segments or folds. Through k iterations, each fold is held out for validation while the remaining k-1 folds are used for training [GOOD16, REFA09].

The first meaningful hyperparameters can be derived from the data extracted in chapter 5. The structure of the data determines the structure of the input and output layers. Thus, the 18 input parameters can enter the neural network through the same number of input nodes. Since the curvature and the feed rate are the only output parameters for each model, the neural networks end in a single node. The number of hidden layers

or nodes is arbitrary. Since the problem is not a simple classification problem, more than one hidden layer should be employed. As mentioned before, the standard scaler was used for all models in this work. The Random Search approach was applied to 10 different validation sets on the basis of cross-validation. The data sets were each used to train 50 iterations with random configurations of the hyperparameters that lie within the specified ranges listed in Table 6.3.

Table 6.3: Conditions and hyperparameter options for Random Search

Random Search					
Iterations	K-Fold		Termination criterion		
50	10		Loss of testing set		
Random Search hyperparameter options					
Layer	Activation functions	Batch size	Learning rate	Neurons	Epochs
1 - 20	Sigmoid, Tanh, Relu, Gelu, Hard Sigmoid, Linear Swish	1 - 4	0.0001 - 0.1	1 - 64	1 - 10

To monitor model training and hyperparameter selection, and to avoid possible overfitting, the loss and accuracy of the test and validation data were evaluated. While the Mean Squared Error MSE is used for the loss function, the accuracy is calculated using the Mean Absolute Percentage Error (MAPE). The MAPE is a measure of the accuracy of a prediction model or a prediction method as a percentage. It indicates the average percentage by which the predictions  $\hat{y}_i$  of the model deviate from the actual values  $y_i$  [KHAI17]. It has been shown that learning under MAPE provides good results for regression models [MYTT16]. It is calculated considering the number of observations  $n$  as follows [KHAI17]:

$$MAPE = \frac{100\%}{n} \sum_{i=1}^n \left| \frac{y_i - \hat{y}_i}{y_i} \right| \quad (6.11)$$

The prediction accuracy is determined by the difference of the MAPE and the theoretical maximum possible accuracy:

$$Accuracy = 100\% - MAPE \quad (6.12)$$

Following the hyperparameter optimization, the loss and accuracy for the test and validation data is plotted in Figure 6.14. Both training and validation curves show improvement, indicating the model is learning effectively. The best results for the validation data were obtained for both the loss and the accuracy with an epoch number below 10. The performance of the model deteriorates for a higher epoch number and indicates overfitting which can be avoided by implementing regularization techniques, using more training data, or early stopping applying a small number of epochs. Therefore,

the best result for the hyperparameter selection was obtained with an epoch number between 1 and 10.

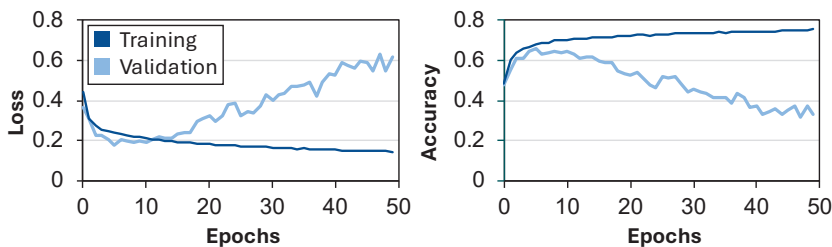


Figure 6.14: Loss and accuracy training and validation sets

6.5 Testing the Regression Model

Initially, the regression models for the evaluation of the quality, in this case by predicting the generated curvature, were built separately for using adjustable and non-adjustable parameters and some results are presented in [KÜPP23]. However, with increasing variance within the curvature or output size, it has been shown that the performance of the models can be improved by increasing the data volume. Therefore, several regression models were developed that use process data from both changing adjustable and non-adjustable parameters. In the following a model is presented, that was built based on three hidden layers which consist of 2, 5, and 1 neurons. The learning rate was set to approx.  $\eta_k = 0.02$  and the batch size to one. The best performing neural network achieved an accuracy of almost 75% indicating a good level of explained variance. Especially, in the field of manufacturing [PATU21] where curvature is predicted in micrometers, the model shows significant potential. Under unchanged process conditions, the curvature remains almost constant, demonstrating the model's capability to provide accurate predictions in practical applications. The final structure of the ANN model and the used hyperparameters are presented in Figure 6.15.

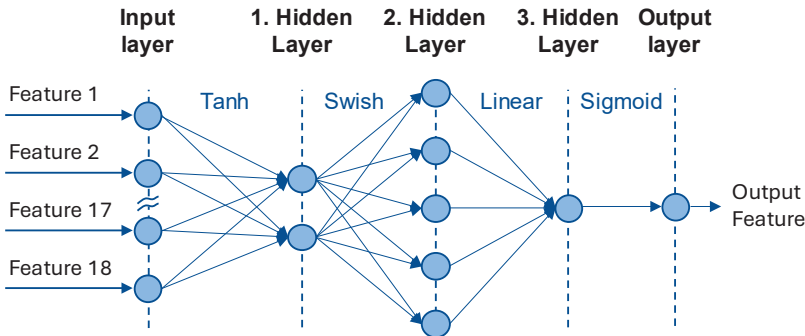


Figure 6.15: Structure of the used neural network

Figure 6.16 shows the results for the test data. The left plot shows both the measured and predicted curvature values for all test data. In the right diagram the predicted



curvatures are plotted over the actual curvatures. Overall, the metrics indicate that the model has a satisfactory ability to predict curvature in the micrometer range. In addition to the MAPE and coefficient of determination  $R^2$ , the MSE and MAE (Mean Absolute Error) were calculated to quantify the average size of the errors. Unlike the MSE, the MAE reflects the absolute differences between the predicted values  $\hat{y}_i$  and actual values  $y_i$  rather than the squared differences. The MAE is therefore less sensitive to outliers than the MSE. Considering the number of observations  $n$  the MAE is calculated as follows [MATZ21]:

$$MAE = \frac{1}{n} \sum_{i=1}^n |y_i - \hat{y}_i| \quad (6.13)$$

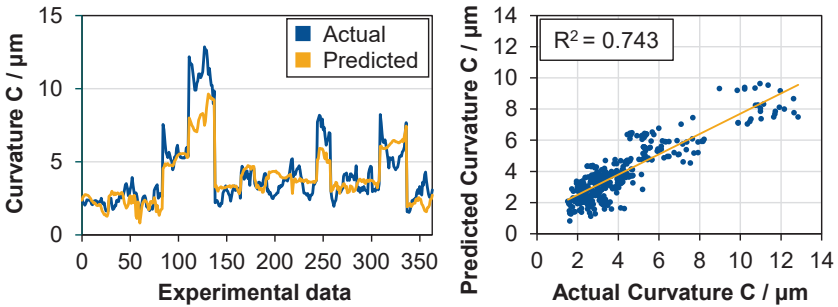


Figure 6.16: Predicted and actual curvature after testing with unknown process data

The prediction accuracy and the ability to explain a considerable part of the variability in the data are good. The absolute error size is very low with an MAE = 0.85 and even when larger outliers are taken into account, the model can still realize a good prediction with an MSE = 1.51. With the achieved coefficient of determination, about 74% of the variability in the curvature can be explained by the model. This is a relatively high value, which indicates that the model has a strong predictive power [MURP12].

This performance can be supported by analyzing SHAP (SHapley Additive exPlanations) values. SHAP values are a method of explaining prediction models in machine learning. They are based on game theory concepts and allow to quantify the contribution of each feature to the prediction of a given instance. They also allow to identify the relative importance of the features in the prediction, which defines the importance of the features and allows to interpret the models [BOWE20, MARC20].

The SHAP feature importance plot displays the impact of different features in predicting the curvature. The features are listed on the y-axis, and their importance is measured on the x-axis in terms of the Mean Absolute SHAP values, see Figure 6.17. As an example, a model was used that had similar performance to the model shown in Figure 6.14. To explain and interpret the importance of each feature, the height of the workpiece has been added here, while it was intentionally left out of the final model. Higher SHAP values indicate greater influence on the model's predictions. As expected, the

workpiece height  $h$  has a significant impact on the model performance. This stands also out in Figure 6.3, where a clear correlation between the workpiece height and the produced curvature can be observed.

After the workpiece height, the effective pulse frequency  $f_e$  has the highest mean absolute SHAP value, indicating it has the most significant impact on predicting the produced curvature. As the most influential feature, variations in  $f_e$  value greatly affect the curvature prediction. The second most influential feature is the presented factor  $e_{max}$ , which already showed correlations with the produced curvature in chapter 5.2.1. This feature is critical in predicting curvature. Its SHAP values suggest that changes in  $e_{max}$  significantly affect the curvature prediction. The median of the normal discharge distribution over the workpiece height  $normal_{median}$  also belongs to the top of the most important features for the presented prediction model.

Finally, the skewness of normal discharges  $normal_{skewness}$  and short circuits  $short_{skewness}$  over the workpiece height have a high importance for the model. The rest of the list contents of moderately influential features, which collectively contribute to the model's predictions, though each individually has a smaller impact compared to the top three. Their SHAP values still need to be considered when analyzing the curvature prediction, as they can influence the model's output in combination with other features. Finally, less influential features such as the kurtosis of short circuit distribution over the workpiece height have almost no effect on the prediction model.

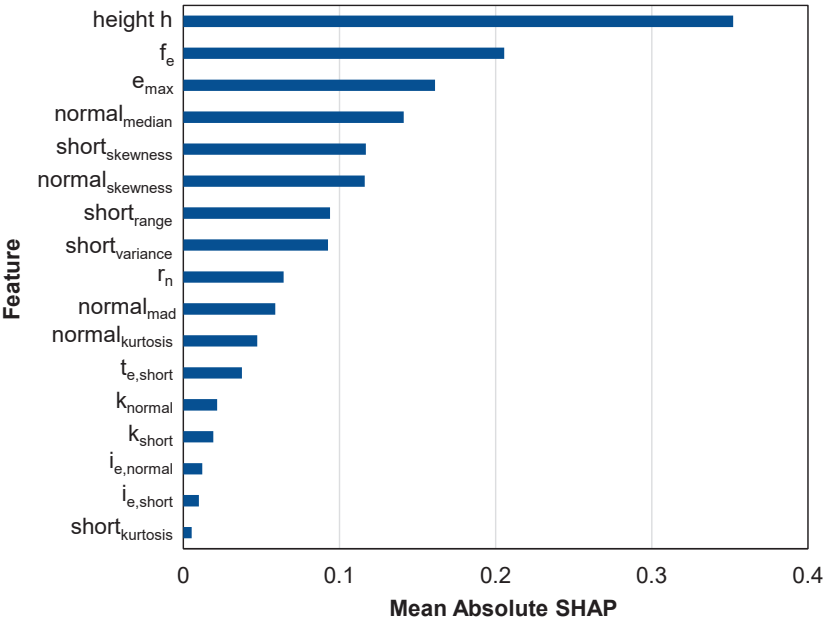


Figure 6.17: Feature importance measured as the Mean Absolute SHAP values

While in Figure 6.17 the feature importance of different input parameters for the curvature is evaluated, only the qualitative influence of the parameters is known. Therefore, in Figure 6.18 the SHAP values are presented in a beeswarm plot to show the exact impact of different features on model prediction. Listed left in the diagram from top to bottom are the parameters that are most important to the prediction accuracy of the model. The SHAP values on the x-axis indicate a positive contribution to the prediction, and negative SHAP values indicate a negative contribution. The color in the plot represents the feature value, thus corresponds to the raw values, with red illustrating high values and blue low values. Each point represents a row of data from the original data set.

For example, the workpiece height  $h$  has a mix of positive and negative values. High values (red) tend to have a positive impact on the model output, while low values (blue) have a negative impact. This means that high workpiece height values produce a high curvature while low values produce a low curvature. This matches the findings from the diagrams in Figure 6.3. On the contrary, it can be seen that for  $f_e$  high pulse effective frequencies will result in a smaller predicted curvature value. Low frequencies do the opposite.

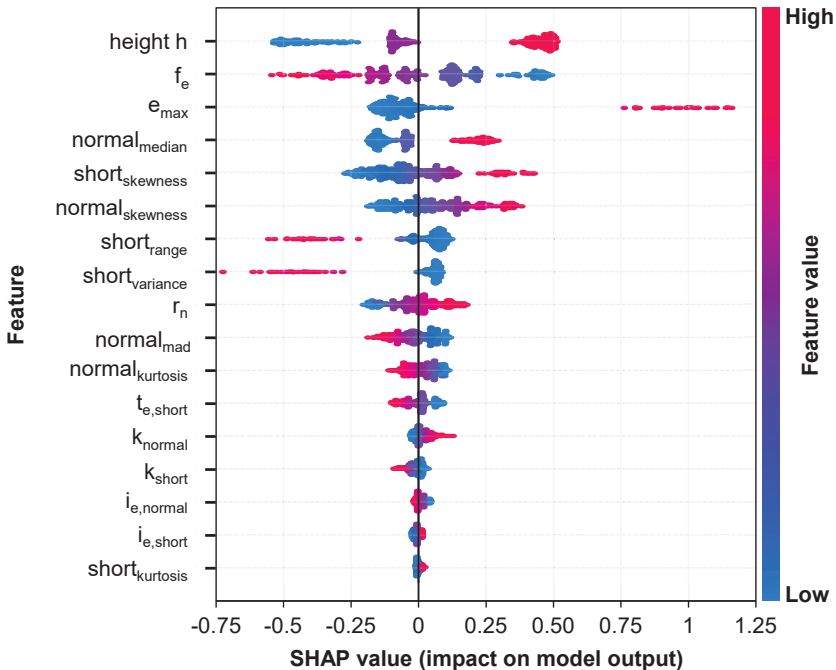


Figure 6.18: SHAP values of the regression model

This is also consistent with the observations in Chapters 6.1 and 6.2, which showed that smaller workpiece heights result in lower curvature but higher discharge frequencies. It is also fitting that the proportion of normal discharges  $r_n$  behaves in the opposite

direction to the discharge frequency. As expected, high values for  $e_{max}$  result in high curvature values for the prediction. The skewness of the discharge distribution over the height of the workpiece also appears to be important. The curvature increases with high skewness values, both of normal discharges and of short circuits. It should be noted here that, depending on the constellation of the model, these correlations could also be mirrored if the features also had different importance for the prediction. Overall, the evaluation shows how important it is to consider the different types of discharges and their distribution along the part height. This is particularly evident in the curvature and kurtosis of the standard discharges.

## 6.6 Summary and Conclusions

In this chapter, a neural network was developed to predict the curvature of the component using continuously recorded data. To generate the data, the process influencing variables were first categorized. A distinction is made between adjustable and non-adjustable variables. Subsequent data preparation and consideration of the influence of data agglomeration led to feature engineering.

An automated feature extraction approach was used to extract a large number of statistical variables from the data sets. In addition to visual analysis, different correlation analysis methods were applied and compared. Based on the results, some of the most important parameters were used as input parameters for the neural network. After a brief description of how neural networks work, the model architecture was determined using the Random Search approach in presented in Figure 6.15. For this purpose, the generated data was divided into training, validation, and test data sets. The training data is used to determine the structure of the neural network, and the validation data is used to carry out a hyperparameter optimization. This is evaluated using various metrics. Finally, the performance of the determined model is evaluated using unknown test data.

The model demonstrates good prediction accuracy and explains a substantial portion of data variability. It has a low mean absolute error of  $MAE = 0.85$  and maintains strong prediction performance with a mean squared error of  $MSE = 1.51$ , even when accounting for larger outliers. The coefficient of determination indicates that approximately 74% of the variability in curvature is explained by the model, reflecting its strong predictive power. Finally, the analyzed SHAP values show the validity of the model by interpreting the most influential input parameters. Moreover, these results can be used to prioritize parameters for further analyses or other machine learning models. This enabled the development of a Digital Twin that represents the generated curvature of the component on the basis of process data.

During the development of the models, the critical importance of data volume became evident. Accounting for different elevations revealed that the complexity of prediction increases due to the involvement of a significant diversity in the target variable (curvature). Based on the results obtained thus far, it can be anticipated that training the models with additional workpiece heights at smaller intervals, such as  $\Delta h = 10$  mm increments, will substantially enhance the model performance.



## 7 Classification Model for Productivity Evaluation

As depicted in Figure 5.1, the process evaluation is mainly divided in quality and productivity evaluation. Based on the approach in chapter 6, the regression models could analogically be trained to predict also the feed rate of the process and result in high prediction accuracies. Since the feed rate is a parameter which results during machining and is displayed on standard wire EDM machines, it is not beneficial or senseful to predict this parameter as a quantitative value. For the evaluation of the process performance, it is still necessary to assess the current feed rate based on the process data considering the process conditions. For this purpose, data-driven classification models are presented that evaluate processing technologies according to various criteria like machining speed, stability and quality. In contrast to the previous chapter, no regression approach is used to predict continuous data; instead, the process is considered as a binary or multi-class problem and classified into specific categories. Due to the variety of process variables and the complexity of the problem, the deep learning approach is a promising method here. Only continuously recorded process data was used for the developed model to evaluate the process performance.

Since this model was specifically designed to evaluate the productivity of a technology, different criteria are analyzed which determine the productivity of a main cut in wire EDM. Figure 7.1 illustrates schematically the classification model built on single sub models which are able to classify the wire EDM based on the criteria. The most important category is the machining speed, since the main cut generally takes up the largest portion of the machining time [WELL15]. Machining speed is represented here as feed rate  $v_r$  instead of cutting rate, since the model should be able to classify process productivity regardless of workpiece height. Equally important is process stability. This is characterized by various factors, but the occurrence of wire breaks is a knock-out criterion for any machining technology setting. There are also secondary factors such as contour accuracy and wire consumption. Wire consumption has a direct impact on costs and can be controlled by wire run-off speed, which in turn affects process stability. Therefore, the influence of the wire run-off speed was included in the experiments.

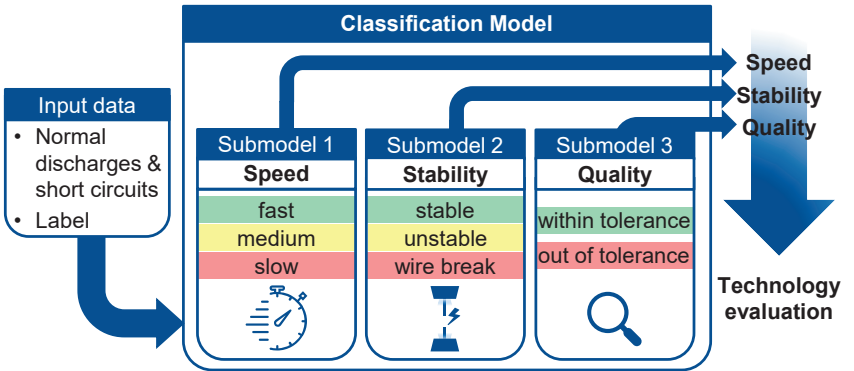


Figure 7.1: Schematic structure of the classification model for productivity evaluation

Adapted experimental setups were conducted to generate a useful large amount of data which covers the various influencing factors. The individual evaluation criteria were each divided into binary or multi-class problems. The collected data was then cleaned and transformed into a form suitable for deep learning methods. After that the performance of different neural networks was tested to develop the best predicting deep learning model architecture. Finally, it was tested whether the generated data could be used to evaluate productivity using the developed deep learning classification model. Not only the classification on a specific range of values was tested, but also the generalization of the model by testing with data which were generated under strongly changed process conditions and other workpiece heights.

## 7.1 Data Generation

The standard technologies for the same used material X155CrVMo12-1 were considered in the tests. In contrast to the previous investigations, the focus here was on the machine settings and therefore a large number of adjustable parameters were varied. The betterbrass one.9, a new generation of brass wire electrode by bedra for productivity increase with a diameter of  $d = 0.25$  mm, was employed [BERK24b]. The discharge current, the pulse interval time, the discharge durations for normal discharges and short circuits as well as the wire run-off speed were changed. These parameters are among the most important factors for the wire EDM productivity [BERG18a, KLOC07, KUNI05].

The challenge is to find the optimum parameter setting. While the cutting rate increases as the discharge energy rises, increasing this parameter beyond a certain point does not improve productivity, but rather expands the risk of wire break and edge deterioration [BERG18b, KÜPP20]. Especially, the dependency of discharge duration and discharge current has never been considered for the continuous process [MARA20]. In particular, the individual electrical process parameters for the two discharge types were neglected, each being considered separately. This means that possible connection or relationships were also considered here. The same trade-off must be made when setting the pulse interval time. Reducing it increases the pulse effective frequency and therefore the cutting rate, but also affects the condition of the working gap, with the risk of accumulation of discharges at the same location due to reduced deionization. In addition to the effects on speed, this can have a particular impact on process stability or an increased risk of wire break [KÜPP20]. Another driving cost factor of the process is the amount of wire used, which can be influenced by the wire speed [KÜPP21b].

Different test series considering two various machining heights applying respective standard steel technologies for the specific height were conducted in this chapter to generate data. An overview of how the different data sets were used for the development of the respective classification models is shown in Figure 7.2. Model development was divided into two phases. In the first phase, a model was selected on the basis of the reference data set. For this purpose, the reference data set was divided up for training, validation, and testing.

The determined model architecture was based only on the reference data sets. After determination of best performing model architecture, all reference test data from the experiments were then used for training only, while the other unknown data sets were used for testing. Thus, the transferability of the model to other heights and to more variable or dynamic process conditions was tested with a large and strongly varied data basis. The data sets generated for wire break detection, were only used for the stability evaluation sub model, while the other testing data sets were employed for all sub models. The percentages in Figure 7.2 show the proportion of data for the phase and for the work step in the model development.

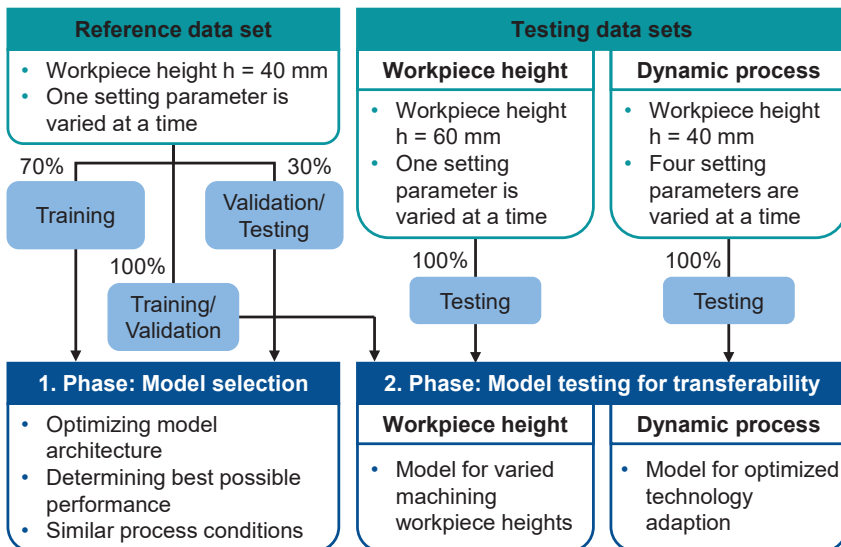


Figure 7.2: Use of the different data sets for training, validation as well as testing to evaluate the transferability of the models

In the first setup, specimens with a cutting height of  $h = 40$  mm and  $h = 60$  mm were machined. The experiments were used to generate the reference data set and testing data sets. A straight cut was applied to produce rectangular samples with a thickness of 5 mm. The thickness of the components was measured at three positions along the workpiece height using a caliper gauge. In order to test as many different technology variations as possible on one sample, a length of  $l = 7$  mm per side was machined on the samples for each variation. With two sides processed for each technology variant, this resulted in data for each variant that was generated on a cutting length of  $l = 14$  mm. Figure 7.3 illustrates schematically the setup. Additional cut-in and cut-out areas of  $l = 3$  mm were created to differentiate between the different areas and, more importantly, to ensure that the process becomes established and constant conditions are set for a variant. The nozzle distance was set regarding to the technology requirement to  $a = 10$  mm. These experiments were used to generate data in order to train,



validate and test different models. The developed models evaluate the speed, process stability and quality.

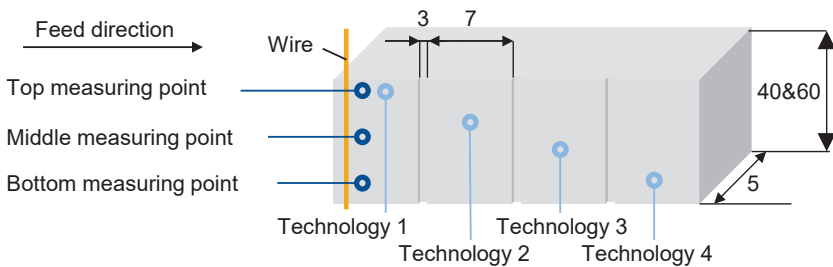


Figure 7.3: Experimental setup recording different technology settings

In this setup, one of the setting parameters was changed in each case and a total of over 180 technology variants were executed. A quantitative view of the range in which each parameter is changed in turn depending on the workpiece height can be found in Table 7.1. First, tests were conducted with a workpiece height of  $h = 40$  mm to generate data for selecting, training, and validating a model. This set of experiments will be referred to as the 'reference tests' throughout this work. This data was used as a reference to identify a model structure with the highest possible performance.

In order to investigate how the model responds to processing different cutting heights, a workpiece height of 60 mm was machined with almost the same parameter setting changes. This is intended to demonstrate the model ability not only to optimize processes, but also to develop machining technologies. The setting parameters are selected as before and are modified regarding the specific standard technology for machining heights of  $h = 60$  mm. These experiments will be referred to as "workpiece height tests".

Table 7.1: Setting parameters of reference data test and testing data set of for changed workpiece height

Machine setting parameter	Machine setting parameter value	
	$h = 40$ mm	$h = 60$ mm
Discharge current $i_e$	12 - 31 (step size 1)	12 - 31 (step size 1)
Pulse interval time $t_0$	35 - 75 (step size 5)	35 - 75 (step size 5)
Normal discharge current rise time $t_{r,n}$	38 - 63 (step size 5)	40 - 60 (step size 5)
Normal discharge current fall time $t_{f,n}$	67 - 97 (step size 5)	58, 63, 67 - 102 (step size 5)
Short circuit discharge duration $t_{e,s}$	4 - 12 (step size 1)	4 - 11 (step size 1)
Wire run-off speed $v_D$	8 and 16	16

Once the model has been selected, trained, and validated, two more test series were conducted for testing. First, another test series was run with a cutting height of

$h = 40$  mm. In contrast to the previous tests, not only one of the selected setting parameters was varied across the different technologies, but four machining setting parameters were changed simultaneously: the discharge current, the pulse interval time, normal discharge duration, and the short circuit discharge duration. This approach is intended to test the transferability of the created model to optimize the process. It was tested how well the model reacts not only to unknown data from similar process conditions, but also to data representing a more dynamic process that was influenced by several factors simultaneously. These tests will be named “dynamic tests” in the following chapters. The parameters were chosen by conducting a Design Of Experiments (DOE) [FISH66] and in total 35 experiments have been conducted. The parameter variations are listed in the appendix in Table 11.1.

Finally, a test series was set up to generate data for the evaluation of process stability, especially, the occurrence of wire breaks. For this purpose, a straight cut was applied for a minimum cutting length of  $l = 2$  mm without an occurrence of a wire break. Based on this setting, first, the electrical parameters were changed with the purpose to rise the feed rate until the wire breaks. Then, the wire run-off speed was increased to compensate the high wire wear until the process reached its limits and the wire broke. These experiments were conducted with different workpiece heights and changing various parameters which are listed in Table 7.2. In total approx. 170 different experiments were executed with a workpiece height of  $h = 40$  mm resulting in over 40 wire breaks.

Table 7.2: Overview of variations to evaluate the occurrence of wire breaks

Machine setting parameter	Machine setting parameter value
Discharge current $i_e$	23 - 32 (step size 1)
Pulse interval time $t_0$	30 - 60 (step size 5)
Normal discharge current rise time $t_{r,n}$	35 - 38 (step size 1)
Normal discharge current fall time $t_{f,n}$	67 - 128 (step size 5)
Short circuit discharge duration $t_{e,s}$	8 - 38 (step size 1)
Wire run-off speed $v_D$	1 – 36 (step size 1)

## 7.2 Data Processing and Defining Classes

In the following, the resulting evaluation parameters are divided into classes. Based on the obtained results, the different data packages and process settings were categorized as shown in Figure 7.1. Only labeled discharges with a resolution of  $res = 0.1 \text{ mm} \times 1 \text{ mm}$  were used as input variables for the model. Since this model focused on the process performance regarding stability and occurrence of wire breaks, a smaller averaging interval was selected based on previous findings [BERG18b]. The number of normal discharges and short circuits was utilized as well as the ratio of these discharge types in each area in relation to the workpiece height as calculated in equations 6.1 and 6.2. The classification of areas for each evaluation criterion was based

partly on experience and partly on data and serves as a criterion for labeling the data. The determination of the threshold was done separately for each sub model.

### 7.2.1 Thresholds for Speed

The speed is treated as a multi-class problem and divided into the three classes naming "slow", "medium" and "fast". First, the sections with the corresponding parameter variations were examined as a database. Figure 7.4 shows an example of the distribution of the feed rate for varied normal discharge duration settings. The speed rises only slightly here with increasing discharge duration. The marked peaks are only used here to illustrate the different feed rate for the various parameter settings. These peak values represent the beginning of a cut and were removed for training as well as testing the data.

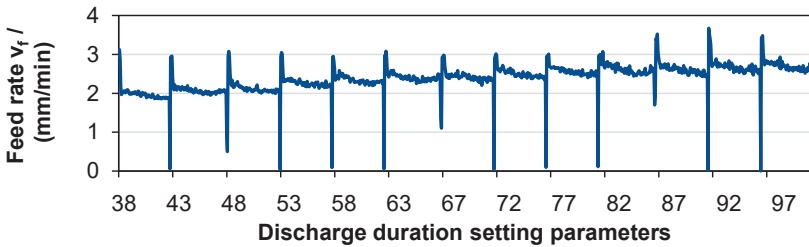


Figure 7.4: Feed rate for machining workpiece of  $h = 40$  mm with different discharge duration parameters

In the following, a possible division of feed rates into different classes is presented. Therefore, the feed rates for different discharge current settings are plotted in Figure 7.5. As expected, the speed rises with increasing discharge current. There are basically two ways to classify the data. The limits can be determined based on the statistical distribution. The initial position is the calculated average feed rate. The achieved feed rate is between  $v_f = 1.4$  to  $3$  mm/min in a stable range. A subdivision of the spectrum results in the following limit values.

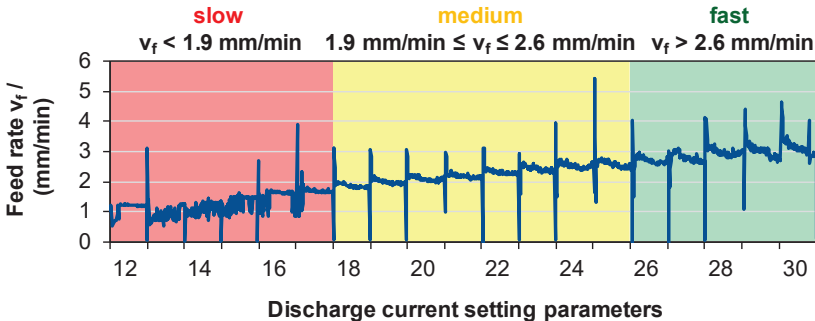


Figure 7.5: Thresholds calculated by average feed rates  $\bar{v}_f$  resulted by machining a workpiece height of  $h = 40$  mm with different discharge current parameters

The second option for consideration is the speed achieved by the used standard technology as reference. The standard technology results in a feed rate of approx.  $v_{f,40} = 2.5$  mm/min and is selected as the basis for the evaluation. A deviation of 10% in both directions around the guide value is defined as classification limit, which leads to the following limit values listed in Table 7.3.

Table 7.3: Thresholds calculated by 10% deviation of the standard feed rate  $v_{f,40}$  for machining  $h = 40$  mm

Threshold based on 10% deviation of standard feed rate $v_{f,40}$ for $h = 40$ mm		
slow	medium	fast
< 2.25 mm/min	2.25 to 2.75 mm/min	> 2.75 mm/min

There are advantages and disadvantages of both approaches. The first classification is statistically determined and reflects a data-based categorization. Due to the more even distribution of the data, this spectrum is likely to provide a more robust model and be less prone to misclassification than classification based on standard technology. The classification based on the standard technology feed rate focuses on the actual machining technology and speeds can be easily interpreted based on reference values. Both threshold approaches have been observed and considered in the model developments.

At the higher workpiece height of  $h = 60$  mm, the process proceeds as expected with a lower feed rate. Accordingly, the classification for these tests changes to the values listed in Table 7.4. The limit values for the different classification approaches are not specified here, since both variants cover the same range of values due to the shift in the speed range.

Table 7.4: Thresholds calculated by 10% deviation of the standard feed rate  $v_{f,60}$  for machining  $h = 60$  mm

Threshold based on 10% deviation of standard feed rate $v_{f,60}$ for $h = 60$ mm		
slow	medium	fast
< 1.25 mm/min	1.25 to 1.55 mm/min	> 1.55 mm/min

## 7.2.2 Threshold for Stability

To classify a process as stable, it must consistently produce predictable results with small variations within a defined range without unexpected stops. Applied to the wire EDM process, this means that the process must run consistently without the risk of a sudden wire break. In the tests, the straight cuts were only allowed to run with slight changes in speed. A strong, sustained fluctuation in the feed rate reflects a strong intervention of the machine control and therefore represents an unstable process. The occurrence of wire breaks in the individual technologies was also recorded and is a direct exclusion criterion for a stable process. In addition to the technology variations directly affected by wire breaks, adjacent parameter settings must also be considered critically, as a wire break risk cannot be ruled out with minimal changes to the processing conditions. The stability was classified on the basis of the standard deviation

of the feed rate of the individual variations and wire breaks. It is illustrated in Figure 7.6. For example, a feed rate that fluctuates more than 20% around the mean value was considered unstable. Technology variations that led to wire breaks were also declared unstable, as were settings that were at the limit before a wire break. In Figure 7.6, the red area includes discharge current setting parameters 29 and 30, which include wire breaks as well as the setting parameter 28 as a threshold.

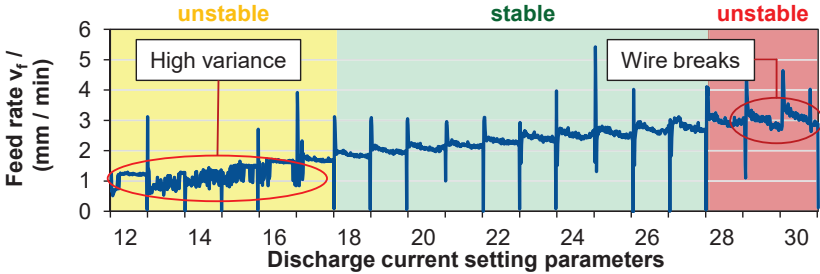


Figure 7.6: Classification of stable and unstable discharge current settings

7.2.3 Threshold Quality

In assessing the contour accuracy yielded by various technologies, these tests computed both the mean deviation from the attained specimen thicknesses and the standard deviation across three measurement points along the height of the workpiece. This approach enables insights into the precision of the generated working gap. Additionally, it serves as an indicator of any produced curvature, albeit with reservation that the accuracy of these measurements may not match that of the CMM measurement outlined in chapter 6. Figure 7.7 provides the average deviation for different tests. A deviation of the mean value between  $\Delta t = -5$  and  $5 \mu\text{m}$  is regarded as within the tolerance for the evaluation.

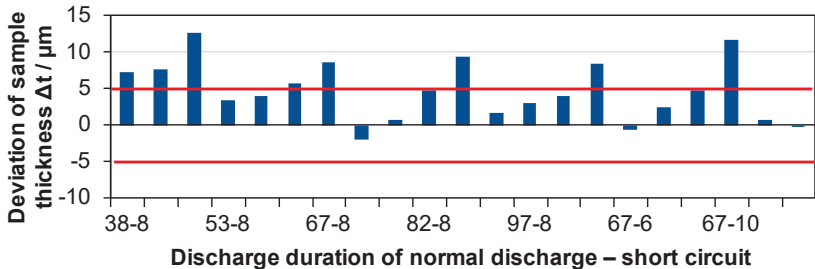


Figure 7.7: Deviation of produced sample thickness with thresholds

The standard deviation of the measured thickness over the workpiece height is depicted in Figure 7.8 and the threshold for classification were determined to  $\sigma_c = 1 \mu\text{m}$ . Everything below this value was declared as within tolerance and everything above it as not in tolerance. It represents a sufficiently good quality of the workpiece straightness for a large number of applications and provides a corresponding amount of data for training.

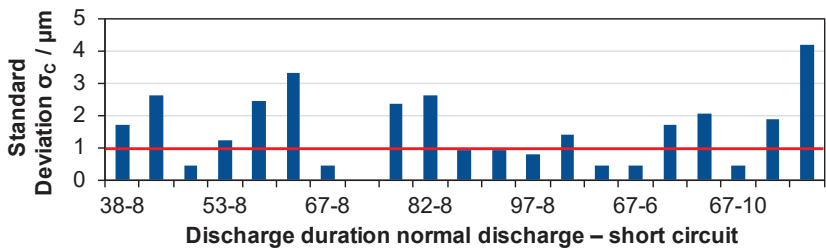


Figure 7.8: Standard deviation of the measurements along the workpiece height

7.2.4 Influence of wire run-off speed on process performance

Wire consumption is an important factor influencing the costs of the wire EDM process. The amount of wire used is determined by the wire run-off speed. Figure 7.9 compares the feed rates of two different wire run-off speeds. For this purpose, one wire run-off speed was halved. It is clear in this chart that the wire run-off speed has only a minor influence on the feed rate. However, it is important to note that a reduced wire run-off speed leads to increased wear of the wire electrode and thus a reduced wire cross section, which increases the risk of wire breaks.

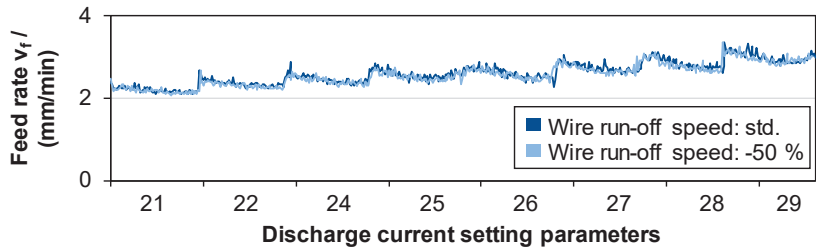


Figure 7.9: Feed rates for a standard and halved wire run-off speed

Furthermore, this can have an impact on the quality of the produced part, in particular the straightness [DICA20, KÜPP21b]. This is confirmed by observing the sample thicknesses shown in Figure 7.10. On average, smaller sample thicknesses are produced due to reduced wire cross section. The curvature produced is slightly greater for some samples.

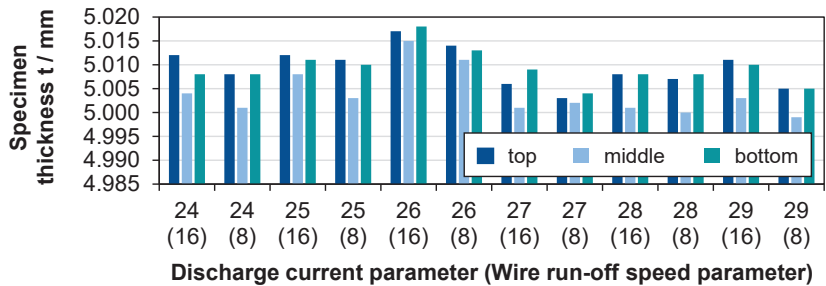


Figure 7.10: Machined geometry applying different wire run-off speeds

When evaluating the wire EDM process, it must be considered whether the cost reduction by reducing wire consumption is proportional to the loss of geometric accuracy and speed. For applications that require high quality parts, higher wire run-off speeds should be used. On the other hand, with larger tolerances, reducing the wire run-off speed could minimize wire consumption without affecting the workpiece quality. This could be useful when the produced accuracy after the main cut is negligible, for example, when cutting additive manufactured components from the substrate plate.

## 7.3 Classification Model Architecture

### 7.3.1 Deep Neural Networks

Following the data generation and the definition of the classes, a suitable classification model is created below. First, the data was transferred to a classic dense model, also known as a fully connected neural network, for training. The use of a simple feed-forward network initially serves to check the usability of neural networks for the problem at hand with the used data. The Deep Learning API (Application Programming Interface) "Keras" in Python is used to create the neural networks. An API is a set of rules and protocols that allows different software applications to communicate with each other, enabling them to request and exchange data or services seamlessly [OFOE19]. Keras serves as an interface to several libraries, including TensorFlow, which provides access to the various applied layers in this chapter. In addition to the basic structure of the models and layers, the API also provides access to tools for examining the performance of the models [KERA24, KETK17].

Convolutional neural networks (CNN) are a class of deep neural networks designed specifically to process structured grid-like data, such as images. They consist of multiple layers, including convolutional layers, pooling layers, fully connected layers (dense layers), dropout layer and flatten layer. The structure of a deeper CNN consisting of several CNN layers and different types of other layers is depicted in Figure 7.11. It consists of the main layers and several auxiliary layers. In convolutional layers, the network learns filters, also called kernels, that are convolved with the input data to extract local features through spatially shared weights [GOOD16, LECU15].

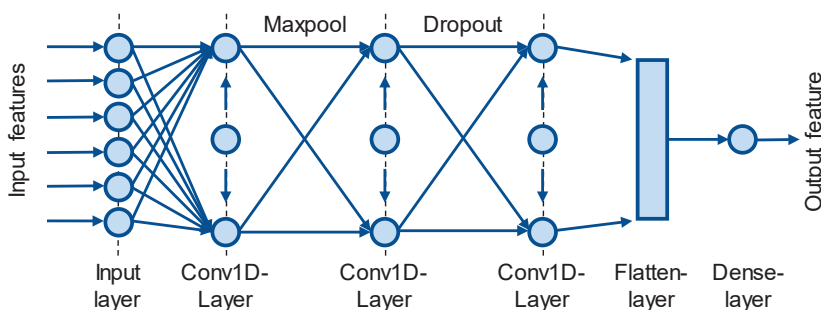


Figure 7.11: CNN architecture with different layer types

One-dimensional CNNs were utilized in this work, see for processing images, a one-dimensional CNN, as the name suggests, uses a one-dimensional input, which allows the concept of CNNs to be optimized for applications in flatter data structures. The reduction to a one-dimensional problem is the decisive feature here and allows this variation of CNNs to achieve faster and better results on these data types due to the reduced complexity. In particular, it is used for pattern recognition in sequential data. The core functionality and structure of the CNN remains the same. Here too, the input is subjected to local convolution and further processed by the activation function and pooling layer [GOOD16, KIRA21].

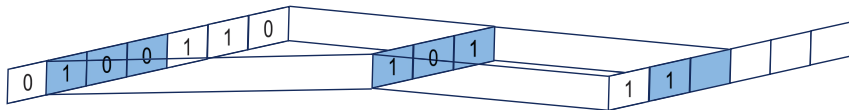


Figure 7.12: Convolution in one-dimensional according to [KIRA21]

At the end of the network are dense layers, which create a connection to all neurons of the previous layers and perform high-level feature extraction and classification. The task of the dense layer here is to reduce the dimensionality to the desired number of output neurons. In classification problems, as discussed in this work, this number of output neurons in the output layer represents in particular the number of classes into which the input data is to be categorized [GOOD16].

In addition to the main components of the network, various auxiliary layers are employed for efficient utilization. A dropout layer uses a regularization technique to prevent overfitting in neural networks. A dropout or "dilution" of the neural network is a stochastic adaptation of the error feedback and is an effective and simple method to avoid overfitting. The idea is to use only a part of the network during training, which is randomly selected with each iteration step. Therefore, these layers randomly switch off individual neurons during training. This simulates the training of several independent neural networks. The result is a reduction in the dependency of the individual neurons in a network and is schematically displayed in Figure 7.13 [PLAU21, SRIV14, GOOD16].

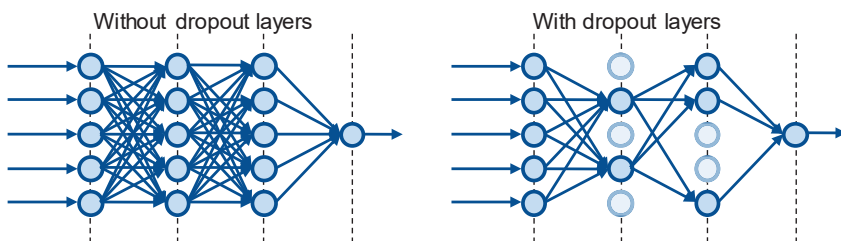


Figure 7.13: Dropout neural network model according to [SRIV14]

Another variant of the auxiliary layer is the so-called pooling layer, which can be set to individual convolution layers of the network. These are used to reduce the dimensionality of the data by aggregating data from neighboring pixels. Figure 7.14 shows an example of a max pooling layer that divides the data string into sections of the desired



size and determines the maximum value from each of these and discards the remaining values. This serves to preserve important features while reducing existing parameters. The most important effect of this step is the improvement of invariance, which enables a more robust recognition of the same features regardless of location, translation or distortion within the input data [GOOD16, LECU15].

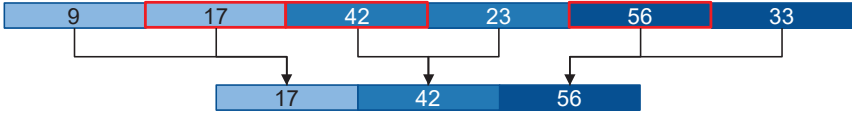


Figure 7.14: Example of a one-dimensional MaxPooling layer of size two [LECU15]

Finally, the multi-dimensional feature maps are converted by the convolution layer into a one-dimensional vector, which then can be fed into a dense layer. CNNs are typically trained by backpropagation to adjust the filters so that they can learn the relevant features automatically [LECU15]. The two parameters learning rate and momentum in this model were also adaptively optimized while training by applying the ADAM algorithm [KING14].

Training is usually done by minimizing a loss function that measures the difference between the actual and predicted results [GOOD16]. In contrast to the training of the regression model in chapter 6, the MSE error is not used as the loss function here. Instead, the loss function Categorical Cross Entropy for multiple classification is applied [ZHAN18a, WANG22]. At its core, the cross entropy is a logarithmic function. The loss increases exponentially the greater the probability of an output determined by the model deviating from the true result. Thereby, the Softmax function ensures that the activation of an output neuron can be interpreted as a probability of class membership [NWAN18, WANG22]. The activation function is defined as follows [PLAU21]:

$$\text{softmax}: \mathbb{R}^K \rightarrow \mathbb{R}^K, \text{softmax}(u) = \left( \sum_{k=1}^K e^{u_k} \right)^{-1} \cdot (e^{u_1}, e^{u_2}, \dots, e^{u_K}) \quad (7.1)$$

The Softmax function has the property that for all  $k \in \{1, \dots, K\}$  and  $u \in \mathbb{R}^K$  its values can always be interpreted as a mass function over the output neurons [PLAU21]:

$$\begin{aligned} (\text{softmax}(u))_k > 0, \sum_{k=1}^K (\text{softmax}(u))_k &= 1 \\ \text{for all } k \in \{1, \dots, K\} \text{ and } u \in \mathbb{R}^K \end{aligned} \quad (7.2)$$

The categorical cross entropy is calculated as follows [PLAU21]:

$$\lambda(y, \hat{y}) = \lambda(y_1, \dots, y_K, \hat{y}_1, \dots, \hat{y}_K) = - \sum_{k=1}^K y_k \ln(\hat{y}_k) \quad (7.3)$$

For a binary classification, a single sigmoid activated neuron can also be used as an output layer to guarantee a class membership probability between zero and one. In this case, the cross entropy takes the following form [PLAU21, WANG22]:

$$\lambda(y, \hat{y}) = -y \ln \hat{y} - (1 - y) \ln(1 - \hat{y}) \quad (7.4)$$

### 7.3.2 Performance of Fully Connected Neural Network

First, the training metrics accuracy and loss function are determined for a simple dense network consisting of the input layer, dense layer and output layer. As described in section 7.1, the model architecture was determined by using the reference data set in the following sections. It can be seen in Figure 7.15, that the model has already achieved an accuracy with a small number of epochs that excludes the possibility of the model predicting correct values by chance and that an application to the data set is therefore valid. The number of epochs was set high enough at 170 to ensure that each model reaches its maximum values. This serves to examine the maximum achievable accuracy with the network used and provides an estimate of the number of epochs at which training should be terminated in order to avoid overfitting. For the purpose to check how the system behaves when the network is deepened, several dense filters were connected in series and analyzed as described for the simple network. To compare the deep network with the simple network, both are plotted in Figure 7.15. These results served as a benchmark for more complex networks, which were considered in the further course of the work.

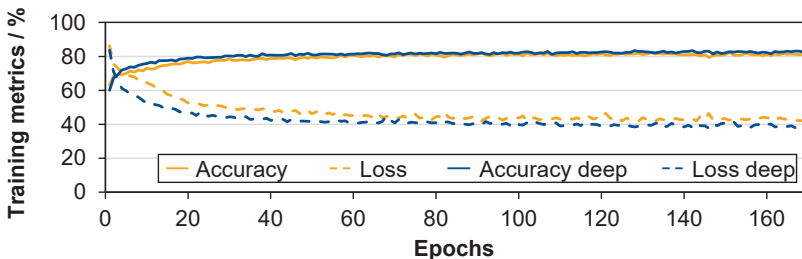


Figure 7.15: Comparison of a simple dense network and a deep network

### 7.3.3 Performance of Convolutional Neural Network

In order to find an optimized network for the problem, it is necessary to include the form and type of data. Due to the form of the utilized data, the implementation of filters that can convert the data into the form of vectors is recommended. For the analysis of vector-like formatted data, one-dimensional convolutional filters, which have been specially developed for this application and are designed to outperform dense layers, are suitable. To further improve the performance of the network, MaxPooling and Dropout layers were employed behind the convolutional layers of the deep network. The procedure for checking the performance of the different networks is again based on observing the behavior over 170 epochs and different network depths. The comparison demonstrated that the change from pure dense to convolutional networks resulted in a significant increase in the accuracy of the network. For direct comparison, the training metrics of the two deep network variants, dense and convolutional, are shown in Figure 7.16. Note that not only the maximum accuracy increases, but also the accuracy of the system rises more with fewer epochs.

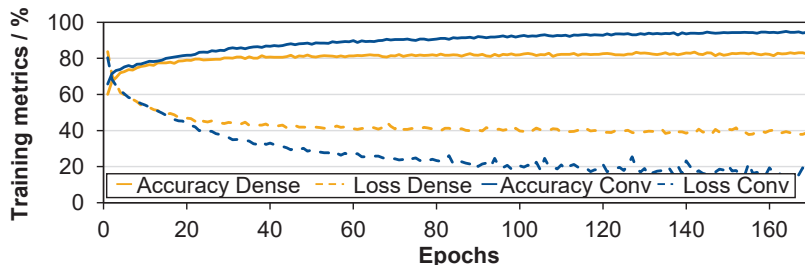


Figure 7.16: Comparison of convolutional one-dimensional and dense network

### 7.3.4 Performance of Recurrent Neural Networks

As mentioned before, the type of data is very important when developing machine learning models. The generated data is time related due to the characteristics of the wire EDM process. Recurrent Neural Networks (RNNs) are specialized neural networks designed for processing sequential data like text, speech, or time series. Unlike feedforward networks or convolutional neural networks, RNNs incorporate feedback between neurons, known as recursion. This recurrent feedback allows RNNs to integrate information from previous steps into current calculations, creating a memory of temporal dependencies. This makes RNNs well-suited for analyzing sequential behavior [DARB22, MANA18, SCHÄ08].

Although RNNs offer a wide range of applications, they face the challenge of the "vanishing gradient problem". This problem has a negative impact on the network ability to learn meaningful information over longer time intervals and can significantly reduce the effectiveness of RNNs in certain applications. The vanishing gradient problem occurs when the gradient propagated back through the network during training decreases exponentially with the length of the sequence. As a result, weight updates for weights further away from the output layer become negligibly small. To counteract this problem, the concept of RNNs was further developed in other networks, which use various protective functions against the occurrence of the problem [MANA18, SCHÄ08]. Figure 7.17 illustrates schematically an RNN.

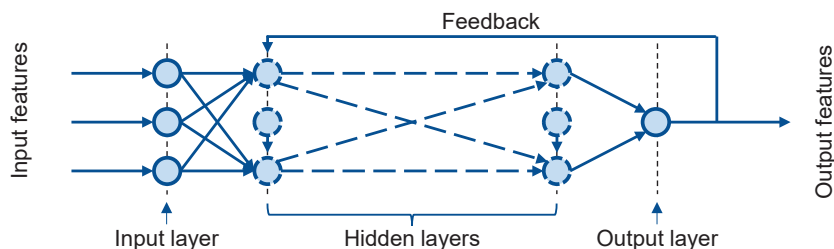


Figure 7.17: Scheme of an RNN [GUPT19]

To address this issue, various advanced RNN architectures have been developed, such as Long Short-Term Memory (LSTM) networks and Gated Recurrent Units (GRUs), which are capable of learning and retaining information over longer time

scales. The LSTM network consists of special cells that have a series of circuits that allow information to be discarded, retained, or added. These circuits are called "gates" and consist of three components: the "forget gate", the "input gate" and the "output gate" [HOCH97, MANA18].

The "forget gate" determines which information in the cell should be discarded, the "input gate" determines which new information should be added and the "output gate" determines which information from the cell should be passed on to the next step. The activation of each gate depends on the new input and the previous state of the cell. To control the gates, a sigmoid function is used to transform values between 0 and 1. In general, it can be said that values close to 0 are ignored and values close to 1 are considered important and saved [MANA18, SCHÄ08].

This control of the information flow within the LSTMs makes it possible to model long-term dependencies in sequences particularly well and yield a preferred use of LSTMs compared to conventional RNNs. For effective use, LSTM networks contain the same auxiliary functions as the CNNs. Here too, the network can be improved by using different pooling or dropout layers. The output layer is then finally reduced to the desired number of neurons by one or more dense layers [PHAM14, LAI15].

Based on this, next RNNs in the form of LSTMs were added to the convolutional network and their performance was tested again. Dropout layers were combined with the LSTM networks as auxiliary layers. Deepening the model did not generate a large jump in final accuracy on the training data, but there is a significant increase in the first 60 epochs. This region is of particular interest, as the training of the sub models is likely to be limited to this region to avoid possible negative effects such as overfitting. This can be seen from the analysis of the previous plots. The exact process can be seen in Figure 7.18.

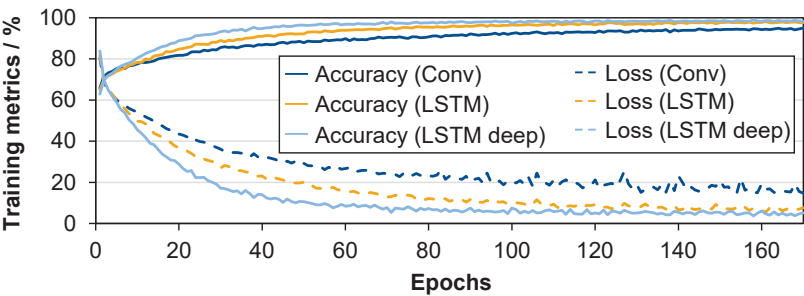


Figure 7.18: Comparison of convolutional network and LSTM-network

The investigation of the different variants revealed that a combination of various filter types achieved the highest performance. The convolutional layers with a downstream MaxPooling layer were well suited to prepare the data for the LSTMs. The combination of multiple LSTMs and dropout layers analyzes the extracted patterns of the convolutional layers over time. The model reached a maximum in this configuration, as further deepening of the network delivered a decrease in accuracy and an increase in loss, as

can be observed in Figure 7.19. It is not advisable to further increase the complexity of the model, especially since a deterioration in performance on the training data set can have an amplified effect on the non-training data.

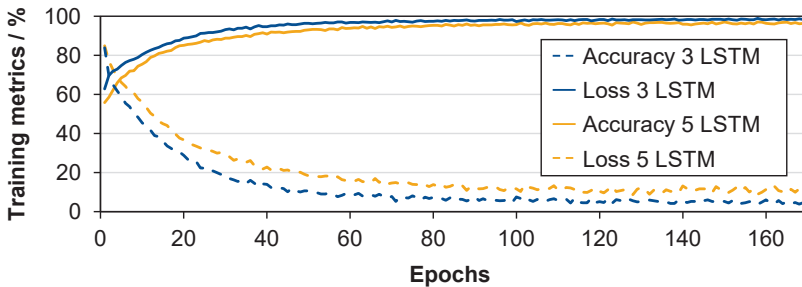


Figure 7.19: Comparison of an LSTM network with 3 LSTM layers (3L) to 5 (5L)

This results in the network shown in Figure 7.20. The final flatten and dense layers act as the necessary transformations to allow the network to perform the classification into the desired labels. The number of nodes in the dense layer corresponds to the label used in the selected sub model. Once the network has been selected for the problems at hand, it can be used to investigate the classification problems. Individual hyperparameters, such as the number of epochs used, are further refined and adapted for different cases. The activation function of the output depends on the problem. In this work, the standard functions for binary problems, the sigmoid function, and for multiclass problems, the Softmax function, are used.

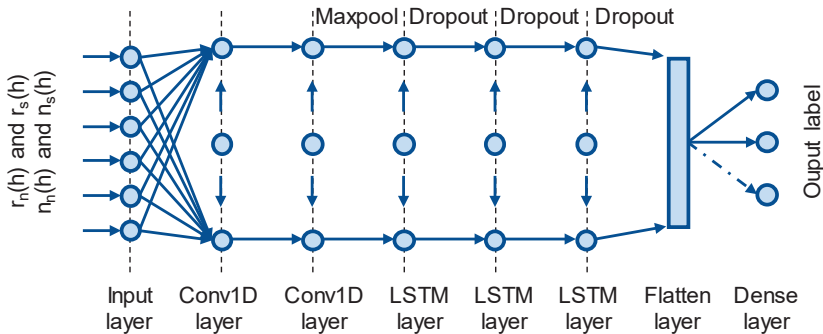


Figure 7.20: Structure of the developed deep neural network

## 7.4 Testing the Classification Models

This chapter presents the training and testing of the classification model. The overall model is built on the individually trained sub models that classify the individual evaluation variables, see Figure 7.1. Information from the sub models can be merged, processed, and then output in the overall model.

For this purpose, the generated process data was divided into different training and test sets. Hence, this ensures that similar but not identical data is compared during the

evaluation. It is important because the model should recognize general patterns regarding the selected factors and not just the specifically selected technologies. First, a model was trained and tested as a basis with the data generated in the reference tests, see Table 7.1. The data set was split so that 70% was used for training and 30% for validation and testing the model.

In order to evaluate the transferability of the models, models were trained and tested with the same architecture but different data. Initially, all data from the reference tests were utilized to train the model. To test the models, the data from the dynamic tests and the data from the modified workpiece height tests were employed separately. The transferability of the model to two different variables should be demonstrated here. Firstly, the model accuracy in more dynamic processes, determined by simultaneously changing several machine settings, should be improved. Secondly, its transferability to different workpiece heights needs to be addressed. Finally, a separate data set was considered for wire break predictions.

#### 7.4.1 Sub Model Speed

Two different groups of limit values were considered for the speed sub model in chapter 7.2.1. In the evaluation, these are examined in parallel in order to assess the differences in the performance of the models more precisely.

First, the classification of the limit values based on the averages of feed rates achieves a good performance to be expected for a model with a balanced database. The evaluation of the model using the confusion matrix in Figure 7.21 clearly underlines the high accuracy on the process-related data sets. The main diagonal of the matrix (yellow marked boxes), which represents the correctly classified data, contains approx. 70% of the results. This indicates that the model can reliably distinguish between the different speed classes. A trained model with the average feed rate  $\bar{v}_f$  defined in Figure 7.5 as classification factor is presented in Figure 7.21 (a). In Figure 7.21 (b) a model with the thresholds based on the standard feed rate from Table 7.3 were used.

This clearly shows that the averaged value provides better results as a threshold for different classes since it is based on the data, especially for the recognition of fast processing technologies. The accuracy of the classes achieved an *F1-score* of approx. 0.7. With the exception of isolated outliers, misclassification almost only occurs between the directly adjacent labels. It should be noted that the feed rate of individual samples is close to the limit of the other speed class, which means that inaccuracies in the evaluation are to be expected.

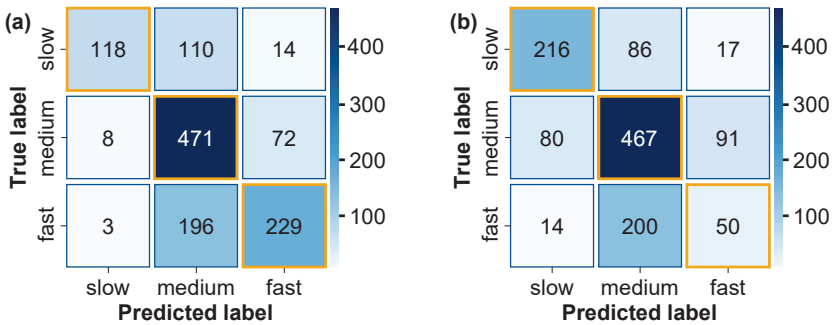


Figure 7.21: Model trained and tested with reference data: confusion matrix using training thresholds for average feed rate  $\bar{v}_f$  (a) and using thresholds for standard feed rate  $v_{f,40}$  (b)

These inaccuracies can be observed in Figure 7.22. Two diagrams are plotted there, both of which consider the same four technologies selected from Table 11.1. The upper diagram depicts the predicted label and the feed rate. Even if a classification model with 3 discrete categories was developed here, the model outputs probabilistic scores which allows prediction to fluctuate between the individual categories. Therefore, the lower diagram shows the accuracy with which the model assigned the label in the classification. This interpretation aligns with more advanced classification models that can represent uncertainty or gradations in predictions, allowing for more nuanced insights into the system's performance across different technologies.

The first two technologies run constantly in their classes "slow" and "medium" in relation to the selected limit values with the cutting speed and are classified correctly accordingly. The last two technologies fluctuate around the feed rate of  $v_f = 2.75$  mm/min, which acts as the limit between the "medium" and "fast" classes. As a result, the classification of the model is also prone to errors at these transition points. In the lower diagram too, in addition to the fluctuations when moving the technologies in and out, the technologies close to the limit value are particularly affected. The classification of the thresholds, which are based on the standard technology, led to a similarly satisfactory performance, albeit with a minimal deterioration compared to the previous configuration. Here too, the confusion matrix still shows a predominantly correct classification, but with slightly more uncertainty in some areas, see Figure 7.21 (b). The main diagonal remains dominant, but the values outside the diagonal are slightly more frequent and indicate a marginally increased number of misclassifications. Despite this, the model remains reliable.

Both classification approaches revealed very good results on the data from the reference tests and the differences in performance are within the expected range. Depending on the evaluation, the advantages and disadvantages of slightly higher accuracy to better containment to the upper spectrum of speed must be weighed up here. In addition to the respective performance on more general data sets, the further

procedure also considers how the different limit value variations affect the robustness of the model.

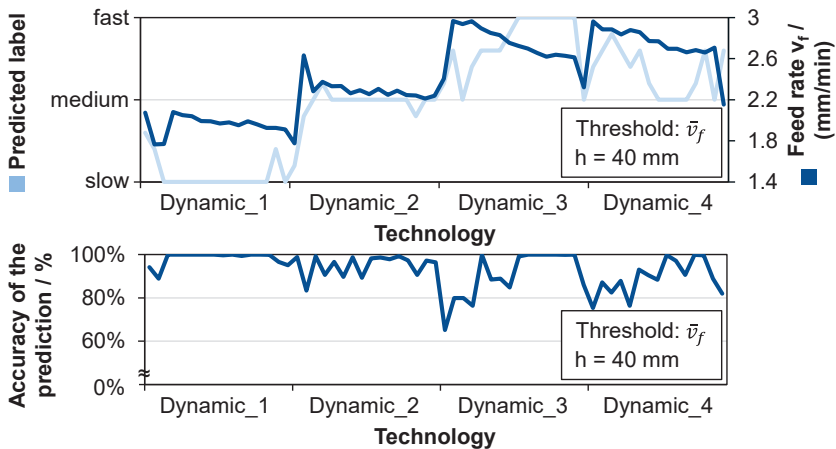


Figure 7.22: Actual feed rate and predicted label (upper diagram); accuracy of the related prediction (lower diagram)

In the following the transferability of the models to more dynamic process conditions are presented. As described models were trained with the reference data and tested with data from dynamic tests changing four machine setting parameters at a time, which is defined in Table 11.1. In Figure 7.23, the comparison was made, using a model based on the averaged  $\bar{v}_f$  (a) and standard feed rate  $v_{f,40}$  (b). The data sets were largely classified correctly and were concentrated in the range of the "fast" speed class, as well as in the limit area to this. It can be observed that both limit value variations performed approximately equally well. It is also evident for both variants that the greatest challenge is to differentiate between "medium" and "fast", which is why a lot of data is assigned from "fast" to "medium". Due to the selected threshold values, the correctly recognized data sets were distributed across different labels. Misinterpretations between the individual groups show a similar number but are distributed differently in each case. The large outliers have remained almost the same in number and suggest that they are probably the same individual data points that do not match the pattern of the other data points or are data errors. However, the number of errors is small enough to be disregarded here.

Overall, the classification works very well on general data with the same machining height. While the categorization as "medium" only has an  $F1$ -score below 0.5, the accuracy predicting "fast" machining almost results in an  $F1$ -score of over 0.75. A more precise classification into the classes "slow", "medium" and "fast" is offered here by the standard technology approach. This is because primarily tests with high cutting speeds were employed here. If the behavior of the two networks is considered in connection with the shift of the limit value range, a specific alignment to a desired speed range or



a finer division into several classes appears to be quite valid here, as long as there is no excessive imbalance in the training data.

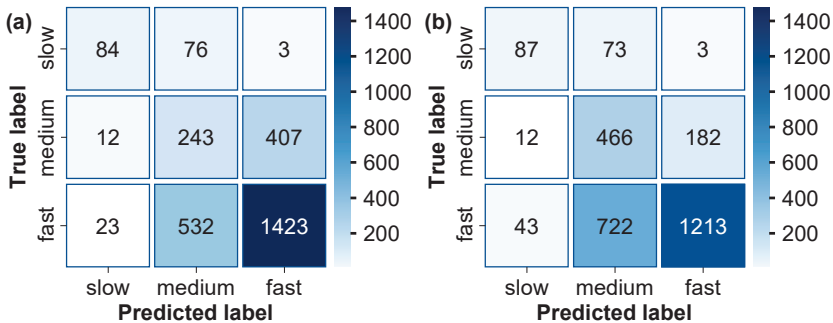


Figure 7.23: Model trained with reference data and predicting dynamic process feed rate: confusion matrix using training thresholds for average feed rate  $\bar{v}_f$  (a) and using thresholds for standard feed rate  $v_{f,40}$  (b)

Finally, both networks were applied to the data sets with a cutting height of  $h = 60$  mm. Due to the greatly reduced feed rate compared to the reference tests, the limits for the workpiece height tests were adjusted here, as described in chapter 7.2.1. Figure 7.24 shows that both networks assign more data sets to the fast or slow class depending on their trained limit values. Here also a lot of data of a fast process is wrongly predicted as medium.

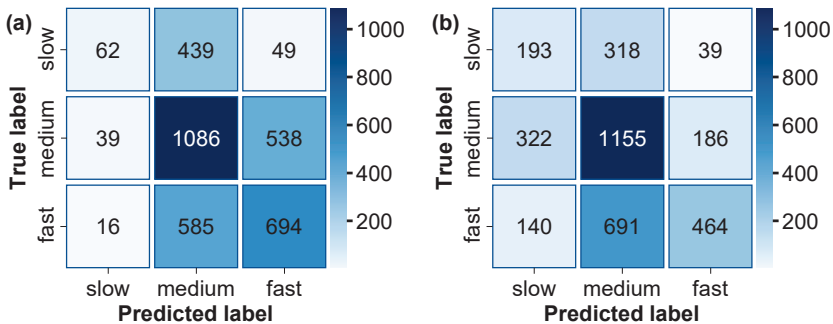


Figure 7.24: Model trained with reference data and predicting changed height feed rate: confusion matrix using training thresholds for average feed rate  $\bar{v}_f$  (a) and using thresholds for standard feed rate  $v_{f,40}$  (b)

Again, both networks behave similarly robustly. The accuracies result in  $F1$ -scores around 0.6 for “medium” and “fast” classes, while a low  $F1$ -score around 0.3 for “slow” predictions is reached – as indicated in Figure 7.24. Accordingly, a choice of both networks is also possible for highly generalized data, which refers to data that captures essential patterns and relationships, making it applicable to a wide range of situations beyond the specific instances it was derived from. Depending on the exact use case, it is therefore possible to use adapted networks. For the case discussed in this work,

the classification based on the averaged feed rate is to be preferred, as this enables a more precise classification of the "fast" class.

7.4.2 Sub Model Stability

The stability sub model is considered a binary problem. The subdivision of the stable versus unstable data sets was based on the boundary value analysis in chapter 7.2.2. Based on the reference test data, the model shows a clear distinction between the two used classes. The misclassified data points are mostly stable data points that are considered unstable, see Figure 7.25 (a). This would be acceptable for monitoring and only the reverse case would be critical. Here, accuracies with an *F1-score* of 0.8 for the prediction of the stable process state and an *F1-score* of 0.85 for the correct classification of unstable process data were achieved.

The selected machine setting parameters for the dynamic tests were at the limit to wire breaks. Due to this limitation, instabilities occur completely in the form of wire breaks. Therefore, an increased misinterpretation of the stable process curves in the direction of unstable processes can be seen in the data displayed in Figure 7.25 (b).

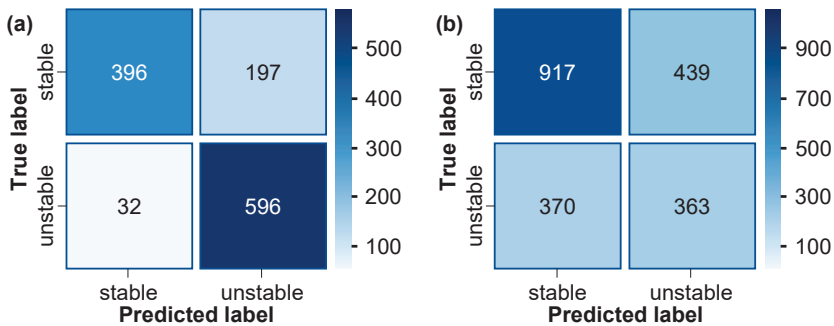


Figure 7.25: Process stability prediction: model trained and tested with reference data (a); model trained with reference data and tested with dynamic process data (b)

The change in cutting height and the associated generalization of the data leads to a decrease in accuracy data of the model predicting instability of process. This can be observed in Figure 7.26 (a). One possible factor that could influence the accuracy is the data density in the area of instability. Here, only an *F1-score* of 0.32 could be reached, while stable process can be predicted with an *F1-score* of approx. 0.9.

A technology that is slightly unstable also contains stable sections in the data that affect the classification. Due to the larger cutting height, the discharges are distributed over a larger area. This has a stabilizing effect on the process as, on the one hand, it is less likely that the discharges will hit the same spot at short intervals when removing material in one area. On the other hand, a longer time elapses after the removal of material until the area is processed again. Accordingly, the algorithm tends towards the "stable" classification.

Due to the problem of the small number of unstable tests, especially those that lead to wire breaks, a further series of tests was produced separately for the case of wire

breaks. This data serves to check whether the used model tends more towards the "stable" label due to the distribution of the data. The investigation revealed that the model is clearly capable of determining unstable processes, see Figure 7.26 (b). The accuracy of the employed tests reached an  $F1$ -score of 0.9 of the individual data points. Considered over the distance, all used data sets can be assigned to the "unstable" label.

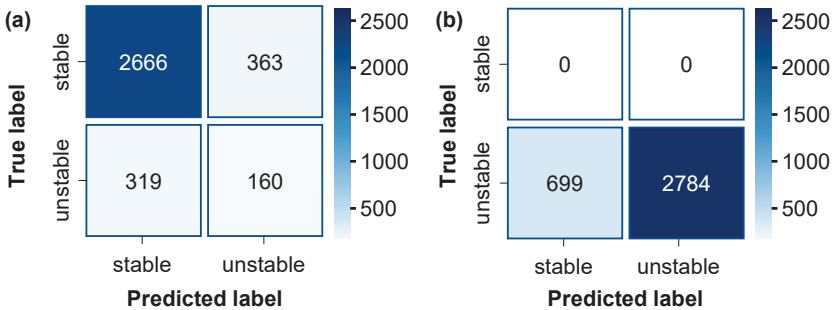


Figure 7.26: Process stability prediction: model trained with reference data and tested with changed workpiece height process data (a); model trained with reference data and tested with wire break process data (b)

### 7.4.3 Sub Model Quality

As stated in chapter 7.2.3, the values based on the deviation of the cutting thickness were used here as labels. The contour accuracy is considered in two ways: the produced workpiece thickness and the standard deviation of the thickness which could indicate a machined curvature. Both characteristic values were evaluated and considered in parallel, see Figure 7.27. The sub model can clearly predict the deviation of the thickness and the standard deviation along the workpiece height. In both cases, thickness measurements defined as good are more often classified as insufficient than the other way round.

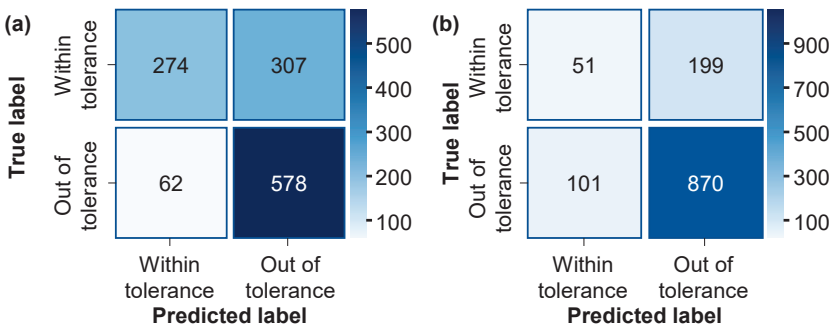


Figure 7.27: Model trained and tested with reference data to predict: the thickness (a); the standard deviation of thickness over workpiece height (b)

The performance of the model using dynamic test data decreases, but the tendencies from the previous evaluation are retained, see Figure 7.28. As with the previous data set, the standard deviation could be determined more precisely. This can be explained by the fact that the discharge types over the length of the cut are used for pattern recognition. With a uniform distribution, they correlate directly with a straighter cut edge, i.e. less construction. The greatest inaccuracies exist in the misinterpretation of "Within in tolerance" quality cuts as "Out of tolerance" quality cuts. Ideally, a more conservative approach is favored to maintain a correspondingly high quality of the produced pieces. However, the current level of misinterpretations leads to excessive waste, necessitating an adjustment of limit values or the facilitation of a finer differentiation through an expanded sample selection.

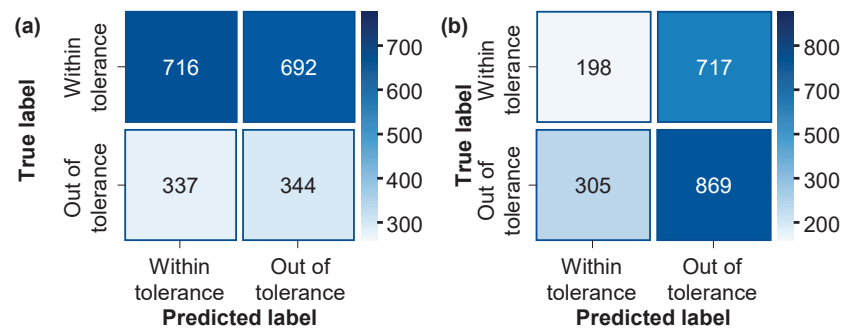


Figure 7.28: Model trained with reference data and tested with dynamic process data to predict: thickness (a); the standard deviation of thickness over workpiece height (b)

Finally, analyzing the quality of workpiece height tests, it can be seen that the inaccuracies continue with the same tendency, see Figure 7.29. The model can no longer be used to classify the samples in this form. The misinterpretation of the good cuts is still the driving error here. In order to use the model for other cutting heights, retraining with appropriate samples that adequately represent both areas are necessary.

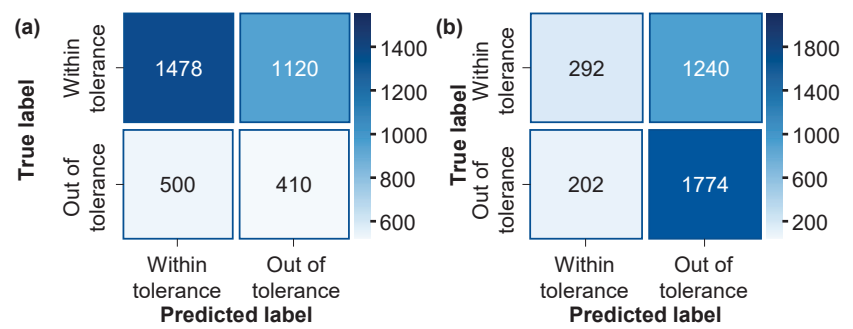


Figure 7.29: Model trained with reference data and tested with changed workpiece height process data to predict: the thickness (a); the standard deviation of thickness over workpiece height (b)

## 7.5 Summary and Conclusions

Based on the findings in the work, this chapter focused on creating a data-driven model for classifying varied machine parameter setups based on process data and categorize them into defined productivity level. A deep learning approach was applied by utilizing different forms of neural networks for the model architecture, see Figure 7.20. Initially, machine setting parameters were selected for data generation, with significant influence on process behavior. Data was then processed and converted into a suitable format for model training, considering important limit values for different characteristic parameters. The dataset was divided into training, validation and test sets, with two training stages conducted on the main data set to assess model efficiency. To identify the best performing model structure for the main data set only one machine setting parameter was changed at a time. The transferability of the model was later tested with data sets generated during machining changed workpiece height and changing four machine setting parameters at once.

Results showed high accuracy for sub models, especially concerning correlations with process parameters like normal discharges and short circuits and their distribution along the workpiece height. However, when varying machine setting parameters, accuracy slightly decreased but remained reasonable. Further analysis at a greater cutting height revealed reduced model accuracy due to significantly altered experimental conditions. Still considering that all testing were conducted with completely unknown data, a good transferability of the models to changed process conditions could be observed.

Despite variations in data, the model accurately classified different datasets, suggesting potential for future expansion. Notably, classification based on process parameters of normal discharge and short circuits, along with their distribution over workpiece height, was successful. Accuracies with an *F1-score* of approx. 0.7 were achieved categorizing different technology variants to various machining speeds depicted in Figure 7.21. Thereby, three different classes were distinguished. For the prediction of process stability categorization even an *F1-score* over 0.9 could be reached. It should be noted that no additional information was used for the models. Thus, an evaluation of the process performance, in particular the speed and stability, could be realized by a discrete categorization of different processes. This fulfils important requirements for the application in practice.

Recommendations for future studies include finer classification, expanding the dataset, considering additional process parameters, and modifying the algorithm for better efficiency. Additionally, it can be assumed that the performance of the models will improve significantly if, in addition to the recorded data, the corresponding machine settings and expert knowledge are also used as input for the machine learning models.

## 8 Development of a Digital Twin

In the machine learning models in chapter 6 and 7 it could be demonstrated that based only on continuously recorded process data, process evaluation could be realized by predicting produced curvature and categorizing the process performance. While the data was recorded and processed in real time online, the training and subsequent testing of the models was conducted offline. In this chapter, the gained knowledge is used to develop a Digital Twin for wire EDM under an industrial environment to make online predictions of the produced curvature real time capable. For this purpose, a cooperative project was carried out with the AI software provider IconPro and the WBA as a user in order to demonstrate that the fundamental technological findings significantly increase the potential of data utilization, and that high-performance AI software can be used to digitally map processes and products. IconPro specializes in digitizing manufacturing processes and developing AI-based software for industrial applications while focusing on predictive calibration, predictive quality, and AI-based process analysis.

The following approach was used to develop a Digital Twin to map the produced work-piece curvature, see Figure 8.1. To implement data-driven models in processes that generate particularly large amounts of data, the data must be continuously reduced and agglomerated while increasing the information density. Data processing and data analysis in wire EDM were described and explained in detail in chapters 4 and 5.



Figure 8.1: Procedure to develop a Digital Twin in production technology [KÜPP22b]

The following system architecture was implemented for the data transfer between the machine, the individual data processing interfaces and the user interface in order to be able to display the Digital Twin representing the machined curvature on a dashboard, see Figure 8.2. Data is processed and condensed at the wire EDM machine, saved every 30 seconds as a CSV-file, and transmitted via a Python script to a cloud server (Data Hub), ensuring spatial decoupling. The Data Hub distributes data for near-real-time display and forwards it to evaluation software. Results are sent back for dashboard display.

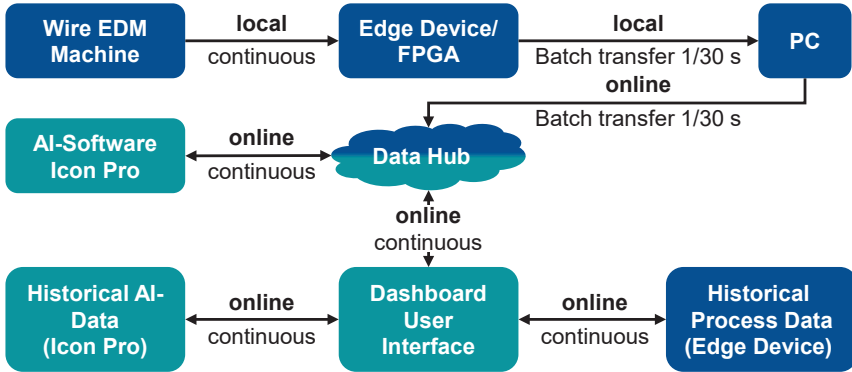


Figure 8.2: System architecture for data transfer to create a Digital Twin in industrial environment – cooperative by the MTI (Manufacturing Technology Institute), IconPro and WBA

While the first steps from data acquisition and processing to transfer to the Data Hub have already been explained in detail in this thesis, the following section describes how the model approaches can be specifically implemented in AI software for industrial use based on the knowledge gained. Paranjape et al. [PARA24] developed an ML ensemble model predicting geometric curvature error with mean absolute error approx. 1  $\mu\text{m}$  and a reported runtime of 2 seconds per 100 predictions in an industrial environment. For this purpose, multiple machine learning models were trained to predict the geometric curvature. Rather than relying on individually trained models, a diverse ensemble of models was developed because ensemble models typically outperform individual models [MOHA23]. Since the target variable geometric curvature is numerical, also regression models were used for training as in chapter 6. These included a mix of simple tree-based models, decision trees, random forests, boosted trees, and neural network models. The training process for these models was automated with a runtime of 60 minutes. The models were trained and fine-tuned on training and validation datasets, respectively. Insights from Gijssbers et al. [GIJS24] were utilized to train the individual models using open-source libraries. These models were subsequently combined into an ensemble. EDM process data, along with quality measurements from CMMs, comprised the training dataset. A custom feature extractor module was used to derive features from the raw generated data [PARA24]. The train and validation sets were used to train an ensemble of ML models, which were finally evaluated on a test split as in chapter 6.

The trained models were grouped to achieve the highest accuracy, resulting in a global model that is an ensemble rather than a single model. This ensemble was created using a voting mechanism, which combines the predictions of multiple individual models and produces a final prediction by averaging these predictions for regression tasks. The final ensemble included a total of 108 models, categorized into major groups as listed on the left in Figure 8.3. The overall ensemble consists of neural networks and various decision tree-based machine learning algorithms. All algorithms were trained

using default hyperparameters for the given runtime. In creating the ensemble, individual models could receive multiple votes. The training was conducted in Python using open-source libraries. The use of a voting mechanism in ensemble creation theoretically ensures that the ensemble outperforms the individual models [PARA24].

The global ensemble model was evaluated on a test split, which the model had not previously seen or used for hyperparameter tuning. Figure 8.3 illustrates a scatter plot comparing true curvature values with predicted values, where a 45-degree line represents perfect predictions. Quantitative metrics showed an R2-score of  $R^2 = 0.82$ , mean absolute error of  $MAE = 0.87 \mu\text{m}$ , and root mean squared error of  $RMSE = 1.29 \mu\text{m}$ , indicating that the prediction errors were within acceptable limits. Only a few samples had an MAE higher than  $2 \mu\text{m}$ , highlighted in yellow in the diagram. To check for bias in dataset splitting, four experiments with different random seeds were conducted, yielding R2-scores of  $R^2 = 0.81, 0.82, 0.79$ , and  $0.82$ . These consistent results suggest negligible bias in the model, despite slight differences in ensemble composition across experiments [PARA24].

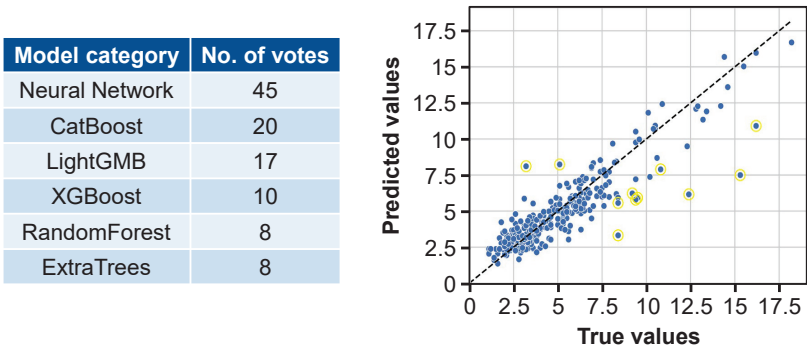


Figure 8.3: Categorized model of the final ML ensemble model (left) and predicted and actual curvature after testing (right) according to [PARA24]

For industrial use, the trained machine learning model was deployed to be accessible to end users. The training and deployment architecture is depicted in Figure 8.4. Deployment was handled within a Kubernetes cluster to utilize its features like non-breaking updates, auto-scaling, resource management, and production readiness [CARR22]. The process begins with a user interacting with the system by sending a request to the Application Programming Interface (API). It serves as the interface between the user and the Kubernetes cluster, receiving the user's request and forwarding it to the Ingress Controller within the cluster. The Ingress Controller then manages and routes the incoming requests to the appropriate services, either the training or inference components.

Model training occurred via a Kubernetes job inside the cluster, and the trained model was stored on S3 (Simple Storage Service) storage for its simplicity and efficiency. It is a scalable object storage service provided by Amazon Web Services (AWS), which is designed to store and retrieve any amount of data from anywhere on the web,



offering high durability, availability, and performance [PALA08, PERS16]. The model was deployed in a pod using a flask server, with an ingress controller managing external connections for both training and inference. The inference requests are routed to the appropriate pod, and the predicted curvature error is returned as a JSON (JavaScript Object Notation) output [PEZO16] for display on the end-user dashboard [PARA24].

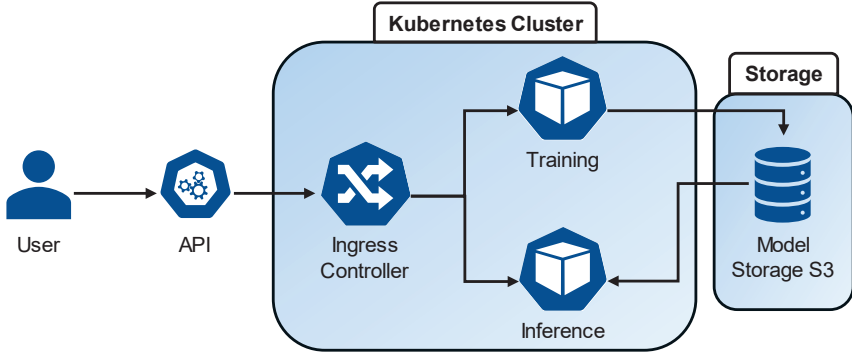


Figure 8.4: Training and deployment architecture under Kubernetes orchestration according to [PARA24]

The deployed model was tested in an industrial setup, showing an average runtime of 2 seconds per prediction for sample sizes from 1 to 200. For batches of 300 and 1000 samples, the runtime increased to 3 and 4.5 seconds, respectively. The model aims to reduce the cost and effort of manual measurement for parts cut with wire EDM by identifying parts with higher geometric curvature errors for inspection, potentially reducing inspection costs and scrap rates.

Based on these results, the end-user dashboard can display near real time process evaluation data, Figure 8.5. Several, parameters can be plotted during the machining process such as the pulse effective frequency, the discharge distribution considering the discharge types. Furthermore, a Digital Twin can be displayed by presenting the produced curvature based on the trained models. This sheet in the dashboard is only for one wire EDM machine and such sheets can be used for the entire production to monitor productivity, quality and efficiency for different machines and processes. The entire system could also be applied on a wire EDM machine from another manufacturer with minimal effort.

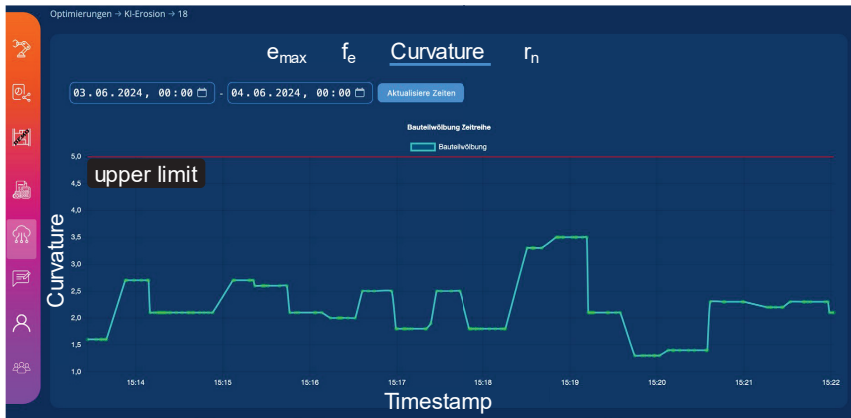


Figure 8.5: Dashboard by WBA Aachen for the user displaying Digital Twin representing produced curvature in real time [WBA24]

The app allows setting warning limits for process data, issuing alerts, and storing events for future analysis. Besides display, permanent storage of data for quality assurance is ensured with a two-part database structure: historical process data basis for dashboard data and historical AI data basis for evaluation results, see Figure 8.2. The dashboard is accessible via a web browser, ensuring device-independent use.

With this approach, an AI-based assistance system for technology development and optimization can be used through the same structure and the use of classification models as in chapter 7. By using reinforcement learning, for example, a self-learning process could even be developed that automatically tests itself through parameter areas and optimizes itself [IPEK08].



## 9 Summary and Outlook

### Summary

The main areas of application for wire EDM are in tool and die making, as well as in aircraft engines and medical technology. Components are often machined that can no longer be produced economically using conventional manufacturing technologies due to their material properties and required tolerances. The technology is mainly used in the production of high-value products and is often the last critical manufacturing step. The process reliability and repeatability of this technology are therefore particularly important and can be guaranteed by correspondingly intelligent control and automation solutions. This, along with the digitalization of manufacturing processes in the context of Industry 4.0, requires the use of data-driven approaches in wire EDM. Machine manufacturers do not offer yet any solutions for end-user data-driven process monitoring or process development. Based on the given state of the art dealing with process data in wire EDM, a deficit was identified for a valid data-driven model to evaluate the wire EDM process.

The objective of the present work was therefore to develop a data-driven model for the evaluation of the wire EDM process. This was to be based primarily on continuously recorded physical respectively electrical process data in order to ensure the transferability and general validity of the model. Machine learning models were trained with process data to evaluate the process solely based on the electrical process signals analyzed in real-time. This goal was to be achieved by developing a regression model to evaluate quality and a classification model to evaluate productivity. Accordingly, the thesis addressed the problem by establishing the research hypothesis that process performance and product quality in wire EDM can be realized with the use of machine learning methods by using continuously recorded electrical signals. The research hypothesis was critically examined using various questions. The scientific design framework in this work is determined in particular by the methods and techniques used in data analysis and the structure of the work is designed accordingly for the development of data-driven models.

The first step was therefore to develop a system for continuous time and spatially resolved recording of process data. To this end, it was first presented how the discharge energy of individual discharges can be determined offline using oscilloscope measurements. The signal processing methodology presented was then transferred to an FPGA system in the next step, with which process signals can be processed in real-time. This made it possible to record individual discharges with corresponding characterization of their discharge type in a continuous process. This measuring chain was then extended to record individual discharge types in a spatially resolved manner. A systematic data reduction was then carried out by agglomerating the process data. The data was agglomerated as much as possible without relevant information being lost. The measuring system and methodology developed therefore not only ensure the acquisition of large amounts of high-quality data.

For wire EDM process evaluation, various criteria for process productivity and product quality were analyzed in the main cut. Continuous process data was recorded to identify possible correlations with productivity and quality. The exploratory analysis revealed initial correlations and trends by examining the speed and occurrence of wire breaks based on the process data. Both macroscopic and microscopic changes were taken into account to evaluate product quality. Initial analyses showed correlations between curvature and discharge distribution over the height of the workpiece. The microscopic changes in surface roughness and the surface layer were not influenced by different process conditions such as nozzle distance or workpiece height.

Based on the initial findings from the process data, a regression model was developed to evaluate product quality. For this purpose, a neural network was trained that predicts the curvature of the component based on continuously recorded data. An automated feature extraction approach was used to extract a large number of statistical variables from the data sets. In addition to visual analysis, different methods of correlation analysis were applied and compared. Based on the results, some of the most important parameters were used as input parameters for the neural network and the network structure was determined using the random search approach. The model shows good prediction accuracy and explains a significant part of the data variability.

Unlike the previous instance, the productivity of the process was evaluated using a classification model. The cutting speed, process stability, and the contour produced, which ultimately also determines the number of trim cuts, were evaluated. This involved classifying different technology variants based on process data and assigning them to specific productivity levels. A deep learning approach was used, in which various forms of neural networks were used for the model architecture. For this purpose, a large number of experiments were carried out with modified machine parameters. The trained models were also validated with data from technology variants with different machining heights and with data from technology variants in which several machine parameters were changed simultaneously. The results showed a high accuracy for the sub models, especially considering that all testing were performed with completely unknown data.

Finally, it was shown how the findings can be transferred to the development of a Digital Twin in an industrial setting. To this end, it was first presented how a Digital Twin is developed in principle. In cooperation with an AI software manufacturer and a wire EDM user, a Digital Twin was developed that can map the machined curvature of the workpiece in a dashboard using data processed in real-time.

## Outlook

The findings in this thesis confirmed the demand in the field of data science for sufficient and high-quality data. Even though a large number of experiments were carried out in this work and a total of over 15 billion individual discharges were used for the models, it can be assumed that a higher amount of data will improve the performance of the machine learning models even further since the information density of the process data is very low and only beneficial by agglomerating the data. Additional work should, therefore, consider implementing data acquisition in systems that are in permanent operation. Based on the findings, such an implementation would be feasible. By linking appropriate optimization algorithms to the output of the prediction models, automated technology adaptation and optimization would be highly conceivable.

Furthermore, in the next step, it would be necessary to map the geometric deviation not only via the workpiece height but also in the cutting direction to predict the determined contour, to extend the applicability of the Digital Twin. This would require training models for the evaluation of edges and curves. Based on these findings, the geometric deviation should be known in all dimensions and direct measures for the application of the first trim cut could be derived. This could be done by adjusting the distance between the wire and the workpiece or by a tapered feed of the wire to eliminate component curvature or skewness over the workpiece height.

Finally, these approaches should be transferred to trim cuts. In addition to the current signals recorded so far, the voltage signal, which reflects the distance between the wire and the workpiece, should be considered. Initial analyses of the trim cuts revealed that characteristic properties can also be identified in the process data here. The used measuring system has also indicated that the signals can, in principle, be recorded in the same way using the methodology. However, a higher sampling frequency must be used here due to the shorter pulses. This was particularly evident when determining the position of trim cut discharges using the presented system. As the discharge currents in the trim cut are considerably smaller than in the main cut, the current difference is correspondingly smaller, and measurement inaccuracies have a much greater impact on the result. Measuring equipment must therefore be replaced by devices with higher sampling rates. In addition, it is no longer possible to differentiate between different discharge types for trim cut processing, as these only consist of one pulse type almost identical to the short circuit pulse forms in the main cut.



## Zusammenfassung und Ausblick

### Zusammenfassung

Die Hauptanwendungsgebiete der Drahtfunkenerosion liegen im Werkzeug- und Formenbau, sowie in der Triebwerks- und Medizintechnik. Bearbeitet werden oft Bauteile, die aufgrund ihrer Werkstoffeigenschaften und geforderten Toleranzen nicht mehr ökonomisch mit konventionellen Fertigungstechnologien gefertigt werden können. Dort kommt sie vor allem bei der Fertigung von hochpreisigen Produkten zum Einsatz und wird oft als letzte maßgebende Fertigungstechnologie eingesetzt. Daher sind die Prozesssicherheit und Wiederholbarkeit dieser Technologie besonders wichtig und können durch entsprechend intelligente Regelungen und Automatisierungslösungen gewährleistet werden. Dies und die Digitalisierung von Fertigungsprozessen im Kontext von Industrie 4.0 erfordern daher den Einsatz von datengetriebenen Lösungen in der Drahtfunkenerosion. Seitens der Maschinenhersteller existieren noch keine Lösungen für eine datengetriebene Prozessüberwachung oder Prozessentwicklung. Auf Basis der vorgestellten Arbeiten, in denen sich die Autoren mit Prozessdaten in der Drahtfunkenerosion auseinandersetzten, ergab sich ein Defizit für ein valides datengetriebenes Modell für die Bewertung des Prozesses.

Die Zielsetzung der vorliegenden Arbeit bestand demnach darin, ein datengetriebenes Modell zur Bewertung des Drahtfunkenerosionsprozesses zu entwickeln. Dieses sollte vor allem auf kontinuierlich aufgezeichneten physikalischen bzw. elektrischen Prozessdaten beruhen, um eine Übertragbarkeit und Allgemeingültigkeit des Modells zu gewährleisten. Mit den Prozessdaten wurden KI-Modelle trainiert, um den Prozess nur auf Basis der in Echtzeit ausgewerteten elektrischen Prozesssignale zu bewerten. Dieses Ziel sollte durch die Entwicklung eines Regressionsmodells zur Bewertung der Qualität und eines Klassifikationsmodells zur Bewertung der Produktivität realisiert werden. Entsprechend widmete sich die Arbeit der Problemstellung, indem die Forschungshypothese aufgestellt wurde, dass die Prozessperformance und die Produktqualität in der Drahtfunkenerosion mit dem Einsatz von Machine Learning Methoden durch Nutzen von kontinuierlich aufgezeichneten elektrischen Signalen realisiert werden können. Die Forschungshypothese wurden über verschiedene Fragestellungen kritisch überprüft. Der wissenschaftliche Gestaltungsrahmen wird in dieser Arbeit besonders durch die Methoden und Techniken in der Datenanalyse bestimmt und der Aufbau der Arbeit ist entsprechend für die Entwicklung datengetriebener Modelle ausgelegt.

In einem ersten Schritt wurde daher ein System zur kontinuierlichen orts- und zeitaufgelösten Aufzeichnung von Prozessdaten entwickelt. Dazu wurde zunächst vorgestellt, wie die Entladeenergie von einzelnen Entladungen offline durch Oszilloskopmessungen bestimmt werden kann. Die vorgestellte Methodik der Signalverarbeitung wurde dann im nächsten Schritt auf ein FPGA-System übertragen, mit dem sich Prozesssignale in Echtzeit verarbeiten lassen. Somit konnte eine Aufzeichnung von einzelnen Entladungen mit entsprechender Charakterisierung bezüglich ihres Entladetyps im kontinuierlichen Prozess realisiert werden. Diese



Messkette wurde anschließend erweitert, um einzelne Entladungstypen orts aufgelöst aufzuzeichnen. Anschließend erfolgte eine systematische Datenreduktion durch Agglomeration der Prozessdaten. Dabei wurden die Daten möglichst stark agglomeriert ohne, dass relevante Informationen verloren gehen. Mit dem entwickelten Messsystem und der Methodik ist somit eine Akquise von großen hoch qualitativen Datenmengen gewährleistet.

Zur Bewertung des Drahtfunkenerosionsprozesses wurden verschiedene Bewertungskriterien für die Prozessproduktivität und die Produktqualität im Hauptschnitt analysiert. Es wurden kontinuierliche Prozessdaten aufgezeichnet, um mögliche Korrelationen mit Produktivität und Qualität zu identifizieren. Die explorative Analyse ergab erste Korrelationen und Trends, indem die Geschwindigkeit und das Auftreten von Drahtbrüchen anhand der Prozessdaten untersucht wurden. Zur Bewertung der Produktqualität wurden sowohl makroskopische als auch mikroskopische Veränderungen berücksichtigt. Erste Analysen zeigten Korrelationen zwischen Wölbung und Entladungsverteilung über die Werkstückhöhe. Die mikroskopischen Veränderungen der Oberflächenrauheit und der Randschicht wurden nicht durch unterschiedliche Prozessbedingungen wie Düsenabstand oder Werkstückhöhe beeinflusst.

Basierend auf den ersten Erkenntnissen der Prozessdaten, wurde ein Regressionsmodell zur Bewertung der Produktqualität entwickelt. Dazu wurde ein neuronales Netz trainiert, das die Wölbung des Bauteils anhand kontinuierlich aufgezeichneter Daten vorhersagt. Ein automatisierter Ansatz zur Merkmalsextraktion wurde verwendet, um eine große Anzahl von statistischen Variablen aus den Datensätzen zu extrahieren. Neben der visuellen Analyse wurden verschiedene Methoden der Korrelationsanalyse angewandt und verglichen. Auf der Grundlage der Ergebnisse wurden einige der wichtigsten Parameter als Eingabeparameter für das neuronale Netz verwendet und mithilfe des Random-Search-Ansatzes die Netzstruktur bestimmt. Das Modell zeigt eine gute Vorhersagegenauigkeit und erklärt einen erheblichen Teil der Datenvariabilität.

Anders als zuvor sollte nun die Produktivität des Prozesses mithilfe eines Klassifikationsmodells bewertet werden. Bewertet wurden dafür die Schnittgeschwindigkeit, die Prozessstabilität und die erzeugte Kontur, die schließlich auch die Anzahl der Nachschnitte bestimmt. Dazu fand eine Klassifizierung verschiedener Technologievarianten auf der Grundlage von Prozessdaten und deren Einstufung in bestimmte Produktivitätsstufen statt. Es wurde ein Deep-Learning-Ansatz angewandt, bei dem verschiedene Formen neuronaler Netze für die Modellarchitektur verwendet wurden. Dazu wurden eine Vielzahl an Versuchen mit veränderten Maschinenparametern durchgeführt. Die trainierten Modelle wurden hierbei auch mit Daten aus Technologievarianten mit unterschiedlicher Bearbeitungshöhe validiert und mit Daten aus Technologievarianten, in denen mehrere Maschinenparameter gleichzeitig verändert wurden. Die Ergebnisse zeigten eine hohe Genauigkeit für die Teilmodelle, insbesondere unter Berücksichtigung, dass alle Validierungen mit völlig unbekannten Daten durchgeführt wurden.

Abschließend wurde im letzten Kapitel gezeigt, wie die Erkenntnisse in die Entwicklung eines Digitalen Zwillings in einem industriellen überführt werden können. Dazu wurde

zunächst vorgestellt, wie ein Digitaler Zwilling prinzipiell entwickelt wird. In kooperativer Arbeit mit einem KI-Software Hersteller und einem Drahtfunkenerosionsanwender, konnte ein Digitaler Zwilling entwickelt werden, der durch in Echtzeit verarbeitete Daten die erzeugte Kontur des Werkstücks in einem Dashboard abbilden kann.

### Ausblick

Die Erkenntnisse in dieser Arbeit bestätigten die Forderung im Data Science Bereich nach ausreichend und qualitativ hochwertigen Daten. Auch wenn in dieser Arbeit eine Vielzahl von Versuchen durchgeführt wurde und insgesamt für die Modelle über 15 Milliarden Einzelentladungen genutzt wurden, kann davon ausgegangen werden, dass sich durch mehr Daten die Performance der KI-Modelle verbessert. Dies liegt an der geringen Informationsdichte der Prozessdaten. Daher sollte für weitere Arbeiten in Betracht gezogen werden, ob die Datenerfassung nicht in Anlagen implementiert werden sollte, die dauerhaft in Betrieb sind. Eine Implementierung des Datenerfassungssystems wäre auf Basis der Erkenntnisse realisierbar. Eine automatisierte Technologieadaption und -optimierung wäre durch Anknüpfung entsprechender Optimierungsalgorithmen an den Output der Prädiktionsmodelle sehr gut vorstellbar. Des Weiteren wäre es im nächsten Schritt notwendig die geometrische Abweichung nicht nur über die Werkstückhöhe abzubilden, sondern auch in Schnittrichtung zur Prädiktion der ermittelten Kontur und somit den DT zu erweitern. Dazu müssten Modelle für die Bewertung von Kanten und Rundungen trainiert werden. Basierend auf diesen Erkenntnissen sollte die geometrische Abweichung in allen Dimensionen bekannt sein und es sollten sich direkte Maßnahmen für die Anwendung des ersten Nachschnitts ableiten. Die kann durch eine Zustellung des Drahtabstands zum Werkstück oder durch eine konische Zustellung des Drahtes, um entsprechend eine Bauteilwölbung oder Bauteilschiefen über die Höhe zu eliminieren.

Zuletzt sollten diese Ansätze auf die Nachschnitte übertragen werden. Dafür sollten neben den bisher aufgezeichneten Stromsignalen auch zusätzlich das Spannungssignal aufgezeichnet werden, welches den Abstand des Drahtes zum Werkstück widerspiegelt. Erste Analysen der Nachschnitte zeigten, dass auch hier charakteristische Eigenschaften in den Prozessdaten identifiziert werden können. Mit dem eingesetzten Messsystem hat sich auch gezeigt, dass die Signale sich prinzipiell mit der Methodik auf die gleiche Weise erfassen lassen. Jedoch muss hier aufgrund der kürzeren Pulse eine höhere Abtastfrequenz genutzt werden. Dies ergab sich besonders bei der Positionsermittlung von Nachschnittentladungen mittels des vorgestellten Systems. Da die Entladeströme im Nachschnitt wesentlich kleiner sind als im Hauptschnitt, ist die Stromdifferenz entsprechend kleiner und Messungenauigkeiten zeichnen sich wesentlich stärker auf das Ergebnis aus. Daher müssen entsprechend Messmittel durch Geräte mit höheren Abtastraten ersetzt werden. Zudem kann für die Nachschnittbearbeitung nicht mehr auf die Unterscheidung von verschiedenen Entladetypen zurückgegriffen werden, da diese nur noch aus einem Pulstypen bestehen, der fast identisch zu den Kurzschlussentladeformen ist.



## 10 References

- [ABEL09] Abel, D.: Umdruck zur Vorlesung Regelungstechnik und Ergänzungen (Höhere Regelungstechnik). 33. Aufl. Aachen: Verlagshaus Mainz, 2009
- [ABHI20a] Abhilash, P.; Chakradhar, D.: ANFIS modelling of mean gap voltage variation to predict wire breakages during wire EDM of Inconel 718. In: CIRP Journal of Manufacturing Science and Technology, 31. Jg., 2020, S. 153–164
- [ABHI20b] Abhilash, P.; Chakradhar, D.: Prediction and analysis of process failures by ANN classification during wire-EDM of Inconel 718. In: Advances in Manufacturing, 8. Jg., 2020, S. 519–536
- [ABHI21a] Abhilash, P.; Chakradhar, D.: Image processing algorithm for detection, quantification and classification of microdefects in wire electric discharge machined precision finish cut surfaces. In: Journal of Micromanufacturing. 2021, S. 116–126
- [ABHI21b] Abhilash, P.; Chakradhar, D.: Failure detection and control for wire EDM process using multiple sensors. In: CIRP Journal of Manufacturing Science and Technology, 33. Jg., 2021, S. 315–326
- [ABHI22a] Abhilash, P.; Chakradhar, D.: Wire EDM failure prediction and process control based on sensor fusion and pulse train analysis. In: The International Journal of Advanced Manufacturing Technology, 118. Jg., 2022, S. 1453–1467
- [ABHI22b] Abhilash, P.; Chakradhar, D.: Machine-vision-based electrode wear analysis for closed loop wire EDM process control. In: Advances in Manufacturing, 10. Jg., 2022, S. 131–142
- [ABHI22c] Abhilash, P.; Chakradhar, D.; Xichun Luo: Machine Learning Based Classification and Analysis of Wire-EDM Discharge Pulses using kernel-based naive Bayes classifier. In: Proceedings of the 8th International Conference on Nanomanufacturing & 4th AET Symposium on ACSM and Digital Manufacturing (Nanoman-AETS). 2022, S. 1–6
- [AHMA07] Ahmad, A.; Dey, L.: A k-mean clustering algorithm for mixed numeric and categorical data. In: Data & Knowledge Engineering, 63. Jg., 2007, S. 503–527
- [AHME17] Ahmed Bufardi; Olcay Akten; Muhammad Arif; Paul Xirouchakis; Roberto Perez: Towards zero-defect manufacturing with a combined online - offline fuzzy-nets approach in wire electrical discharge machining. In: WSEAS Transactions on Environment and Development, 13. Jg., 2017, S. 401–409
- [ARTH07] Arthur, D.; Vassilvitskii, S.: K-Means++: The Advantages of Careful Seeding (Hrsg): Proceedings of the Eighteenth Annual ACM-SIAM Symposium on Discrete Algorithms, S. 1027–1035
- [ARUN01] Arunachalam, C.; Aulia, M.; Bozkurt, B.; Eubank, P.: Wire vibration, bowing, and breakage in wire electrical discharge machining. In: Journal of Applied Physics, 89. Jg., 2001, S. 4255–4262

- [ASKH13] Askham, N.; Cook, D.; Doyle, M.; Fereday, H.; Gibson, M.; Landbeck, U.; Lee, R.; Maynard, C.; Palmer, G.; Schwarzenbach, J.: The six primary dimensions for data quality assessment. In: DAMA UK working group. 2013, S. 432–435
- [AUST21] Aust, H.: Das Zeitalter der Daten. Was Sie über Grundlagen, Algorithmen und Anwendungen wissen sollten. Berlin, Heidelberg: Springer, 2021
- [BACH04] Bach, F.; Jordan, M.: Learning Spectral Clustering. In: In Proceedings of 17th Advances in Neural Information Processing Systems, 16. Jg., 2004
- [BACH10] Bacher, J.; Pöge, A.; Wenzig, K.: Clusteranalyse. Oldenbourg Wissenschaftsverlag, 2010
- [BADI20] Badillo, S.; Banfai, B.; Birzele, F.; Davydov, I.; Hutchinson, L.; Kam-Thong, T.; Siebourg-Polster, J.; Steiert, B.; Zhang, J.: An Introduction to Machine Learning. In: Clinical pharmacology and therapeutics, 107. Jg., 2020, S. 871–885
- [BAHL20] El-Bahloul, S.: Optimization of wire electrical discharge machining using statistical methods coupled with artificial intelligence techniques and soft computing. In: SN Applied Sciences, 2. Jg., 2020
- [BANE93] Banerjee, S.; Prasad, B.; Mishra, P.: A simple model to estimate the thermal loads on an EDM wire electrode. In: Journal of Materials Processing Technology, 39. Jg., 1993, S. 305–317
- [BERG12] Bergstra, J.; Bengio, Y.: Random search for hyper-parameter optimization. In: Journal of Machine Learning Research, 13. Jg., 2012
- [BERG18a] Bergs, T.; Tombul, U.; Herrig, T.; Klink, A.; Klocke, F.: Experimental Analysis of Influence of Discharge Current, Pulse Interval Time and Flushing Conditions on WEDM Performance. In: Procedia Manufacturing, 18. Jg., 2018, S. 130–137
- [BERG18b] Bergs, T.; Tombul, U.; Herrig, T.; Olivier, M.; Klink, A.; Klocke, F.: Analysis of Characteristic Process Parameters to Identify Unstable Process Conditions during Wire EDM. In: Procedia Manufacturing, 18. Jg., 2018, S. 138–145
- [BERG20a] Bergs, T.; Tombul, U.; Mevissen, D.; Klink, A.; Brimmers, J.: Load Capacity of Rolling Contacts Manufactured by Wire EDM Turning. In: Procedia CIRP, 87. Jg., 2020, S. 474–479
- [BERG20b] Bergs, T.; Tombul, U.; Herrig, T.; Klink, A.; Welling, D.: Influence of an Additional Indexing Rotary Axis On Wire Edm Performance for the Automated Manufacture of Fir Tree Slots. In: Journal of Engineering for Gas Turbines and Power. 2020
- [BERG20c] Bergs, T.; Gierlings, S.; Augspurger, T.: Mit dem Digitalen Zwilling Prozessgrenzen überwinden. In: Internet of Production-Turning Data into Value: Statusberichte der Produktionstechnik. 2020, S. 81–113, Aachen.
- [BERG20d] Bergs, T.; Welschhof, L.; Herrig, T.; Klink, A.: Energetic Characterization of Trim Cut Process Signals in Wire EDM. In: Procedia CIRP, 95. Jg., 2020, S. 262–267

- [BERG21] Bergs, T.; Gierlings, S.; Auerbach, T.; Klink, A.; Schraknepper, D.; Augspurger, T.: The Concept of Digital Twin and Digital Shadow in Manufacturing. In: *Procedia CIRP*, 101. Jg., 2021, S. 81–84
- [BERK24a] Berkenhoff GmbH: bedraEDM. bercocut pro 900. URL: <https://www.bedra.com/europe/products/bedraedm/bercocut-pro-900> [25.07.2024]
- [BERK24b] Berkenhoff GmbH: bedraEDM. betterbrass ONE.9. URL: <https://www.bedra.com/europe/products/bedraedm/betterbrass/> [25.07.2024]
- [BERO93] Beroual, A.: Electronic and gaseous processes in the prebreakdown phenomena of dielectric liquids. In: *Journal of Applied Physics*, 73. Jg., 1993, S. 4528–4533
- [BEZD81] Bezdek, J.: *Pattern Recognition with Fuzzy Objective Function Algorithms*. Boston, MA: Springer US, 1981
- [BISH06] Bishop, C.: *Pattern recognition and machine learning*. New York, NY: Springer, 2006
- [BLEC18] Bleck, W.; Moeller, E.: *Handbuch Stahl. Auswahl, Verarbeitung, Anwendung*. München: 2018
- [BOCC18] Boccadoro, M.: Spark Track: A Breakthrough in WEDM. In: *Experts Corner EDM Today*, 2018, S. 70–73
- [BOCC20] Boccadoro, M.; D'Amario, R.; Baumeler, M.: Towards a better controlled EDM: industrial applications of a discharge location sensor in an industrial wire electrical discharge machine. In: *Procedia CIRP*, 95. Jg., 2020, S. 600–604
- [BOOS18] Boos, W.; Salmen, M.; Kelzenberg, C.; Johannsen, L.; Helbig, J.; Ebbecke, C.: *Tooling in Germany 2018*. 2. Aufl. Aachen: RWTH Aachen Werkzeugmaschinenlabor, 2018
- [BOWE20] Bowen, D.; Ungar, L.: *Generalized SHAP: Generating multiple types of explanations in machine learning*, 2020
- [BRAN10] Brans, K.: *Electrical Discharge Machining of Advanced Ceramics*. Dissertation Katholieke Universiteit Leuven, 2010
- [BREC11] Brecher, C.: *Integrative Produktionstechnik für Hochlohnländer*. 1. Aufl. Berlin, Heidelberg: 2011
- [BUND21] Bundesministerium für Wirtschaft und Klimaschutz (BMWK): *Deutsche Klimapolitik. Verbindlicher Klimaschutz durch das Bundes-Klimaschutzgesetz*. URL: <https://www.bmwk.de/Redaktion/DE/Artikel/Industrie/klimaschutz-deutsche-klimaschutzpolitik.html> [20.05.2024]
- [BURS24] Burstedde, A.; Kolev-Schaefer, G.: *Die Kosten des Fachkräftemangels*. IW-Kurzbericht Nr. 27/2024, 2024
- [BUXM21] Buxmann, P.; Schmidt, H.: *Künstliche Intelligenz. Mit Algorithmen zum wirtschaftlichen Erfolg*. 2., aktualisierte und erweiterte. Aufl. Berlin, Heidelberg: Springer Gabler, 2021

- [CABA08a] Cabanes, I.; Portillo, E.; Marcos, M.; Sánchez, J.: On-line prevention of wire breakage in wire electro-discharge machining. In: *Robotics and Computer-Integrated Manufacturing*, 24. Jg., 2008, S. 287–298
- [CABA08b] Cabanes, I.; Portillo, E.; Marcos, M.; Sánchez, J.: An industrial application for on-line detection of instability and wire breakage in wire EDM. In: *Journal of Materials Processing Technology*, 195. Jg., 2008, S. 101–109
- [CAGG15] Caggiano, A.; Teti, R.; Perez, R.; Xirouchakis, P.: Wire EDM Monitoring for Zero-defect Manufacturing based on Advanced Sensor Signal Processing. In: *Procedia CIRP*, 33. Jg., 2015, S. 315–320
- [CAGG16] Caggiano, A.; Perez, R.; Segreto, T.; Teti, R.; Xirouchakis, P.: Advanced Sensor Signal Feature Extraction and Pattern Recognition for Wire EDM Process Monitoring. In: *Procedia CIRP*, 42. Jg., 2016, S. 34–39
- [CAGG20] Caggiano, A.; Napolitano, F.; Teti, R.; Bonini, S.; Maradia, U.: Advanced die sinking EDM process monitoring based on anomaly detection for online identification of improper process conditions. In: *Procedia CIRP*, 88. Jg., 2020, S. 381–386
- [CARR22] Carrión, C.: Kubernetes as a Standard Container Orchestrator - A Bibliometric Analysis. In: *Journal of Grid Computing*, 20. Jg., 2022
- [ÇAYD09] Çaydaş, U.; Hasçalık, A.; Ekici, S.: An adaptive neuro-fuzzy inference system (ANFIS) model for wire-EDM. In: *Expert Systems with Applications*, 36. Jg., 2009, S. 6135–6139
- [CHEN10] Chen, H.-C.; Lin, J.-C.; Yang, Y.-K.; Tsai, C.-H.: Optimization of wire electrical discharge machining for pure tungsten using a neural network integrated simulated annealing approach. In: *Expert Systems with Applications*, 37. Jg., 2010, S. 7147–7153
- [CHEN15] Chen, Z.; Huang, Y.; Huang, H.; Zhang, Z.; Zhang, G.: Three-dimensional characteristics analysis of the wire-tool vibration considering spatial temperature field and electromagnetic field in WEDM. In: *International Journal of Machine Tools and Manufacture*, 92. Jg., 2015, S. 85–96
- [CHOU18] Choudhuri, B.; Sen, R.; Kumar Ghosh, S.; Saha, S.: Study of surface integrity and recast surface machined by Wire electrical discharge machining. In: *Materials Today: Proceedings*, 5. Jg., 2018, S. 7515–7524
- [COND16] Conde, A.; Sanchez, J.; Plaza, S.; Ramos, J.: On the Influence of Wire-lag on the WEDM of Low-radius Free-form Geometries. In: *Procedia CIRP*, 42. Jg., 2016, S. 274–279
- [COND18a] Conde, A.; Sanchez, J.; Plaza, S.; Ostolaza, M.; La Puerta, I. de; Li, Z.: Experimental Measurement of Wire-lag Effect and Its Relation with Signal Classification on Wire EDM. In: *Procedia CIRP*, 68. Jg., 2018, S. 132–137
- [COND18b] Conde, A.; Arriandiaga, A.; Sanchez, J.; Portillo, E.; Plaza, S.; Cabanes, I.: High-accuracy wire electrical discharge machining using artificial neural networks

- and optimization techniques. In: *Robotics and Computer-Integrated Manufacturing*, 49. Jg., 2018, S. 24–38
- [ÇPUN90] Çpun C.: A technique and its application for evaluation of material removal contributions of pulses in electric discharge machining (EDM). In: *International Journal of Machine Tools & Manufacture*, 30. Jg., 1990, S. 19–31
- [DARB22] Darban, Z.; Webb, G.; Pan, S.; Aggarwal, C.; Salehi, M.: *Deep Learning for Time Series Anomaly Detection: A Survey*, 2022
- [DAUW86] Daww, D.; Snaeys, R.: ADAPTIVE CONTROL OPTIMIZATION OF THE ELECTRO-DISCHARGE MACHINING PROCESS BY REAL TIME PULSE DETECTION. In: *Advanced Manufacturing Processes*, 1. Jg., 1986, S. 45–81
- [DEKE85] Dekeyser, W.; Snoeys, R.; Jennes, M.: A thermal model to investigate the wire rupture phenomenon for improving performance in EDM wire cutting. In: *Journal of Manufacturing Systems*, 4. Jg., 1985, S. 179–190
- [DEKE88] Dekeyser, W.; Snoeys, R.; Jennes, M.: Expert system for wire cutting EDM, based on pulse classification and thermal modeling. In: *Robotics and Computer-Integrated Manufacturing*, 4. Jg., 1988, S. 219–224
- [DEKE89] Dekeyser, W.; Snoeys, R.; Kruth, J.: Geometrical accuracy of wire-EDM. In: *Engineering, Materials Science*. 1989
- [DICA20] Di Campli, R.; Maradia, U.; Boccadoro, M.; D'Amario, R.; Mazzolini, L.: Real-Time Wire EDM Tool Simulation Enabled by Discharge Location Tracker. In: *Procedia CIRP*, 95. Jg., 2020, S. 308–312
- [DIN03]: DIN 8590:2003-09, *Fertigungsverfahren Abtragen\_- Einordnung, Unterteilung, Begriffe*, 2003
- [DIN22]: DIN EN ISO 21920-2:2022-12, *Geometrische Produktspezifikation\_(GPS)\_- Oberflächenbeschaffenheit: Profile\_- Teil\_2: Begriffe und Kenngrößen für die Oberflächenbeschaffenheit (ISO\_21920-2:2021, korrigierte Fassung 2022-06)*; Deutsche Fassung EN\_ISO\_21920-2:2022.
- [DIN98]: DIN EN ISO 13565-1:1998-04, *Geometrische Produktspezifikationen (GPS)\_- Oberflächenbeschaffenheit: Tastschnittverfahren\_- Oberflächen mit plateauartigen funktionsrelevanten Eigenschaften\_- Teil\_1: Filterung und allgemeine Meßbedingungen (ISO\_13565-1:1996)*; Deutsche Fassung EN\_ISO\_13565-1:1997.
- [DING08] Ding, S.; Jia, W.; Su, C.; Xu, X.; Zhang, L.: PCA-Based Elman Neural Network Algorithm. Kang, L.; Cai, Z.; Yan, X.; Liu, Y. (Hrsg): *Advances in Computation and Intelligence*. (Reihe: *Lecture Notes in Computer Science*, Berlin, Heidelberg: Springer Berlin Heidelberg, 2008, S. 315–321
- [DRZA22] Držajić, D.; Wiessner, M.; Maradia, U.; Piga, D.: Virtual Operators with Self and Transfer Learning Ability in EDM. In: *Procedia CIRP*, 113. Jg., 2022, S. 17–22
- [DURA13] Durairaj, M.; Sudharsun, D.; Swamynathan, N.: Analysis of Process Parameters in Wire EDM with Stainless Steel Using Single Objective Taguchi Method and Multi



- Objective Grey Relational Grade. In: *Procedia Engineering*, 64. Jg., 2013, S. 868–877
- [EBIS18] Ebisu, T.; Kawata, A.; Okamoto, Y.; Okada, A.; Kurihara, H.: Influence of Jet Flushing on Corner Shape Accuracy in Wire EDM. In: *Procedia CIRP*, 68. Jg., 2018, S. 104–108
- [ELLI07] Elliott, C.; Vijayakumar, V.; Zink, W.; Hansen, R.: National Instruments LabVIEW: A Programming Environment for Laboratory Automation and Measurement. In: *JALA: Journal of the Association for Laboratory Automation*, 12. Jg., 2007, S. 17–24
- [ERB93] Erb, R.: Introduction to backpropagation neural network computation. In: *Pharmaceutical research*, 10. Jg., 1993, S. 165–170
- [ERTE16] Ertel, W.: *Grundkurs Künstliche Intelligenz. Eine praxisorientierte Einführung*. 4., überarbeitete Auflage. Aufl. Wiesbaden: Springer Vieweg, 2016
- [FAHR16] Fahrmeir, L.; Heumann, C.; Künstler, R.; Pigeot, I.; Tutz, G.: *Statistik. Der Weg zur Datenanalyse*. 8. Aufl. Berlin, Heidelberg: Springer Spektrum, 2016
- [FEDO18] Fedorov, A.; Blesman, A.; Postnikov, D.; Polonyankin, D.; Russkikh, G.; Linovsky, A.: Investigation of the impact of Rehbinder effect, electrical erosion and wire tension on wire breakages during WEDM. In: *Journal of Materials Processing Technology*, 256. Jg., 2018, S. 131–144
- [FERG22] Fergus, P.; Chalmers, C.: *Supervised Learning*. Fergus, P.; Chalmers, C. (Hrsg): *Applied Deep Learning*. (Reihe: Computational Intelligence Methods and Applications, Cham: Springer International Publishing, 2022, S. 63–93
- [FISH66] Fisher, R.; Genetiker, S.; Genetician, S.; Britain, G.; Généticien, S.: *The design of experiments*. Oliver and Boyd Edinburgh, 1966
- [FLOU09] Floudas, C.; Pardalos, P.: *Encyclopedia of optimization*. With 247 tables. 2. ed. Aufl. New York: Springer Science+Business Media LLC, 2009
- [FRAU18] Fraunhofer - Gesellschaft: *Maschinelles Lernen - Kompetenzen, Anwendungen und Forschungsbedarf*. URL: [https://www.bigdata-ai.fraunhofer.de/content/dam/bigdata/de/documents/Publikationen/Fraunhofer\\_Studie\\_ML\\_201809.pdf](https://www.bigdata-ai.fraunhofer.de/content/dam/bigdata/de/documents/Publikationen/Fraunhofer_Studie_ML_201809.pdf) [10.07.2024]
- [FREI02] Freitas, A.; Rozenberg, G.; Bäck, T.; Eiben, A.; Kok, J.; Späink, H.: *Data Mining and Knowledge Discovery with Evolutionary Algorithms*. Berlin, Heidelberg: Springer Berlin Heidelberg, 2002
- [FROC21] Frochte, J.: *Maschinelles Lernen. Grundlagen und Algorithmen in Python*. 3., überarbeitete und erweiterte Auflage. Aufl. München: Hanser, 2021
- [FUJI12] Fujimoto, T.; Okada, A.; Okamoto, Y.; Uno, Y.: Optimization of Nozzle Flushing Method for Smooth Debris Exclusion in Wire EDM. In: *Key Engineering Materials*, 516. Jg., 2012, S. 73–78

- [GAD22] Gad, A.: Particle Swarm Optimization Algorithm and Its Applications: A Systematic Review. In: Archives of Computational Methods in Engineering, 29. Jg., 2022, S. 2531–2561
- [GAMA16] Gamage, J.; DeSilva, A.: Effect of Wire Breakage on the Process Energy Utilisation of EDM. In: Procedia CIRP, 42. Jg., 2016, S. 586–590
- [GIJS24] Gijssbers, P.; Bueno, M. L. P.; Coors, S.; LeDell, E.; Poirier, S.; Thomas, J.; Bischl, B.; Vanschoren, J.: AMLB: an AutoML Benchmark. In: Journal of Machine Learning Research, 25. Jg., 2024, S. 1–65
- [GINZ02] Ginzel, J.: Funkenerosives Senken mit Neuro-Fuzzy Prozeßführung und Fehlentladungsbehandlung unter Berücksichtigung der Bahn- und Planetärerrosion. Zugl.: Hamburg, Univ. der Bundeswehr, Diss., 2002, München: Utz Wiss, 2002
- [GOOD16] Goodfellow, I.; Courville, A.; Bengio, Y.: Deep learning. Cambridge, Massachusetts: The MIT Press, 2016
- [GOST12] Gostimirovic, M.; Kovac, P.; Sekulic, M.; Skoric, B.: Influence of discharge energy on machining characteristics in EDM. In: Journal of Mechanical Science and Technology, 26. Jg., 2012, S. 173–179
- [GOYA21] Goyal, A.; Gautam, N.; Pathak, V.: An adaptive neuro-fuzzy and NSGA-II-based hybrid approach for modelling and multi-objective optimization of WEDM quality characteristics during machining titanium alloy. In: Neural Computing and Applications, 33. Jg., 2021, S. 16659–16674
- [GOYA22] Goyal, K.; Sharma, N.; Dev Gupta, R.; Singh, G.; Rani, D.; Banga, H.; Kumar, R.; Pimenov, D.; Giasin, K.: A Soft Computing-Based Analysis of Cutting Rate and Recast Layer Thickness for AZ31 Alloy on WEDM Using RSM-MOPSO. In: Materials (Basel, Switzerland), 15. Jg., 2022
- [GUO03] Guo, Z.; Yue, T.; Lee, T.; Lau, W.: Computer simulation and characteristic analysis of electrode fluctuation in wire electric discharge machining. In: Journal of Materials Processing Technology, 142. Jg., 2003, S. 576–581
- [GUO23] Guo, Y.; Klink, A.; Bartolo, P.; Guo, W.: Digital twins for electro-physical, chemical, and photonic processes. In: CIRP Annals, 72. Jg., 2023, S. 593–619
- [GURU17] Gurupavan, H.; Devegowda, T.; Ravindra, H.; Ugrasen, G.: Estimation of Machining Performances in WEDM of Aluminium based Metal Matrix Composite Material using ANN. In: Materials Today: Proceedings, 4. Jg., 2017, S. 10035–10038
- [HADA12] Hada, K.; Kunieda, M.: Analysis of Discharge Current in Wire-EDM Considering Electromagnetic Fields in and between Electrodes. In: Key Engineering Materials, 523-524. Jg., 2012, S. 281–286
- [HADA13] Hada, K.; Kunieda, M.: Analysis of Wire Impedance in Wire-EDM Considering Electromagnetic Fields Generated around Wire Electrode. In: Procedia CIRP, 6. Jg., 2013, S. 244–249

- [HAN04] Han, F.; Kunieda, M.; ASANO, H.: Improvement of Controllability of Discharge Locations in WEDM. In: Journal of The Japan Society of Electrical Machining Engineers, 38. Jg., 2004, S. 31–36
- [HAN08a] Han, F.; Cheng, G.; Feng, Z.; Isago, S.: Thermo-mechanical analysis and optimal tension control of micro wire electrode. In: International Journal of Machine Tools and Manufacture, 48. Jg., 2008, S. 922–931
- [HAN08b] Han, F.; Grangure, P.; Kunieda, M.: Improvement in accuracy in potential method for detecting EDM spark locations. In: Journal of Materials Processing Technology, 206. Jg., 2008, S. 328–332
- [HASH09] Hashimoto, T.; Yamada, H.; Hattori, K.; Ishii, S.: Study of the Machining Shape Monitor in Wire EDM. In: Journal of The Japan Society of Electrical Machining Engineers, 43. Jg., 2009, S. 1–8
- [HEID21] Heidemanns, L.; Seelbach, T.; Küpper, U.; Seimann, M.; Bergs, T.: Manufacturing Technologies for Fir Tree Slots: A Technological and Economic Evaluation (Hrsg): Proceedings of ASME Turbo Expo 2021: Turbomachinery Technical Conference and Exposition. June 7-11, 2021, virtual, online. 6/7/2021 - 6/11/2021, Virtual, Online
- [HENS17] Hensgen, L.: Auswirkung der Drahtfunkenerosion auf die mechanischen Eigenschaften von Festkörpergelenken. Dissertation RWTH Aachen University.1. Aufl. Aachen Apprimus Wissenschaftsverlag, 2017
- [HENS84] Hensgen, G.: Werkzeugspezifische Einflüsse beim funkenerosiven Schneiden mit ablaufender Drahtelektrode. Dissertation RWTH Aachen, 1984
- [HESS22] Hess, R.; Grethe, P.; Heidemanns, L.; Herrig, T.; Klink, A.; Bergs, T.: Simulation based derivation of changed rim zone properties caused by thermal loadings during EDM process. In: Procedia CIRP, 113. Jg., 2022, S. 41–46
- [HO03] Ho, K.; Newman, S.: State of the art electrical discharge machining (EDM). In: International Journal of Machine Tools and Manufacture, 43. Jg., 2003, S. 1287–1300
- [HOCH97] Hochreiter, S.; Schmidhuber, J.: Long short-term memory. In: Neural computation, 9. Jg., 1997, S. 1735–1780
- [HOCK67] Hockenberry, T.; Williams, E.: Dynamic Evolution of Events Accompanying the Low-Voltage Discharges Employed in EDM. In: IEEE Transactions on Industry and General Applications, IGA-3. Jg., 1967, S. 302–309
- [HOFM13] Hofmann, H.; Spindler, J.: Werkstoffe in der Elektrotechnik: Grundlagen - Struktur - Eigenschaften - Prüfung - Anwendung - Technologie. Hanser, Carl, 2013
- [HOLS18] Holsten, M.: Polarity-dependent removal interferences in sink EDM of titanium alloys. Dissertation RWTH Aachen University.1. Aufl. Aachen Apprimus Wissenschaftsverlag, 2018

- [HOLS19] Holsten, M.; Klink, A.; Bergs, T.: Concepts for Advancing the Use of Process Data in Electrical Discharge Machining. In: *Procedia CIRP*, 82. Jg., 2019, S. 220–223
- [HUAN18] Huang, G.; Xia, W.; Qin, L.; Zhao, W.: Online Workpiece Height Estimation for Reciprocated Traveling Wire EDM Based on Support Vector Machine. In: *Procedia CIRP*, 68. Jg., 2018, S. 126–131
- [HWAN81] Hwang, C.; Yoon, K.: Multiple attribute decision making. Methods and applications ; a state-of-the-art-survey. Berlin, Heidelberg: Springer, 1981
- [IPEK08] Ipek, E.; Mutlu, O.; Martínez, J.; Caruana, R.: Self-Optimizing Memory Controllers: A Reinforcement Learning Approach (Hrsg): 2008 International Symposium on Computer Architecture. 21.06.2008 - 25.06.2008, Beijing, China, S. 39–50
- [IWAI20] IWAI, H.; Ebisu, T.; Okada, A.; Kurihara, H.: Influence of Nozzle Jet Flushing on Working Fluid Flow and Wire Electrode in Trim-cut WEDM. In: *Procedia CIRP*, 95. Jg., 2020, S. 250–254
- [JABB14] Jabbar, H.; Khan, R.: Methods to Avoid Over-Fitting and Under-Fitting in Supervised Machine Learning (Comparative Study) (Hrsg): Computer Science, Communication and Instrumentation Devices. 27.12.2014 - 27.12.2014, S. 163–172
- [JANG93] Jang, J.-S.: ANFIS: adaptive-network-based fuzzy inference system. In: *IEEE Transactions on Systems, Man, and Cybernetics*, 23. Jg., 1993, S. 665–685
- [JAVA23] Javid, M.; Haleem, A.; Singh, R.: A study on ChatGPT for Industry 4.0: Background, potentials, challenges, and eventualities. In: *Journal of Economy and Technology*, 1. Jg., 2023, S. 127–143
- [JIAW12] Jiawei Han; Micheline Kamber; Jian Pei: 11 - Advanced Cluster Analysis. Jiawei Han; Micheline Kamber; Jian Pei (Hrsg): *Data Mining (Third Edition)*. (Reihe: The Morgan Kaufmann Series in Data Management Systems). Third Edition. Aufl. Boston: Morgan Kaufmann, 2012, S. 497–541
- [JONE20] Jones, D.; Snider, C.; Nassehi, A.; Yon, J.; Hicks, B.: Characterising the Digital Twin: A systematic literature review. In: *CIRP Journal of Manufacturing Science and Technology*. 2020
- [KERA24] Keras: About Keras 3. Keras 3 is a multi-framework deep learning API. URL: <https://keras.io/about/> [09.03.2024]
- [KETK17] Ketkar, N.: Introduction to Keras. Ketkar, N. (Hrsg): *Deep Learning with Python. A Hands-on Introduction*. (Reihe: For professionals by professionals, Berkeley, CA, New York, Ny: Apress; Springer Science+Business Media, 2017, S. 97–111
- [KHA17] Khair, U.; Fahmi, H.; Hakim, S.; Rahim, R.: Forecasting Error Calculation with Mean Absolute Deviation and Mean Absolute Percentage Error. In: *Journal of Physics: Conference Series*, 930. Jg., 2017, S. 12002
- [KIM18] Kim, D.-H.; Kim, T.; Wang, X.; Kim, M.; Quan, Y.-J.; Oh, J.; Min, S.-H.; Kim, H.; Bhandari, B.; Yang, I.; Ahn, Sung-Hoon: Smart Machining Process Using Machine Learning. A Review and Perspective on Machining Industry. In: *International*

- Journal of Precision Engineering and Manufacturing-Green Technology, 5. Jg., 2018, S. 555–568
- [KIMU22] KIMURA, S.; IWAI, H.; LIU, S.; Okada, A.; Kurihara, H.: Influence of Nozzle Jet Flushing in Wire EDM of Workpiece with Stepped Thickness. In: *Procedia CIRP*, 113. Jg., 2022, S. 149–154
- [KING14] Kingma, D.; Ba, J.: Adam: A Method for Stochastic Optimization. In: 3rd International Conference for Learning Representations CoRR, San Diego. 2014
- [KINO82] Kinoshita, N.; Fukui, M.; Gamo, G.: Control of Wire-EDM Preventing Electrode from Breaking. In: *CIRP Annals*, 31. Jg., 1982, S. 111–114
- [KIRA21] Kiranyaz, S.; Avci, O.; Abdeljaber, O.; Ince, T.; Gabbouj, M.; Inman, D.: 1D convolutional neural networks and applications: A survey. In: *Mechanical Systems and Signal Processing*, 151. Jg., 2021, S. 107398
- [KIRK83] Kirkpatrick, S.; Gelatt, C.; Vecchi, M.: Optimization by simulated annealing. In: *Science*, 220. Jg., 1983, S. 671–680
- [KLIN09] Klink, A.: Funkenerosives und elektrochemisches Abrichten feinkörniger Schleifwerkzeuge. 1. Aufl. Zugl.: Aachen, Techn. Hochsch., Diss., 2009, Aachen: Apprimus-Verl., 2009
- [KLIN14] Klink, A.: Electric Discharge Machining. Laperrière, L. (Hrsg): *CIRP Encyclopedia of production engineering*. (Reihe: Springer reference, Heidelberg, Berlin: Springer, 2014, S. 439–443
- [KLIN16] Klink, A.: Process Signatures of EDM and ECM Processes – Overview from Part Functionality and Surface Modification Point of View. In: *Procedia CIRP*, 42. Jg., 2016, S. 240–245
- [KLIN17] Klink, A.; Holsten, M.; Hensgen, L.: Crater morphology evaluation of contemporary advanced EDM generator technology. In: *CIRP Annals - Manufacturing Technology*, 66. Jg., 2017, S. 197–200
- [KLOC07] Klocke, F.; König, W.: *Fertigungsverfahren 3. Abtragen, Generieren Lasermaterialbearbeitung*. 4. Aufl. Berlin, Heidelberg: Springer-Verlag Berlin Heidelberg, 2007
- [KLOC13] Klocke, F.; Zeis, M.; Klink, A.; Veselovac, D.: Technological and economical comparison of roughing strategies via milling, sinking-EDM, wire-EDM and ECM for titanium- and nickel-based blisks. In: *CIRP Journal of Manufacturing Science and Technology*, 6. Jg., 2013, S. 198–203
- [KLOC14a] Klocke, F.; Klink, A.; Veselovac, D.; Aspinwall, D.; Soo, S.; Schmidt, M.; Schilp, J.; Levy, G.; Kruth, J.-P.: Turbomachinery component manufacture by application of electrochemical, electro-physical and photonic processes. In: *CIRP Annals*, 63. Jg., 2014, S. 703–726
- [KLOC14b] Klocke, F.; Welling, D.; Klink, A.; Perez, R.: Quality Assessment through In-process Monitoring of Wire-EDM for Fir Tree Slot Production. In: *Procedia CIRP*, 24. Jg., 2014, S. 97–102

- [KLOC16] Klocke, F.; Hensgen, L.; Klink, A.; Ehle, L.; Schwedt, A.: Structure and Composition of the White Layer in the Wire-EDM Process. In: *Procedia CIRP*, 42. Jg., 2016, S. 673–678
- [KOBA99] Kobayashi, M.; Ohta, T.; Yoshino, H.; Saga, S.; Kunieda, M.: Control of Discharge Location in EDM by Locally Superimposing High Electric Field. In: *Journal of the Japan Society for Precision Engineering*, 65. Jg., 1999, S. 1492–1496
- [KUNI01] Kunieda, M.: Control of Discharge Locations in EDM with Locally Imposed High Electric Field. In: *Proc. ISEM 13th*. 2001
- [KUNI05] Kunieda, M.; Lauwers, B.; Rajurkar, K.; Schumacher, B.: Advancing EDM through Fundamental Insight into the Process. In: *CIRP Annals - Manufacturing Technology*, 54. Jg., 2005, S. 64–87
- [KUNI90] Kunieda, M.; Kojima, H.; Kinoshita, N.: On-Line Detection of EDM Spark Locations by Multiple Connection of Branched Electric Wires. In: *CIRP Annals*, 39. Jg., 1990, S. 171–174
- [KUNI91] Kunieda, M.: Study on Distribution of Spark Locations in EDM. In: *Journal of the Japan Society for Precision Engineering*, 57. Jg., 1991, S. 941–944
- [KUNI95] KUNIEDA M.: Relation Between Debris Concentration and Discharge Gap Length in EDM Process. In: *Proceeding of ASIAN Electrical-Machining Symposium '95*, 1. Jg., 1995
- [KUNI97] KUNIEDA M.: Study on Debris Movement in EDM Gap. In: *IJEM*, 2. Jg., 1997, S. 43–49
- [KUNI99] Kunieda, M.; Kowaguchi, W.; Takita, T.: Reverse Simulation of Die-Sinking EDM. In: *CIRP Annals*, 48. Jg., 1999, S. 115–118
- [KÜPP20] Küpper, U.; Herrig, T.; Klink, A.; Welling, D.; Bergs, T.: Evaluation of the Process Performance in Wire EDM Based on an Online Process Monitoring System. In: *Procedia CIRP*, 95. Jg., 2020, S. 360–365
- [KÜPP21a] Küpper, U.; Herrig, T.; Bergs, T.: Visualization of Spatially Resolved Energy in Wire Electrical Discharge Machining. In: *Procedia CIRP*, 104. Jg., 2021, S. 1512–1517
- [KÜPP21b] Küpper, U.; Herrig, T.; Welling, D.; Bergs, T.: Process Performance of High Energy Wire EDM. In: *Procedia CIRP*, 101. Jg., 2021, S. 230–233
- [KÜPP22a] Küpper, U.; Seelbach, T.; Heidemanns, L.; Prinz, S.; Herrig, T.; Bergs, T.: Effects of the Manufacturing Chain on the Surface Integrity when Machining Fir Tree Slots with Alternative Manufacturing Processes. In: *Procedia CIRP*, 108. Jg., 2022, S. 728–733
- [KÜPP22b] Küpper, U.; Tchoupe, E.; Klink, A.; Bergs, T.: Prediction of Geometrical Accuracy in Wire EDM by Analyzing Process Data. In: *Procedia CIRP*, 113. Jg., 2022, S. 23–28
- [KÜPP23] Küpper, U.; Klink, A.; Bergs, T.: Data-driven model for process evaluation in wire EDM. In: *CIRP Annals*, 72. Jg., 2023, S. 169–172

- [KÜPP24] Küpper, U.; Schulze Brock, D.; Klink, A.; Herrig, T.; Bergs, T.: Wire EDM for the Manufacture of Fir Tree Slots Using Different Wire Electrodes (Hrsg): Proceedings of ASME Turbo Expo 2024: Turbomachinery Technical Conference and Exposition (GT2024). June 24-28, 2024, London, United Kingdom. 6/24/2024 - 6/28/2024, London, United Kingdom
- [KWON06] Kwon, S.; Yang, M.-Y.: The benefits of using instantaneous energy to monitor the transient state of the wire EDM process. In: The International Journal of Advanced Manufacturing Technology, 27. Jg., 2006, S. 930–938
- [LAI15] Lai, S.; Xu, L.; Liu, K.; Zhao, J.: Recurrent Convolutional Neural Networks for Text Classification. In: Proceedings of the AAAI Conference on Artificial Intelligence, 29. Jg., 2015
- [LAR014] Larose, D.; Larose, C.: Discovering Knowledge in Data: An Introduction to Data Mining. Wiley, 2014
- [LECU15] LeCun, Y.; Bengio, Y.; Hinton, G.: Deep learning. In: Nature, 521. Jg., 2015, S. 436–444
- [LEE07] Lee, W.; Liao, Y.: Adaptive control of the WEDM process using a self-tuning fuzzy logic algorithm with grey prediction. In: The International Journal of Advanced Manufacturing Technology, 34. Jg., 2007, S. 527–537
- [LI13] Li, L.; Guo, Y.; Wei, X.; Li, W.: Surface Integrity Characteristics in Wire-EDM of Inconel 718 at Different Discharge Energy. In: Procedia CIRP, 6. Jg., 2013, S. 220–225
- [LI16] Li, C.; Ding, J.; Yang, S.; Fang, Y.; Kong, Q.: Discharge current shape control method and experiment in wire EDM. In: The International Journal of Advanced Manufacturing Technology, 87. Jg., 2016, S. 3271–3278
- [LI97] Li, Y.; Zhao, W.; Feng, X.; Wei, H.: Research advancement on on-line detection of EDM spark locations. In: Measurement, 22. Jg., 1997, S. 29–35
- [LIAO00] Liao, Y.; Woo, J.: Design of a fuzzy controller for the adaptive control of WEDM process. In: International Journal of Machine Tools and Manufacture, 40. Jg., 2000, S. 2293–2307
- [LIAO02] Liao, Y.; Yan, M.; Chang, C.: A neural network approach for the on-line estimation of workpiece height in WEDM. In: Journal of Materials Processing Technology, 121. Jg., 2002, S. 252–258
- [LIAO04a] Liao, Y.; Yu, Y.: The energy aspect of material property in WEDM and its application. In: Journal of Materials Processing Technology, 149. Jg., 2004, S. 77–82
- [LIAO04b] Liao, Y.; Yu, Y.: Study of specific discharge energy in WEDM and its application. In: International Journal of Machine Tools and Manufacture, 44. Jg., 2004, S. 1373–1380

- [LIAO13] Liao, Y.-S.; Chuang, T.-J.; Yu, Y.-P.: On-line Workpiece Height Estimation and its Application in Servo Feed Control of WEDM Process. In: *Procedia CIRP*, 6. Jg., 2013, S. 226–231
- [LIAO97a] Liao, Y.; Woo, J.: The effects of machining settings on the behavior of pulse trains in the WEDM process. In: *Journal of Materials Processing Technology*, 71. Jg., 1997, S. 433–439
- [LIAO97b] Liao, Y.; Chu, Y.; Yan, M.: Study of wire breaking process and monitoring of WEDM. In: *International Journal of Machine Tools and Manufacture*, 37. Jg., 1997, S. 555–567
- [LIAS19] Liashchynskiy, P.; Liashchynskiy, P.: Grid Search, Random Search, Genetic Algorithm: A Big Comparison for NAS, 2019
- [LIKA03] Likas, A.; Vlassis, N.; J. Verbeek, J.: The global k-means clustering algorithm. In: *Pattern Recognition*, 36. Jg., 2003, S. 451–461
- [LIPT14] Lipton, Z.; Elkan, C.; Naryanaswamy, B.: Optimal Thresholding of Classifiers to Maximize F1 Measure. In: *Machine learning and knowledge discovery in databases : European Conference, ECML PKDD ... : proceedings. ECML PKDD (Conference)*, 8725. Jg., 2014, S. 225–239
- [LIU11] Liu, B.: *Web Data Mining*. Berlin, Heidelberg: Springer Berlin Heidelberg, 2011
- [LIU16a] Liu, J.; Guo, Y.: Residual Stress Modeling in Electric Discharge Machining (EDM) by Incorporating Massive Random Discharges. In: *Procedia CIRP*, 45. Jg., 2016, S. 299–302
- [LIU16b] Liu, J.; Guo, Y.: Modeling of White Layer Formation in Electric Discharge Machining (EDM) by Incorporating Massive Random Discharge Characteristics. In: *Procedia CIRP*, 42. Jg., 2016, S. 697–702
- [LODH14] Lodhi, B.; Agarwal, S.: Optimization of Machining Parameters in WEDM of AISI D3 Steel Using Taguchi Technique. In: *Procedia CIRP*, 14. Jg., 2014, S. 194–199
- [ŁUCZ16] Łuczak, M.: Hierarchical clustering of time series data with parametric derivative dynamic time warping. In: *Expert Systems with Applications*, 62. Jg., 2016, S. 116–130
- [LUO95] Luo, Y.: An energy-distribution strategy in fast-cutting wire EDM. In: *Journal of Materials Processing Technology*, 55. Jg., 1995, S. 380–390
- [MAHE15] Maher, I.; Ling, L.; Sarhan, A.; Hamdi, M.: Improve wire EDM performance at different machining parameters - ANFIS modeling. In: *IFAC-PapersOnLine*, 48. Jg., 2015, S. 105–110
- [MAHR19] Mahr GmbH: MarSurf. MarSurf XC basic. URL: <https://metrology.mahr.com/fileadmin/assets/files/MarSurf--XC%20basic--3751585--FL--EN--2019-02-21.pdf> [13.03.2024]
- [MAJU15] Majumder, A.: Comparative study of three evolutionary algorithms coupled with neural network model for optimization of electric discharge machining process



- parameters. In: Proceedings of the Institution of Mechanical Engineers, Part B: Journal of Engineering Manufacture, 229. Jg., 2015, S. 1504–1516
- [MAKI24] Makino Europe GmbH: U6 H.E.A.T Wire EDM. URL: <https://www.makino.com/machine-technology/machines/wire-edm/u6-h-e-a-t> [19.02.2024]
- [MANA18] Manaswi, N.: Deep learning with applications using Python. Chatbots and face, object, and speech recognition with TensorFlow and Keras. New York: Apress, 2018
- [MARA20] Maradia, U.; Filisetti, E.; Wiessner, M.; Schneider, S.; Boccadoro, M.: The influence of energy input characteristics on surface integrity in wire EDM. In: Procedia CIRP, 95. Jg., 2020, S. 268–272
- [MARC20] Marcilio, W.; Eler, D.: From explanations to feature selection: assessing SHAP values as feature selection mechanism (Hrsg): 2020 33rd SIBGRAPI Conference on Graphics, Patterns and Images (SIBGRAPI). 07.11.2020 - 10.11.2020, Recife/Porto de Galinhas, Brazil, S. 340–347
- [MATZ21] Matzka, S.: Künstliche Intelligenz in den Ingenieurwissenschaften. Maschinelles Lernen verstehen und bewerten. Wiesbaden, Heidelberg: Springer Vieweg, 2021
- [MAYR16] Mayr, P.; Awiszus, B.; Bast, J.; Dürr, H.: Grundlagen der Fertigungstechnik. 6., aktualisierte Auflage. Aufl. Aufl. München, 2016
- [MING15] Ming, W.; Hou, J.; Zhang, Z.; Huang, H.; Xu, Z.; Zhang, G.; Huang, Y.: Integrated ANN-LWPA for cutting parameter optimization in WEDM. In: The International Journal of Advanced Manufacturing Technology. 2015
- [MIRF22] Mirfendreski, A.: Künstliche Intelligenz für die Entwicklung von Antrieben. Mirfendreski, A. (Hrsg): Künstliche Intelligenz für die Entwicklung von Antrieben. Berlin, Heidelberg: Springer Berlin Heidelberg, 2022, S. 83–172
- [MITC13] Mitchell, T.: Machine learning. [Nachdr.]. Aufl. New York: McGraw-Hill, 2013
- [MOEL10] Moeller Fachverlag: Das Dielektrikum bei der Funkenerosion. Der Stahlformenbauer. 2010
- [MOHA21] Mohammadnejad, M.: Phase field simulation of microstructure evolutions in the heat affected zone of a spark-eroded workpiece. Dissertation RWTH Aachen University. 1. Aufl. Aachen Apprimus, 2021
- [MOHA23] Mohammed, A.; Kora, R.: A comprehensive review on ensemble deep learning: Opportunities and challenges. In: Journal of King Saud University - Computer and Information Sciences, 35. Jg., 2023, S. 757–774
- [MOHD07] Mohd Abbas, N.; Solomon, D.; Fuad Bahari, M.: A review on current research trends in electrical discharge machining (EDM). In: International Journal of Machine Tools and Manufacture, 47. Jg., 2007, S. 1214–1228
- [MONM07] Monmasson, E.; Cirstea, M.: FPGA Design Methodology for Industrial Control Systems—A Review. In: IEEE Transactions on Industrial Electronics, 54. Jg., 2007, S. 1824–1842

- [MURP00] Murphy, K.; Lin, Z.: The influence of spatially nonuniform temperature fields on the vibration and stability characteristics of EDM wires. In: *International Journal of Mechanical Sciences*, 42. Jg., 2000, S. 1369–1390
- [MURP12] Murphy, K.: *Machine learning. A probabilistic perspective*. Cambridge, Mass.: MIT Press, 2012
- [MYTT16] Myttenaere, A. de; Golden, B.; Le Grand, B.; Rossi, F.: Mean Absolute Percentage Error for regression models. In: *Neurocomputing*, 192. Jg., 2016, S. 38–48
- [NA10] Na, S.; Xumin, L.; Yong, G.: Research on k-means Clustering Algorithm: An Improved k-means Clustering Algorithm (Hrsg): 2010 Third International Symposium on Intelligent Information Technology and Security Informatics. 02.04.2010 - 04.04.2010, Jian, China, S. 63–67
- [NARE20] Naresh, C.; Bose, P.; Rao, C.: ANFIS based predictive model for wire edm responses involving material removal rate and surface roughness of Nitinol alloy. In: *Materials Today: Proceedings*. 2020
- [NATI20c] National Instruments: Was ist DIAdem? URL: <https://www.ni.com/de-de/shop/data-acquisition-and-control/application-software-for-data-acquisition-and-control-category/what-is-diadem.html> [23.07.2020]
- [NATI24a] National Instruments: NI-5731/5732/5733 User Guide and Specifications, 2024
- [NATI24b] National Instruments: NI-7931R Controller for FlexRIO, 2024
- [NATI24c] National Instruments: What Is LabVIEW? URL: <https://www.ni.com/de/shop/lab-view.html> [20.05.2024]
- [NWAN18] Nwankpa, C.; Ijomah, W.; Gachagan, A.; Marshall, S.: *Activation Functions: Comparison of trends in Practice and Research for Deep Learning*, 2018
- [OBAR95] H. Obara, Y. Makino, T. Ohsumi: Single Discharging Force and Single Machining Volume of Wire EDM. In: *Proc. of ISEM*, 1995, 11. Jg., 1995, S. 85-93
- [OBAR97] Obara, H.; ABE, M.; OHSUMI, T.: Prevention of Wire Breakage on Wire EDM. 1st Report. Comparison of Spark Gap Detecting Signals on Wire EDM. In: *Journal of The Japan Society of Electrical Machining Engineers*, 31. Jg., 1997, S. 11–17
- [OBAR98] Obara, H.; ABE, M.; OHSUMI, T.: Prevention of Wire Breakage during wire EDM. 2nd Report. Grouping Method of Gap Signals according to Discharged Location. In: *Journal of The Japan Society of Electrical Machining Engineers*, 32. Jg., 1998, S. 8–15
- [OFOE19] Ofoeda, J.; Boateng, R.; Effah, J.: Application Programming Interface (API) Research. In: *International Journal of Enterprise Information Systems*, 15. Jg., 2019, S. 76–95
- [OKAD09] Okada, A.; Uno, Y.; Onoda, S.; Habib, S.: Computational fluid dynamics analysis of working fluid flow and debris movement in wire EDMed kerf. In: *CIRP Annals*, 58. Jg., 2009, S. 209–212

- [OKAD15] Okada, A.; Konishi, T.; Okamoto, Y.; Kurihara, H.: Wire breakage and deflection caused by nozzle jet flushing in wire EDM. In: CIRP Annals - Manufacturing Technology, 64. Jg., 2015, S. 233–236
- [OLIV23] Olivier, M.: Abtragmechanismen beim drahtfunkenerosiven Bearbeiten elektrisch leitfähiger Keramiken im kohlenwasserstoffbasierten Dielektrikum. Dissertation RWTH Aachen University, 2023
- [OLSO04] Olson, D.: Comparison of weights in TOPSIS models. In: Mathematical and Computer Modelling, 40. Jg., 2004, S. 721–727
- [OBWA18] Oßwald, K.; Lochmahr, I.; Schulze, H.-P.; Kröning, O.: Automated Analysis of Pulse Types in High Speed Wire EDM. In: Procedia CIRP, 68. Jg., 2018, S. 796–801
- [PALA08] Palankar, M.; Iamnitchi, A.; Ripeanu, M.; Garfinkel, S.: Amazon S3 for science grids (Hrsg): Proceedings of the 2008 international workshop on Data-aware distributed computing. 24 06 2008 24 06 2008, Boston MA USA, S. 55–64
- [PANT90] Panten, U.: Funkenerosive Bearbeitung von elektrisch leitfähigen Keramiken. Dissertation RWTH Aachen, 1990
- [PARA24] Paranjape, A.; Küpper, U.; Schulze Brock, D.; Schmitt, R.; Ohlenforst, M.; Peterek, M.: Real-time Quality Monitoring of Wire EDM Process Using Machine Learning. 2024. in press.
- [PART24] Parthasarathy, P.; Vetter, G.; Koerber, B.; Flood, C.; Min, S.: Global Machinery & Equipment Report 2024. Artificial Intelligence Rockets to the Top of the Manufacturing Priority List, 2024
- [PATR15] Patro, S.; Sahu, K.: Normalization: A Preprocessing Stage, 2015
- [PATU21] Paturi, U.; Cheruku, S.: Application and performance of machine learning techniques in manufacturing sector from the past two decades: A review. In: Materials Today: Proceedings, 38. Jg., 2021, S. 2392–2401
- [PERS16] Persico, V.; Montieri, A.; Pescape, A.: On the Network Performance of Amazon S3 Cloud-Storage Service (Hrsg): 2016 5th IEEE International Conference on Cloud Networking (Cloudnet). 03.10.2016 - 05.10.2016, Pisa, Italy, S. 113–118
- [PEZO16] Pezoa, F.; Reutter, J.; Suarez, F.; Ugarte, M.; Vrgoč, D.: Foundations of JSON Schema (Hrsg): Proceedings of the 25th International Conference on World Wide Web. 11 04 2016 15 04 2016, Montréal Québec Canada, S. 263–273
- [PHAM14] Pham, V.; Bluche, T.; Kermorvant, C.; Louradour, J.: Dropout Improves Recurrent Neural Networks for Handwriting Recognition (Hrsg): 2014 14th International Conference on Frontiers in Handwriting Recognition
- [PLAU21] Plaue, M.: Data Science. Berlin, Heidelberg: Springer Berlin Heidelberg, 2021
- [PORT07] Portillo, E.; Cabanes, I.; Marcos, M.; Orive, D.; Sanchez, J.: Design of a Virtual-Instrumentation System for a Machining Process. In: IEEE Transactions on Instrumentation and Measurement, 56. Jg., 2007, S. 2616–2622

- [PORT08a] Portillo, E.; Marcos, M.; Cabanes, I.; Zubizarreta, A.; Sánchez, J.: ANN for Interpolating Instability Trends in WEDM. In: IFAC Proceedings Volumes, 41. Jg., 2008, S. 2230–2235
- [PORT08b] Portillo, E.; Marcos, M.; Cabanes, I.; Zubizarreta, A.; Sanchez, J.: Artificial Neural Networks for detecting instability trends in different workpiece thicknesses in a machining process (Hrsg): 2008 American Control Conference. 11.06.2008 - 13.06.2008, Seattle, WA, S. 1064–1069
- [PORT09] Portillo, E.; Marcos, M.; Cabanes, I.; Orive, D.: Real-time monitoring and diagnosing in wire-electro discharge machining. In: The International Journal of Advanced Manufacturing Technology, 44. Jg., 2009, S. 273–282
- [PURI03] Puri, A.; Bhattacharyya, B.: An analysis and optimisation of the geometrical inaccuracy due to wire lag phenomenon in WEDM. In: International Journal of Machine Tools and Manufacture, 43. Jg., 2003, S. 151–159
- [QU02] Qu, J.; Shih, A.; Scattergood, R.: Development of the Cylindrical Wire Electrical Discharge Machining Process, Part 1. Concept, Design, and Material Removal Rate. In: Journal of Manufacturing Science and Engineering, 124. Jg., 2002, S. 702
- [RAHU23] M, R.; V, B.; S, N.: Optimization of wire-EDM process parameters for Ni–Ti–Hf shape memory alloy through particle swarm optimization and CNN-based SEM-image classification. In: Results in Engineering, 18. Jg., 2023, S. 101141
- [RAJU20] V N Ganapathi Raju; K Prasanna Lakshmi; Vinod Mahesh Jain; Archana Kalidindi; V Padma: Proceedings of the 3rd International Conference on Smart Systems and Inventive Technology (ICSSIT 2020). 20-22, August 2020. Piscataway, NJ: IEEE, 2020
- [RAJU91] Rajurkar, K.; Wang, W.; Lindsay, R.: On-Line Monitor and Control for Wire Breakage in WEDM. In: CIRP Annals, 40. Jg., 1991, S. 219–222
- [RAJU93] Rajurkar, K.; Wang, W.: Thermal modeling and on-line monitoring of wire-EDM. In: Journal of Materials Processing Technology, 38. Jg., 1993, S. 417–430
- [RAJU94] Rajurkar, K.; Wang, W.; McGeough, J.: WEDM Identification and Adaptive Control for Variable-Height Components. In: CIRP Annals - Manufacturing Technology, 43. Jg., 1994, S. 199–202
- [RAJU97] Rajurkar, K.; Wang, W.; Zhao, W.: WEDM-Adaptive Control with a Multiple Input Model for Identification of Workpiece Height. In: CIRP Annals - Manufacturing Technology, 46. Jg., 1997, S. 147–150
- [RANI13] Rani Y.; Dr. Harish Rohil: A Study of Hierarchical Clustering Algorithm.
- [RAO11] Rao, R.; Savsani, V.; Vakharia, D.: Teaching–learning-based optimization: A novel method for constrained mechanical design optimization problems. In: Computer-Aided Design, 43. Jg., 2011, S. 303–315
- [RASA20] Rasamoelina, A.; Adjailia, F.; Sincak, P.: A Review of Activation Function for Artificial Neural Network (Hrsg): SAMI 2020. IEEE 18th World Symposium on Applied

- Machine Intelligence and Informatics : proceedings : January 23-25, 2020, Herl'any, Slovakia. 1/23/2020 - 1/25/2020, Herlany, Slovakia, S. 281–286
- [RAY23] Ray, P.: ChatGPT: A comprehensive review on background, applications, key challenges, bias, ethics, limitations and future scope. In: Internet of Things and Cyber-Physical Systems, 3. Jg., 2023, S. 121–154
- [REFA09] Refaeilzadeh, P.; Tang, L.; Liu, H.: Cross-Validation. LIU, L.; ÖZSU, M. (Hrsg): Encyclopedia of Database Systems Boston, MA: Springer US, 2009, S. 532–538
- [RICH19] Richter, S.: Statistisches und maschinelles Lernen. Berlin, Heidelberg: Springer Berlin Heidelberg, 2019
- [ROCK24] Rockwell Automation: Annual State of Smart Manufacturing. How global manufacturers are harnessing emergent technology to maximize workforce potential, reduce risk, increase quality and deliver sustainable growth. 9th, 2024
- [SAEE21] Saeedi, J.; Dotta, M.; Galli, A.; Nasciuti, A.; Maradia, U.; Boccadoro, M.; Gambardella, L.; Giusti, A.: Measurement and inspection of electrical discharge machined steel surfaces using deep neural networks. In: Machine Vision and Applications, 32. Jg., 2021
- [SAHA04] Saha, S.; Pachon, M.; Ghoshal, A.; Schulz, M.: Finite element modeling and optimization to prevent wire breakage in electro-discharge machining. In: Mechanics Research Communications, 31. Jg., 2004, S. 451–463
- [SAHA22a] Saha, S.; Gupta, K.; Maity, S.; Dey, S.: Data-driven probabilistic performance of Wire EDM: A machine learning based approach. In: Proceedings of the Institution of Mechanical Engineers, Part B: Journal of Engineering Manufacture, 236. Jg., 2022, S. 908–919
- [SAHA22b] Saha, S.; Kumar Gupta, K.; Ranjan Maity, S.; Dey, S.: Probabilistic investigation of geometric responses in Wire EDM machined complex-shaped profile: A machine learning based approach. In: Proceedings of the Institution of Mechanical Engineers, Part B: Journal of Engineering Manufacture. 2022, S. 095440542211386
- [SAHA23] Saha, S.; Maity, S.; Dey, S.: Prediction of WEDM Performances Using Clustering Techniques in ANFIS During Machining of A286 Superalloy. In: Journal of The Institution of Engineers (India): Series C, 104. Jg., 2023, S. 315–326
- [SANC18] Sanchez, J.; Conde, A.; Arriandiaga, A.; Wang, J.; Plaza, S.: Unexpected Event Prediction in Wire Electrical Discharge Machining Using Deep Learning Techniques. In: Materials (Basel, Switzerland), 11. Jg., 2018
- [SCHA04] Schacht, B.: Composite Wires and Alternative Dielectrics for Wire Electrical Discharge Machining. Dissertation, Katholieke, Leuven, Belgium, 2004
- [SCHÄ08] Schäfer, A.: Reinforcement learning with recurrent neural networks Osnabrück, Univ., Diss., 2008, 2008

- [SCHN21] Schneider, S.: Modellierung der Energiedissipation in der Funkenerosion. Dissertation RWTH Aachen University. 1. Aufl. Aachen Apprimus Wissenschaftsverlag, 2021
- [SCHW17] Schwade, M.: Automatisierte Analyse hochfrequenter Prozesssignale bei der funkenerosiven Bearbeitung von Magnesium für die Medizintechnik. Dissertation RWTH Aachen University. 1. Aufl. Aachen Apprimus Wissenschaftsverlag, 2017
- [SHAH16] Shahane, S.; Pande, S.: Development of a Thermo-Physical Model for Multi-spark Wire EDM Process. In: Procedia Manufacturing, 5. Jg., 2016, S. 205–219
- [SHAM22] Shami, T.; El-Saleh, A.; Alswaitti, M.; Al-Tashi, Q.; Summakieh, M.; Mirjalili, S.: Particle Swarm Optimization: A Comprehensive Survey. In: IEEE Access, 10. Jg., 2022, S. 10031–10061
- [SHAO20] Shao, G.; Helu, M.: Framework for a digital twin in manufacturing: Scope and requirements. In: Manufacturing Letters, 24. Jg., 2020, S. 105–107
- [SHAR20] Sharma, S.; Sharma, S.; Athaiya, A.: ACTIVATION FUNCTIONS IN NEURAL NETWORKS. In: International Journal of Engineering Applied Sciences and Technology, 04. Jg., 2020, S. 310–316
- [SHOD92] Shoda K., Kaneko Y., Nishimura H., Kunieda M., Fan M.X.: Adaptive control of WEDM with on-line detection of spark locations. In: International Symposium of Electromachining (ISEM X). 1992, S. 410–416
- [SIEG94] Siegel, R.: Funkenerosives Feinstschneiden Verfahrenseinflüsse auf die Oberflächen- und Randzonenausbildung. Düsseldorf: VDI Verlag, 1994
- [SINA20] Sinaga, K.; Yang, M.-S.: Unsupervised K-Means Clustering Algorithm. In: IEEE Access, 8. Jg., 2020, S. 80716–80727
- [SING20] Singh, N.; Singh, Y.; Kumar, S.; Sharma, A.: Predictive analysis of surface roughness in EDM using semi-empirical, ANN and ANFIS techniques: A comparative study. In: Materials Today: Proceedings, 25. Jg., 2020, S. 735–741
- [SMIT13] Smith, C.; Koshy, P.: Applications of acoustic mapping in electrical discharge machining. In: CIRP Annals - Manufacturing Technology, 62. Jg., 2013, S. 171–174
- [SPED97] Spedding, T.; Wang, Z.: Parametric optimization and surface characterization of wire electrical discharge machining process. In: Precision Engineering, 20. Jg., 1997, S. 5–15
- [SRIV14] Nitish Srivastava; Geoffrey E. Hinton; Alex Krizhevsky; Ilya Sutskever; Ruslan Salakhutdinov: Dropout: a simple way to prevent neural networks from overfitting. In: J. Mach. Learn. Res., 15. Jg., 2014, S. 1929–1958
- [STAR19] Stark, R.; Damerau, T.: Digital Twin. Chatti, S.; Tolio, T. (Hrsg): CIRP Encyclopedia of Production Engineering Berlin, Heidelberg: Springer Berlin Heidelberg, 2019, S. 1–8

- [STE18] Stearns, S.; Hush, D.: Digitale Verarbeitung analoger Signale / Digital Signal Analysis. 7., durchgesehene Auflage. Reprint 2018. Aufl. Berlin, Boston: Oldenbourg Wissenschaftsverlag, 2018
- [STYC17] Styczynski, Z.; Rudion, K.; Naumann, A.: Einführung in Expertensysteme. Grundlagen, Anwendungen und Beispiele aus der elektrischen Energieversorgung. Berlin, Heidelberg: Springer Berlin Heidelberg, 2017
- [SUCK20] Sucky Rashida Nasrin: Data Binning with Pandas Cut or Qcut Method. URL: <https://towardsdatascience.com/sort-and-segment-your-data-into-bins-to-get-sorted-ranges-pandas-cut-and-qcut-7785931bbfde> [04.01.2021]
- [SUDH22a] Sudhir; Kumar Sehgal, A.; Singh Nain, S.: Machine learning models behavior analysis for WEDM of super alloy. In: Materials Today: Proceedings. 2022
- [SUDH22b] Sudhir; Sehgal, A.; Nain, S.: Machine learning algorithms evaluation and optimization of WEDM of nickel based super alloy: A review. In: Materials Today: Proceedings, 50. Jg., 2022, S. 1793–1798
- [SURY17] Surya, V.; Kumar, K.; Keshavamurthy, R.; Ugrasen, G.; Ravindra, H.: Prediction of Machining Characteristics using Artificial Neural Network in Wire EDM of Al7075 based In-situ Composite. In: Materials Today: Proceedings, 4. Jg., 2017, S. 203–212
- [SWAM17] Swamynathan, M.: Mastering Machine Learning with Python in Six Steps. A Practical Implementation Guide to Predictive Data Analytics Using Python. Berkeley, CA: Apress, 2017
- [TARN95] Tarn, Y.; Ma, S.; Chung, L.: Determination of optimal cutting parameters in wire electrical discharge machining. In: International Journal of Machine Tools and Manufacture, 35. Jg., 1995, S. 1693–1701
- [TEKT18] Tektronix, I.: Digital Phosphor Oscilloscopes DPO7000 Series Datasheet. URL: <https://download.tek.com/datasheet/DPO7000C-Oscilloscope-Datasheet-48W2654321.pdf> [19.02.2024]
- [TEKT23a] Tektronix, I.: High-voltage Differential Probes TMDP0200 - THDP0200 - THDP0100 - P5200A - P5202A - P5205A - P5210A. URL: <https://download.tek.com/datasheet/TMDP-P5200Datasheet-51W1119515.pdf> [19.02.2024]
- [TEKT23b] Tektronix, I.: AC/DC Current Measurement Systems TCPA300, TCP312A, TCP305A, TCP303, TCPA400, TCP404XL Datasheet. URL: <https://download.tek.com/datasheet/TCPA300-400-Datasheet-EN-US-60W-16458-14.pdf> [19.02.2024]
- [THAN19] Thankachan, T.; Soorya Prakash, K.; Malini, R.; Ramu, S.; Sundararaj, P.; Rajandran, S.; Rammasamy, D.; Jothi, S.: Prediction of surface roughness and material removal rate in wire electrical discharge machining on aluminum based alloys/composites using Taguchi coupled Grey Relational Analysis and Artificial Neural Networks. In: Applied Surface Science, 472. Jg., 2019, S. 22–35

- [TING10] Ting, K.: Confusion Matrix. Sammut, C.; Webb, G. (Hrsg): Encyclopedia of Machine Learning Boston, MA: Springer US, 2010, S. 209
- [TOMU09] Tomura, S.; Kunieda, M.: Analysis of electromagnetic force in wire-EDM. In: Precision Engineering, 33. Jg., 2009, S. 255–262
- [TRAS09] Traskin, V.: Rehbinder effect in tectonophysics. In: Izvestiya, Physics of the Solid Earth, 45. Jg., 2009, S. 952–963
- [TULL93] Tulleken, H.: Grey-box modelling and identification using physical knowledge and bayesian techniques. In: Automatica, 29. Jg., 1993, S. 285–308
- [UGRA14] Ugrasen, G.; Ravindra, H.; Prakash, G.; Keshavamurthy, R.: Estimation of Machining Performances Using MRA, GMDH and Artificial Neural Network in Wire EDM of EN-31. In: Procedia Materials Science, 6. Jg., 2014, S. 1788–1797
- [UGRA15] Ugrasen, G.; Ravindra, H.; Prakash, G.; Prasad, Y.: Optimization of Process Parameters in Wire EDM of HCHCr Material Using Taguchi's Technique. In: Materials Today: Proceedings, 2. Jg., 2015, S. 2443–2452
- [ULAS20] Ulas, M.; Aydur, O.; Gurgenc, T.; Ozel, C.: Surface roughness prediction of machined aluminum alloy with wire electrical discharge machining by different machine learning algorithms. In: Journal of Materials Research and Technology, 9. Jg., 2020, S. 12512–12524
- [VDI94]: Norm VDI. Anwendung der Funkenerosion - VDI 3402 Blatt 4, März 1994
- [VENK23] Venkatarao, K.; Reddy, M.; Kumar, Y.; Raju, L.; Rao, B.; Azad, D.: Multi-response optimization in WEDM process of Al–Si alloy using TLBO-graph theory algorithm towards sustainability. In: The International Journal of Advanced Manufacturing Technology, 126. Jg., 2023, S. 3679–3694
- [VIEI20] Vieira, S.; Garcia-Dias, R.; Lopez Pinaya, W.: A step-by-step tutorial on how to build a machine learning model (Hrsg): Machine Learning Elsevier, 2020, S. 343–370
- [WANG18a] Wang, J.; Sanchez, J.; Ayesta, I.; Iturrioz, J.: Unsupervised Machine Learning for Advanced Tolerance Monitoring of Wire Electrical Discharge Machining of Disc Turbine Fir-Tree Slots. In: Sensors (Basel, Switzerland), 18. Jg., 2018
- [WANG18b] Wang, D.; Tan, D.; Liu, L.: Particle swarm optimization algorithm: an overview. In: Soft Computing, 22. Jg., 2018, S. 387–408
- [WANG19a] Wang, J.; Sanchez, J.; Iturrioz, J.; Ayesta, I.: Geometrical Defect Detection in the Wire Electrical Discharge Machining of Fir-Tree Slots Using Deep Learning Techniques. In: Applied Sciences, 9. Jg., 2019, S. 90
- [WANG19b] Wang, J.; Sánchez, J.; Iturrioz, J.; Ayesta, I.: Artificial Intelligence for advanced non-conventional machining processes. In: Procedia Manufacturing, 41. Jg., 2019, S. 453–459
- [WANG22] Wang, Q.; Ma, Y.; Zhao, K.; Tian, Y.: A Comprehensive Survey of Loss Functions in Machine Learning. In: Annals of Data Science, 9. Jg., 2022, S. 187–212



- [WANG23] Wang, J.; Sánchez, J.; Izquierdo, B.; Ayesta, I.: Effect of discharge accumulation on wire breakage in WEDM process. In: *The International Journal of Advanced Manufacturing Technology*, 125. Jg., 2023, S. 1343–1353
- [WARR05] Warren Liao, T.: Clustering of time series data—a survey. In: *Pattern Recognition*, 38. Jg., 2005, S. 1857–1874
- [WATA90] Watanabe, H.; Sato, T.; Suzuki, I.; Kinoshita, N.: WEDM Monitoring with a Statistical Pulse-Classification Method. In: *CIRP Annals - Manufacturing Technology*, 39. Jg., 1990, S. 175–178
- [WATS85] Watson, P.: Electrostatic and Hydrodynamic Effects in the Electrical Breakdown of Liquid Dielectrics. In: *IEEE Transactions on Electrical Insulation*, EI-20. Jg., 1985, S. 395–399
- [WBA24] WBA Aachener Werkzeugbau Akademie GmbH: Tooling in Series. URL: <https://werkzeugbau-akademie.de/en/> [28.02.2024]
- [WEIC19] Weichert, D.; Link, P.; Stoll, A.; Rüping, S.; Ihlenfeldt, S.; Wrobel, S.: A review of machine learning for the optimization of production processes. In: *The International Journal of Advanced Manufacturing Technology*, 104. Jg., 2019, S. 1889–1902
- [WEIN12] Weingärtner, E.; Wegener, K.; Kuster, F.: Wire electrical discharge machining applied to high-speed rotating workpieces. In: *Journal of Materials Processing Technology*, 212. Jg., 2012, S. 1298–1304
- [WEIN13] Weingärtner, E.; Wegener, K.; Kuster, F.: Influence of Workpiece Circumferential Speed in Wire Electrical Discharge Machining. In: *Procedia CIRP*, 6. Jg., 2013, S. 238–243
- [WEIß15] Weißgerber, W.: *Elektrotechnik für Ingenieure - Formelsammlung*. Elektrotechnik kompakt. 5., durchges. Aufl. Aufl. Wiesbaden: Springer Vieweg, 2015
- [WELL15] Welling, D.: Wire EDM for the manufacture of fir tree slots in nickel-based alloys for jet engine components. Dissertation RWTH Aachen University. 1. Aufl. Aachen Apprimus, 2015
- [WELS22] Welschof, L.; Schäfer, N.; Herrig, T.; Klink, A.; Bergs, T.: Effect of electrode material on removal efficiency regarding single discharges in wire EDM. In: *The International Journal of Advanced Manufacturing Technology*, 120. Jg., 2022, S. 1583–1589
- [WERB88] Werbos, P.: Generalization of backpropagation with application to a recurrent gas market model. In: *Neural Networks*, 1. Jg., 1988, S. 339–356
- [XU10] Xu, Y.; Guo, X.; Liu, C.: Study on Wire Breakage in WEDM by 3D Technology. In: *Applied Mechanics and Materials*, 44-47. Jg., 2010, S. 1442–1448
- [YAN96] Yan, M.; Liao, Y.: Monitoring and self-learning fuzzy control for wire rupture prevention in wire electrical discharge machining. In: *International Journal of Machine Tools and Manufacture*, 36. Jg., 1996, S. 339–353

- [YAN98] Yan, M.; Liao, Y.: Adaptive control of the WEDM process using the fuzzy control strategy. In: *Journal of Manufacturing Systems*, 17. Jg., 1998, S. 263–274
- [YAN99] Yan, M.; Li, H.; Liang, J.: The Application of Fuzzy Control Strategy in Servo Feed Control of Wire Electrical Discharge Machining. In: *The International Journal of Advanced Manufacturing Technology*, 15. Jg., 1999, S. 780–784
- [YUEN21] Yuen, B.; Hoang, M.; Dong, X.; Lu, T.: Universal activation function for machine learning. In: *Scientific reports*, 11. Jg., 2021, S. 18757
- [ZEIS17] Zeis, M.: Verformung dünnwandiger Graphitelektroden mit hohen Aspektverhältnissen beim funkenerosiven Senken. Dissertation RWTH Aachen University. 1. Aufl. Aachen Apprimus Wissenschaftsverlag, 2017
- [ZEIS23] Carl Zeiss AG: ZEISS Smartzoom 5. URL: <https://www.zeiss.de/messtechnik/produkte/systeme/industrielle-mikroskopie/smartzoom-5.html> [02.06.2023]
- [ZELN04] Zelnik-Manor, L.; Perona, P.: Self-Tuning Spectral Clustering (Hrsg): *Advances in Neural Information Processing Systems*
- [ZHAN15] Zhang, Z.; Ming, W.; Zhang, G.; Huang, Y.; Wen, X.; Huang, H.: A new method for on-line monitoring discharge pulse in WEDM-MS process. In: *The International Journal of Advanced Manufacturing Technology*, 81. Jg., 2015, S. 1403–1418
- [ZHAN18a] Zhang, Z.; Sabuncu, M.: Generalized cross entropy loss for training deep neural networks with noisy labels (Hrsg): *Proceedings of the 32nd International Conference on Neural Information Processing Systems*, S. 8792–8802
- [ZHAN18b] Zhang, Z.: Improved Adam Optimizer for Deep Neural Networks (Hrsg): *2018 IEEE/ACM 26th International Symposium on Quality of Service (IWQoS)*. 04.06.2018 - 06.06.2018, Banff, AB, Canada, S. 1–2



## 11 Appendix

Table 11.1: Machine setting parameters of test series “dynamic process” for workpiece height  $h = 40$  mm

Discharge current $i_e$	Pulse interval time $t_0$	Normal discharge duration $t_{e,n}$	Short circuit discharge duration $t_{e,s}$
23	60	67	6
23	70	82	8
23	50	97	10
23	40	53	11
26	50	67	8
26	40	82	6
26	60	97	11
26	70	53	10
29	40	67	10
29	50	82	11
29	70	97	6
29	60	53	8
20	70	67	11
20	60	82	10
20	40	97	8
20	50	53	6
23	55	97	10
23	50	97	6
26	45	82	6
26	55	67	8
26	65	97	11
29	45	67	10
29	55	82	11
23	60	97	10
26	50	82	6
26	70	97	11
29	50	67	10
29	60	82	11
29	55	67	10
29	65	82	11
29	60	67	10
29	70	82	11
29	65	67	10
29	75	82	11
29	75	67	10
29	75	67	10

